Iowa State University

Digital Repository

1979

Random-walk variable wind model for loess deposits

Alan James Lutenegger

Iowa State University

Recommended Citation

INFORMATION TO USERS

This was produced from a copy of a document sent to us for microfilming. While the most advanced technological means to photograph and reproduce this document have been used, the quality is heavily dependent upon the quality of the material submitted.

The following explanation of techniques is provided to help you understand markings or notations which may appear on this reproduction.

1. The sign or "target" for pages apparently lacking from the document photographed is "Missing Page(s)". If it was possible to obtain the missing page(s) or section, they are spliced into the film along with adjacent pages. This may have necessitated cutting through an image and duplicating adjacent pages to assure you of complete continuity.

2. When an image on the film is obliterated with a round black mark it is an indication that the film inspector noticed either blurred copy because of movement during exposure, or duplicate copy. Unless we meant to delete copyrighted materials that should not have been filmed, you will find a good image of the page in the adjacent frame.

3. When a map, drawing or chart, etc., is part of the material being photo-graphed the photographer has followed a definite method in "sectioning" the material. It is customary to begin filming at the upper left hand corner of a large sheet and to continue from left to right in equal sections with small overlaps. If necessary, sectioning is continued again—beginning below the first row and continuing on until complete.

4. For any illustrations that cannot be reproduced satisfactorily by xerography, photographic prints can be purchased at additional cost and tipped into your xerographic copy. Requests can be made to our Dissertations Customer Services Department.

5. Some pages in any document may have indistinct print. In all cases we have filmed the best available copy.

LUTENEGGER, ALAN JAMES

RANDOM-WALK VARIABLE WIND MODEL FOR LOESS DEPOSITS

Iowa State University   PH.D.   1979

PLEASE NOTE:

In all cases this material has been filmed in the best possible way from the available copy. Problems encountered with this document have been identified here with a check mark ✓.

1. Glossy photographs _____

2. Colored illustrations _____

3. Photographs with dark background __✓__

4. Illustrations are poor copy _____

5. Print shows through as there is text on both sides of page _____

6. Indistinct, broken or small print on several pages __✓__ throughout _____

7. Tightly bound copy with print lost in spine _____

8. Computer printout pages with indistinct print _____

9. Page(s) _____ lacking when material received, and not available from school or author _____

10. Page(s) _____ seem to be missing in numbering only as text follows _____

11. Poor carbon copy _____

12. Not original copy, several pages with blurred type _____

13. Appendix pages are poor copy _____

14. Original copy with light type _____

15. Curling and wrinkled pages _____

16. Other _____

Random-walk variable wind model for loess deposits

by

Alan James Lutenegger

A Dissertation Submitted to the

Graduate Faculty in Partial Fulfillment of

The Requirements for the Degree of

DOCTOR OF PHILOSOPHY

Department: Civil Engineering
Major: Geotechnical Engineering

Approved:

In Charge of Major Work

For the Major Department

For the Graduate College

Iowa State University
Ames, Iowa
1979

ii

TABLE OF CONTENTS

LIST OF FIGURES

.

ix

		Page

LIST OF TABLES

LIST OF ABBREVIATIONS

The following list of abbreviations is presented to simplify the reading of this manuscript, and pertains only to current research methods:

α	angle (measured from perpendicular) between source and wind direction
BST	Borehole Shear Test
BWS	Basal Wisconsin Soil
β	trajectory angle (measured from horizontal) of an individual particle
d	grain diameter
d_m	maximum grain diameter
ESW	Effective Source Width
IES	Iowan Erosion Surface
LH	Iowa River Traverse
LSP	Late Sangamon Paleosol
ME	Missouri-East Traverse
MW	Missouri-West Traverse
NPR	Number of Prevailing Repetitions
PC	Particle Concentration
P_f	probability of particle fall
P_p	probability of prevailing wind
P_r	probability of particle rise
P_{v_i}	probability of variable wind

PWC   Prevailing Wind Component

RCYBP   Radiocarbon Years Before Present

Sed   Sediment

SEM   Scanning Electron Microscopy

SL   Step Length

SW   Source Width

V_s sedimentation velocity

V_x horizontal wind velocity

V_y vertical wind velocity

X_m maximum transport distance

YSP   Yarmouth-Sangamon Paleosol

INTRODUCTION

General Statement

The extent of eolian silt which occurs throughout the world has been documented extensively during the past fifty years and has been summarized in the United States by Thorp and Smith (157), who in the early 1950's attempted to quantify the thickness and extent of known eolian deposits. Loess deposits, because of their vast areal occurrence and unique characteristics, have been the attention of considerable research -- by soil scientists, because of the agronomic importance of loess-derived soils, by geologists, because of the need to understand the genesis and distribution, and by engineers, because of the associated geotechnical problems. The recognition of loess as an engineering material whose properties can be quantified is a prerequisite to any corresponding geotechnical research. Certain property variations which occur in loess deposits, such as thickness and particle size, have been given specific empirical relationships which help demonstrate the systematics involved. These variations will be discussed further.

Variable Winds Hypothesis

In the central United States, loess is generally considered to be a periglacial deposit associated with the

eolian transport of silts derived from glacial outwash
(18 , 43, 118).   The source of these silts is meltwater
streams, i.e. river valleys, which become choked with debris
from glacial melting. The eolian theory of formation has
typically included the concept of deposition by prevailing
winds (18 , 43) usually considered in the U.S. to be north-
westerly. However, observations of significant loess
deposits in the world, particularly those of the upper mid-
west U.S., reveal an interesting point: material occurs on
both sides of valley sources. Figure 1 displays this trend
for the central U.S.

The prevailing wind concept for loess deposition does
not account for loess on the "upwind" side of sources or
"upwind" thinning away from a source, providing that the
source can be identified. Prevailing wind theory also does
not explain situations such as in northcentral Missouri and
southcentral Iowa where thickness isopach's appear as closed
contours, Figure 1. Rather, a more striking relation is
shown between source and thickness. This does not refute
that seasonal prevailing winds existed during the period
of loess deposition, as studies of dune form and lineation
(42 ,167), wind aligned drainage patterns (63, 98), as well
as paleoclimatic interpretations of wind directions (94),
have all substantiated the paleowind regimes to a certain
extent. However, the prevailing wind may not have
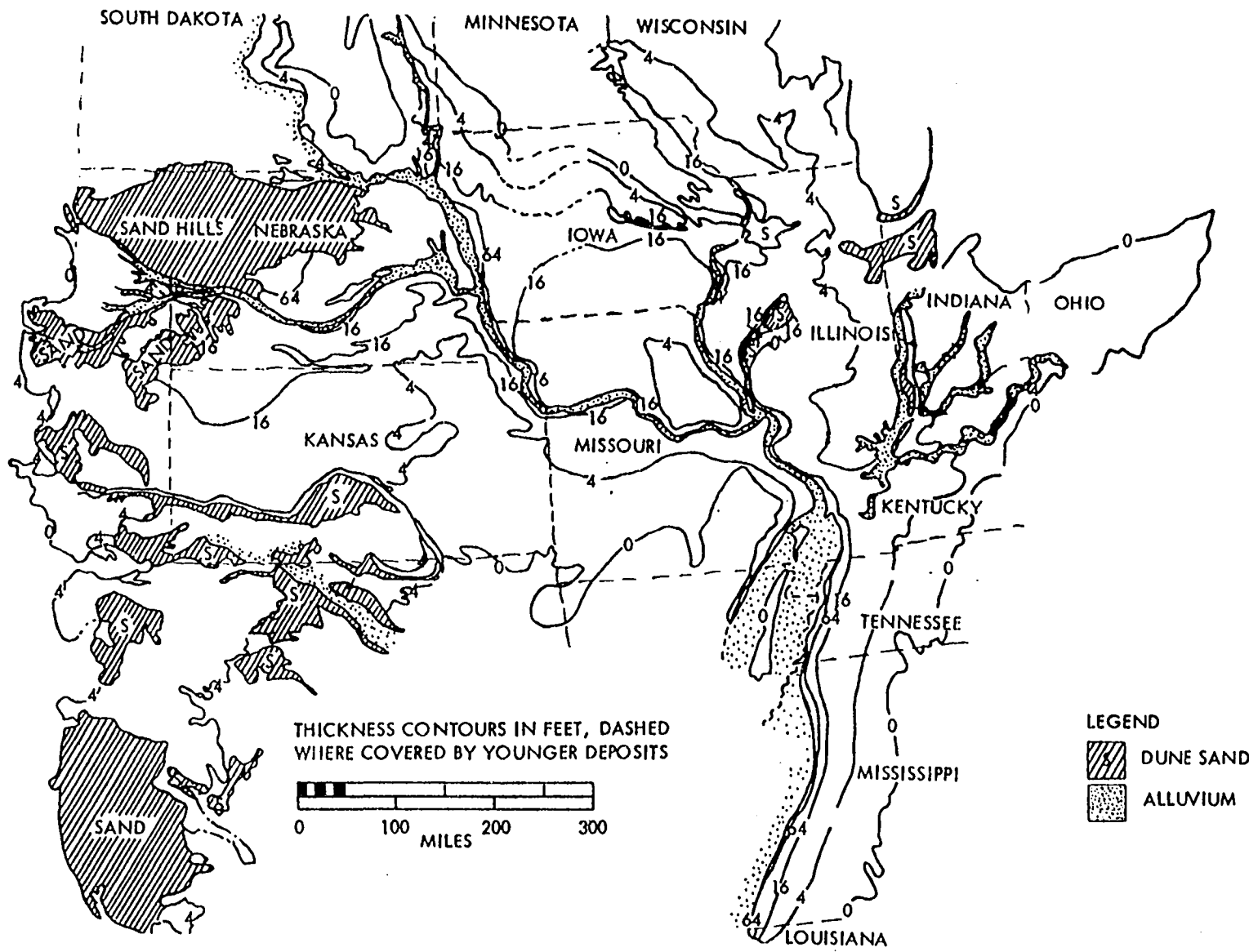
Figure 1. Loess thickness in the central U.S.

contributed to the formation of loess deposits as strongly as believed. A more logical approach to this problem might be to define a number of "prevailing" wind directions to account for seasonal direction changes, hence in effect a variable wind system. This has been suggested (67) and appears to have significant merit. Although this is not necessarily a new concept and has been mentioned by a number of investigators it was not pursued further until recently.

The classical work of Smith (142) in Illinois, was the first successful attempt to establish relationships between loess thickness and textural changes with distance from the proposed source. He accounted for a two-part mathematical expression of thickness by stating:

> "A more logical explanation of the change in the constants of the equation expressing the thinning of the loess can be developed from the probability that the wind direction was not constant during the deposition of the loess. If the loess was deposited by winds of varying direction, the shape of the flood plains would bring about the observed phenomenon."

It is interesting to note the reference to source configuration, a factor which had previously been neglected.

Hutton's (80) two traverses in southwestern Iowa, like Smith's in Illinois, were oriented in a northwest-southeast direction, in keeping with the prevailing winds concept; however, a comment was made concerning depositional wind direction:

"There undoubtedly were winds from many directions
during the long period as is shown by the fact that
Peorian loess is deposited close to the Missouri River
in Nebraska, but the loess does not attain the thick-
ness there that it does in Iowa."

Obviously,winds were not uniform in all directions, other-
wise thickness would be uniform. This observation also was
made by Leighton and Willman (96), concerning Mississippi
valley loess. "Wind directions also were variable, as at
present, but in the main were westerly." Note the
reference to the concept of uniformitarianism.

As recent as 1973, Frye and Willman (52) made reference
to variable winds by stating:

"The dominance of westerly winds is indicated by
thicker loess on the east sides of valleys than on
the west. However perhaps a third as much loess
occurs on the west side of valleys, which indicates
wind shifts comparable to those accompanying the
passing of high and low-pressure weather systems
such as we have at present."

The concept of variable winds in relation to loess
deposition has mainly been used as the "catchall" explana-
tion for trends in thickness and particle size which could
not otherwise be explained (39, 49).

An explanation for the deposition of loess by winds
from variable rather than a prevailing direction was
presented in the form of a theoretical mathematical model
by Handy (67). This approach suggests that the linear
relationship between loess thickness and logarithm of

distance from the source can be demonstrated by adding a prevailing wind component to a random variable wind direction. While the model is somewhat simplified, the author concluded that the importance of such an approach is not in describing in detail the entire mechanism of eolian sedimentation, but in emphasizing the most important features in the process while temporarily disregarding the others.

The important point is not whether the wind directions were constant during loess deposition, which does not appear to be the case, or for that matter what climatic conditions were required to generate eolian activity. Rather, the question should be how well the deposit can be quantified using a theoretical approach on the basis of reasonable and logical assumptions, in this case variable winds.

SCOPE AND OBJECTIVES

Geologic materials ultimately provide the basis of geotechnical engineering and since the engineer must be constantly aware of changes in any deposit, a complete understanding of the materials is essential. No other widely occurring geologic deposit shows more systematic variation in properties than does loess. This is in part demonstrated by the large number of empirical relationships that have been published since the beginning of formal quantitative geomorphology. The eolian origin for loess provides a natural means of studying these variations from a theoretical sense, by: 1) making preliminary assumptions based on extrapolated observations or theory; 2) developing a model which mathematically describes general trends and, 3) comparing the developed model to observed data and making adjustments to the model if needed. This certainly implies an iterative process, considering that geologic materials, even if quite uniform, do not always behave as ideal, theoretical media. In short, what looks good on paper may not look good in the field.

The unique characteristics of loess deposits make this an interesting material to study, and the widespread occurrence throughout the United States and the world makes loess an important material to study. Furthermore, the

progressive geographical changes in properties which influence mechanistic behavior may further our understanding of soil behavior.

Qualitatively, engineering variations which occur in loess have been related to changes in thickness and particle size. Thicker, coarse textured loess exhibits behavior which resembles cohesionless soil (sand) with apparent cohesion. Ability to maintain steep slopes, and sudden collapse of structure upon saturation are typically associated with thick loess deposits. Thin, fine textured loess displays behavior more typical of cohesive soils. In fact, excessive amounts of expandable clay minerals present in thin loess areas can create shrink-swell problems (62) a hazard which is often overlooked in loess provinces. One would suspect, then, that a transition zone occurs between these two end members wherein the material would display certain qualities of both a cohesive and a cohesionless soil.

In addition, as distance from the source increases, loess may change through a sequence which might be described in the classical soil mechanics sense as: (1) underconsolidated, (2) normally consolidated, and (3) overconsolidated, the latter being produced by shrinkage as a result of desiccation. Theories of soil mechanics

have generally been developed for cohesive and cohesion-
less materials in an idealized sense, and thus provide a
framework to approach the geotechnical study of loess.

The engineering properties of loess as with other
soils are a function of the genetic process of formation,
and of any alterations that have occurred as a result of
the post-depositional changes. This reflects not only the
importance of the sedimentation processes; erosion,
transportation, and deposition, but also the subsequent
geologic processes which exert external forces on the
deposit. One objective of this study is to examine these
processes and describe the relative influence on the
resulting deposit and resultant engineering characteristics.

The overall objective is to develop a theoretical
model based on the variable winds hypothesis, that will
explain observed changes in thickness and particle size
distribution relative to a source, and secondly, to relate
the engineering properties to these changes. Assuming
that loess was deposited by winds from variable directions,
the most important variable which influences the deposit
should be source geometry, i.e., width, length, inclina-
tion, and efficiency. Resulting deposits of finite thick-
ness and uniform particle-size should be controlled by
source variables, all other things being constant. In turn,

the thickness and particle size should then control
measureable engineering properties, such as density and
shear strength.

REVIEW OF LITERATURE

General Statement

This study deals with a general model for describing the genesis of eolian loess deposits, and the relation of engineering properties to that process. The review of background material pertinent to the present research is presented in four sections. The first two discuss the general nature of loess deposits in the midcontinental U.S., and deal with occurrence, stratigraphy, complexity, and quantitative variations, the latter of which are empirical. The last two sections provide background material necessary for development of the variable-winds statistical model, and discuss previous attempts to establish theoretical models for eolian deposition.

Stratigraphy of midcontinent loess

Pleistocene loess in the United States, particularly the Midwest, has been used in this study to compare the results of model predictions with observed trends, the majority of attention being given to Wisconsinan loess. Since some confusion may exist concerning time-stratigraphy of the loess throughout the Midwest, a general review of the subject is in order.

Frye et al. (54) presented a schematic diagram showing the stratigraphy of loess deposits from eastern Nebraska-

northeastern Kansas to eastern Illinois, plotted with the Sangamon (Illinoian) soil as a horizontal plane, Figure 2. The Sangamon soil separates Illinoian from Wisconsinan aged deposits, and thus Loveland (Illinoian) from Peorian (Wisconsin) loess. In eastern Nebraska and south-western Iowa, Wisconsin loess is shown as being comprised of three units; a basal zone, a middle zone, and a upper unit, the Bignell loess. The lower increment of loess was reclassified as Early Wisconsin and named the Gilman Canyon (115).

Lugn (100) was of the opinion that the majority of loess in Nebraska originated from the sand hills and thus was associated with desert conditions. This hypothesis of origin has not been fully supported (114), and quantitative data indicate that the Missouri and Platte River Valleys, and not the sand hills, were the major sources for loess in Nebraska (9, 38). Radiocarbon dates from alluvium over-lain by as much as 19.7 ft. (6.0 m) of dune sand in the sand-hills region all date less than 7200 RCYBP (radiocarbon years before present) (103), which places the formation as mid-Holocene. This would seem to conflict with attempts to equate the deposition of Wisconsin loess with the formation of large scale dunes.

In Nebraska, the Bignell loess is separated from the

WEST   EAST

SE. Neb.   S. Iowa
NE. Kan.   N. Missouri   Illinois
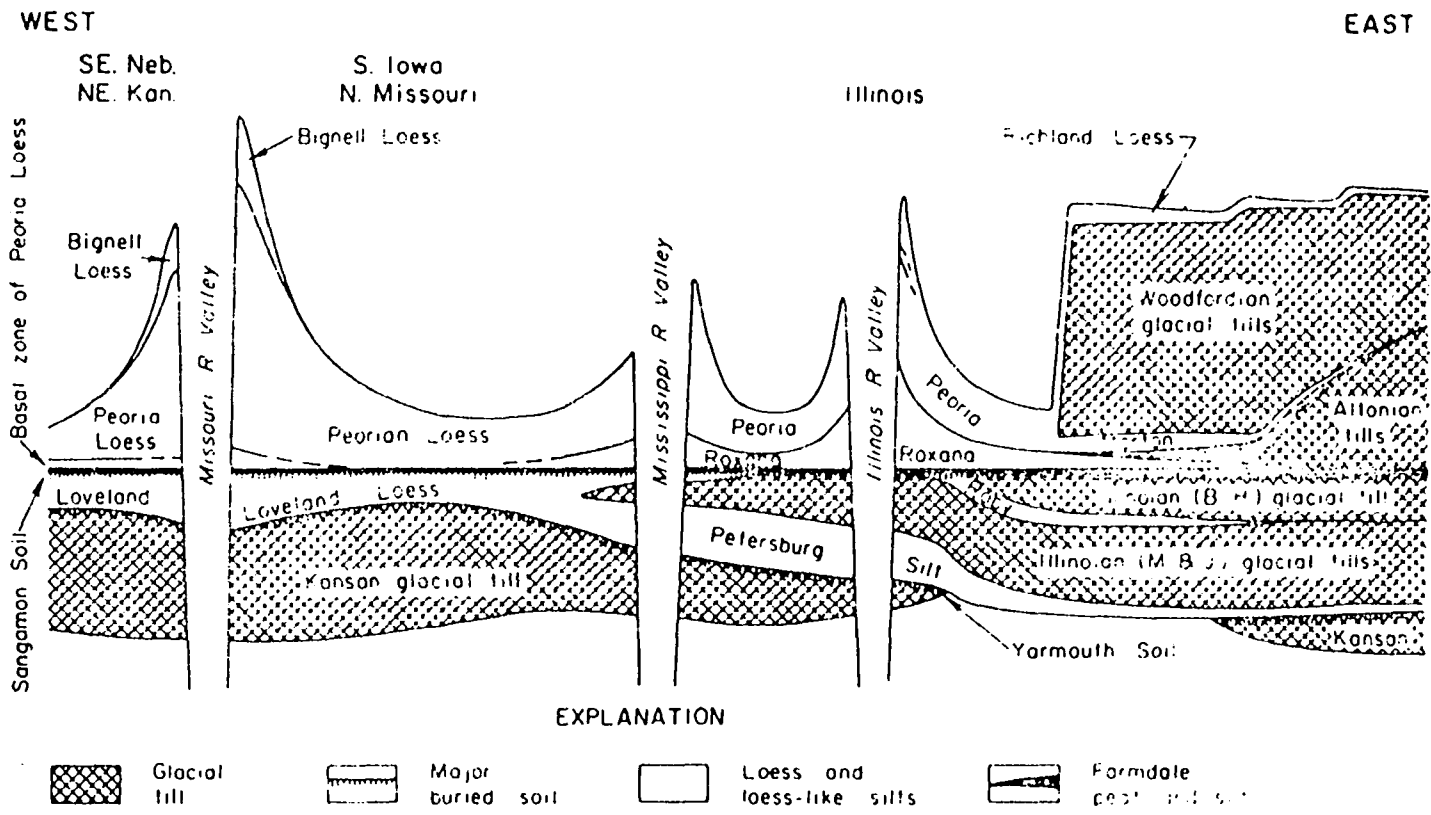
Figure 2. Stratigraphy of midcontinental U.S. loess

medial Wisconsinan by the Brady soil and in much of the
upland areas cannot be separated from the modern soil
making identification nearly impossible (115). Caspall
(16) concluded that in northeastern Kansas the Brady soil
is nonexistent and Bignell loess is separated from Peorian
on the basis of calcite-dolomite content. Because of the
difficulty in distinguishing the Bignell, the thickness
map of Peoria loess in Nebraska (88) although incomplete
in some areas, probably includes some Bignell in the
measurements.[1]

There is still some difficulty in distinguishing the
age of the Bignell, whether Wisconsinan or Holocene, since
no modern radiocarbon dating is available (121). However,
dates obtained from mollusk shells about 8 ft (2.4 m) above
the Brady soil in northeastern Kansas are 12,500 ± 400 BP
(before present) and 12,700 ± 300 BP (115), while spruce wood
taken from base of the Wisconsin loess in the same area was
dated at 18,200 ± 500 RCYBP. This would seem to put the
Bignell clearly as Wisconsinan.

In northeastern Kansas (51) and northwestern Missouri
(77) the stratigraphic column is basically in agreement
with that of Nebraska for Wisconsinan loess, again divided

---

[1]Written communication, J. Swinehart, Research
Geologist, Nebraska Geological Survey, January, 1979.

into three units. Bignell loess and the Brady Soil
tentatively have been identified along the Missouri River
Valley, as far east as central Missouri (113).

In Iowa, the lower unit of Wisconsinan loess has been
called Farmdale (126) but radiocarbon dates ranged from as
old as 29,000 RCYBP to as young as 16,000 RCYBP (118). In
southwestern Iowa, this unit decreases in age systematically
with distance from the Missouri River valley (119) according
to the expression:

$$A = 24,750 - 45D$$

where

A = age in radiocarbon years

D = distance in miles from the Missouri River valley.
Because of the time-transgressive nature of this unit, the
name Farmdale was dropped and replaced with "Basal
Wisconsin" or basal loess paleosol, to indicate the first
increment of Wisconsinan loess (118). In some cases this
zone is too thin to be recognized, or has undergone
morphologic changes after burial, such as carbonate enrich-
ment, making it difficult to distinguish.

Bignell loess although tentatively identified by
several investigators in Iowa (56, 68, 122), is not
recognized as a formal unit. This seems a bit peculiar

considering its extensive identification in Nebraska, Kansas, and Missouri. One possible explanation may lie in the problem of the "dark-colored bands", which will be discussed in the next section.

Progressing eastward across Iowa and northern Missouri, Wisconsin loess decreases in thickness, again making identification of any separate loess units almost impossible. In northcentral and northeastern Missouri, the Wisconsinan loess is quite thin, and identified as Peoria, and no attempt at separation has been made (77). This is also the case in thin loess areas of eastern Iowa; however, where the loess is sufficiently thick, Basal Wisconsin loess can still be distinguished (65, 105).

Loveland loess of Illinoian age is shown in Figure 2 as extending from eastern Nebraska across through eastern Iowa. Loveland loess has been identified throughout eastern Nebraska (88, 115) and southwestern Iowa (118, 171) but has not been recognized beyond about 74 miles (119.1 km) (118, 171) from the Missouri Valley, although it may extend farther. For example, Handy (67) converted Ruhe's (118) data for Loveland loess in southwestern Iowa to semi-log, and extrapolated a distance of about 142 miles (228.6 km) for zero thickness, almost twice as far as the maximum observed distance. Loveland loess presumably adjacent to the

Mississippi Valley in eastern Iowa has not been identified, although it does extend along the southern Mississippi Valley (96, 168).

In Illinois, the Wisconsinan loess outside the terminous of Woodfordian glacial advance is divided into Peoria and Roxana, the latter projected to be as old as 75,000 RCYBP (121). However, most radiocarbon dates range from 27,500 to 20,000 RCYBP (121). The latter dates fit well within the time-frame of the "Basal Wisconsin" in Iowa. The Peorian loess has also been subdivided into zones based on clay mineralogy (53, 87), believed to reflect changes in outwash source mineralogy correlative to specific glacial events (53, 57) in Illinois.

To summarize, the Wisconsinan loesses in midcontinent United States are generally divided into two major units - a lower and an upper loess (121). Radiocarbon chronology throughout the Midwest from Nebraska to Indiana substantiates this classification, although there is some physical stratigraphic data which indicate a much more complex system within this duality. The lack of any continuous discontinuity such as that which separates Illinoian from Wisconsinan loess has forced this two-fold system to be used.

Complexity of loess deposits

In the past, regional studies of loess deposits have

almost universally contained the inherent assumption of uniform deposition rate. Except where major units are separated by well-recognized paleosols, such as the Sangamon Soil, loess deposits have generally been considered single sediment bodies (124). Using this assumption and radiocarbon dating, Ruhe (119) calculated the rate of deposition along his southwestern Iowa traverse, and found that the rate decreases rapidly up to about 40 miles (64.4 km), decreases less rapidly to about 120 miles (193.2 km), and then increases for distances greater than 120 miles (193.2 km). Even assuming uniform deposition at any given site, the rate of deposition is not uniform, which simply says that more material was deposited closer to the source at a faster rate. The increase in deposition rate after 120 miles (193.2 km) has not been discussed, but may indicate influence of an alternate source.

The occurrence of "dark-colored bands" as indicators of a pause in deposition or nondeposition, was first recognized in Iowa (31a), where they parallel the underlying geomorphic surface and resemble weak A-horizons. The presence of more than one band at a section suggests that more than one slowdown in deposition occurred. Prior to the discovery of the bands, evidence had been presented which suggested a multiple sequence of deposition in western

Iowa (68). Clayey zones which were thought to indicate lulls in deposition were correlated to the advances of Wisconsinan glaciation.

Ruhe et al. (124) used the bands to demonstrate the complexity of loess deposition by calculating the relative rates of deposition within a site, based on radiocarbon dating. The results varied considerably, from 0.86 to 9.92 in./100 years (2.18 to 25.5 cm/100 years). The bands were not considered as relict pedologic features, but rather as indicators of depositional rate changes, reflected by higher clay content than the material directly above and below. In western Iowa bands have been recognized up to 19.5 miles (31.4 km) from the source, however, probably because of post-depositional weathering they may not be identified at greater distances, as loess thickness decreases. Similar features have been recognized in other areas; Nebraska (115), Missouri (113), Wisconsin (74), Indiana (125), and in Illinois some have even been given formal names, such as the Jules Soil (121). This raises the question of the Brady Soil of presumably late Wisconsin age. Dark band or paleosol?

In Illinois (86) rates of loess deposition also have been shown to be quite varied, ranging from 0.04-8.03 in./ 100 years (0.1-20.4 cm/100 years), supporting the complexity

of deposition. In addition, differences in clay mineralogy have been used to separate zones of loess which otherwise appear as single units (53, 58, 87).

Weathering zones can indicate discontinuous deposition, for example where leached zones occur buried by calcareous loess (78, 126). Often the "Basal Wisconsin" loess in Iowa is only recognized by a thin leached zone at the bottom of the deposit. Where secondary enrichment of calcium carbonate has occurred, this increment may even go unnoticed.

In Nebraska, zones of carbonate accumulation, in the form of a concretion concentration, have been used as indicators of nonuniform loess deposition (47). Fluctuations in the percent dolomite content with depth have also been used to suggest nonuniform deposition (16).

In short, there are several lines of evidence which support nonuniform loess deposition; (1) occurrence of "dark bands" or incipient paleosols, (2) changes in particle size distribution such as clay accumulation, (3) differences in clay mineralogy, (4) complex weathering zone sequences, (5) carbonate concentrations and (6) differences in carbonate mineral composition. Although the bulk of evidence unequivically supports this viewpoint, loess studies have retained the application of uniform deposition and the single body concept, as indicated by the use of empiricism

to describe morphologic changes. Not only is separation
of individual loess increments impractical on a regional
basis, from the foregoing discussion it appears impossible.
Since evidence for major regional breaks is lacking, this
tends to support the continued use of the single body
concept.

Quantitative Variations in Loess

Quantitative variations in loess deposits of the mid-
continental United States have been the subject of numerous
investigations in recent years, primarily by soil scientists
and geologists. The empirical relationships which evolve
display unique systematic properties resulting from eolian
deposition. For example, Ruhe (118) gives some eleven
relationships which describe the loesses of southwestern
Iowa. These include changes in thickness, physical composi-
tion, age, and topography with respect to the source. By
far the greatest amount of interest has been devoted to
changes in thickness and particle-size distribution.
Although most investigations have been conducted in such a
manner as to provide information on the "downwind" side of
sources, there are some data available for appropriate
"upwind" trends, a necessary addition when considering a
variable winds hypothesis. In all cases, a valley source
has been indicated.

Thickness

The trend of decreasing loess thickness away from an assumed source has received considerable attention throughout the U.S. during the past 50 years (80, 90, 118, 142), and a number of forms of mathematical equations have been used to describe this change. The approach was initiated by Krumbein (90) who used a decreasing exponential function in the form of $Y = ae^{-bX}$, where

Y = thickness

X = distance

a = thickness at X = 0

b = rate of thickness change.

Krumbein's measurements of thickness were taken in western Illinois and were scattered instead of being along a straight line traverse, and only represented a short distance, 13.2 miles (21.2 km). The data were plotted on semilogarithmic scale, log-thickness versus distance, and showed a linear decrease within the first 9 miles (14.5 km), after which a horizontal line was fitted. This indicated that the exponential function might be valid up to about 9 miles (14.5 km), beyond which a more or less uniform blanket of loess is spread over the upland. Although it was acknowledged that this expression would underestimate the actual thickness at the bluff, this was explained by the potential for

excessive piling-up of sand adjacent to the source. In reality, this is not found in many cases and this exponential form has not seen further application.

Table 1 presents a summary of loess thinning relationships for the United States extracted from published data. Mathematical expressions used to describe the thinning have been of several forms including:

Semilogarithmic: $Y = a - b \log X$

Linear: $Y = a - bX$

Hyperbolic: $Y = 1/(a + bX)$

Additive Exponential: $Y = ae^{-bX} + ce^{-dX} + fe^{-gX}$

where

Y = thickness

X = distance

Note that the semilogarithmic expressions which have been most commonly used differ from Krumbein's in that the logarithmic term is distance rather than thickness.

Log-linear relationships, where thickness is plotted versus logarithm of distance, have seen the most abundant use, but frequently more than one equation must be used to fully describe the thinning, such as seen in Smith's traverse 2 in Illinois (142) and Frazee et al.'s work in Illinois and Indiana (49). Near-source extraordinary thickness and changes in rate of decrease presumably account for this

Table 1. Summary of loess thinning equations

Traverse or Area	Source Floodplain	Range (Miles)	Angle α[a] (deg)	Equation[b]	Reference
Iowa					
Hutton Northern	Missouri R.	10.3 - 167.5	45	$Y = 1250.5 - 528.5 \log X$	80
Hutton Southern	Missouri R.	0.1 - 6.9	45	$Y = 1100.2 - 325.8 \log X$	80
Ruhe R.I. roadcuts	Missouri R.				
Wisconsinan		13.0 - 64.0	0	$Y = 1/(9.51 \times 10^{-4} + 7.99 \times 10^{-5} X)$	118
Loveland		13.0 - 41.4	0	$Y = 1/(2.13 \times 10^{-3} + 1.04 \times 10^{-4} X)$	118
Davidson & Associates					
3	Missouri R.	0.01 - 78.2	45	$Y = 874.3 - 284.6 \log X$[c]	34b
Worcester	Missouri R.	11.7 - 173.2	-	$Y = 1/(4.75 \times 10^{-4} + 6.5 \times 10^{-5} X)$	171
Illinois					
Scattered Observations	Mississippi R.	2.0 - 13.2	-	$Y = 26 e^{-0.17X}$	90
Smith 1	Illinois R.				
Peorian		4.0 - 100.0	0	$Y = 434 - 200 \log X$	142
Late Sangamon		4.0 - 50.0	0	$Y = 87 - 38 \log X$	142
Smith 2	Mississippi R.	2.0 - 20.0	45	$Y = 523 - 352 \log X$	142
		20.0 - 70.0		$Y = 153 - 621 \log X$	142
Frazee 4 "leeward"	Mississippi R.	0.2 - 81.8	53	$Y = 328 e^{-2.8X} + 190 e^{-.17X} + 87 e^{-10}$	49
N.E. of Ohio & Mississippi Confluence	Ohio & Mississippi R.		-		
Total loess		1.0 - 40.0		$Y = 303 - 157 \log X$	39
Farmdale		1.0 - 40.0		$Y = 129 - 80 \log X$	39

[a]Angle between source and traverse, measured from perpendicular.

[b]Y = thickness in inches, X = distance in miles.

[c]Fitted by least squares method.

Table 1. continued

Traverse or Area	Source Floodplain	Range (Miles)	Angle α^a (deg)	Equation[b]	Reference
Peorian loess on Wis. Till	Wabash R.	0.2 – 50.0	–	$Y = 56 - 30 \log X$	39
Peorian loess on Ill. Till	Wabash R.	0.1 – 2.0	–	$Y = 60 - 90 \log X$	39
		2.0 – 50.0		$Y = 46 - 28 \log X$	39
Indiana					
Caldwell Northern (total loess)	Wabash R.	5.0 – 66.0	20	$Y = 122 - 47 \log X$	13
Caldwell Southern (total loess)	Wabash? R.	4.0 – 88.0	5	$Y = 125 - 53 \log X$	13
	White R. (westfork)	15.0 – 37.0		$Y = 148 - 67 \log X$	13
	White R. (eastfork)	37.0 – 88.0		$Y = 169 - 78 \log X$	13
Frazee 6	Wabash R.	0.05 – 3.4	5	$Y = 175 - 142 \log X^d$	49
		3.4 – 42.0		$Y = 138 - 60 \log X^d$	49
Peorian loess on Wis. Till	Wabash R.	0.7 – 40.0	–	$Y = 75 - 24 \log X$	39
Peorian loess on Ill. Till	Wabash R.	0.1 – 2.0	–	$Y = 114 - 99 \log X$	39
		2.0 – 50.0	–	$Y = 96 - 29 \log X$	39
N.E. of Ohio & Wabash Confluence	Wabash R. & Ohio R.				
Total loess		0.1 – 80.0	–	$Y = 304 - 151 \log X$	39

[d]Calculated by Harlan and Franzmeier (72).

Table 1. continued

Traverse or Area	Source Floodplain	Range (Miles)	Angle α^a (deg)	Equation[b]	Reference
Farmdale		0.4 – 60.0	–	Y = 38 – 17 logX	39
Hall A (total loess)	Wabash & White R.	2.0 – 50.0	0	Y = 133 – 50 logX	60
Hall B (total loess)	Wabash & White R.	2.0 – 40.0	15	Y = 121 – 40 logX	60
Hall C (total loess)	Wabash R.	2.0 – 40.0	0	Y = 142 – 57 logX	60
Hall D (total loess)	Wabash R.	2.0 – 40.0	0	Y = 108 – 40 logX	60
Minnesota					
Foss & Rust	Mississippi R.	5.0 – 15.0	23	Y = 201 – 3.3 X	44
	Zumbro R.	2.0 – 10.0	22	Y = 229 – 4.4 X	44
Louisiana					
Lafayette "windward"	Mississippi R.	0 – 16.0	0	Y – 164.3 – 96.8 logX	30
Ville Platte "windward"	Mississippi R.	0 – 16.0	0	Y = 66.3 – 31.2 logX	30
Youngsville "windward"	Mississippi R.	0 – 26.0	0	Y = 185.0 – 6.7 X	30
Maryland					
Foss et al. 2	Chesapeake Bay	2.5 – 13.7	0	Y = 235 – 9.8 X[e]	45

[e] Y = thickness in cm, X = distance in km.

bilinearity. In the Matanuska Valley of Alaska, three such
equations must be used for loess thickness relationships
over a distance of only 27 miles (43.5 km) (158). The
application of this function from Alaska (158) throughout
the Midwest (39, 80, 142) and down the Mississippi Valley as
far south as Tennessee (12), and Louisiana (30), as an almost
universal form, warrants further discussion.

The form of semi-logarithmic equation $Y = a - b \log X$
is such that the constant $\underline{a}$ is equal to the loess thickness
at a distance X equal to unity, and the value of Y is un-
defined for X equal to zero. Since the maximum possible
thickness immediately adjacent to the valley wall thus can-
not be described, measurements made at the valley wall are
usually plotted somewhere in the first mile or so. The
semilog function also implies that a finite distance can be
determined for the maximum transport capability, solving
for Y equal to zero thickness. The constant $\underline{b}$ is the rate
of change of thickness with distance, larger values indicat-
ing more rapid decrease away from the source.

A hyperbolic function was used by Ruhe (118) for both
Wisconsinan and Loveland loess in Western Iowa, and more
recently has also been applied to the "Basal Wisconsin"
increment of loess (121). Worchester (171) also applied

this form to a traverse perpendicular to loess thickness
isopach's in southwestern Iowa. Similar to the semilog plot,
the rate of thinning decreases per equal unit of distance.
A significant advantage of this form over the preceding
function is in the ability to evaluate the maximum thickness
by solving $Y = 1/(a + bX)$ for X equal to zero. By using
Ruhe's expression for Wisconsinan loess, the maximum thickness
is calculated as 87.6 ft. (26.7 m), considerably less than
the maximum recorded thickness of about 150 ft (45.7 m) (68).
Similarly, Worchester's expression yields 175.4 ft. (53.5 m),
somewhat greater than the observed maximum.

The other dissimilar feature provided by hyperbolic
equations is the inadequacy to project a maximum distance of
transport, since X is undefined for Y equal to zero. This
could be rationalized and may relate to atmospheric phenomenan
where some particles remain continually suspended, and the
thickness is asymptotic, resulting in a near uniform blanket
of cover at great distances.

The use of linear equations to describe loess thinning
provides the capability for defining both a maximum thickness
adjacent to the source, and a maximum transport distance.
However, where this form has been used, the range of distance
measurement has been relatively short, and loess deposits
have not been extensive (30, 44, 154). For example, in

southeastern Minnesota, Foss and Rust (44) used linear
equations to indicate that the Mississippi River and its
major tributary valleys are the source areas for loess.
Similarly, Daniels and Young (30) used linear and log-linear
equations to describe loess thinning in south-central
Louisiana for three traverses on the "upwind" side of the
source.

The additive exponential model was introduced by Frazee
et al. (49) and was first expressed as:

$$Y = ae^{-bX} + ce^{-dX},$$

the first term describing the rapid decrease in thickness
near the source as a result of particle size changes, and the
second term describing the regional decrease in thickness
as a function of the number of loess particles. The thickness
at the bluff is then given by a + c. For Frazee's traverse 4,
a three term exponential model was fitted to explain a near-
source rate of thinning because of winds from different
directions. They concluded that the additive exponential
form more accurately describes both thinning and particle-
size variations for several traverses in Illinois and
Indiana.

The systematic variations in loess thickness presented
in Table 1 illustrate the degree of empiricism which has been

used to express the thickness-source relation. One problem
in analyzing the mathematical expressions for loess thinning
is the method used to measure the distance from the source.
Depending on the direction of measurement, the constants in
any expression may change, and even the form of the function
may be different (67).

Unfortunately, not all trends can be fit as nicely as
might seem possible. In Kansas, for example, Hanna and
Bidwell (71) reported a thickness decrease from 100 ft
(30.5 m) adjacent to the Missouri River to less than 6 ft
(1.8 m) at a distance of only 13 miles (20.9 km). In fact
after about 6 miles (9.7 km) the thickness was more or less
uniform.

In summary, it appears that loess thinning equations
which have been used to fit observed thicknesses can be of a
variety of forms. For the most part, equations which produce
the best statistical reliability have been utilized in these
empirical relations, disregarding any theoretical rationale.
As is commonly known, a curve can fit through any set of
data points, providing enough terms are used, as with a
polynominal.

Differences within any given family of curves, such as
semilog, can be attributed to a number of variables, including:
orientation of the observations with respect to the source,

source width, deposition rate, and paleoclimatic conditions. The equations presented in Table 1, while all statistically significant, are only applicable in the direction of each individual traverse, and only over the distance indicated. Extrapolation to other directions or distances only proves to demonstrate the inadequacy of the expression. In short, universal empiricism is not valid.

Another form of relationship between thickness and distance from the source, logarithm thickness versus logarithm distance, was suggested by Waggoner and Bingham (165), but is not presented in this section, and will be discussed in a later section on mathematical modeling.

Particle size

Similar to thickness-distance relationships, empirical equations which express the changes in particle size with distance from the source are of a variety of forms. Table 2 summarizes the available textural data for a variety of locations throughout the U.S. As can be seen, textural variations have been described using linear, semi-logarithmic, hyperbolic, and quadratic functions. In addition, Frazee et al. indicate that the additive exponential model predicts the decrease in mean particle size with distance from the source, although the actual equations were not published.

Table 2. Summary of loess textural change equations

Traverse or Area	Source Floodplain	Range (Miles)	Angle α[a] (deg)	Equation[b]	Reference
Iowa					
Ruhe R.I. roadcuts	Missouri R.	13.0 - 64.0	0		
Wisconsinan					
C. Silt (62 - 16μm)				$Y = 1/(1.56 \times 10^{-2} + 6.64 \times 10^{-5}X)$	118
F. Silt (16 - 2μm)				$Y = 1/(4.91 \times 10^{-2} - 3.59 \times 10^{-5}X)$	118
Clay (<2μm)				$Y = 17.39 + 0.15 \ X$	118
Median Size (μm)				$Y = 1/(4.75 \times 10^{-2} + 2.01 \times 10^{-4}X)$	118
Loveland		13.0 - 41.4	0		
C. Silt (62 - 16μm)				$Y = 52.9 - 0.34 \ X$	118
F. Silt (16 - 2μm)				$Y = 21.2 - 0.11 \ X$	118
Clay (<2μm)				$Y = 22.9 - 0.51 \ X$	118
Davidson & Associates 3	Missouri R.	0.01 - 78.2	45		
Silt (74 - 5μm)				$Y = 80.3 - 0.242 \ X$[c]	34b
Clay (<5μm)				$Y = 17.6 + 0.259 \ X$[c]	34b
Worcester (calcareous loess)	Missouri R.	11.7 - 84.4	-		
C. Silt (62 - 31μm)				$Y = 2.83 - (1.71 \times 10^{-1}) \ X + (1.47 \times 10^{-4}) \ X^2$	171
M. Silt (31 - 16μm)				$Y = 34.25 - 0.033 \ X$	171
M.F. Silt (16 - 8μm)				$Y = 11.91 + (7.19 \times 10^{-2}) \ X + (7.24 \times 10^{-6}) \ X^2$	171
F. Silt (8 - 4μm)				$Y = 4.3 + 00.041 \ X$	171

[a] Angle between source and traverse, measured from perpendicular.

[b] Y = thickness in inches, X = distance in miles.

[c] Fitted by least squares method.

Table 2. continued

Traverse or Area	Source Floodplain	Range (Miles)	Angle α[a] (deg)	Equation[b]	Reference
V.F. Silt (4 - 2μm)				$Y = 3.48 + 0.016\ X$	171
C. Clay (2 - 1μm)				$Y = 3.39 + 0.017\ X$	171
C. Silt (16 - 2μm)		11.7 - 173.2	-	$Y = 59.95 - 0.19\ X^c$	171
F. Silt (16 - 2μm)				$Y = 22.30 + 0.08\ X^c$	171
Clay (<2μm)				$Y = 16.42 + 0.11\ X^c$	171
Illinois					
Smith 1	Illinois R.	0.6 - 60.0	0		
Mean Size (μm)				$Y = 30.83 - 7.75\ \log X$	142
Indiana					
Hall-Silty Loess					
A	Wabash & White R.	2.5 - 45.0	0		
Coarse Silt (62 - 16μm)				$Y = 63.01 - 0.47X + 0.002X^2$	60
F. Silt (16 - 2μm)				$Y = 31.13 + 8.29\ \log X$	60
Mean Size (μm)				$Y = 10.56 - 0.08X$	60
B	Wabash & White R.	2.5 - 36.0	15		
Coarse Silt (62 - 16μm)				$Y = 65.46 - 0.84X + 0.01\ X^2$	60
F. Silt (16 -μm)				$Y = 26.92 + 12.97\ \log X$	60
Mean Size (μm)				$Y = 11.72 - 0.08X$	60
C	Wabash R.	2.5 - 44.5	0		
Mean Size (μm)				$Y = 10.59 - 0.05X$	60
D	Wabash R.	1.5 - 30.0	0		
Mean Size (μm)	Wabash R.			$Y = 12.21 - 0.13X$	60

[d]Y = log phi median diameter.

Table 2. continued

Traverse or Area	Source Floodplain	Range (Miles)	Angle α[a] (deg)	Equation[b]	Reference
Kansas					
Hanna and Bidwell	Missouri R.	0 - 23.5	0	$Y = 14.29 + 19.15 \log X$	119
Swineford & Frye A	Arikaree & Republican R.	0 - 180	10	$Y = 4.58 + .0037X^d$	152
Swineford & Frye B	Arikaree & Republican R.	0 - 125	40	$Y = 4.55 + .0044X^d$	152
Swineford & Frye D	Platte R. (Republican?)	0 - 225	25	$Y = 4.41 + .0046X^d$	152
Swineford & Frye F	Platte R. (Republican?)	0 - 255	5	$Y = 4.41 + .0032X^d$	152
Ohio[e,f]					
C. Silt (50 - 20μm)	Scioto R.	0.2 - 6.8	0	$Y = 43.9 - 20.97 \log X$	127
M. Silt (20 - 5μm)				$Y = 38.7 + 14.61 \log X$	127
F. Silt (5 - 2μm)				$Y = 8.7 + 5.39 \log X$	127
C. Silt (50 - 20μm)	Little Miami R.	0.6 - 11.8	0	$Y = 31.0 - 5.62 \log X$	127
M. Silt (20 - 5μm)				$Y = 53.2 + 1.53 \log X$	127
F. Silt (5 - 2μm)				$Y = 10.4 + 2.93 \log X$	127
Arkansas					
Crowley's Ridge[e,f]					
Peorian	Mississippi R.	0.3 - 4.0	0		
C. Silt (50 - 20μm)				$Y = 49.7 - 5.8 \log X$	168
M. Silt (20 - 5μm)				$Y = 45.2 + 4.0 \log X$	168
F. Silt (5 - 2μm)				$Y = 4.5 + 1.9 \log X$	168

[e]Clay-free basis (2mm - 2μm = 100%)

[f]X = distance in km.

34

One of the greatest ambiguities which abounds in
textural investigations of loess deposits is in the reported
particle size for a given site. Almost without exception,
the depths of samples within a profile are left out of the
discussion. The reader is left to believe that one value
represents the entire section below the soil solum. In
general, the discussion does not include the method which
was used to derive the value for particle size at each site.
In some cases, noncalcareous loess has been disregarded
(49 , 142) in order to "remove the effects of weathering",
and in thin loess regions, particle size has been expressed
on a clay-free basis (127, 168) to eliminate pedologic
variations.

Krumbein (90) had suggested that the average size of
loess grains should decrease away from the source in a manner
similar to the exponential decrease he had shown for thickness.
No data were available, and it was not until Smith (142) had
re-evaluated the nature of Illinois loess that a relation
between particle size and distance from the source was
apparent. A linear relationship was described between
particle size and the logarithm of distance for Peorian loess
and indicated an increase in the 10 to 20μm fraction, a de-
crease in the 30 to 50μm fraction, and a decrease in the
sand-free arithmetic mean particle size. This semi-log plot

indicated rapid changes in the particle size close to the source, and only slight changes at distance.

In western Iowa, Ruhe (118) used both hyperbolic and linear expressions to describe the changes in particle size of both Wisconsinan and Loveland loess. In general, as distance from the source increases, finer fraction materials (clay and fine silt) increase, while coarse silt and median grain diameter decrease. This would seem to suggest some form of selective sorting based on particle size. These trends have been established in many locations throughout the midwest (60, 142, 171) and other parts of the U.S. (117, 156), in fact particle size changes have frequently been used to identify sources (15, 45, 127). However, this should not necessarily be taken to represent all cases.

For example, in northeastern Kansas, loess particle size was observed to become finer with increased distance from the bluff up to 16 miles (25.8 km), but beyond that point there was little or no decrease. Similar results have been found in other areas where no difference in mean diameter of loess has been evident along traverses (30, 71).

In areas of thin loess where unweathered material is no longer available for mechanical analysis, the clay-free particle size data, where the sum of particles 2 mm to 2 μm = 100%, appear to be useful in determining the source (127, 168). In a transect on Crowley's Ridge in Arkansas, West

et al. (168) have identified three loess deposits correlated
from the surface downward as Peoria, Roxana, and Loveland.
Since major rivers flowed on both sides of Crowley's Ridge
during the Pleistocene, the source of the loess could be
either to the west or the east. Using clay-free particle
size plotted on log distance scale, the source of the Peoria
and Roxana Loess was identified as lying to the east, while
the Loveland loess was presumably deposited from both the
east and the west. This scheme has also been used to
identify the source for thin loess in Southern Ohio (127),
where the Scioto and Muskingum River Valleys are indicated
as the chief sources.

In the silty mantle of southeastern Pennsylvania, (15)
over a distance of 22 miles (35.4 km) the mean percent very
fine sand changed from about 7 to 2%. Bartlett's χ^2 test was
used to check for homogeniety of the thin mantle by treating
the percent clay-free silt as the variable. The mean
variance was checked against silt from loess-derived soils,
(the Fayette & Memphis series) and other deposits, namely
alluvium, residuum, and colluvium. Based on uniformity, it
was concluded that the silty mantle was loess.

Foss et al. (45) sampled at the base of the Ap horizons
over a distance of 11.2 miles (18 km), and indicated a
decrease in silt content with increasing distance away from

the eastern shore of Chesapeake Bay. Mixing of coarser
material in shallow loess (in this case locally derived
sands) was evident. The mixing was shown in the decrease
in mean and median particle-size up to 7.4 miles (11.9 km),
after which an increase was shown. Similar results were
also shown by Tamura et al. (154) for loess in Connecticut.

Density

An important property of soil materials which affects
many geotechnical designs, is the in situ density, or
weight per unit volume. The vertical stresses used in slope
stability analysis and for estimation of consolidation
settlement, and the determination of the in situ stress pro-
file, all depend to some degree on in situ density and
moisture content. Loess soils have been shown to display a
wide range of density values (35, 75), but most
geotechnical emphasis has been on low density, collapsible
loess (75, 76), no doubt because of its troublesome be-
havior.

Western Iowa loess has been the topic of numerous
research studies pertaining to engineering properties, includ-
ing in situ density (32, 35, 68). Davidson and Handy
(35) presented in-place density data taken at five sampling
locations over the range of 80 miles (128.7 km) in south-
western Iowa, and demonstrated a linear relation of

increasing density with increasing distance from the
Missouri River valley. Since tests were conducted at
approximately the same depth throughout, 2 to 3 ft (0.6 to
0.9 m) below the top of C-horizon, and would thus approximate
near-uniform overburden stress, this increase was considered
to be related to changes in texture.

Tests made at greater depths generally indicated higher
densities. Corresponding moisture contents showed the same
trends, i.e. increasing with depth, and with distance from
the valley wall. The apparent increase in density with depth
was verified at several sections throughout southwestern
and eastern Iowa (35, 102). Referring to a specific location,
Handy and Davidson (68) made a further study of the density-
depth relationship, producing the following expression for a
section adjacent to the bluff:

$$Y = 54 + 17 \log X$$

where

Y = field density ($1b/ft^3$)

X = depth from surface (ft)

This best-fit line was drawn for tests conducted on C-horizon
material over a range from 10 to 90 feet (3.0 to 27.4 m) in
depth and therefore constitutes a rather complete section.

Relations of density and moisture content to particle-
size were presented by Davidson and Sheeler (34a) for western

Iowa loess using clay content only. Expressions for density and moisture content were given as:

$$Y = 65.0 + 0.5 X$$

where

Y = field density (lb/ft^3)

X = % < 2 μm clay

and

$$Y = 3.52 + 1.11 X$$

where

Y = field moisture content (%)

X = % < 2 μm clay

Note that both equations are linear. Density measurements, as before, represent only samples taken from 2 to 3 ft. (0.6 to 0.9 m) below the top of the C-horizon at a variety of locations, while moisture content was determined at several depths and locations.

The dependency of in situ density on both depth and textural variations was put in quantitative form by Handy (66) to account for changes in two-dimensional space and expressed by the multiple regression:

$$\gamma_d = 1.11 + 0.116Z + 0.0048X_{005}$$

where

γ_d = bulk density (g/cm^3)

Z = depth (m)

X_{005} = % < 5 μm clay

In areas of thin loess, where the thickness is entirely within the developed soil profile, bulk density has been shown to increase both with depth and distance from the source (117).

Shear strength

Shear strength in loessial soils is considered to reflect three variables; (1) moisture content, (2) density, and (3) clay content (1, 75, 104). Recognizing that strength may change depending upon physical state of the material, Gibbs et al. (55) divided loess into two distinct classes; (1) "dry" loess with cohesion (C) generally ranging between 5 and 10 psi (3.5 - 6.9 KN/m^2) and a friction angle (φ) of about 31.0 - 33.00, (2) wetted loess which is reduced in strength, primarily through the reduction of cohesion to about 1 psi (0.7 KN/m^2). Friction angles of all tests were very close, variations presumably occurring as a result of changes in particle size.

Fox, et al., (46) conducted in situ shear tests on western Iowa loess and found an increase in angle of internal friction with increasing depths, attributed to increased density. Cohesion also increased slightly with depth, although these data were more scattered. Tests were also

conducted at various orientations at open cuts, with essentially the same results. Additional bore-hole shear data were presented by Lohnes and Handy (99) for loess in Iowa and Tennessee. They concluded that horizontal tests tended to be more erratic and scattered, attributed to slight stratification of the deposit.

Anderson (3) indicated that friction angle increased as field density increased, and that cohesion increased with increasing clay content and decreased with increasing moisture content. These results were based on borehole shear tests conducted on loess in western Iowa. However, he did conclude that regional trends in these shear strength parameter were "overshadowed by the properties of the individual soil horizons."

The reduction or loss of cohesion upon wetting is an indication that this property may be attributed to moisture films at grain-to-grain contacts, and is thus termed "apparent" cohesion. This is in contrast to true cohesion, which involves actual binding between particles, a result of clay or carbonate cementation. Olson (108) indicated that for saturated loess in Western Iowa, where preconsolidation was zero, cohesion was zero.

The changes in shear strength resulting from increasing moisture content in collapse-prone loess have been investigated (145) and indicate a reduction in both ϕ and c during the

collapse phase. No "regain" in strength was shown after the material had been allowed to dry, even though an increase in density from 92.4 to 113.6 lb/ft^3 (1.48 - 1.82 g/cm^3) had occurred. The results of wetting on the shear strength of loess appear somewhat irreversible, in this case reduction of cohesion.

Variations in the shear strength of loess would appear to occur in two distinct manners; (1) vertical variations at a site related to collapse and change of soil structure on saturation and (2) lateral variations, as distance from the source increases. The latter should be related to overburden, texture, and seasonal moisture fluctuations.

Eolian Mechanics

Smalley (137) recognized that three distinct operations influence the nature of sedimentary deposits: P actions (those concerned with the production of the material and the mechanism of its formation), T actions (those involving transportation), and D actions (those concerned with deposition). He further suggested the events leading to the formation of glacial loess as:

P_1: Rocks pulverized by glaciers yield detritus of varying hardness and solubility. Single crystal quartz grains are formed, and crushed crystals of feldspar and other rock materials traversed by the glacier.

P_2: The quartz particles may be deformed and broken by the glacier.

T_1: The detritus is transported by the glacier.

D_1: The glacier, on melting, deposits the mixed (coarse and fine) detritus of quartz and other rock material.

T_2: The fine material is raised and transported by the wind.

D_2: The material is deposited in homogeneous deposits.
Although somewhat simplified, this system recognizes that a natural division of material may be achieved based on process. The present discussion of wind mechanics will be limited to the process T_2, being comprised of wind erosion, and vertical and lateral transport. Assuming a continuous supply of sediment, the formation of loess deposits is presumed almost entirely dependent on the action of wind.

Properties of wind

For most practical purposes, the atmosphere can be treated as an ideal gas (130), in which case, the universal gas law can be stated as:

$$\frac{P}{\rho} = RT$$

where P is pressure, ρ is the density, T the absolute temperature in degrees Kelvin, and R is the universal gas constant. Even in a static condition, variations occur in atmospheric properties with height, such as the exponential decrease in density (149) and the decrease in temperature which in turn

affect pressure.

For turbulent blowing wind, the von Karman-Prandtl logarithmic velocity distribution law is commonly used (149), and is of the form:

$$\frac{\bar{u}}{u_*} = \frac{2.3}{K} \log \frac{y}{y_1}$$

where

$\bar{u}$ = average wind velocity at a height y from a rough surface.

u_* = $(\tau_o/\rho)^{1/2}$ friction velocity over surfaces with an equivalent sand roughness height, k_s, <1.5mm

τ_o = shear stress at the bed

ρ = mass density of the fluid

K = von Karman universal constant for turbulent flow

y_1 = reference distance equal to that value of y at which $\bar{u} = 0$

Zingg (172) found y_1 to vary as the logarithm of grain diameter, d_s, according to the relationship

$$y_1 = 0.081 \log \frac{d_s}{0.18}$$

where

y_1 and d_s are in millimeters.

Atmospheric diffusion

The theory of atmospheric diffusion is a phenomenon in

the lower layers of the atmosphere, which is attributed to turbulence (109). The transportation of sediment in suspension can be treated as a diffusion process, if it is assumed that the vertical components of velocity fluctuation because of turbulence are larger than the fall velocity of individual particles. Taking this criterion into account, Kalinske (83) gave the general diffusivity equation as

$$\frac{\partial N}{\partial t} = \frac{D_y \partial^2 N}{\partial y^2} + \frac{D_x \partial^2 N}{\partial x^2} + \frac{c \partial N}{\partial y} - \frac{\bar{U} \partial N}{\partial x}$$

where

    c = relative concentration at the ground

    N = sediment concentration at point (x, y) at time t

D_x, D_y = lateral and vertical diffusion coefficient

    $\bar{U}$ = mean fluid velocity at the point considered.

By experimentation, Kalinske found D_x to be greater than D_y. The simplest solution to this equation would be for equilibrium in which

$$\frac{\partial N}{\partial T}, \frac{\partial N}{\partial x}, \frac{\partial^2 N}{\partial x^2} = 0$$

and therefore at equilibrium

$$cN = D_y \, dN/d_y$$

or the average rate of upward diffusion of silt by turbulence is equal to the average rate of its dropping by gravity.

    Sutton (147) derived the equation for density at any point (x, y, z) from a continuous line source emitting

Q gm/sec. per centimeter from $(0, y_0, 0)$ to $(0, -y_0, 0)$ as:

$$\chi = \frac{Q \exp \left[-\left\{ \frac{z^2}{C^2 x^m} \right\} \right]}{2\sqrt{\pi}\, C u x^{1/2m}} \left[\text{Erf}\left(\frac{y_0 - y}{C x^{1/2m}} \right) + \text{Erf}\left(\frac{y_0 + y}{C x^{1/2m}} \right) \right]$$

By letting y_0 go to infinity, the infinite line case can be deduced as:

$$\chi = \frac{Q}{\sqrt{\pi}\, C u x^{1/2m}} \exp \left[-\left(\frac{z^2}{C^2 x^m} \right) \right]$$

χ = density in grams/cubic centimeter

u = mean velocity of the wind

C = diffusion coefficient

Erf(x) = error function

m = a constant which describes the degree of tur-
bulence.

This assumes that the correlation between the motion to which the particle is initially subjected, and the motion which it experiences at some later instant tends to vanish with increasing time. Also, in following the motion of the particle, the average size of the eddies continually increases.

Turner (160) simplified Sutton's equation for the infinite case, taking the wind normal to the source, and found:

$$\chi(x, y, 0;H) = \frac{2_q}{\sqrt{2\pi}} \sigma_z u \exp [-1/2 (\frac{H}{\sigma_z})^2]$$

where

χ = concentration at x, y, z from a source with effective emission height H

q = source strength per unit distance, $g\ sec^{-1}\ m^{-1}$

u = mean wind speed

σ_z = standard deviation of vertical cloud spread, which is assumed to be Gaussian.

Since it was assumed that no lateral dispersion takes place, the term for standard deviation of lateral spread, σ_y, is not present. For winds blowing at an angle φ to the source, the value of 2_q is replaced by $2q/\sin φ$, which strengthens the influence of the source.

The diffusion of particles can also be viewed as a statistical process, such as the random walk used by Sutton (149). In this case, the motion of a particle is only influenced by (1) its inertia, (2) viscous drag, and (3) extraneous influences, including collisions, which are regarded as random. Sutton wrote the equation for one-dimensional motion as:

$$m \frac{d^2x}{dt^2} + f \frac{dx}{dt} + R_x = 0$$

in which

m = mass of the particle

$f \frac{dx}{dt}$ = viscous drag

R_x = extraneous forces

Taking the mean rate of dispersion, S, as

$$\overline{\frac{d}{dt} (x^2)} = \frac{d}{dt} (\overline{x^2}) = S$$

the motion equation is written as

$$\frac{1}{2} m \frac{d^2}{dt^2} (x^2) - m \left(\frac{dx}{dt}\right)^2 + \frac{1}{2} f \frac{d}{dt} (x^2) +$$

$$xR_x = 0$$

With a very large number of particles, xR_x goes to zero, because of the randomness. By substituting for S:

$$\frac{1}{2} m \frac{dS}{dt} + \frac{1}{2} fS = \overline{mu^2}$$

where

$$u = \frac{dx}{dt}, \text{ the velocity}$$

Integrating with respect to time:

$$S = \frac{2m}{f} \overline{u^2} \, [1 - \exp(-\frac{tf}{m})]$$

Since $F = 6\pi\mu r$ (Stokes viscous drag), and $m = 4/3 \, \pi r \, \gamma$, then $f/m = 9\mu/2r^2$. It can be seen that the dispersion rate is a function of particle size, wind velocity u, and time t.

Work performed by the wind

Erosion   Generally speaking, lifting of exposed material by the wind is largely considered to be the work of eddy currents or irregularities of wind movement (50). Material may either be picked up as individual particles or aggregates by wind which exceeds the threshold velocity, or propelled upward by impact of saltating sand-sized grains. In either case, the competence of the wind to erode is a function of particle size and wind velocity (161b). Bagnold (5) indicated that the critical diameter of quartz grains which gives a minimum value of threshold velocity of air is about 80 μm. That is, for particles larger or smaller than this, the threshold velocity increases -- higher for larger grains because of their weight, and for smaller grains because of their cohesion and formation of layer of air in laminar flow.

Chepil (21) showed experimentally that in fine soil

fractions silt between 5 μm and 10 μm is least wind-erodible and has the ability to form clods, because it exhibits considerable cohesion. Larger silt fractions, have less cohesion, are easily separated by wind action, and therefore are readily picked up. Coarse silt in the range 20 μm to 50 μm was found to have no cohesion, and was easily picked up by the wind. A moderate degree of erodibility was found for clay, which formed small granules that were then easily eroded. In mixtures of silt and clay, the greatest degree of clodiness and resistance to wind erosion was found when about 20 percent clay was mixed with 80 percent silt.

Smalley (138) described a simple soil system in which all wind erosion results from the impact of saltating sand grains. The ideal eroded system was composed of "silt-type quartz particles, such as found in loess." Smalley's model depends on soil cohesion, which can be obtained from the tensile strength. The tensile strength in the ideal system was given as:

$$\sigma = NB \cos\theta \ A_a$$

where

σ = tensile strength

N = average number of bonds in the fracture section

B = average bond strength

θ = angle at which the bonds act with respect to the tensile direction

A_a = cross-sectional area of the whole system

This equation reduces to:

$$\sigma = 0.55\ B\rho Kt/d^3$$

which states that the tensile strength of an ideal soil system, and thus cohesion, is directly proportional to the packing density, ρ, coordination number, K, and inter-particle bond strength, B and inversely proportional to the cube of the particle diameter, d; the failure zone having a thickness of t. Thus, a decrease in the particle size greatly increases the tensile strength and improves stability. However, Smalley did indicate that since small particles are lighter, once disturbed they are easily eroded.

Transportation   Udden (161a) in his classic work initiated the experimental approach and examined samples of road dust, volcanic dust and river floodplain dust. He concluded that particles which are carried in suspension by strong winds must have a diameter less than .0625 mm and that particles with a diameter less than about .0156 mm were

hindered from promptly settling out. He presented the following table for distance of transport in strong winds for various size particles:

Fine Sand (0.25 - .125 mm)	<mile
Very Fine Sand (.125 - .0625 mm)	a few miles
Coarse Dust (.0625 - .03125 mm)	200 miles (321.8 km)
Medium Dust (.03125 - .0156 mm)	1000 miles (1609 km)
Fine Dust (< .0156 mm)	around the globe

The settling of finer particles was thought to be a function of the load; increasing the load should cause flocculation.

In a simple experiment where different size fractions were thrown into the air with an average velocity of about 8 mi/hr. (12.9 km/hr), Udden (161b) observed the paths of the particles and reported the following:

Average Diameter	Behavior of Particle
.75 mm	Described a path about 10° from vertical
.37 mm	Described a path about 45° from vertical
.18 mm	Described a path but a few degrees from horizontal, blown upward by eddies
.08 mm	Could scarcely be noticed to settle
.04 mm	Apparently completely borne up by the wind
.007 mm	Completely borne up by the wind
.001 mm	Completely borne up by the wind

It was concluded that the average size of the largest particles carried depends on the wind velocity, since some sand grains are occasionally found at great distances.

Chepil (20) found that the equivalent diameter of suspended particles in dust storms decreased with height above the ground. Particles carried at 2 feet (0.6 m) above the ground had an average diameter of 86 µm, while those at 20 feet (6.1 m) had an average diameter of about 50 µm. By extrapolation from previous studies (22), the average diameter of dust particles carried at one mile (1.6 km) was 22 µm. Differences in the composition of suspended dust and the reported composition of loess were attributed to variations in wind velocity.

This form of initial selective sorting had previously been studied, (19), and in dust storms, only about 60 percent of the total dust content with particles less than 100 µm had resulted from actual deflation at the source. The remainder of material was created by secondary abrasion during transport. Initial breakdown of soil aggregates was caused by impact of saltating grains on the ground surface. It has been pointed out that sediments generally become more poorly sorted as median diameter decreases (81). This can be quantified by defining a sorting coefficient as:

$$\sigma_\phi = \frac{\phi_{84} - \phi_{16}}{2}$$

where

σ_ϕ = sorting coefficient

ϕ_{84} = diameter in phi units of lower 84% on cumulative size curve

ϕ_{16} = diameter in phi units of lower 16% on cumulative curve.

A smaller value of σ_ϕ indicates a better sorted material.

Fisher (41) used this coefficient to analyses loess data from Illinois, and showed that Smith's (142) data indicates that median particle diameter decreases at a constant (log-log) rate away from the source. Sorting values increase, i.e. sorting becomes poorer, with decreasing median diameter and thus with increasing distance from the source.

The sorting of eolian deposits was approached by Franzmeier (48) in an attempt to explain the variations among glacial till, river terrace deposits, dune sands, and loess. Material in the range 40 to 80 μm, most abundant in the glacial till, was essentially absent in loess. It was postulated that this fraction has been selectively removed, either by water or wind, and deposited elsewhere.

The clay dilemma

The clay fraction in loess presents a problem when related to the mode of deposition. It has already been discussed that fine particles have sedimentation velocities which are considered smaller than the turbulent wind velocity. This raises a question of how clay particles can be deposited and show obvious trends away from the source, similar to changes in silt fractions.

Beavers (10) suggested that the majority of clay particles in loess did not come from local floodplains but were carried from scattered sources. These air-borne clay minerals were then electrostatically attracted to larger silt grains, adsorbed onto the surface, such that the clay and silts were deposited together. Further evidence for this mechanism is the generally massive or unstratified nature of loess deposits, in that differential settling of clay and silt presumably would not produce homogeneous, unstratified material.

Scholtes and Smith (133), who investigated the paha or isolated loess-covered hills of northeast Iowa, postulated that silt and clay size particles present in these dune-like features may have moved as aggregates of sand size. This interpretation was based on the lack of sorting in the paha, while the surrounding loess was well-sorted.

Teller (155) reported that sand-size aggregates of clay particles were subject to eolian erosion, and deposited as dune-like features on snowdrifts in Manitoba. Although these aggregates were thought to eventually break down, they remained stable throughout the summer following deposition.

Wind tunnel experiments performed to study artificial abrasion of quartz particles during eolian suspension have shown that the abrasion dust formed from crushed quartz is composed of angular fragments with a minimum size of about 50 μm (92). Chips from the corners were considerably smaller, generally less than 2μm. Silt particles showed no loss from abrasion, and therefore were considered to be unaffected. This led Kuenen (92) to believe that the abrasion products only yielded the coarse and fine fractions in loess, and therefore the other major size fractions must have been available for transport at the beginning. Nieter and Krinsley (107) also found that clay-size particles of about 1 μm could be produced as a result of silt abrasion during eolian transport.

Davidson and Handy (33), showed photomicrographs from a polarizing microscope of clay particles attached to silt grains in loess samples. Continuous clay coatings covered the surface of some larger grains, while individual clay

particles were also found adhered. After vigorous dispersion with a malted milk mixer, noticeable amounts of clay coatings still persisted on host grains. Similar continuous coatings had previously been mentioned by Swineford and Frye (152) for loess of Kansas and identified as montmorillonite.

Scanning Electron Microscopy (SEM) analysis of the microtexture of loess has been helpful in studying the surface structure of loess grains, and the nature of silt particles. Smalley and Cabrera (139) presented SEM micrographs of loess from Nebraska and Karlsruhe, Germany in which the majority of grains < 64 µm were angular and had an abundance of very fine (1 µm) particles adhering to them. These fine particles were tentatively identified as quartz chippings, a possible result of glacial grinding. Grabowska-Olszewska (59), identified clay mineral particles up to 8 µm adhering to silt in loess from Poland. In addition, the micrographs revealed a number of smaller quartz particles attached to larger silt grains. Other studies have revealed similar fine particles on larger silt grains (4, 17, 166).

Worchester (171) concluded that in southwestern Iowa loess x-ray diffraction analysis indicated depositional clay occurred as aggregates of silt size and as coatings on silt particles. This aggregation and coating was presumably

enhanced by carbonates present in the silt at the time of deposition.

In Texas, Gillette and Walker (56) studied the nature of airborne soil particles which had been eroded from sandy parent material by wind action. Size distribution of airborne particles showed two modes, (1) a coarser mode between 10 and 100 μm and (2) a finer mode between 1 and 10 μm. The coarse mode was attributed to loose erodable quartz particles present in the parent soil. The finer particles consisted of clay minerals and were considered to be the result of sand blasting during erosion. SEM micrographs showed that clay was removed as individual platelets, as coatings on quartz grains, and as coarse aggregates of platelets. "Sand blasting" during transport removed the clay from quartz grains and separated aggregates. SEM analysis also revealed that at higher wind speeds, a higher percentage of the large particles consisted of eroded clay aggregates.

Dust storms

The study of eolian mechanics: erosion, transportation and deposition of suspended load, can be supplemented if the analogy to modern dust storms is considered. Comparisons of the particle size distribution of loess samples with wind-blown dust have been made (70, 111, 151) and show close similarities. Even thickness-distance relationships of dust resemble observed trends in loess distribution (143),

except they occur over a much more widespread area.

Nickling (106) reported the results of the analysis of dust storms originating on the delta of the Slims River in the Yukon. Material was comprised of fine sand and silt originating from outwash of the Kaskawulsh Glacier. The lack of vegetation, low annual precipitation, and fine texture of the sediments make this area extremely susceptible to erosion by strong off-glacier winds. Log-log plots of suspended sediment flow rate versus height above the ground approximated straight-line relationships and could be expressed as a power function:

$$F = a/Z^b$$

where F is the suspended sediment flow rate (mg/cm.s) at height Z(m). This is the same form which had previously been given by Chepil and Woodruff (22), for dust storms in Kansas and Colorado during the mid 1950's. Nickling concluded that for suspended material, the flow rate was more directly controlled by the degree of air turbulence than the shear velocity. It should be noted that sediment transport in creep and saltation varied with the cube of the shear velocity.

Present-day dust storms in Alaska, which are producing accumulations of loess (110, 159), give some insight into the most important variables required for the eolian mechanism to operate. The periodic flooding of glacial streams and the continual influx of sediment (36, 107) would seem to be the most critical prerequisite for wind deflation to be effective. Apparently, the winds which are currently active are of sufficient magnitude to cause modern loess deposition.

Rieger and Juve (116) concluded from studies of soil development, or more precisely, lack of development, that there is at present, continual loess deposition in Alaska. Pedologic evidence indicates that soils close to the source are subject to continual accretion. Since radiocarbon dating of the Alaskan loess spans from 30,000 RCYBP to 4,000 RCYBP (111), this encompasses not only the age of Wisconsinan loess in the Midwest but transgresses into Holocene. The lack of any Holocene loess throughout the Midcontinent thus may be because of the lack of ample material for transport.

Mathematical Modeling

Ash falls

Systematic variations in properties of volcanic ash have been reported (37) and show some trends as seen in

loess deposits. Decreasing thickness and decreasing particle size downwind are typical. Resulting patterns of thickness contours are related to the wind direction at the time of eruption and commonly are elongated with an axis away from the source and oriented in the direction of the wind (37). If the wind direction varies with altitude, the resulting ground pattern may be highly irregular and non-indicative of a predominant wind direction.

Scheidegger and Potter (132) suggested that the variations in thickness and particle size downwind follow an exponential decay, and developed a physical model to explain these trends. Their model included the following assumptions:

(1) An initial volume of ash ejected has particle size distribution and cloud density given as power functions of the settling velocity.

(2) The material is suspended in turbulent motion, with turbulence decaying with time and distance.

(3) With decay of the turbulence there is deposition, with total deposition time proportional to eruption time.

(4) A constant mean wind.

The rate of sedimentation, S, can be expressed as a function of time t, and fall velocity W, which is related to particle diameter d, and density γ:

$$S = S(W, t) = S(\gamma, d, t)$$

By using the analogous turbulent decay function for water, and the sediment load density, n, a function for the sedimentation rate at some distance, x, from the source can be written as:

$$S = mn_o \; (CWh \; (x/v))^{m-1} \; e^{-(CWh \; (x/v))^m}$$

where

m = turbulent decay constant

n_o = initial number of particles per unit volume of air

c = a constant

W = fall velocity

h = height above ground

v = velocity of wind.

By differentiating this equation with respect to W and maximizing the result, an expression for the relation between fall velocity and distance can be given:

$$W_m = \frac{1}{Ch} \; \frac{v^m}{x^m}$$

This simply states that as x increases away from the source, then W_m, the settling velocity of "main" grains becomes

smaller, i.e., larger particles fall out first.

The initial size distribution was taken as a power function:

$$n_o \ (W) = cW^p$$

where c and p are constants. Fall velocity relates to the size distribution according to Stoke's Law where $W = const \ \gamma d^2$.

The thickness of the deposit, H, is dependent on the duration of the eruption, T, and is given by:

$$H = T \ \alpha \ (\tfrac{v}{x})^{\beta m + 1}$$

where α and β are constants of integration related to the initial size distribution. To further display the intimate relation between thickness and particle size, this equation can be modified by substituting the appropriate expression for v/x already given. The thickness equation then becomes:

$$H = T \ \alpha \ (chW_m)^{\beta + 1/m}$$

The total thickness is now expressed as a function of time and fall velocity.

Slaughter and Hamil (136) also used atmospheric turbulence to develop a model for volcanic ash deposition taking into account aggregation of particles. They assumed that

violent eruption created a "mushroom" cloud, which is
spherical at first, and then expands and becomes flat as it
rises. An initial particle-size distribution was assumed
from Rosin's crushing law:

$$W_r = 100 \exp -b \ (\log r)^n$$

where

W_r = weight percent of rock of particle radius r,
and b and n are empirical constants.

Because volcanic clouds contain a significant amount
of water and are highly electrically charged, aggregation
of the finer ash becomes an important factor. It was
indicated that such aggregation should decrease as particle
size increases. The distribution of aggregated particles
which best fit observations of ash beds was produced by
the Maxwell-Boltzmann function. Settling velocity was based
on Oseen's law for particles outside the cloud, and

$$u_r = c \ (r + a)^{1/2}$$

where

u_r = mean horizontal speed of the particle in the cloud

a = a constant which compensates for increased
viscosity because of turbulence

c = horizontal wind speed.

The volume of particles at point x, y on the ground, with 0, 0 taken as the volcano orifice is:

$$W_{r_j} (x,y) = [c \ (r_i+a)^{1/2} \ dx/wh) \ \Sigma_n \ W_{r_i}^{*} \ (x_n, y_k)]$$

where

W_{r_j} (x,y) = volume of material on the ground of aggregated radius, r_j

$W_{r_i}^{*}$ = weight percent of particles of effective radius, r_i at point x_n, y_k in the cloud

h = thickness of the cloud

w = cloud velocity.

One of the requirements of this model is that particle motion is fixed to straight line segments or steps of specified length before changing direction.

Loess deposition

The theoretical study of loess deposition has in the past been approached from two distinctly different aspects. The application of turbulent atmospheric diffusion to loess deposition was first suggested by Sundborg (146) in a general discussion, and later presented in detail by Waggoner and Bingham for some specific trends (165). Both of these studies relied heavily on the meteorological

theories developed by Sutton (149), previously discussed.

An alternative approach to this problem was more recently presented by Handy (67) who based his theoretical development on sedimentation and variable winds hypothesis in an attempt to explain both "upwind" and "downwind" thicknesses. The developed mathematical model suggested that the linear relation between loess thickness and logarithm of distance from the source is a result of variable rather than prevailing winds. This model still did not sufficiently explain near source thickness, which he labelled as "extraordinary." Since the model developed in the present is in reality a combination of these two approaches, turbulent diffusion and variable-winds sedimentation, a complete understanding of these models is required.

Turbulent diffusion   Waggoner and Bingham (165) perceived that previous attempts to explain the thinning relationship for the loess of Illinois were inadequate. They believed that since very little change takes place in particle diameter with distance, neglecting the coarsest zone immediately adjacent to the source, Stoke's Law did not govern the sedimentation process. Therefore, they were convinced that a simple process was responsible for loess deposition, and that a simple hypothesis should explain it.

Waggoner and Bingham observed that the terminal velocity of silt and finer particles must be less than the vertical velocities of turbulent air. They therefore assumed that all loess particles regardless of size have a uniform rate of deposition. In addition, the downwind concentration was taken to be normally distributed with elevation, and the variance, σ^2, in the vertical direction was assumed 4/9 that of the down-and cross-wind variance. Assuming that (1) turbulence in three dimensions is not correlated, (2) since the ground surface bisects the normal distribution, concentration is twice the three-dimensional distribution about the origin, and (3) distribution of concentration remains constant downward, they presented the following expression for concentration, χ, at any point X, Y, Z from the center of the cloud:

$$\chi = \frac{2q(r)}{2\pi^{3/2} \sigma^2 (2/3\sigma)} \exp - 1/2 \left[\frac{x^2}{\sigma^2} + \frac{y^2}{\sigma^2} + \frac{9Z^2}{4\sigma^2} \right]$$

The quantity of material in the cloud, an emission from 1 cm of line source, is q(r) of material remaining after drift of r cm.

An infinite line source was taken and the length of deposition along the wind direction was summed over infinity to produce an expression for deposition, d:

$$d = \int_{-\infty}^{\infty} \int_{-\infty}^{\infty} p\, \chi\, dy\, dx$$

where

p = proportion of particles which settle upon 1 cm^2

downwind.

The thickness of material can be written as:

$$b = kd$$

where

k = a constant of proportionality.

This takes the place of summing one dust cloud over the
numerous clouds during the time of loess deposition. This
expression, which is the basis of their hypothesis, was then
refined for depletion of the cloud and for source width.
The total thickness of blanket B, at distance r_1 from the
lee side and r_w from the windward side of the source is, the
sum of deposits b from 1 cm strips of source:

$$B = \int_{r_1}^{r_w} b\, dr$$

$$B = \frac{3pq(r)}{c\pi^{1/2}(1-(m/2))} \cdot (r_w^{(1-(m/2))} - r_1^{(1-(m/2))})$$

where

    c = a constant near 1

    m = varies between 1 and 2, and describes the degree

       of turbulence.

The depletion of the cloud results in a percentage settling
of silt from a 1 cm zone immediately above the ground:

$$q(r) = q(o)\exp\left(-\frac{2pr\ (1-(m/2))}{(\pi^{1/2}(1-(m/2))}\right)$$

Because the basic equation is of the form $b = kr^{-m/2}$,
this predicts that the logarithm of thickness will be a
linear function of logarithm of distance with slope $-m/2$.
Increasing values of p indicate more rapid settling and
will steepen the slope. At the same time, the influence of
wide sources will be to flatten the slope.

Variable-wind sedimentation   An alternative approach
based on sedimentation rather than turbulent diffusion was
presented by Handy (67) and produces a semi-logarthmic thick-
ness-distance relation through variable rather than prevailing
wind. He pointed out that the occurrence of material on both
sides of a valley source and the multidirectional thinning of
loess might be explained by defining a number of prevailing
wind directions, hence in effect a variable wind system.

The initial model introduced the statistical probability of a variable wind direction, an intuitive observation based on the current occurrence of frequent changes in ground winds. Some basic parameters set forth in this model included:

(1) Linear source of eolian silt (uniform size of material)

(2) Randomly variable wind direction with no prevailing wind. (Ability to rotate 360° where α = angle between source and wind direction.)

(3) Deposition is essentially a sedimentation phenomenon, therefore Stoke's Law applies.

(4) Vertical dispersion of dust and the horizontal wind velocity are uniform throughout the height of the dust cloud.

By assuming a linear source of infinite length, and specifying a random wind direction and maximum deposition length, the system of erosion and deposition has distinct boundaries which now becomes convenient for analysis. By allowing a change in wind direction then, during any given time period an incremental thickness would be deposited. Where the wind direction can complete a full sweep of the source area a total accumulation of material is developed. The time period for deposition from any wind position must be

the same as all others to give a uniformity to direction
and dispell any dominance by one direction. An expression
for thickness H, in terms of distance, X, normal to the
source was given as:

$$H = -2 \ln \tan (1/2 \sin^{-1} X)$$

A semilogarithmic plot of this equation between thickness and
perpendicular distance from the source showed excellent
linearity, leading to the linear approximation of

$$H = 1.3 - 2 \ln X$$

It was then suggested that modification of this simple
variable winds model could show seasonal prevailing winds by
additional probability of certain wind directions over
others, with the wind speed constant. However, it was
stated that this would "still give semilogarithmic thickness
distributions both directions from sources, which does not
appear to be the case." This model was therefore rejected
in favor of a constant prevailing wind added vectorially to
the variable winds. This resulted in extending the deposit
downwind and reducing it upwind, a common observation from
field evidence.

A prevailing wind function, R_x, equal to the ratio of

prevailing to variable wind velocities was introduced to account for the relative influence of both wind types. Integration gave the following equation for loess thickness:

$$H = \left[\frac{1}{\sqrt{1 - R_x^2}} \ln \frac{1 \pm R_x \tan \frac{\alpha}{2} \sqrt{1 - R_x^2}}{1 \pm R_x \tan \frac{\alpha}{2} + \sqrt{1 - R_x^2}} \right]_{\alpha_p}^{180 - \alpha_p}$$

Some discussion was made concerning important contributing factors such as source width, parallel sources, terminating sources, short sources, time of deposition and source efficiency, all of which apply to certain locations.

Statistical models in geomorphology

Random-walk process as a statistical model to describe certain geomorphic patterns was first suggested by Leopold and Langbein (97) for the generation of drainage networks. Hillslope development by soil creep has also been based on the idea of a random-walk process (28), and the theory of flow of fluids through porous media has also been viewed as a random-walk (128, 129). In addition, the formation of alluvial fans, was described as a random walk (112).

Dacey (29), developed a random walk model for sediment transport which included only absorbing barriers, through

which particles could transcend. The loss of particles by removal was compensated by additions to the space at periodic intervals, giving a recurring random walk. The application was for particles entering a stream at the top and drifting to the bottom in turbulent water.

The motion of particles in turbulent fluid, as in the case of stream flow, has been refined by stochastic models, to the point of using a random number generator for distance and duration of the step (23). Although such models are generally utilized to produce a concentration profile, or show diffusion from point sources (11, 26), they substantiate the applicability of such methods.

The use of statistical mechanics in this case is based solely on the assumption of randomness of process. It has been pointed out (13) that in geomorphology nothing is really random; the evolution of landforms is clearly related to mechanics, which determines specific events. However, on a grand scale, the transport process which produces landforms may be treated as if it were random, as the sum effect of complicated small-scale effects which act on individual particles.

PRESENT RESEARCH

Random Walk Model

Particles which exhibit erratic, unpredictable movements have been modeled as a random walk, the most classic of which is Brownian motion for very small particles (8). An example often given to illustrate the simple random walk is the "gambler's ruin," wherein a gambler plays against an opponent until one or the other of the players is bankrupt (7, 25, 27). Perhaps more easily understood, and more appropriate to the present application, is the case of the "drunkards walk" (149).

Consider an inebriated individual who starts for home at time t = 0 walking from a tavern located on an arbitrary x-y axis at point 0, 0. His plan is to walk a straight line along the path y = 0. But considering his condition, at subsequent times t = 1, 2, ... he takes a number of steps of the same length 45° to his right or left with probabilities of movement p or q = 1 - p, respectively. With equal probabilities, of a transition to the left or right, i.e. p = q = 1/2, we consider this to be a symmetric walk and might appear as in Figure 3. If for some reason the probabilities are not equal and p > 1/2, there is a drift to the right, and if p < 1/2 the drift is to the left. By
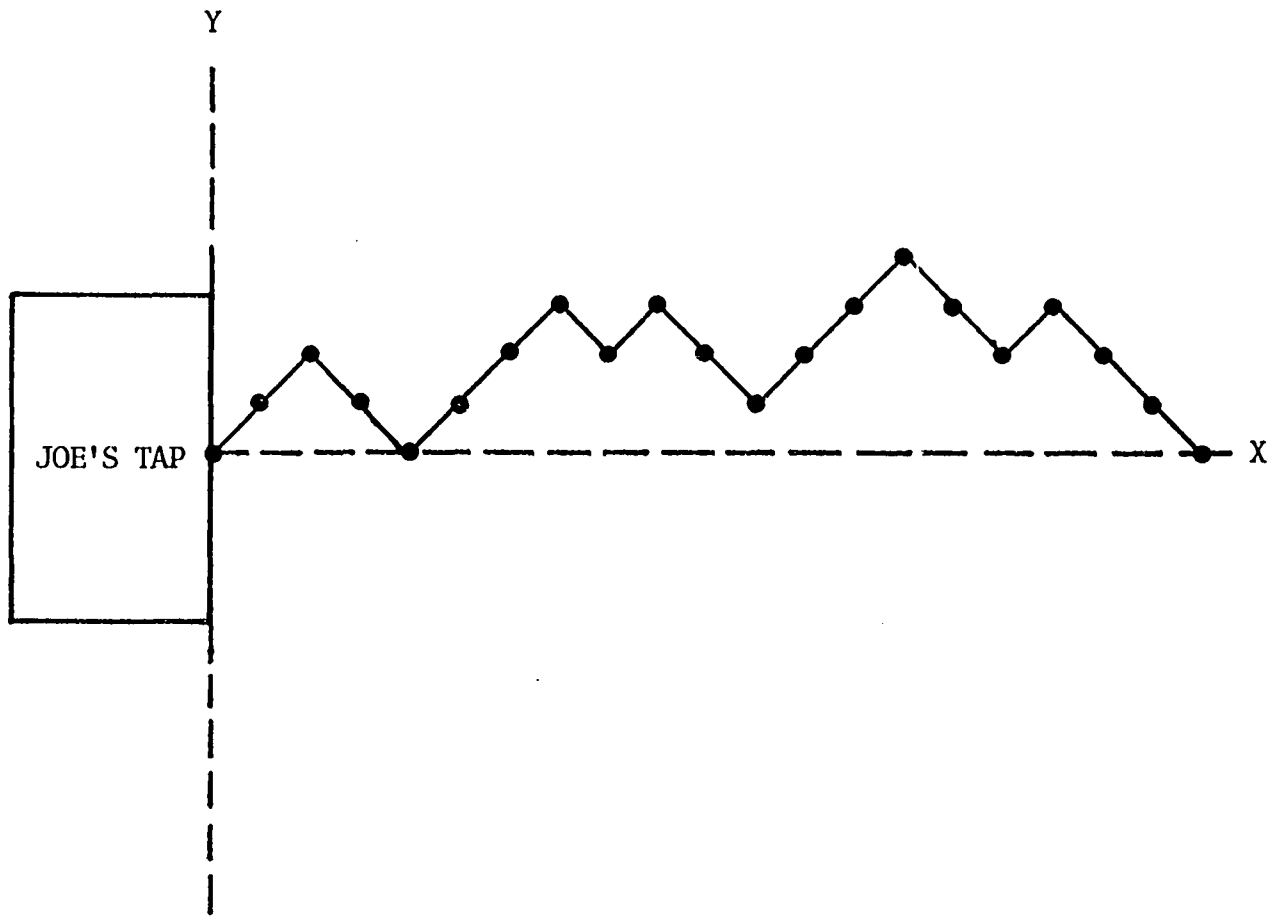
Figure 3. Drunkard's walk

assuming a completely open space for the walk to take
place, we would say that the walk is unrestricted, without
barriers, and our friend could continue walking to infinity.
It has been shown (40) that with equal probabilities the
walker would eventually return to his path, no matter how
far he has deviated.

Suppose now that in reality, the tavern is located along
a wharf, with a dock and warehouse located as shown in
Figure 4. Now the walk is not without restriction, and
should the walker attempt to walk too far to his left and
run into the warehouse, he would be bounced back into his
open field. The warehouse is considered a "reflecting"
barrier. In the same respect, if he should drift too far to
the right, he would fall off the dock, and be removed from
the space. In this case, the dock becomes an "absorbing"
barrier.

The vagaries of horizontal wind velocity coupled with
vertical wind turbulence are herein described as a random
walk - an interrupted stepwise progression in which there
is a given probability of the next step being upward or
downward. Each step is completely independent of the
preceding steps and all steps are of equal length. Regimes
of eolian erosion, transportation and deposition are then
simulated by restrictions on the walk.
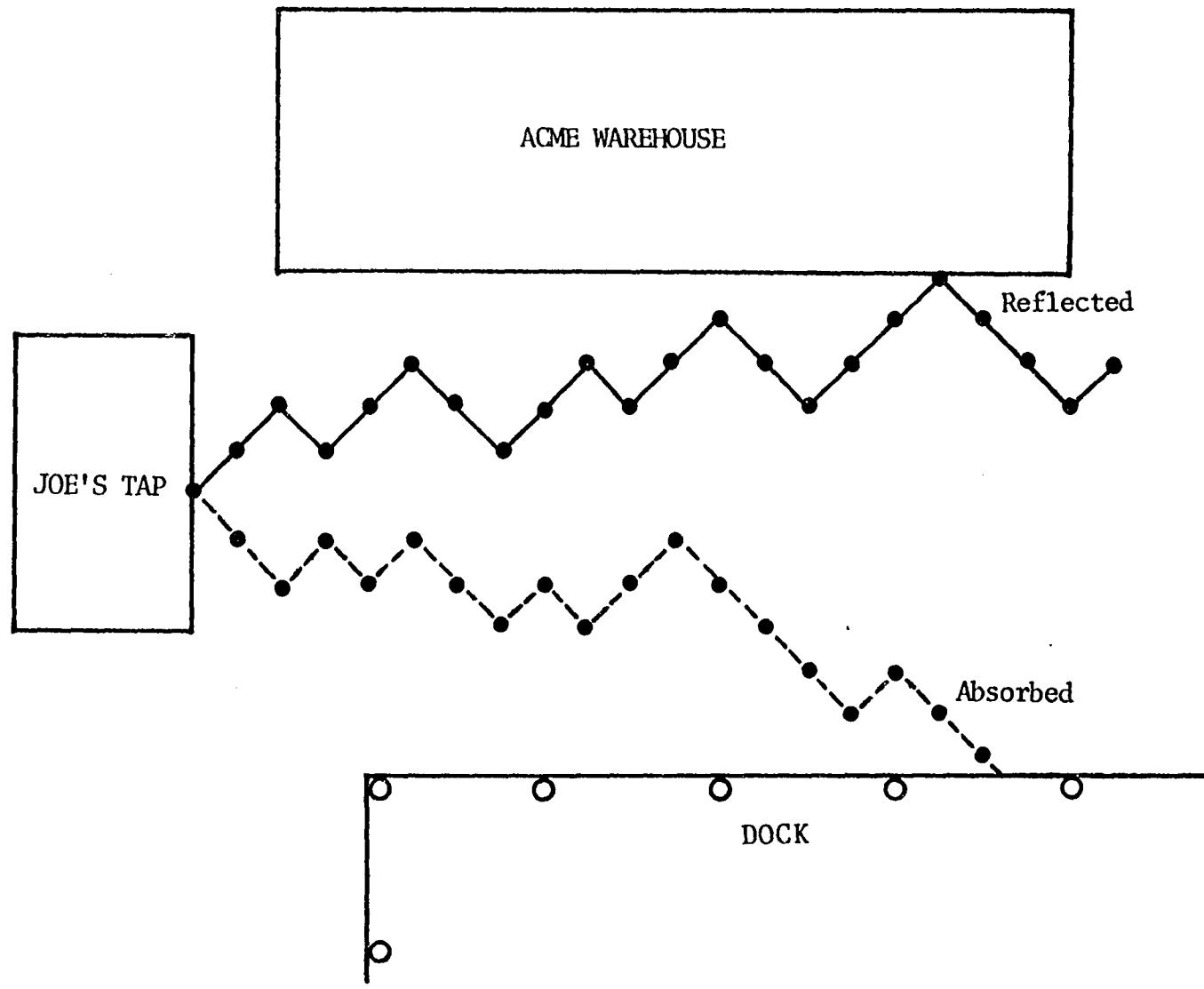
Figure 4. Restricted walk, with reflecting and absorbing barriers

The simplest random walk is a one-dimensional lattice walk, with equal probabilities, in which the walker eventually returns to the origin, in this case the ground surface (8). Even with zero net settling velocity because of turbulence, the implication is a conformation of the old adage, "What goes up must come down." The probability of the walker being on the mth lattice point, or in this case the mth level after step n is

$$P_n (m) = (1/2)^n \frac{n!}{(\frac{n+m}{2})! \ (\frac{n-m}{2})!}$$

A large number of steps results in an asymptotic behavior, and the distribution falls off with increasing level m, becoming zero at m equal to infinity. This distribution has been shown to tend towards Gaussian, with a differential equation describing diffusion (27).

For the ground level, m = 0 and this equation reduces to

$$P_n (0) = (1/2)^n \frac{n!}{(\frac{n}{2})!^2}$$

This function is shown in Figure 5 , and represents the probability of encounter of a particle with the ground surface given zero settling velocity. Also shown are
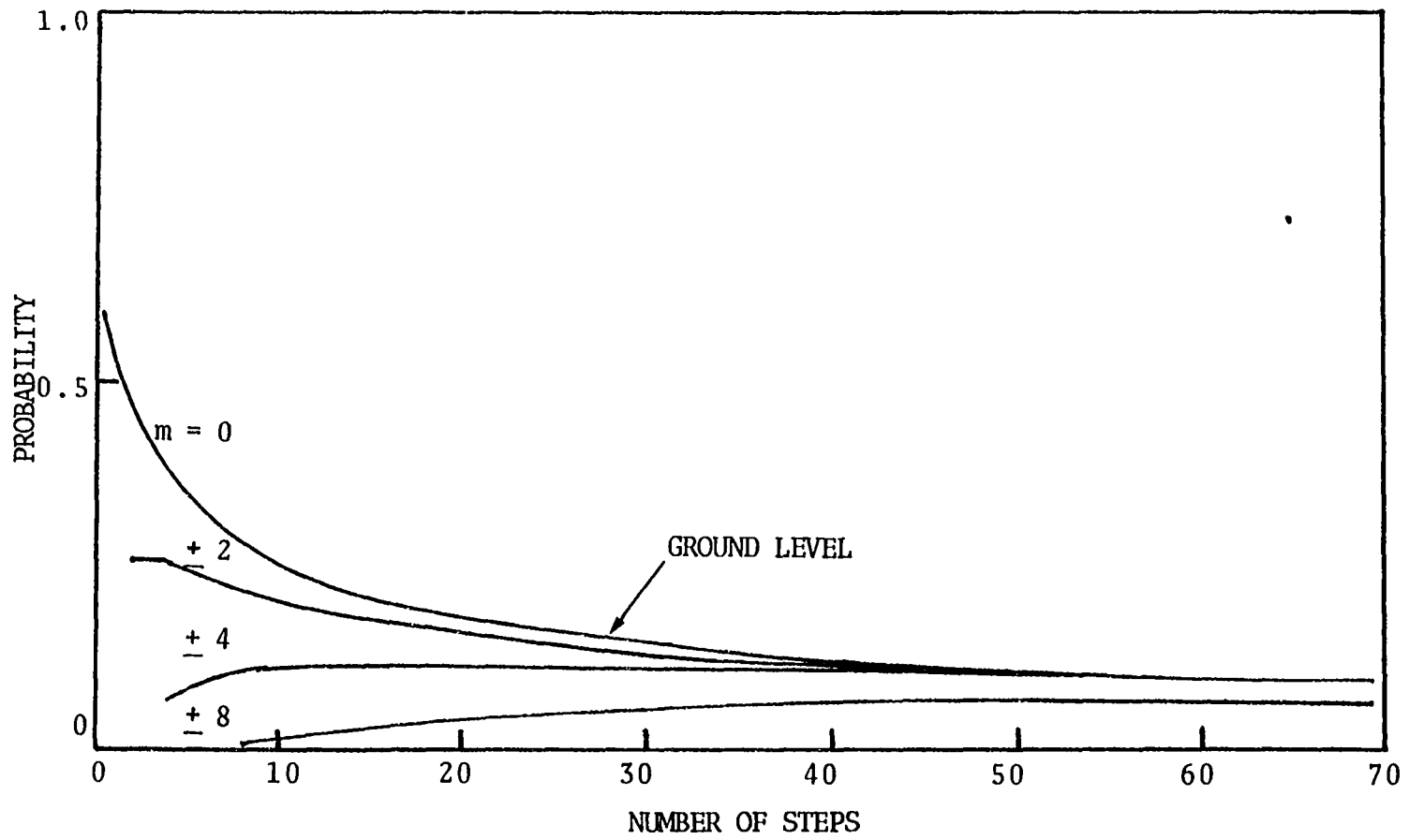
Figure 5. Probability of walker on mth point after n steps

solutions for m = ± 2, ± 4 and ± 8. As n becomes large
the relationships may be seen to converge. Even as m is
larger, the probabilities tend to remain constant, the
implication being that the likelihood of sedimentation remains
almost constant because of the high concentration of particles
close to the ground.

Particles which settle out on the source area will bounce
away and become resuspended from turbulent wind and saltating
sand grains. In the random-walk model, the source area is a
reflecting barrier. Probability equations must be modified
to account for the reflection, and the result will add to
the probabilities of particles at a particular height. The
added probability is for the mirror reflection, and the
probability sum for both a real level m and a reflected level
m_1, is

$$P_n (m, m_1) = P_n(m) + P_n (2m_1 - m)$$

As before, letting the reflected level $m_1 = 0$, this expres-
sion becomes

$$P_n' (m, 0) = P_n(m) + P_n (-m)$$

$$= 2 P_n (m)$$

Then the probability of particles at any level m within a source is doubled by the reflection, and the general shape of Figure 5 remains unchanged.

In the deposition area, particles which settle should remain lodged because of vegetation, and thus are not subject to further erosion and resuspension. An expression similar to the previous one, only now considering absorption, can be written as

$$P_n (m, m_1) = P_n (m) - P_n (2m_1 - m)$$

$$P_n = 0$$

which simply states that if there is no reflective source, there is no airborne silt. If however $P_n (m) = P'_n(m)$; there is already an established probability coming off of the source, $P'_n (m) = 2P_n(m)$ and varies with level m and step n. Then at $m_1 = 0$

$$P_n(m,0) = 2P_n (m) - P_n(-m)$$

$$= P_n(m)$$

and the probability for particles to reach an absorbing barrier after bouncing along a source reflecting barrier is the same as if there were no barriers at all.

The ground-level (m = 0) probability curve of Figure 5 shows a sharp rise at low values because of the higher likelihood that particles beginning their walk and thus within a step of the ground will in fact step to the ground. In actual eolian transport and deposition, this effect should be reduced or damped because the walk starting points are dispersed across a source area. The amount of damping should depend on source width and may be approximated by averaging probabilities obtained from starting points n = 1, 2, ...n_s, where n_s equals the source width, Figure 6. As can be seen, the wider the source, the less pronounced is the near-source rise in probability of deposition.

The approach used here to simulate the genetics of loess deposits is the trial walk, wherein certain variables are initially given values and particles walk out of the source area. The use of a microprocessor or small computer to generate a large number of particles in effect produces a simulated dust cloud. Three cases will be presented, (1) unidirectional wind normal to the source (2) randomly variable wind directions, and (3) variable plus a prevailing component. All cases initially use an equal probability for up or down particle motion.

Case I: unidirectional wind

Considering an infinite line source the scheme the

SOURCE AREA

RANGE OF ORIGINS
FOR WALKS

MEAN PROBABILITIES WHEN
SOURCE WIDTH IS:

2
10
20

RANGE IN PROBABILITIES FOR
WALKS ORIGINATING FROM:

WINDWARD SIDE, and

LEEWARD SIDE, OF SOURCE

PROBABILITY

NUMBER OF STEPS
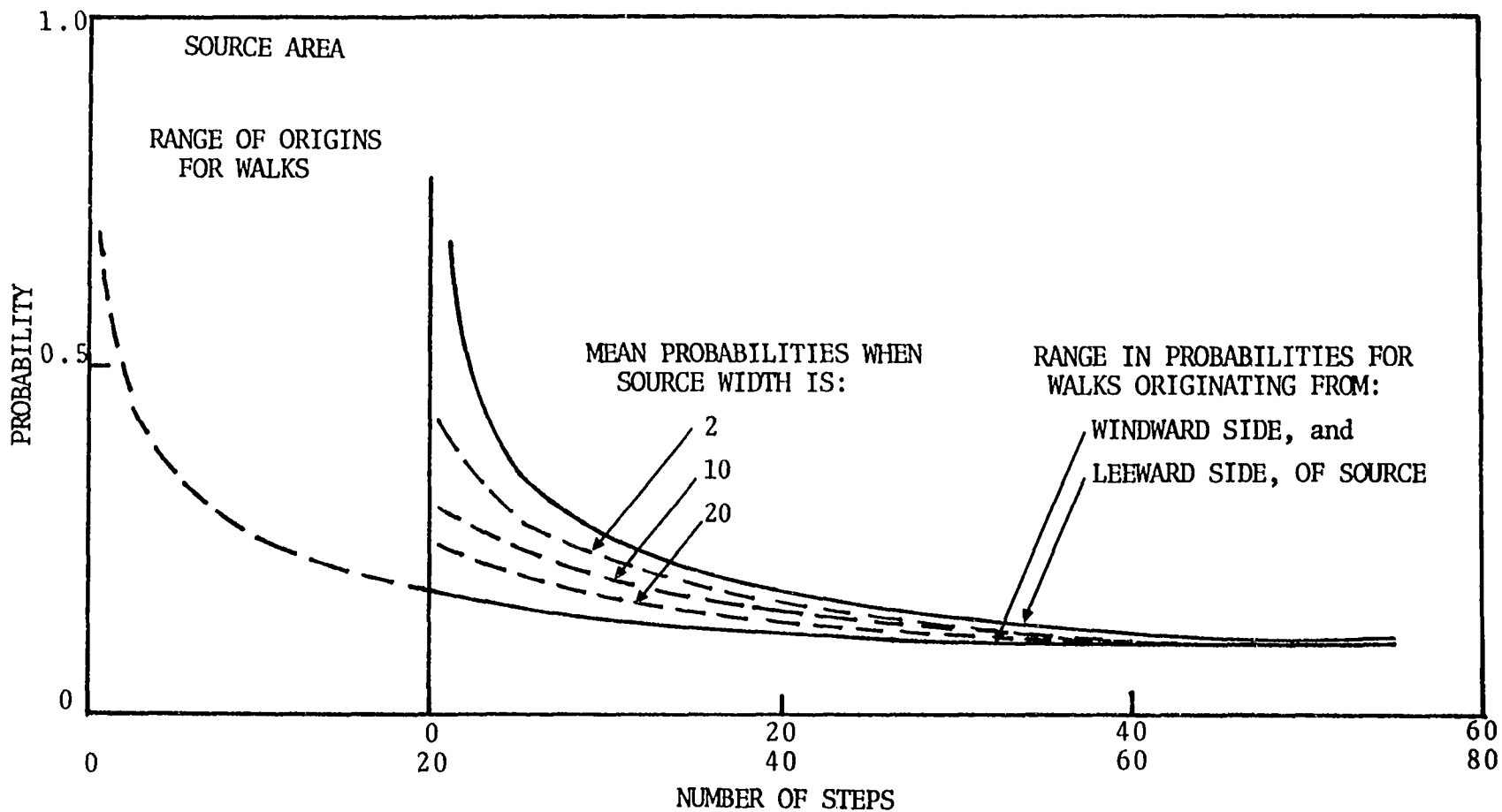
Figure 6. Damping effect of starting point on probability

computer simulation begins with specifying source width
and a deposition area width of relative units, the latter
arbitrarily chosen as 200 to limit computer time. This
system can be viewed as a series of buckets, placed in a
single line, the length of which is equal to the sum of
source and deposition zones. In each of the source
buckets, a number of particles is specified, while at time
zero the deposition buckets are empty. The program
essentially empties each source bucket in sequence, using
a random number between zero and one for each step motion
of individual particles. A number less than 0.5 yields a
step downward, and greater than 0.5 a step upward. Since
a constant horizontal wind is imposed, the path of an indi-
vidual particle is taken as one step forward and either one
step up or down, resulting in a net movement of 45°. The
total path of a particle might appear as a series of steps,
Figure 7.

A simple scheme of accumulation for the number of
particles landing at each location along the deposition area
produces a plot as shown in Figure 8 . The number of
particles recorded at each location is somewhat sporadic
and at some locations no particles fell, as indicated by a
zero, while at great distance some "local" numbers are
indicated. Increasing the particle concentration at the

SOURCE

ZONE OF DEPOSITION
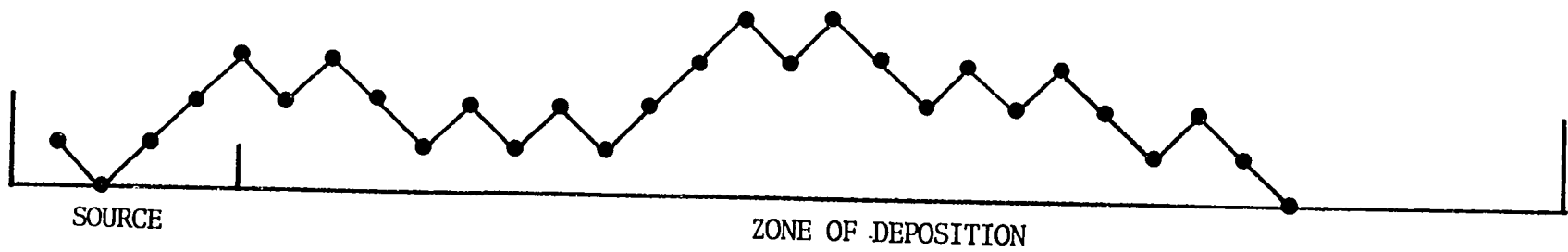
Figure 7. Path of an individual particle described from a symmetric random walk

```
5138  ####################################################
2187  ##################
2170  ##################
1457  ##############
1401  ##############
 980  #########
1047  #########
 817  ########
 904  ########
 691  ######
 688  ######
 578  #####
 569  #####
 473  ####
 482  ####
 421  ####
 420  ####
 366  ###
 377  ###
 320  ###
 343  ###
 285  ##
 306  ###
 287  ##
 275  ##
 258  ##
 242  ##
 202  ##
 234  ##
 201  ##
 202  ##
 164  #
 193  #
 156  #
 144  #
 159  #
 140  #
 121  #
 147  #
 126  #
 119  #
 130  #
 128  #
 116  #
 136  #
```

PARTICLE COUNT
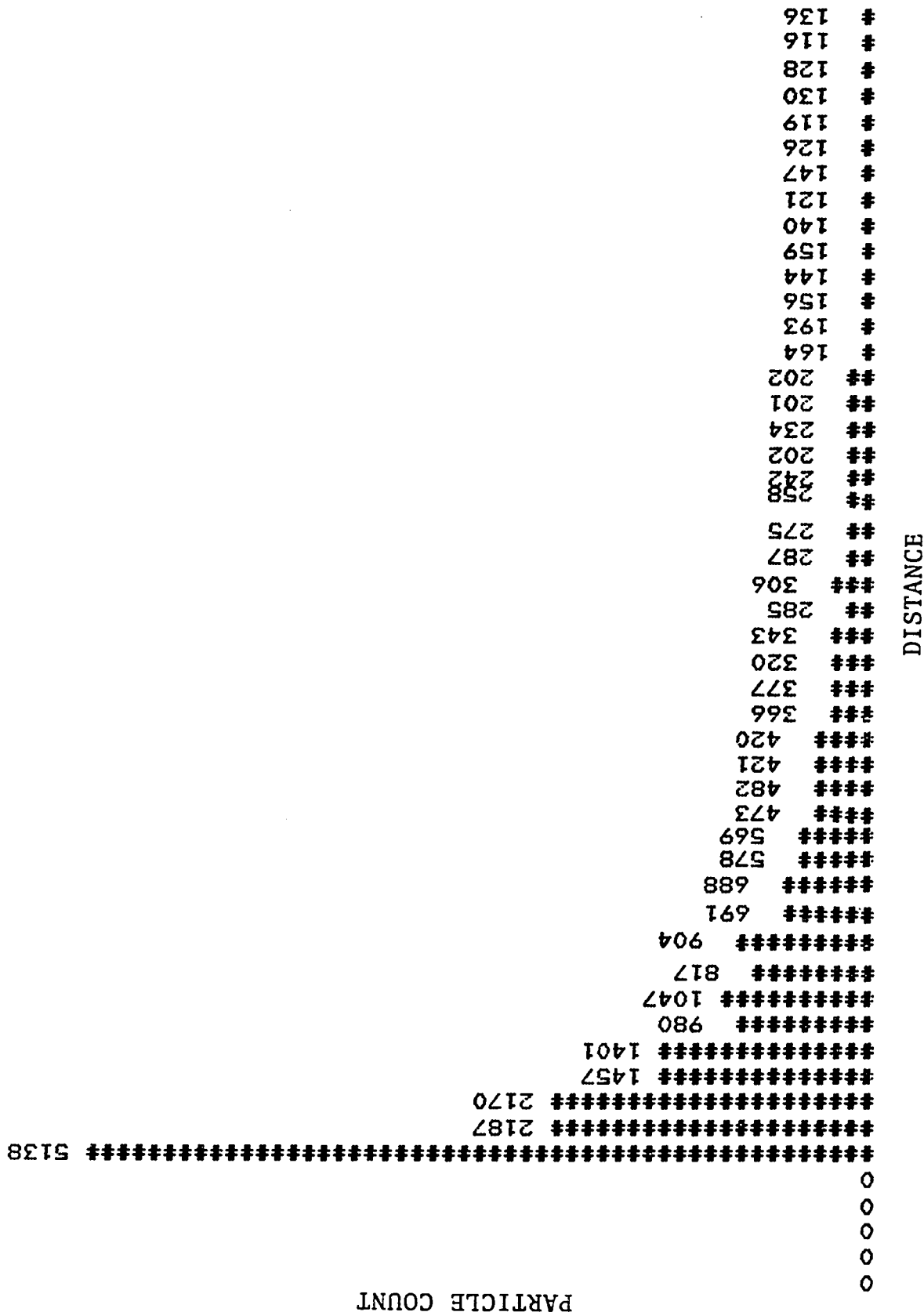
DISTANCE

Figure 8. Typical particle count versus distance plot

source points produce greater numbers, and a smoother curve.

Since initial suspension of material at the source is a prerequisite to any lateral movement, particles along the source points begin their walk from level one, i.e. $m = 1$. In addition, should a particle land on the source, it is set back into resuspension at level one and advanced a step. This accounts for the bouncing motion of a particle striking the surface.

The maximum height of suspension of particles coming off of the source is equal to the source width, since particles are moving in a net direction of 45°. The height of maximum suspension moving across the deposition zone is limited to some level, h, and can be written as

$$h \leq kn$$

where

    k = proportionality constant

    n = number of steps

This would tend to coincide with field observations from active eolian sources; the height of rise appears discrete and limited at the edge of a source, and becomes higher and more diffuse farther downwind. Some particles then may not fall within the range of the deposition area but remain suspended.

Case II: variable wind

Adaptation of the unidirectional case to a variable wind direction model is relatively simple, and is accomplished by specifying a number of individual wind directions. Again, an infinite line source is specified, and particle motion is as before. Ideally, we would like the wind to rotate through a full sweep of positions, considering one quadrant, from 0° to 90°. To limit computer time, positions were taken from 5° to 85° in 10° segments, Figure 9, α being the angle of the wind, measured as the deviation from normal. For $\alpha = 0^\circ$, the wind blows perpendicular to the source as in Case I, whereas at $\alpha = 90^\circ$, the direction is parallel, with no deposition.

Assuming that the amount of material available for transport is directly proportional to source width, as α increases the effective source width increases by $1/\cos \alpha$, or $\sec \alpha$. As an example, a source width of 5 units gives the following effective widths for various values of α:

α	effective source width
0°	5
5°	5.02
25°	5.52
45°	7.07
65°	11.83
85°	57.37

AVERAGE AREA COVERED BY
EACH POSITION
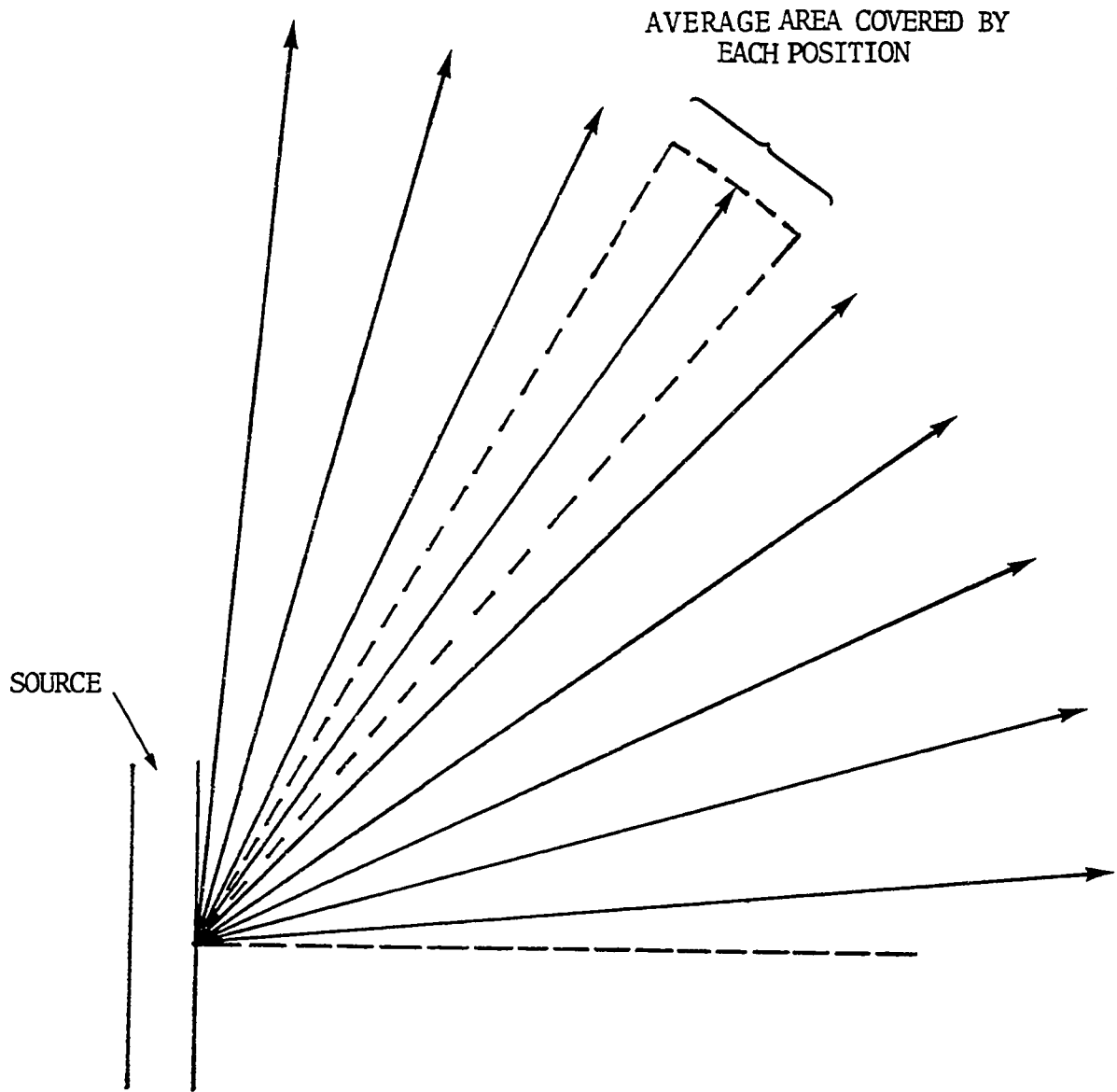
SOURCE

Figure 9. Position of wind direction in any given quadrant

At large angles, the effect of angle on source width is greatly accentuated. With no prevailing wind direction, the resulting deposit is distributed uniformly on both sides of the source, which generally is not the case for loess.

Case III: variable plus prevailing wind

To account for a seasonal prevailing wind, the variable-wind model can be easily modified to model an increased duration of wind in one direction, with all others staying the same. In effect, this simply increases the probability of one direction over the others. This would increase the amount of material on the leeward side of the source, hence increasing the thickness. In the case of sources aligned in the direction of the prevailing component, the thickness on both sides should be identical, a result of the variable-wind model essentially acting alone. Sources lined perpendicular to the prevailing component would show the least influence, the maximum being achieved at high angles of α, as indicated before. Typical situations are shown in Figure 10.

We may note that thus modelled, the distribution on the windward side of the source is identical to that described by the variable wind model, whereas on the leeward side, the distribution is the result of a uni-directional component superimposed onto the variable-wind model. The strength
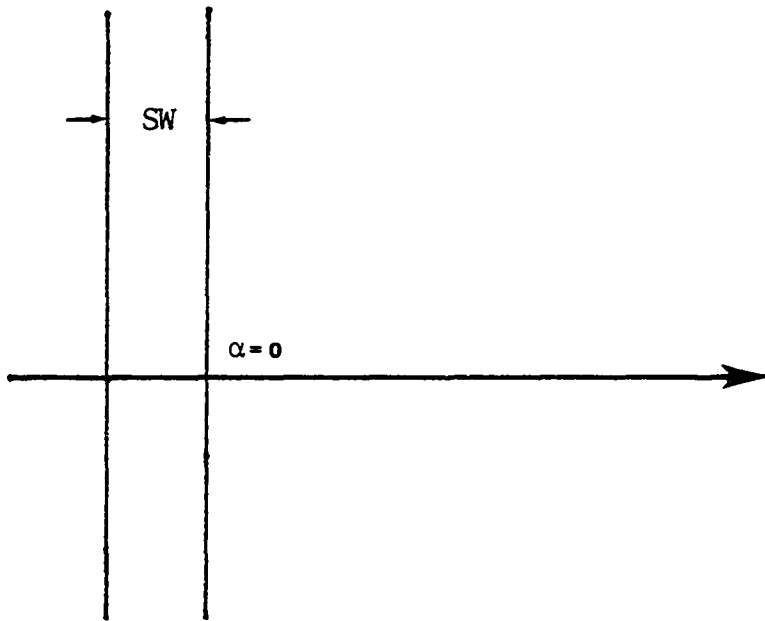
Figure 10a. Wind blowing normal to a source
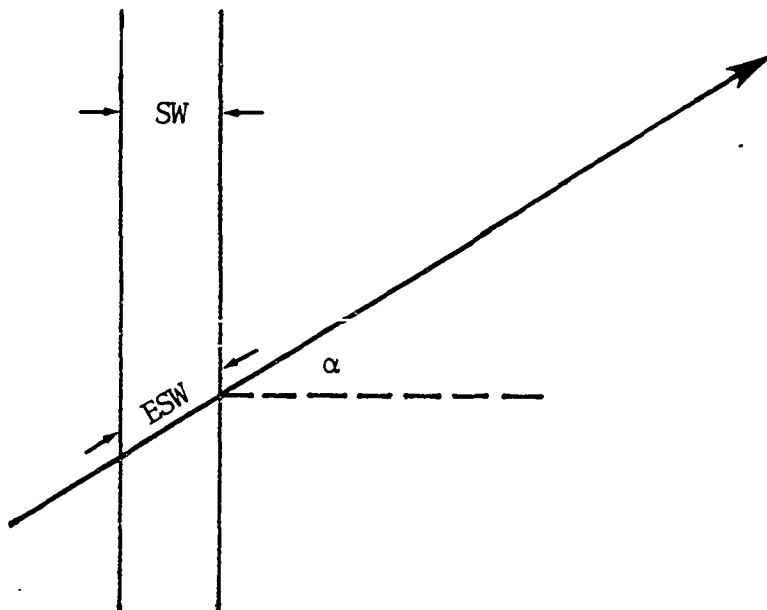
Figure 10b. Wind blowing at any angle, α, to a source

of the prevailing wind can be adjusted by specifying a number of cycles or repetitions in that direction.

Particle size

The above discussion ignores gravitational settling, and predicts sedimentation purely from the probability of random encounter of a particle with the ground. Superimposed upon the random walk must be some biasing of up vs. down movements to account for net settling velocity for particles heavier than air. Furthermore, if Stoke's Law is in effect, the larger the particle the larger must be this bias.

At the source area, erosion occurs when turbulent velocities are sufficient to remove particles from their lodgement, and this is often assisted by the impact energy from saltating particles such as sand or aggregated silt (5). Partial suspension of eroded particles will occur whenever this turbulent velocity exceeds the sedimentation velocity, since some particles will be lifted faster than they fall. Complete suspension occurs only if fallen particles rebound or are re-eroded.

The magnitude of vertical turbulent wind velocities at a source can be estimated on the basis that particles larger than about 60 μm generally do not remain suspended. Stoke's equation for settling velocity is given as (82):

$$V_s = \frac{d^2 g (\gamma)}{18 \eta}$$

where

V_s = sedimentation velocity

d = particle diameter in millimeters

γ = density of particle (2.65 for quartz)

η = fluid viscosity (183 micro poises @ 18°C)

g = acceleration due to gravity (980 cm/sec^2)

Substituting,

$$V_s = 7880 d^2$$

Using 60 μm in this equation gives a vertical sedimentation velocity of about 28.4 km/hr (17.6 m/hr). Thus, vertical wind turbulence must only occasionally exceed this velocity near the ground. For an average silt particle of 20 μm, this turbulent velocity represents 9 times the sedimentation velocity, indicating an excellent likelihood for suspension of unaggregated silt-size particles.

The biasing of particle sedimentation can be viewed in two ways: (1) one may consider that the distribution from the zero-settling velocity (P = 0.5) represents the minimum size particle, and increase the probability of fall P_f, to simulate larger grain sizes, or (2) take the zero-settling velocity distribution as representing the largest size

available to transport by suspension, and adjust the step length to account for smaller grain sizes. Both of these schemes will be presented.

Probability adjustment[1]   If V_s = the sedimentation velocity and V_y the vertical wind velocity (downward positive), and if the instantaneous $V_s = 0$, there is an equal probability of rise or fall for the next step; hence for $V_s/V_y = 0$, $P_r = P_f = 0.5$ (since $P_r + P_f = 1$). Similarly, if V_y upward exceeds V_s downward, i.e. $V_s \leq - V_y$, $V_s/V_y \leq - 1$, the probability of rise is $P_r = 0$ and therefore the probability of fall $P_f = 1$. For grains heavier than air, all values of P_f will fall within the limits $0.5 \leq P_f \leq 1$. Thus, for $P_f = 0.75$ and $P_r = 0.25$, three particles must fall for every one that rises, and the mean direction is $\frac{3-1}{4} = 0.5 = V_s/V_y$. A generalized equation can be written as:

$$P_f = 0.5 \left(1 + \frac{V_s}{V_y}\right)$$

When the largest grain diameter, d_m is just on the verge of immobility, $V_s/V_y = 1$ and $P_f = 1$. Since V_s is proportional to d^2, corresponding diameters may be calculated from

---

[1] This approach was suggested in an unpublished Progress Report by R. L. Handy (personal communication).

$$\frac{V_s}{V_y} = (\frac{d}{d_m})^2$$

and substituting for $\frac{V_s}{V_y}$ gives:

$$P_f = 0.5 \ (1 + (\frac{d}{d_m})^2)$$

Since wind velocities vary, different values of d_m should correspond to $P_f = 1$. Calculating probabilities of fall for different values of d_m:

Grain Size d, mm	Probability of Fall		
	$d_m = 0.10$ mm	$d_m = 0.08$ mm	$d_m = 0.06$ mm
0.10	1.0	1.0	1.0
0.08	0.820	1.0	1.0
0.06	0.680	0.781	1.0
0.04	0.580	0.625	0.722
0.02	0.520	0.531	0.556
0.01	0.505	0.508	0.514
0.005	0.501	0.502	0.503
0.002	0.500	0.500	0.501

Despite the use of different values for the maximum size of erodable material, thus indicating variations in wind velocity, the probability for clay size (.002 mm) particles essentially corresponds to zero settling velocity,

i.e. P_f = 0.5. Therefore the zero-settling velocity random walk simulates the transport and deposition of the clay fraction. By increasing P_f, other size fractions can be included.

Step length adjustment   Another approach to account for particle size variations is to modify the path of the particle, or trajectory, based on the fall velocity. This assumes that the distribution from the zero-settling velocity represents the maximum particle diameter, d_m, which the wind is capable of eroding and transporting in suspension. This is a reasonable assumption considering that the maximum grain size in loess deposits does not change appreciably with increasing distance from the source, and is about 60 μm. Considering that turbulent mixing is of sufficient magnitude to transport this maximum size, this technique also assumes that for all size fractions, the mean path of particles is horizontal, Figure 11.

The zero-settling velocity random walk assumes that the trajectory, β, or path of each step, is at 45° to the horizon since movement is either up or down. This is achieved by advancing equal distances both horizontally and vertically, and thus constitutes the limiting value of β. Since this describes the path of the maximum grain size, smaller sizes should be described by smaller values of β. For a sedimentation velocity, V_s and a constant value of horizontal wind
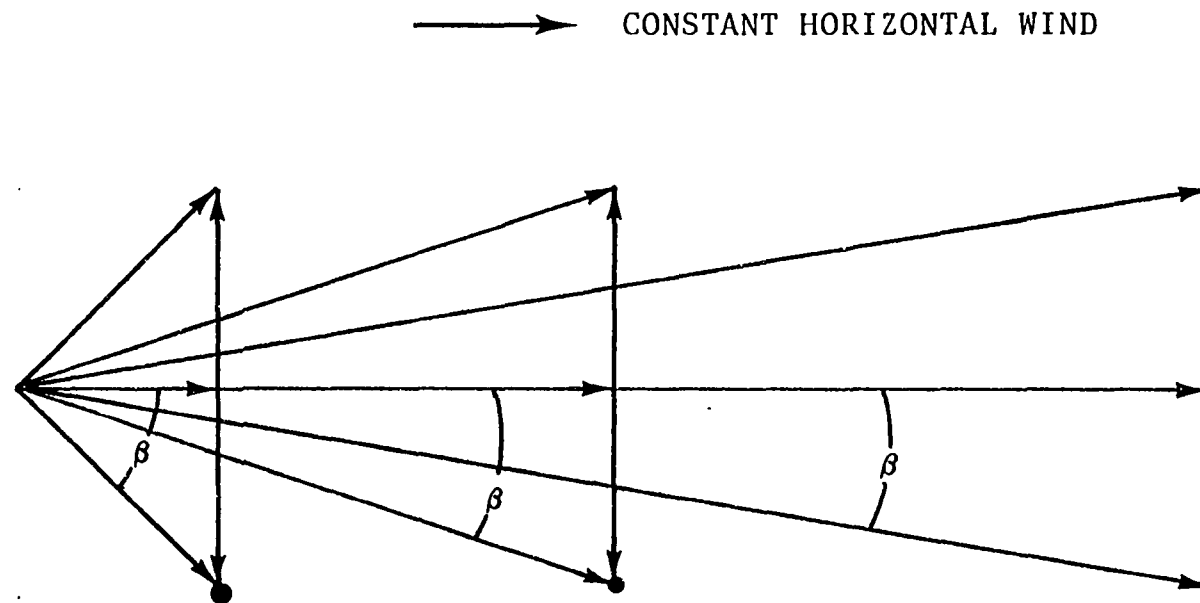
Figure 11. Mean path of particles, step length adjustment

velocity, V_x, the trajectory is expressed as

$$\beta = \tan^{-1} \frac{V_s}{V_x}$$

For d_m, $V_s/V_x = 1$ and $\beta = 45°$. Since V_s is proportional to d^2, and V_x is constant for any value of d_m, β can be expressed in terms of particle size as:

$$\beta = \tan^{-1} (\frac{d}{d_m})^2$$

The trajectory can then be calculated for various values of d_m:

Grain Size d, mm	Trajectory Angle		
	$d_m = 0.10$ mm	$d_m = 0.08$ mm	$d_m = 0.06$ mm
0.10	45	-	-
0.08	32.6	45	-
0.06	19.8	29.4	45
0.04	9.1	14.0	24.0
0.02	2.3	3.6	6.3
0.01	0.6	0.9	1.6
0.005	0.1	0.2	0.4
0.002	0.02	0.04	0.06

This indicates that for small particles (0.02 mm), the path only slightly deviates from horizontal, and hence these particles may not add significantly to the deposit. Taking the limiting value of d_m, the horizontal transport distance, X, is one unit. If all particles started downward from the same height, with a constant horizontal wind, the downwind distance can be stated as

$$X_d = \frac{d}{\tan \beta_d}$$

For $\beta_d < 0.29$, the transport distance is outside the range of the deposition zone. This might suggest deposition of the fine fractions by aggregation or by rain.

For computational purposes, it is easier to increase the horizontal component of step, rather than decrease the vertical component and β may be calculated for various values of step length.

Step Length	β
1	45°
2	26.6°
4	14.0°
8	7.1°
16	3.6°
32	1.8°

Although this technique gives the correct value for β, it is not the same as reducing the vertical component; however, over a large number of steps and a large number of particles, the resulting trend should be the same. Along the source, the path is still described by movement along β = 45°, to allow for continual suspension.

Model Verification

The worth of any model is its ability to forecast the specific trends for which it was developed. To test the accuracy of the random-walk model against observed trends in loess deposits, the results could be compared with available data which, as has been shown, are numerous. This will be done in part. Since many of the loess transects which are reported in the literature have not been oriented normal to the source, any correction of distances could introduce unknown errors, particularly where source width changes.

To provide additional information for model verification, sampling transects were located in Missouri and Iowa. Frye, et al., (54) presented a map of Iowa and Missouri on which the major source valleys for loess were indicated, Figure 12. In central Missouri, the Missouri River Valley width changes, presumably influenced by bedrock in the

MINNESOTA
IOWA

SOUTH DAKOTA

NEBRASKA

WISCONSIN
ILLINOIS

IOWA
MISSOURI

NEBRASKA
KANSAS

WISCONSINAN
(WOODFORDIAN)

WISCONSINAN
(ALTONIAN)

ILLINOIAN

KANSAN

MAJOR SOURCE
VALLEYS FOR
LOESS
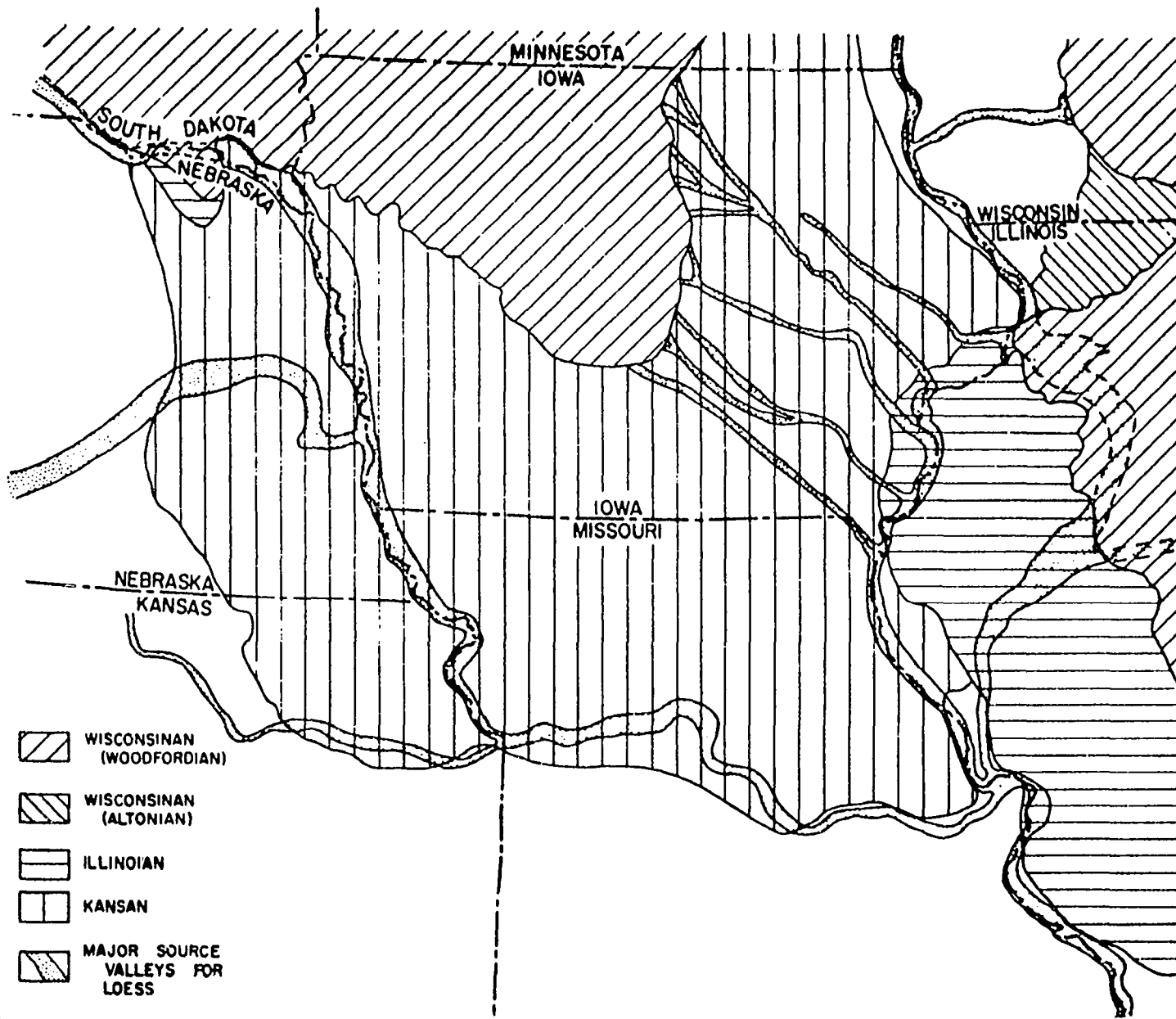
Figure 12. Sources of loess in the central U.S. (54)

east-central part of the state, and thus provides a chance
to investigate this effect of source width. In east-central
Iowa, the Iowa River is indicated as a source, along with a
number of other streams, however this has yet to be
established by any formal investigation. Since the distri-
bution of loess surrounding the Iowa River is complex, a
transect across the river could provide useful data.

These two areas were chosen to further test the random-
walk model for thickness and particle-size trends. Some
understanding of the extent of loess in these areas is
essential, therefore a brief background will be presented.

Loess in central Missouri

The distribution of loess in Missouri, not unlike most
major loess deposits, displays a graphic relationship to
the source area, in particular, the Missouri and Mississippi
Rivers, Figure 13. The thickness contours are essentially
the same as indicated by Thorp and Smith (157) in their map
of the United States, and are considered only general, since
no evidence of an organized investigation could be found.

Shrader (135) indicated that the loess in northern
Missouri had been derived from the Missouri River flood-
plain in northwestern Missouri and southwestern Iowa, and
estimated that the maximum thickness varied from at least
70 ft (21.3 m) adjacent to the river to about 50 inches
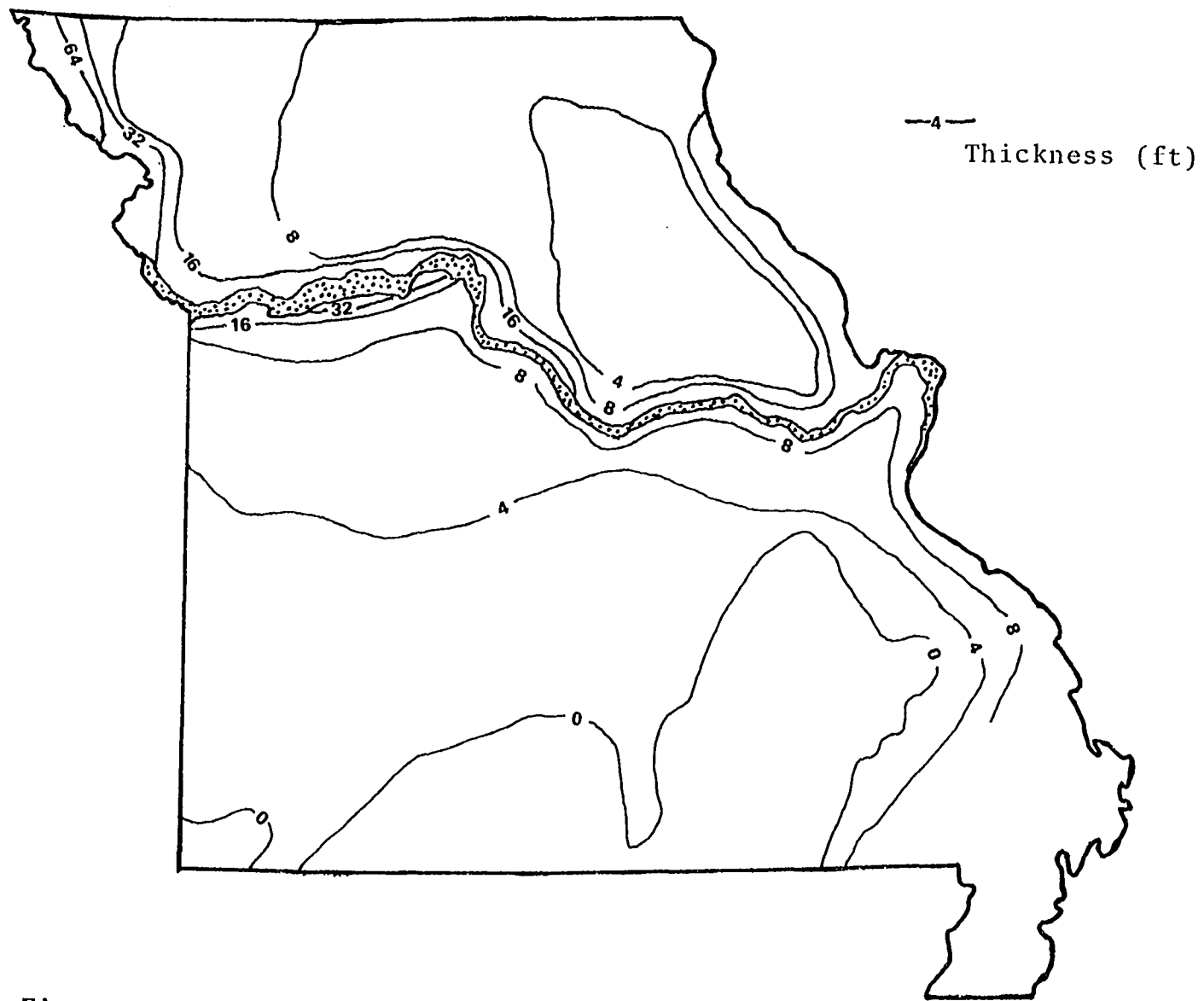
Figure 13. Generalized loess thickness in Missouri

(127 cm) in northcentral Missouri. Deposition along the lower Missouri River and along the Mississippi River was considered to be of lesser magnitude and it was suggested that a portion of the loess in northeastern Missouri may have been derived from a source in east-central Iowa. Krusekopf (91) made essentially the same observations and again indicated that the maximum thickness was in the north-western part of the state, about 75 ft (22.9 m).

The variations in texture of loess parent material, particularly in relation to soil development, were investigated by Springer (144) who studied soils with increasing distance from the bluff. He indicated that thicknesses up to 100 ft (30.5 m) along the bluff were present in north-western Missouri where the study was conducted. Samples tested from scattered sites up to 9 miles (14.5 km) from the bluff showed a decrease in the coarse silt (50-20 μm) fraction which was roughly considered exponential. The fine silt (20-2 μm) and clay (<2 μm) fractions both showed increasing trends away from the bluff which were more or less linear.

Pritchard (113), described two sections adjacent to the Missouri River in central Missouri where late, medial, and early Wisconsin loess were all separated by recognizable paleosols. In both sections, Loveland loess was also

identified. At the Miami section, a radiocarbon date of 15,134 ± 1,684 RCYBP in medial Wisconsin loess was reported. At Rock Port in extreme northwestern Missouri, a date of 21,360 ± 1,150 RCYBP was also reported at the base of the medial Wisconsin loess, above the Gilman Canyon.

Loess in east-central Iowa

East-central Iowa has been an area of considerable attention concerning loess occurrences and possibly one of the most abused. It is perhaps the only loess deposit in the world that has had its source area identified as a till plain. In 1897, Chamberlin (18) referred to this region in presenting the "Supplementary Hypothesis..." i.e. eolian origin for loess and made an observation that still persists:

> "Next to the border of the ice-sheet the loess is thick and typical, but graduates away with increasing distance from the ice border in a manner similar to the graduation away from the river valleys."

Although most researchers agreed that the "Iowan drift" was the significant source of loess in this area, the extent of deposits and relation to the supposed source were never sufficiently quantified. The influence of major streams as sources was not investigated extensively and therefore has long been neglected. In general, the trend of decreasing loess thickness away from the Iowan border has been considered to be the observed norm. In circular fashion the "Iowan drift" border was frequently mapped based on

discontinuities in loess thickness. In turn the "Iowan drift" terminous was then interpreted to be the source. Qualitative evidence has generally been presented to support the genetic relationship between the loess and the "Iowan drift", (2, 14, 18, 96) and this point was summarized by Leighton and Willman (96):

> "The outstanding feature of the loess deposits in eastern Iowa is the marginal relationship of the loess to the Iowan drift sheet."

Some discussion has been presented in support of riverine sources of loess as Leighton (95) had earlier observed that the loess associated with the Iowan area is thickest in three situations: (1) along the river valleys leading from the "Iowan drift"; (2) around the border of the Iowan drift, and (3) in the isolated paha (loess-covered hills). However, Shimik (134) also stated:

> "It is the writer's opinion that the accumulation of a comparatively large amount of loess along the border of the Iowan drift is explained by the fact that this border follows the larger streams of this part of the state, the Iowa, Cedar, Wapsipinicon... The deposit is thickest in the southern portions of the area, where the river valleys are broad..."

Hunter et al. (79), had studied loess-derived soils along a southeasterly traverse from Marshall to Henry County, and indicated that the source area for these soils was not clearly defined. Although they concluded that much of the loess of east-central Iowa originated from the "Iowan drift" plain, it was also suggested that Wisconsinan

drift had obliterated the source for some of the loess.
In addition, the Skunk and Des Moines Rivers were cited as
possible sources for lesser amounts of loess, presumably
derived from Wisconsinan outwash carried along these streams.

Lyon et al. (102) conducted mechanical analysis of loess
samples taken at uniform depth from three traverses in
east-central Iowa and indicated that the textural changes
showed a more pronounced relationship to the Iowa River than
the Iowan drift border. Complete sections were not sampled
in all cases; therefore loess thickness was not studied.

The work of Ruhe and associates (123) showed that the area
previously considered to be a drift plain was in reality an
erosional feature; the Iowan Erosion Surface (IES). Their
work concluded that although the Iowan was genetically
different than previously believed, i.e., not a separate
drift sheet or substage of a prior glaciation, it still
could be a source of loess. Running water was suggested
as the agent in formation of the Iowan surface, and the time
of formation was shown to be concurrent with loess deposi-
tion. Evidence for the depletion of fines was in the
presence of a stoneline or "pebble-band", the occurrence
of sand zones between an upper and lower loess zone,
particularly in the paha, representing the time of cutting
of the erosion surface.

The current concept of the Iowan is as a loess-mantled or loess-free erosion surface, indicated by the lack of a paleosol. The extent of Iowan surfaces has recently been presented by Hallberg et al. (65) and is considerably modified from the border given by Alden and Leighton (2) in that there is no clear-cut border, and the Iowan in effect is found throughout Iowa. The concept of a thin-loess mantled surface does not even hold up, as shown by Miller (105) who described thick loess sequences over an erosion surface on till. Vreeken (163) attributed such locally thick loess above Iowan surfaces to different rates of loess deposition.

The abundance of upland eolian sand in east-central Iowa, predominantly adjacent to the major streams (65, 169), suggests that eolian activity was more than sufficient to cause deflation on flood plains. The fact that these sands occur on both sides of the rivers indicates variable wind directions for deposition. The generalized loess thickness map for this area (118), indicates decreasing loess thickness away from the Iowa River in a southerly and northeasterly direction, the latter essentially leading to a loess-free surface, Figure 14. More detailed mapping, with the help of county soil surveys, produces a much better picture of local and regional trends (65), Figures 15a and 15b.
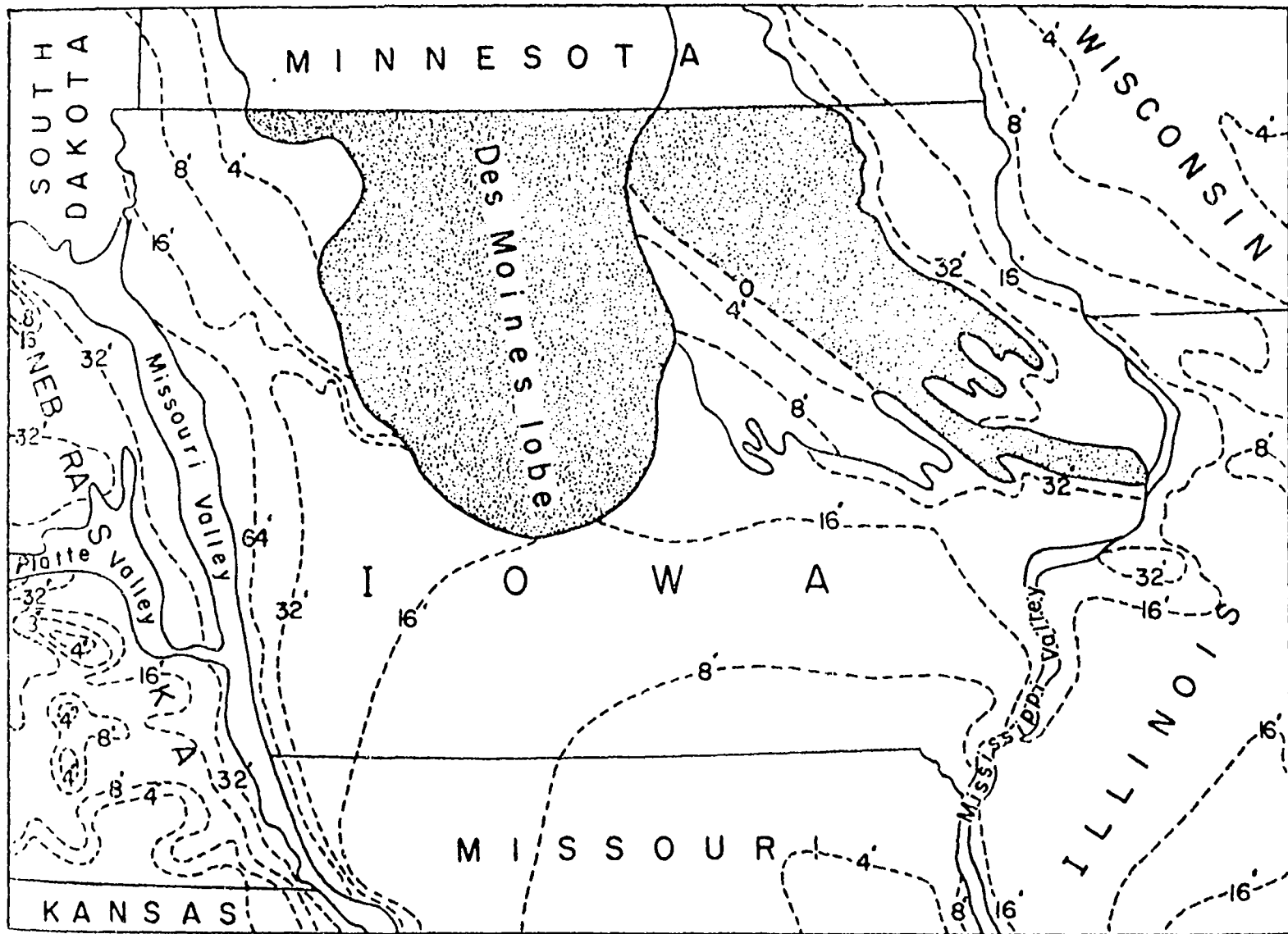
Figure 14. Generalized loess thickness in Iowa (118)

Thickness measurements on non-Iowan surfaces, where the
paleosol has been preserved, show thicker loess deposits
than adjacent Iowan areas. The change in thickness on
the Iowan surface appears directly related to the stream
valleys, except where inliers of preserved landscape in the
form of paha indicate locally thick loess. These isolated
areas might be considered local anomalies, unrelated to
the regional trends in loess deposition. The thicknesses
attained here, along with the presence of stratified sand
zones, indicate <u>local</u> sources for eolian sediments, i.e.
local drainageways. The amount of material being stripped
on summits and sideslopes certainly would have provided an
abundant supply for deflation. However, consider that the
amount of water required to erode in excess of 4 feet (1.2 m)
over such a large area as the Iowan would have been of a
magnitude to produce continual sheet wash, and possibly the
development of braided streams.

The time of Wisconsinan loess deposition in Iowa has
already been established and is sandwiched between 29,000
RCYBP in western and east-central Iowa and 14,000 RCYBP
where it is buried by Wisconsinan till in central Iowa.
Dates on organic matter from "Basal Wisconsin" loess in
east-central Iowa range from 20,700 $\pm$ 500 at Alburnett in
Linn County, to 29,000 $\pm$ 3,500 at Salt Creek in Tama County
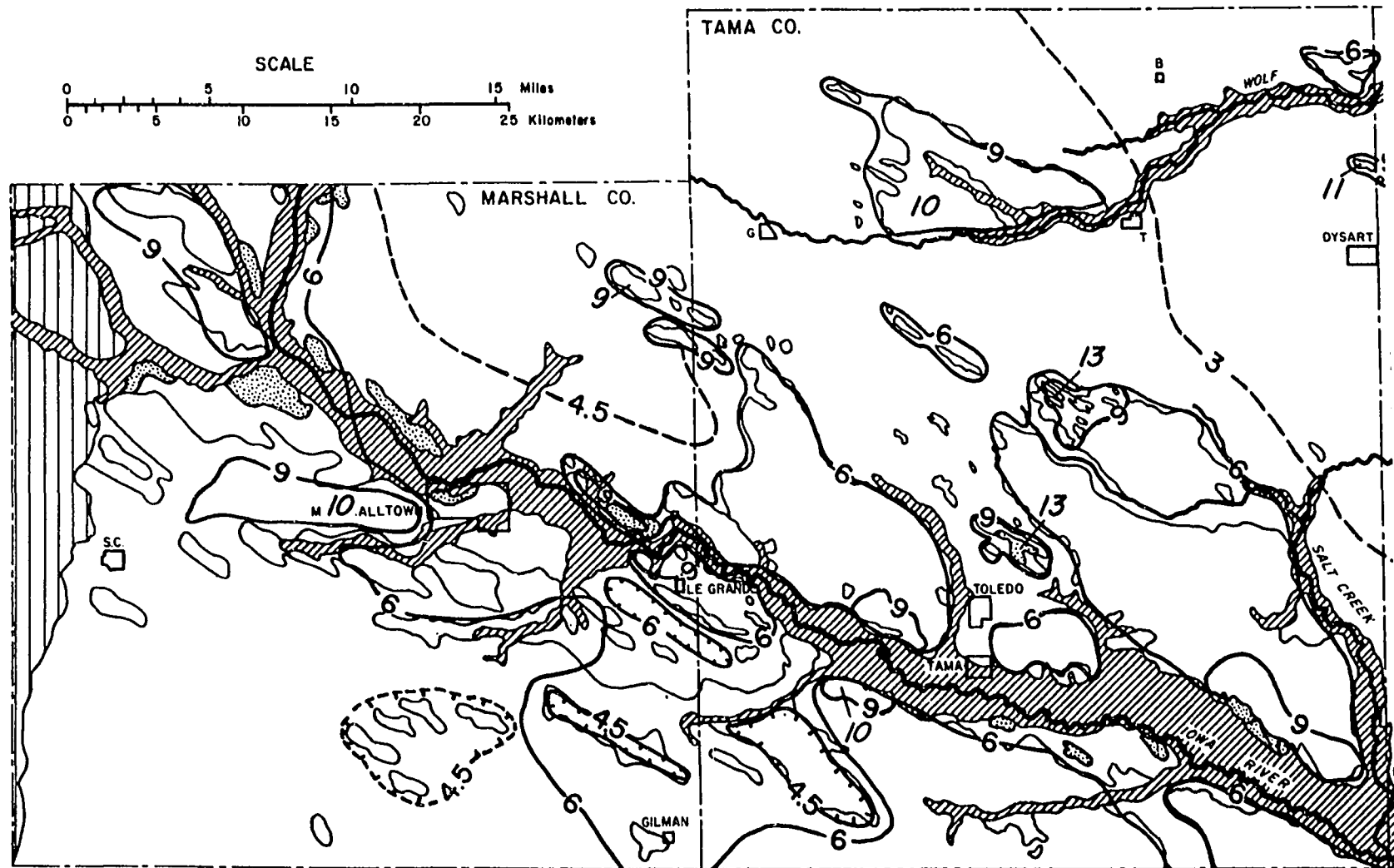
Figure 15a. Loess thickness in and around the Iowan Surface in Eastern Iowa
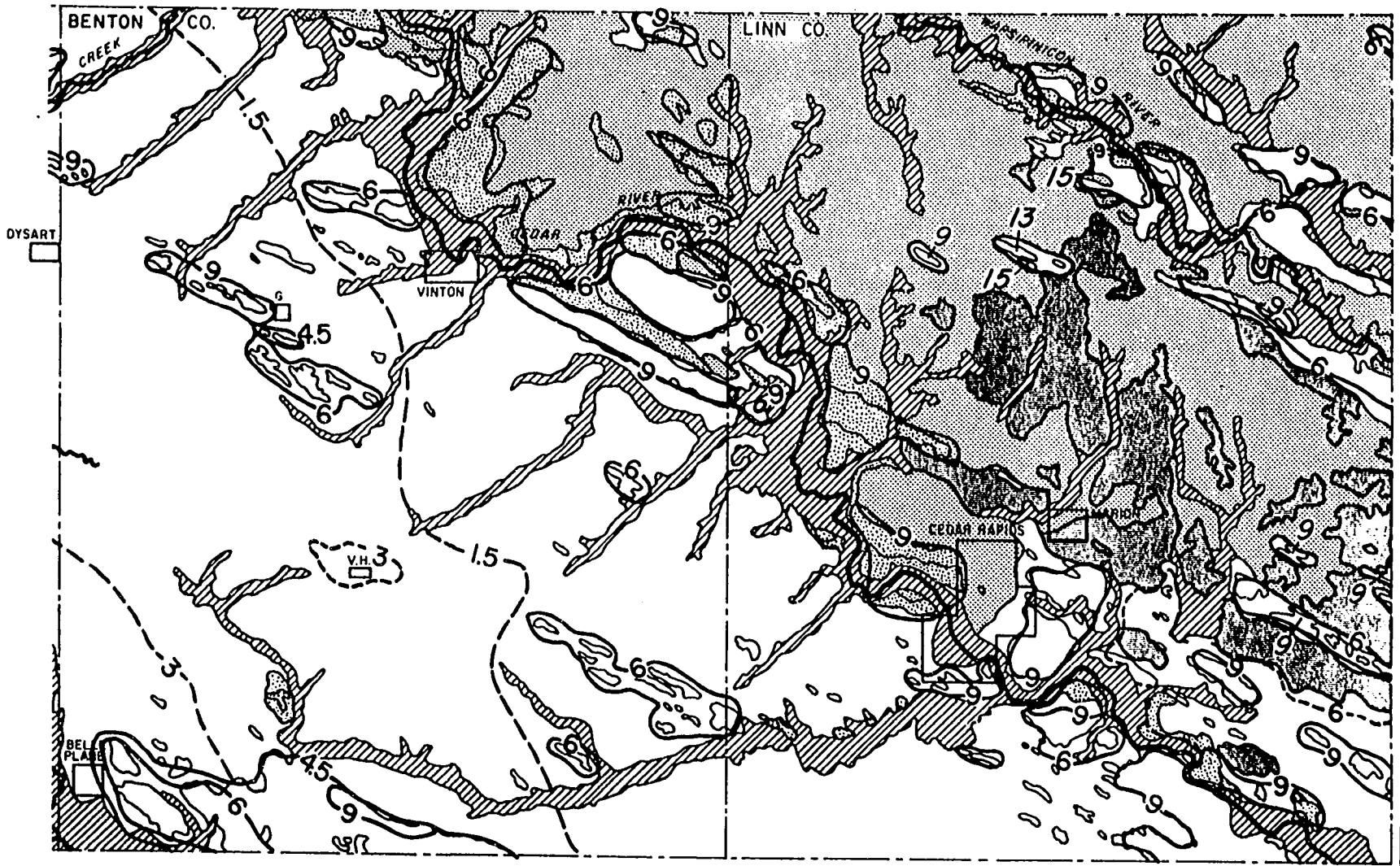
Figure 15b. Loess thickness in and around the Iowan Surface in Eastern Iowa

(118). Based on radiocarbon dates, Vreeken (163) placed the cutting of the Iowan between 18,300 and 20,300 RCYBP. Since this time span is concurrent with loess deposition, loess was being deposited while running water was eroding the land surface. Any material being deposited would have been subject to erosion. Since loess deposition ceased at approximately 14,000 RCYBP, this leaves about 5,000 years for loess deposition on the IES.

The fact that loess mantles the Erosion Surface conflicts with the concept of the Iowan as a source for loess. This is especially true where thick loess covers Iowan surfaces. The presence of "Basal Wisconsin" in and around the Iowan conflicts with the Iowan as a source, since the "Basal Wisconsin" predates the formation of the Iowan. Regionally, loess thins away from the major streams, in particular the Iowa River. Thick loess mapped on the basis of the former Iowan boundary, does not fit the concept of the Iowan as a source, as previously thought. The Iowan as a _local_ source of sand and silt certainly enhanced thick loess on locally preserved landscape, however this cannot be accepted as controlling the regional variations.

Field investigations

Field procedures   In order to provide data to test the theoretical loess thickness and particle-size models

presented, field measurement and sampling programs were
conducted. These consisted of traverses in west-central
and east-central Missouri, and east-central Iowa. Supplement-
al holes located off of the main traverses were used to
help establish a more regional view of the deposits. Sites
were selected from 7 1/2 minute topographic maps after a
general field review of the area being investigated. Except
where otherwise indicated, sample sites were situated on
primary upland divides, where measured thickness was
assumed to be maximum.

Boreholes were made with a Giddings hydraulic soil
probe mounted on a four-wheel drive 3/4 ton pickup truck.
Three-inch diameter borings were made to a depth of refusal,
after which a two-inch diameter sampler was used. Except
for a few supplemental observations for particle size
samples, all borings were advanced through the loess, and
samples of the underlying stratigraphic unit were also
taken. Sampling with this technique produces a continuous
core which was laid out in entirety.

Description of the core was made, noting thickness,
stratigraphic unit, weathering zones, Munsell moist color,
existence of carbonate concretions or nodules, iron and
magnesium staining, and general consistency. Bag samples
for mechanical analysis were taken at 1 1/2 to 2 ft.

(0.5 to 0.6 m) intervals, or at naturally occurring material breaks. Except where loess thickness was less than 60 inches (152.4 cm), samples of the soil profile were not taken.

Three-inch diameter core samples were wrapped in plastic wrap and aluminum foil and transported back to the laboratory for bulk density and moisture content determination. Where time permitted, these measurements were made in the field. In addition, the Iowa Borehole Shear Test (BST) was used to measure in situ drained shear strength at selected sites.

<u>Central Missouri</u>   In central Missouri, two north-south traverses spanning the Missouri River were sampled. The location of these traverses was designed to investigate the influence of width as an important source variable. The present width of floodplain as measured from topographic maps for traverses MW and ME are 7.05 miles (11.3 km) and 1.80 miles (2.9 km) respectively. In addition to the main traverses, isolated sites were also chosen to supply information in critical areas, e.g. where the course of the river changed abruptly. Sampling sites are regionally shown in Figures 16 and 17. Individual sites are located on topographic quadrangles and given in Appendix B.

Loess investigations in Missouri, as previously

Scale 1:500,000
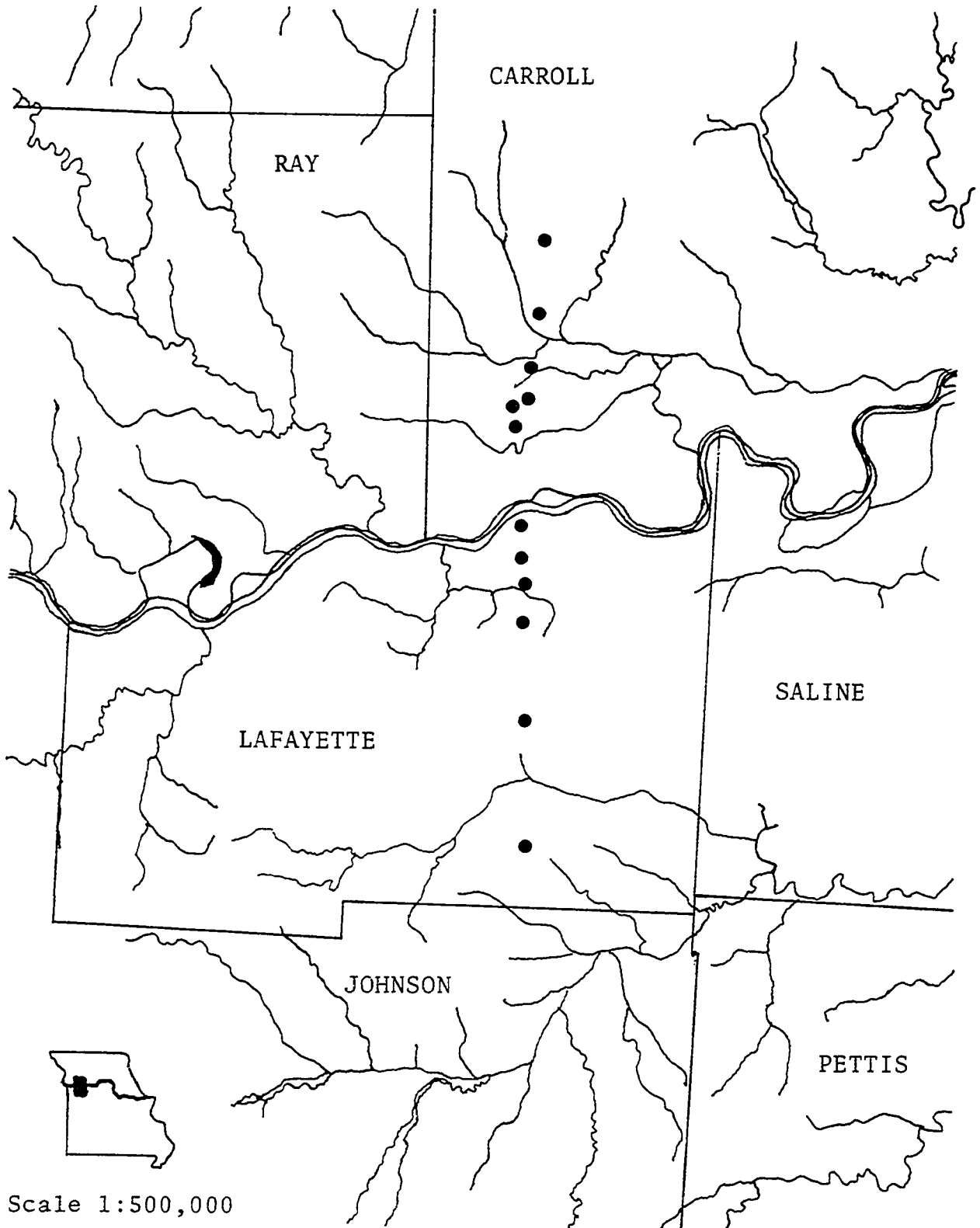
Figure 16. Location of sampling sites: MW traverse
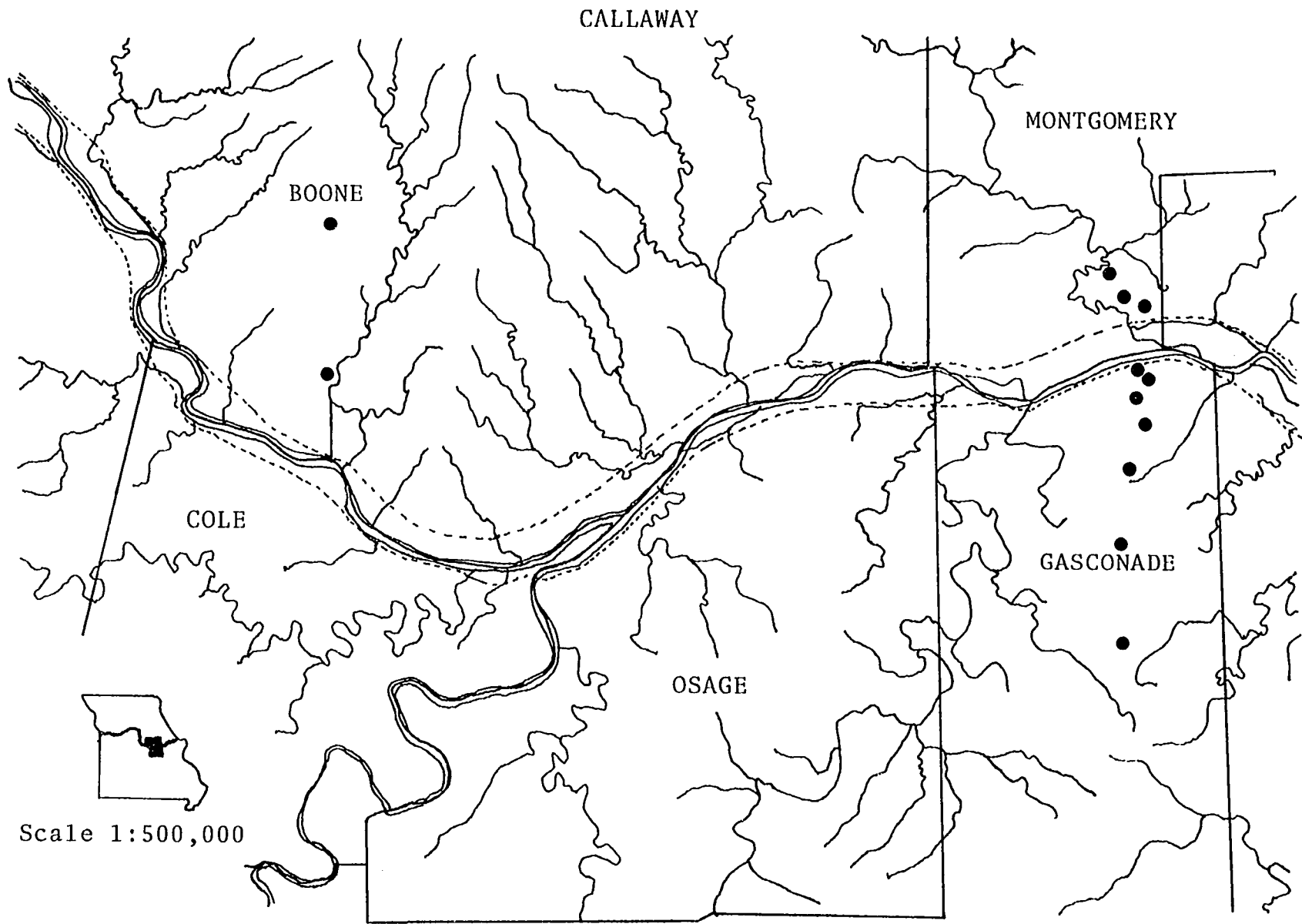
Figure 17. Location of sampling sites: ME traverse

outlined, have not been conducted extensively and for the most part have been on a localized basis, with little attention given to regional trends. This area is a key location in presenting evidence for the variable winds hypothesis, in that the configuration of the source is predominantly east-west, and the source width changes abruptly and remains fairly constant over large distances.

East-Central Iowa   In Iowa, observations were made across the Iowa River in the east-central portion of the state. The Iowa River, previously neglected as a potential source because of the controversey of the "Iowan", presents a chance to investigate deposits in this geologically complex area. Regional location of sites is shown in Figure 18, and individual sites are again given in Appendix B.

Supplemental sampling   In addition to the two main sampling areas described above, supplemental sites for density and shear strength data were investigated. These locations were mainly in northeast, southeast, and central Iowa, with a few additional scattered sites. The locations of all sites for density measurements and shear strength tests are shown in Figures 19 and 20 respectively.
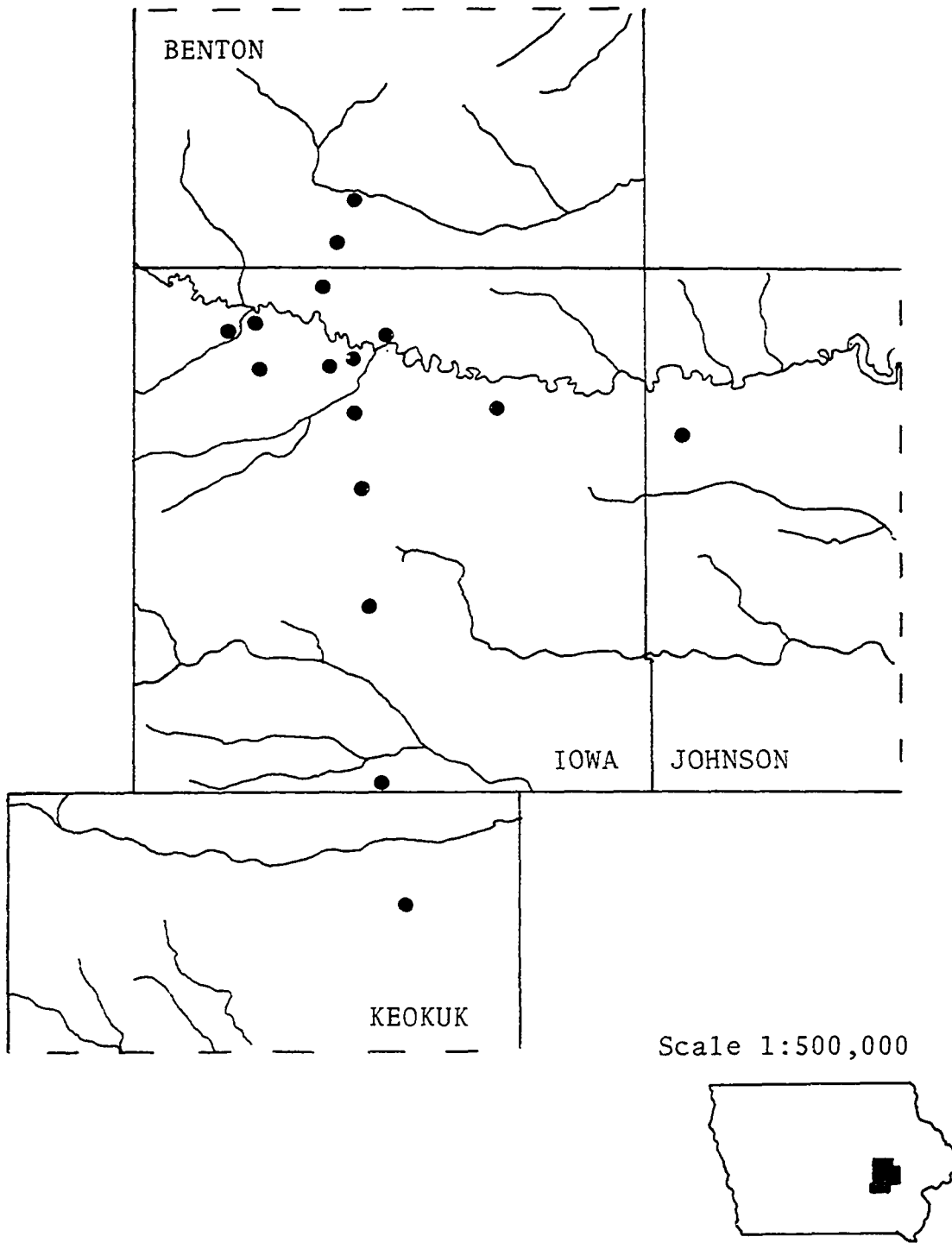
Figure 18. Location of sampling sites: LH traverse
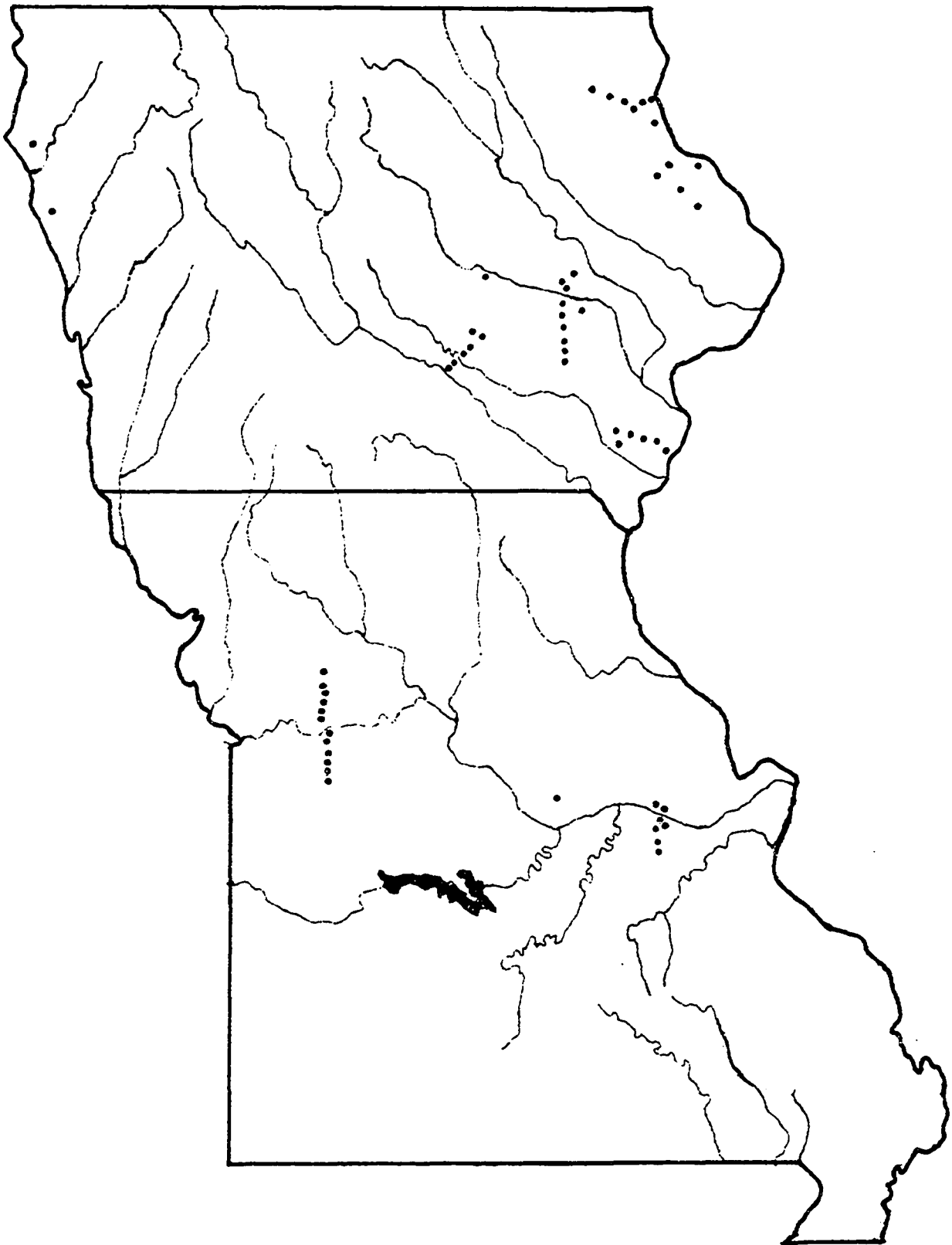
Figure 19. Location of density measurement sites
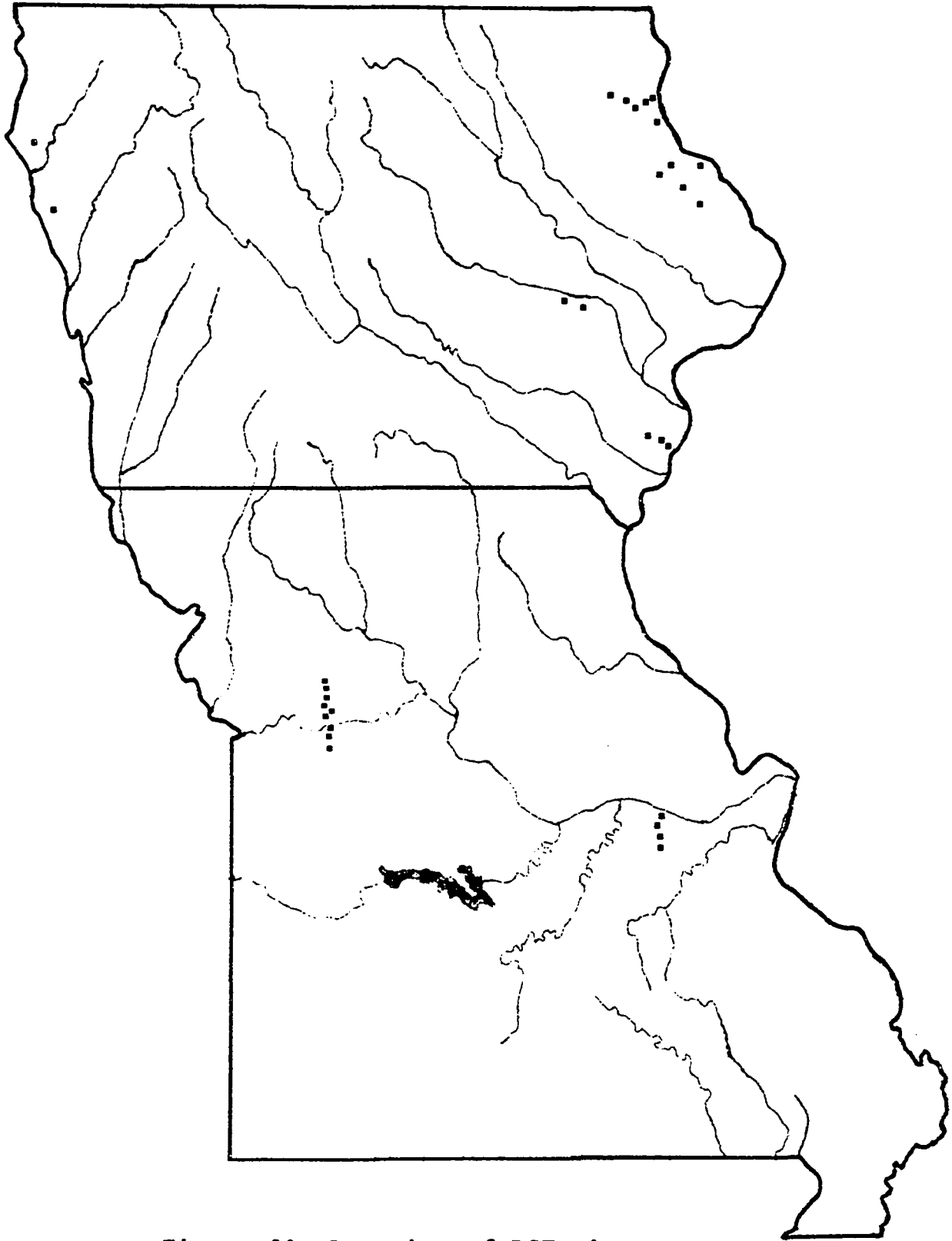
Figure 20. Location of BST sites

Particle size analysis

Laboratory procedure   Particle size analysis of
selected samples was determined by a modification of the
pipette method of Kilmer and Alexander (85), and more
recently of Walter et al. (164). Samples were allowed to
air-dry to hygroscopic moisture content before pulveriza-
tion and were then hand pulverized with mortar and rubber-
tipped pestle to pass a #40 (.42 mm) sieve. A sample of
approximately 10 grams was first placed in a 300° F oven
for a minimum of 24 hours to remove hygroscopic moisture.
The exact ovendry weight was then determined to the nearest
0.0001 gram using an analytical balance. The sample was
then placed in a beaker with 100 ml distilled water, and to
this soil-water suspension 10 ml of dispersing agent was
added. The dispersing agent was composed of a 4.8%
solution of Calgon (sodium hexametaphospate) buffered with
0.8% sodium carbonate.

The suspension was then transferred to a 1000 ml grad-
uated cylinder (hydrometer jar) and distilled water was
added to produce a total suspension of 250 ml. This was
then allowed to stand for a minimum of two hours. Disper-
sion was attained utilizing the air-jet dispersion apparatus
described by Chu and Davidson (24), and shown in Figure 21.
All suspensions were agitated at 25 psi (1.76 kg/cm^2) for 5
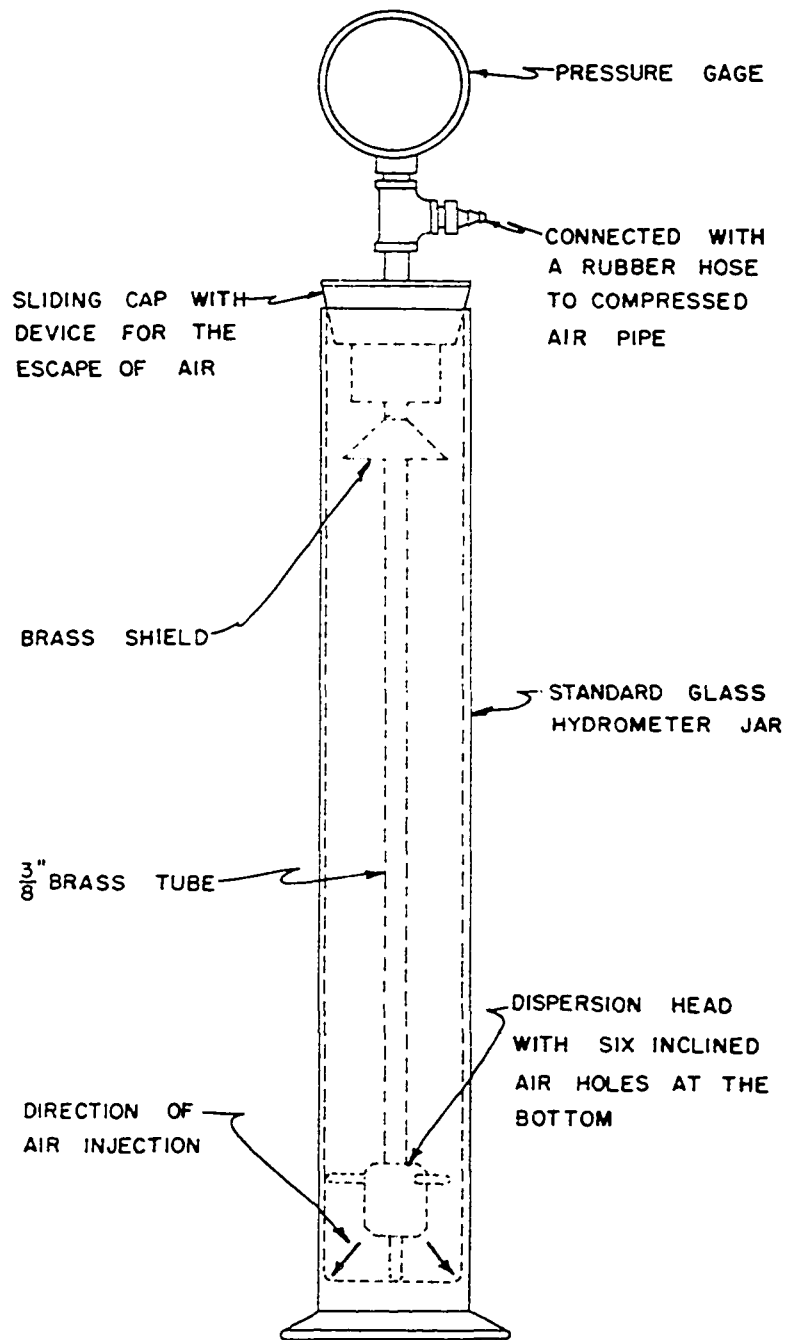
Figure 21. Air-jet dispersion apparatus

minutes. Following dispersion, the suspension was brought
to final 1000 ml volume with distilled water.

Suspensions were hand stirred vigorously for a period
of time greater than 30 sec., but less than 1 min., and
then allowed to begin settling. Samples were drawn from
the suspension using a Shaw pipette rack and a 25 ml pipette,
at depths and settling times calculated from Stoke's Law.
Size fractions were designated as follows:

>0.074 mm	Sand
0.074-0.020 mm	Coarse silt
0.020-0.002 mm	Fine silt
<0.002 mm	Total clay
<0.001 mm	Fine clay

The sand fraction was collected following completion of the
pipette procedure by washing the remaining soil through a
#200 sieve. All samples were oven dried for a minimum of
24 hours after which the exact weight to the nearest 0.0001
gm was determined and corrected for the addition of the
dispersing agent.

Statistical control   To provide a measure of proce-
dure variance and reliability of particle size data, stan-
dard control samples were repeatedly analyzed throughout the
duration of pipette analysis. Two control samples were

Table 3. Pipette control statistics

	Number of Observations	Mean	Standard Deviation	Range	Std Error of Mean	Variance	Coefficient of Variation
Control Sample 1							
Coarse Silt	9	33.8	1.7	4.1	0.6	2.8	4.9
Fine Silt	9	32.7	1.6	6.2	0.5	2.5	4.9
Total Clay	9	32.9	1.5	3.9	0.5	2.3	4.6
Fine Clay	9	27.7	2.3	7.2	0.8	5.2	8.2
Control Sample 2							
Coarse Silt	30	36.3	2.1	9.2	0.4	4.6	5.9
Fine Silt	30	30.7	1.5	7.8	0.3	2.1	4.7
Total Clay	30	32.1	1.2	4.0	0.2	1.4	3.7
Fine Clay	30	28.4	1.4	5.8	0.3	2.1	5.0

repeatedly analyzed throughout the duration of pipette
analysis. Two control samples were used and results of
the individual tests are given in Appendix D. An analysis
of variance on these results is presented in Table 3.

Data presentation   Because of the ambiguities which
are present in current literature concerning the location
of samples for reporting trends in particle size, a scheme
was devised to describe and integrate the texture of the
loess at each site through the entire thickness. As
previously discussed, the complexity of loess deposition
results in some variation in textural composition with
depth. To account for this and yet describe each site with
one discrete particle size distribution, an areal summation
method was used.

A typical textural profile is shown in Figure 22, with
cumulative percent plotted versus depth. The amounts of
total clay, fine silt, and coarse silt at each sample
location have been shown as points. Straight line connection
of these points identifies the limit of each fraction. The
total particle size of the site is taken as the area
bounded by the lines 0 to 100% between the base of the
loess and the upper limit of 60 inches (152.4 cm). The
individual fractions are represented by the area between
limiting lines as shown. The percent of each fraction is
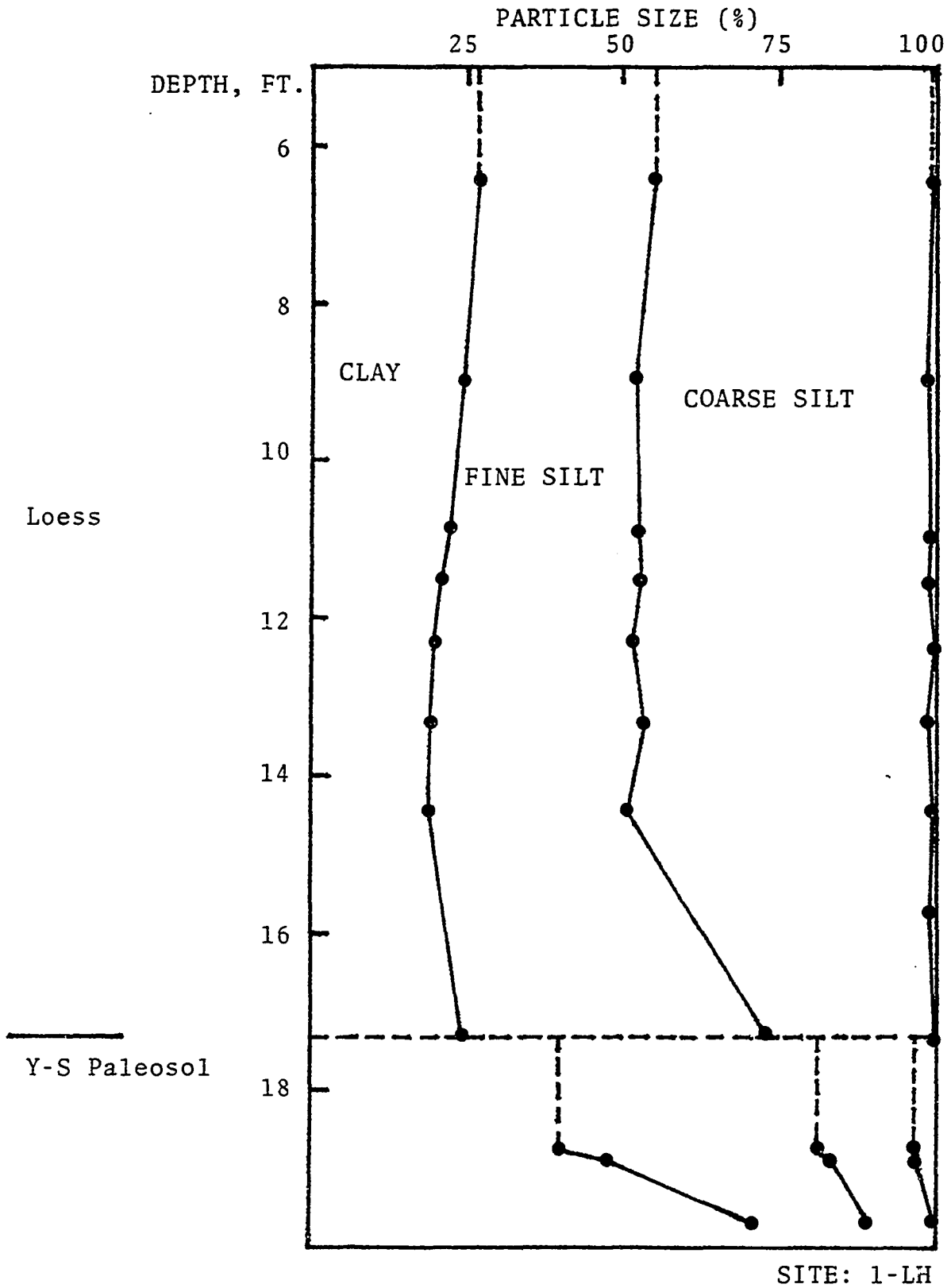
Figure 22. Area method particle-size determination

a simple ratio of fraction area to total area. Areas of
individual fractions were measured using an electronic
digitizer; essentially a automatic planimeter. The average
of three determinations was used to report respective
percentages.

This method assumes a linear relation between
successive points with depth, and a vertical distribution
from the upper limit to the first point, and likewise from
the last sampling point to the base, the latter being used
where samples were not taken immediately above the contact
with the underlying material. The area-method was used to
describe the unweathered texture for both the Missouri-West
transect and the Iowa River transect. However, for the
Missouri-East transect, where the loess was too thin to
describe the condition of unweathered material, clay-free
silt fractions were calculated based on the total sampling
profile.

Bulk density - moisture content

Field density and gravimetric moisture content deter-
minations were made at selected depths on intact 3-inch
cores to establish spatial and vertical variations. All
volume measurements were made using the Eley Volumeter,
essentially a core measurement method which accurately

measures soil volume to 0.01 cm^3. The device is inserted into one end of a core and the excess material trimmed to give an initial volume. A "disk" of the measuring core is extruded with the plunger screwhandle, trimmed flush, and weighed to the nearest 0.01 gm. A final volume reading is taken, the difference from the initial volume being the volume of the disk. With wet weight and volume, the wet or field density is calculated. A minimum of four measurements was made from each core sample horizon with the average of these individual values reported.

Field moisture content was made on samples taken from density core trimmings to convert field density to dry or bulk density. When made in the field, moisture content was measured with the Speedy Moisture Meter; in the lab, oven dry moisture content was measured. Variation between results of these two methods is considered negligible.[1]

Shear strength

The Iowa Borehole Shear Test (BST) was used to give a measure of the consolidated-drained in situ shear strength. This device has been discussed elsewhere (69 , 101 , 170) and is essentially a direct shear test performed on the inside walls of a borehole. This technique was considered to be

_____

[1]Personal communication, G.R. Hallberg, Iowa Geological Survey.

more useful for this investigation, since discreet values
of internal friction, ϕ, and cohesion, c, could be deter-
mined rapidly at a variety of locations. Data are reduced
in the field, and typically appear very linear, Figure 23 .

Clay aggregation-dispersion

The degree to which clay minerals and clay-size particles
may be aggregated together or attached to host silt grains
has been demonstrated to be an pertinent factor in eolian
processes. Gradation changes in a loess deposit, with
increasing distance from the source, normally do not consider
such aggregation. This is primarily because of the fact
that standard procedures of particle-size analysis tend to
destroy any natural particle cementation (31b). This
brief study was directed towards determining the existence
and/or extent of such agglomerates. Modified-dispersion
pipette analysis and scanning electron microscopy (SEM)
were used to investigate aggregation effects on gradation.

Samples from selected profiles were prepared for
pipette analysis as previously discribed with the following
modification; dispersing agent was not added to the soil-
water suspension. The effects of air jetting are still
present, however the impact of particles in water has less
influence than in air (92). Therefore, results may give a
better representation to the particle size distribution
immediately following eolian transport and deposition. These

IOWA BOREHOLE SHEAR TEST

PROJECT __Loess__

SITE __3-ME__ HOLE __1__

DEPTH __40 in.__ W.T. __—__

DATE __31 May, 1978__

SOIL __loess__

TECHNICIANS __Al Lutenegger &__

__Ron Elsner__

BHS PLATE SIZE (5) (1)SQ IN.

MOISTURE CONTENT _____ %

DRY UNIT WEIGHT _____

	TRIAL	1	2	3	4	5	6	7	8	RESULTS	
τ_1	Gauge	21.5	28.0	35.0	42.0	48.0				RUN # 1	
	psi	5.85	7.6	9.5	11.4	13.0				r: 0.999	
σ_1	Gauge	12.5	27.0	40.0	55.0	70.0				c: 4.5	psi
	psi	2.8	6.6	10.0	14.0	17.9				φ: 25.7	deg
REMARKS											
τ_2	Gauge									RUN #2	
	psi									r:	
σ_2	Gauge									c:	psi
	psi									φ:	deg
REMARKS											
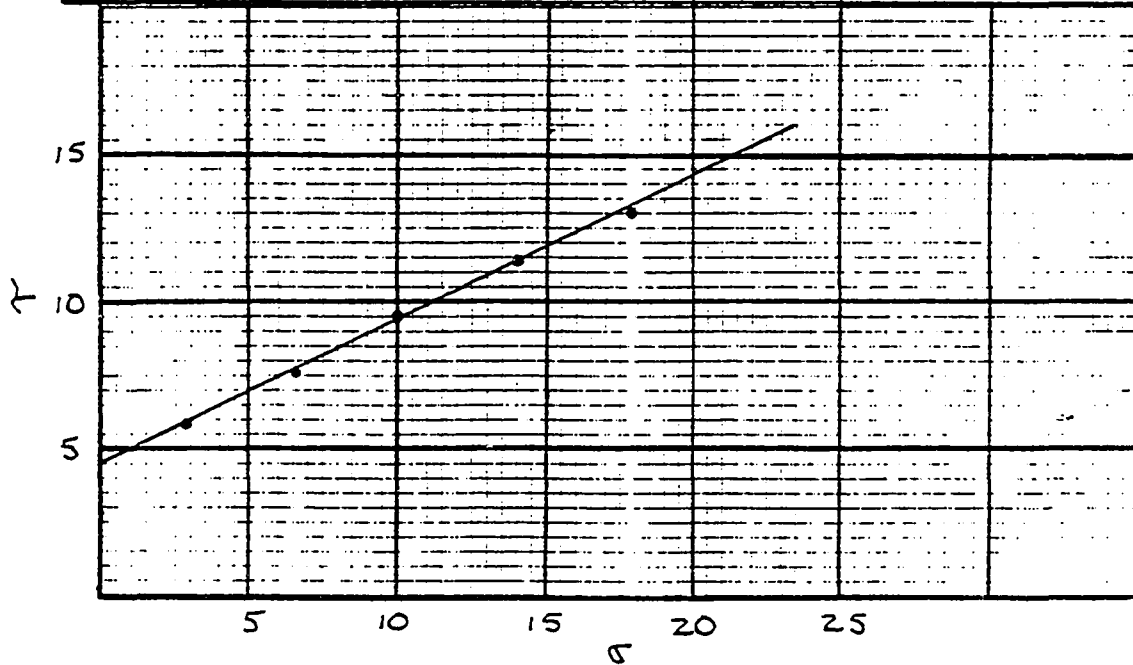
Figure 23.   Typical BST data

results will be compared to standard test results.

Particle size analysis using the air-jet dispersion apparatus have also shown that the time of dispersion affects results (24), and in studying particle size changes, this may be an important factor. An attempt was made to illustrate the importance of this variable by testing two samples from the Iowa River transect; 4-LH-3 and 17-LH-9. These samples were chosen to represent typical near-source material, and sediment at some distance from the source. Dispersion times were varied from 0.5 to 5.0 minutes, and in addition, no dispersing agent was used. Extrapolation to zero time on a plot of percent of each fraction versus time should give an indication of the undis-turbed particle size. The mean value of three repetitions was used to test this hypothesis, and results will be presented in a later discussion.

As previously discussed, SEM has been used quite effectively to display the microstructure of loess particles and the nature of dust. With this in mind, samples were selected from both the Iowa River transect and Missouri-West transect for SEM observation. Air dried loess samples were hand-pulverized with a mortar and rubber-tipped pestle, the identical preparation to that used for the standard pipette

analyses. Following pulverization, samples were sieved with a vibratory shaker for ten minutes through a #200 (74 μm) and #325 (44 μm) sieve, with the material passing the #325 retained in a pan. Random samples were extracted from each of the three sizes; > 74 μm, 74-44 μm, and < 44 μm for viewing, and in addition, clod samples of untreated loess were also selected for viewing. This work was primarily conducted to visually verify any occurrence of agglomerated particles before pipetting.

RESULTS

Random Walk Model

Case I: unidirectional wind

The random walk simulation of particle motion for wind blowing normal to an infinite linear source was used to investigate the effect of source efficiency on the trend of particle accumulation versus distance. In order to smooth-out the generated distributions, a three-point running average was used to calculate the number of particles falling within the first 10 units. Thereafter the three-point average was also used to determine the number of particles at specific locations; for example, the number of particles at a distance of 40 is calculated as: $(P_{39} + P_{40} + P_{41})/3$. It should be noted that this three-point averaging technique destroys the maximum accumulation at the first deposition location since the first average utilizes points 1, 2 and 3. Values less than one indicate that fewer than three particles fell within the averaging zone. This occurs at large distances, a result of the random nature of movement. For zero-settling velocity, all particles are taken as the same size, hence the number of particles may be used as a measure of thickness. Linear regressions presented are based on particle counts greater than one.

Figures 24 thru 26 present the results of trial walks
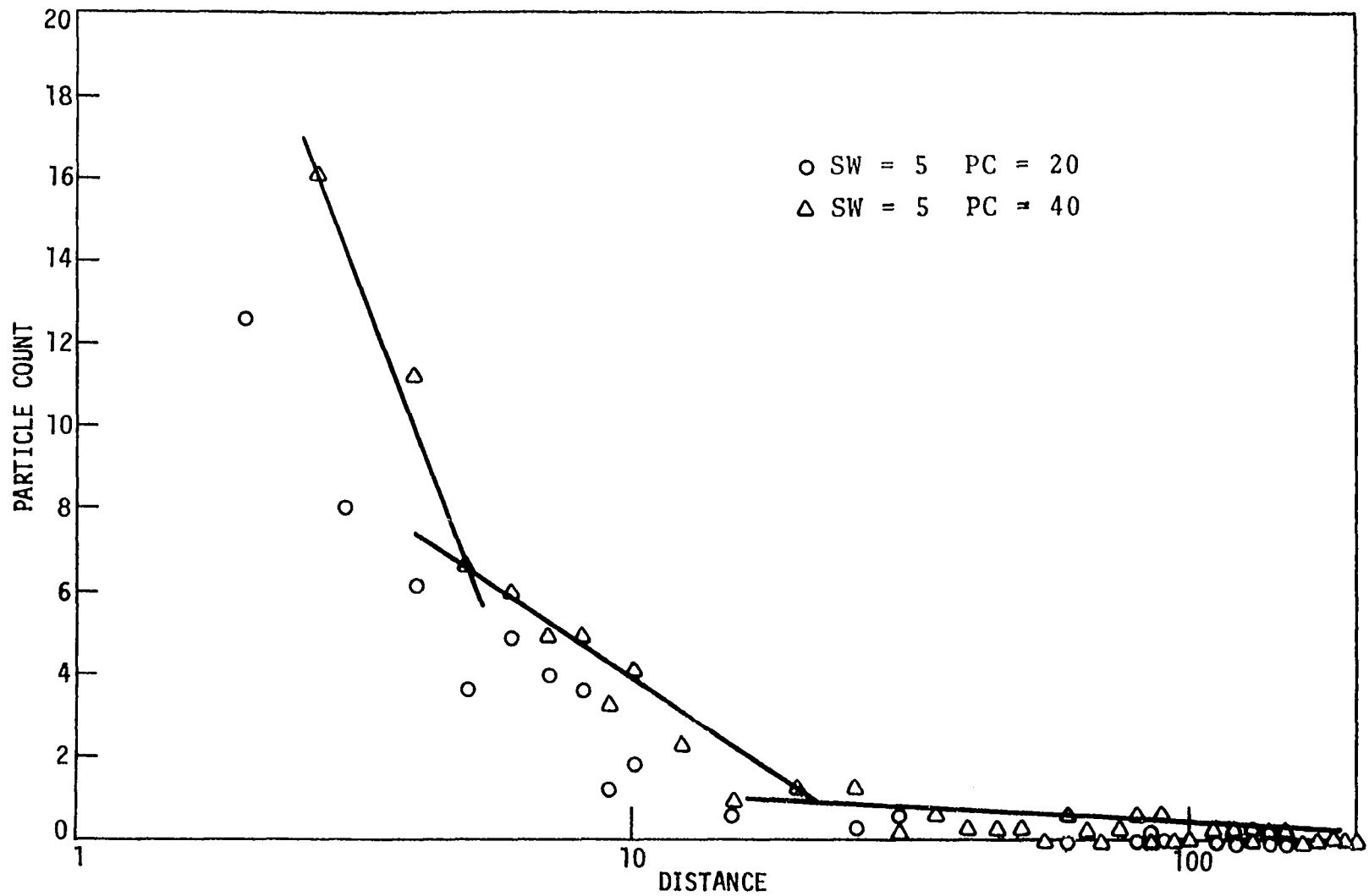
Figure 24. Unidirection wind: source width = 5; particle
concentration = 20 and 40
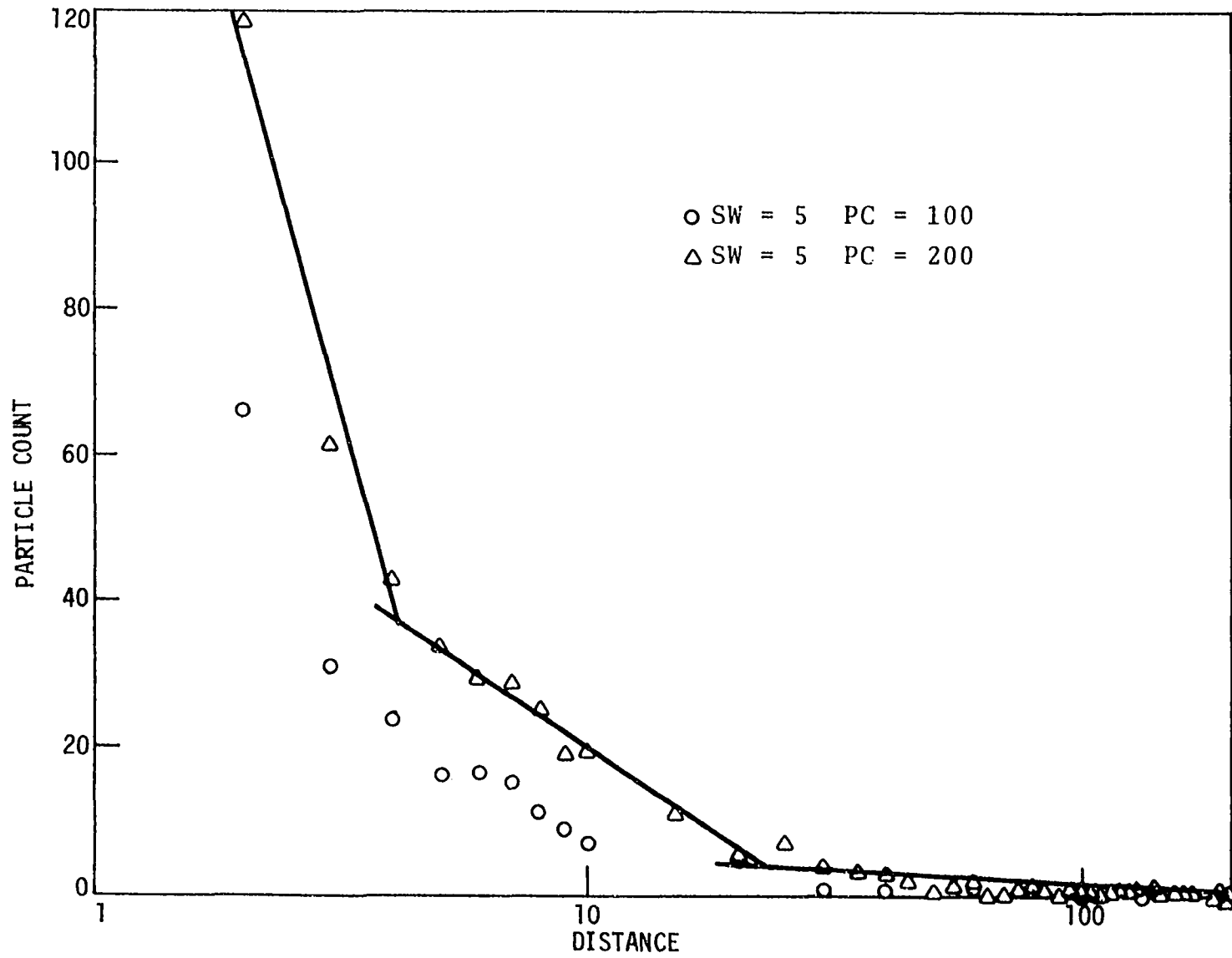
Figure 25. Unidirectional wind: source width = 5; particle
concentration = 100 and 200
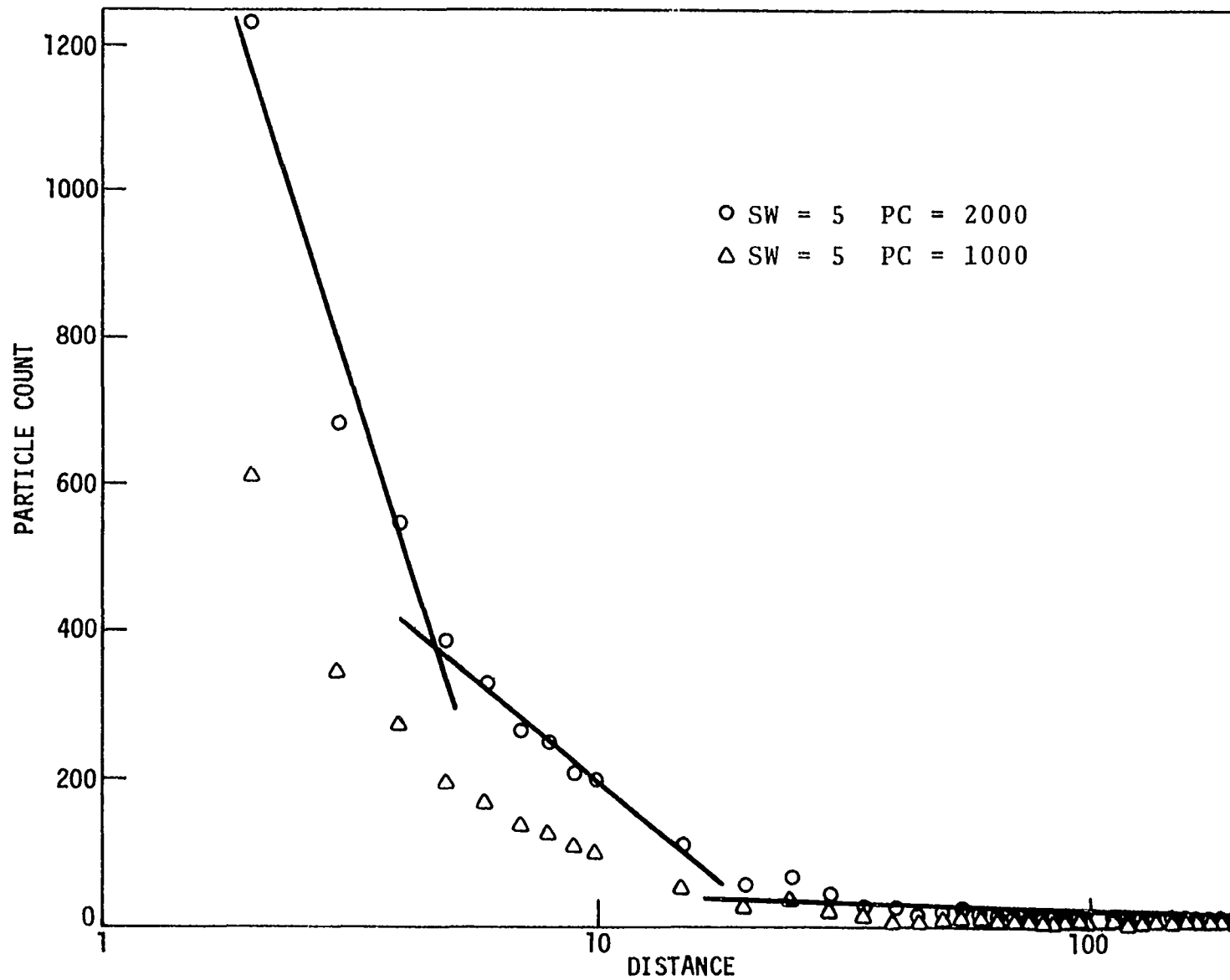
Figure 26. Unidirectional wind: source width = 5; particle concentration = 1000 and 2000

in which source width (SW) was held constant at five units while source point particle concentration (PC) was varied from 20 to 2000. Semilog plots of distance vs particle count, Figures 24, 25, and 26, show a somewhat curvilinear trend which may be represented by a series of straight-line segments as shown. In this case, trilinearity results in an fairly good description of the decreasing number of particles with increasing distance. Note that at distances greater than about 100 units, the number of particles is very low, resulting in near uniform minor increments of thickness. Transformation of these data to log-log scale results in linear distance vs particle count trends, Figures 27 and 28. At low values of particle concentration, low resolution occurs and therefore scatter is greatest at larger values of distance, indicating that the variance of particle count may not be a constant but rather increases with distance.

The accumulation of particles at various positions can also be viewed as accumulations with time, and as such is represented statistically as a Poisson event. A unique property of the Poisson distribution is the fact that the variance is equal to the mean.

The variance can be calculated by letting

$$Y = \log C$$

Figure 27. Log distance vs log particle count: Case I,
SW = 5, PC = 20, 40 and 100
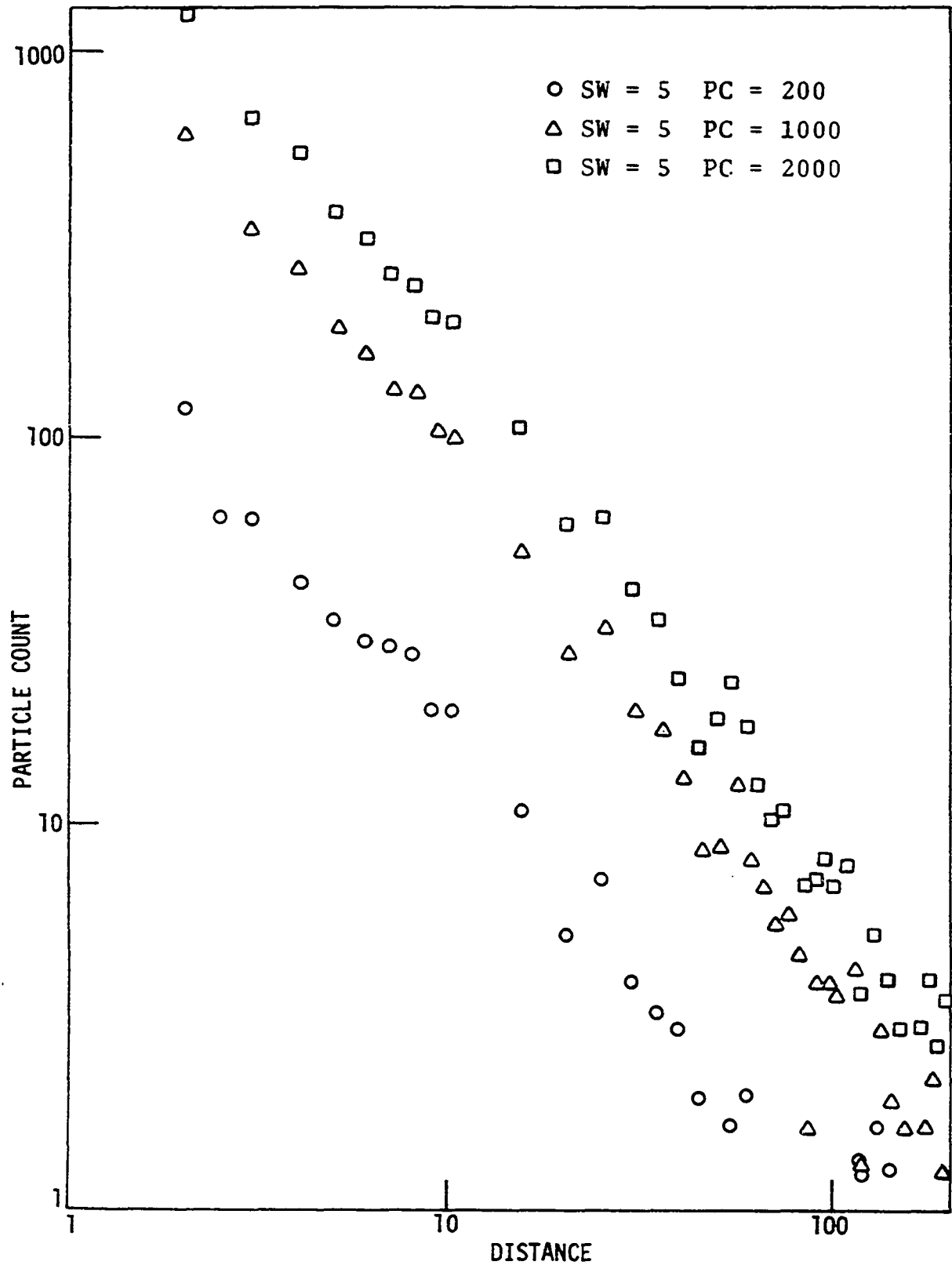
Figure 28. Log distance vs log particle count: Case I,
SW = 5, PC = 200, 1000 and 2000

where

    C = particle count

then

$$V[Y] = V[C] \times \left(\frac{\partial \log(X)}{\partial X} \right) \Big|_C^2$$

and

$$V[Y] = V[C] \times \frac{1}{C^2}$$

substituting gives

$$V[Y] = \frac{1}{C}$$

Therefore, the variance of particle count is equal to the reciprocal of the count itself.[1] Note that in Figures 27 and 28, an increase in particle concentration (and hence total number of particles) appears to increase resolution and shows less scatter. This is particularly evident for particle concentrations of 1000 and 2000 shown in Figure 28. Because of the apparent goodness of fit of log-log plots, this form of data presentation will be used for the remainder of the data. It should be noted that all regressions which will be presented are significant at 1%.

Increasing particle concentration may be considered analogous to either increased duration of blowing wind or

[1] This proof was suggested by H. T. David, personal communication, July 13, 1979.

increased velocity. Considering constant wind velocity, the capacity for the wind to transport should be constant. Increasing the time of blowing then should result in increasing a proportional amount of eroded material. Where source width has been held constant, increased particle concentration is shown to change the distance-particle count plot by "offsetting" the linear relationship, Figures 27 and 28. The slope of the lines appears to be essentially the same and the results may be described as a "family" of curves for a given source width. In fact, the intercept of a least squares regression calculated for each case, increases systematically with increasing particle concentration, from 25.7 to 3861, as shown in Figure 29. Slopes of the individual plots are nearly identical:

PC	Slope	r
20	-1.0599 $\pm$ 1.2773	0.9263
40	-1.2913 $\pm$ 1.0797	0.9702
100	-1.2754 $\pm$ 0.7594	0.9817
200	-1.1512 $\pm$ 0.6180	0.9762
1000	-1.3650 $\pm$ 0.5145	0.9887
2000	-1.3723 $\pm$ 0.4993	0.9937

The $\pm$ entry represents a 95% confidence interval and r is the correlation coefficient of the linear regression.

Figures 30, 31 and 32 show the results of three cases where source width has been changed, while particle concentration has been held constant. The total amount of material being transported is equal to SW x PC, therefore wider sources
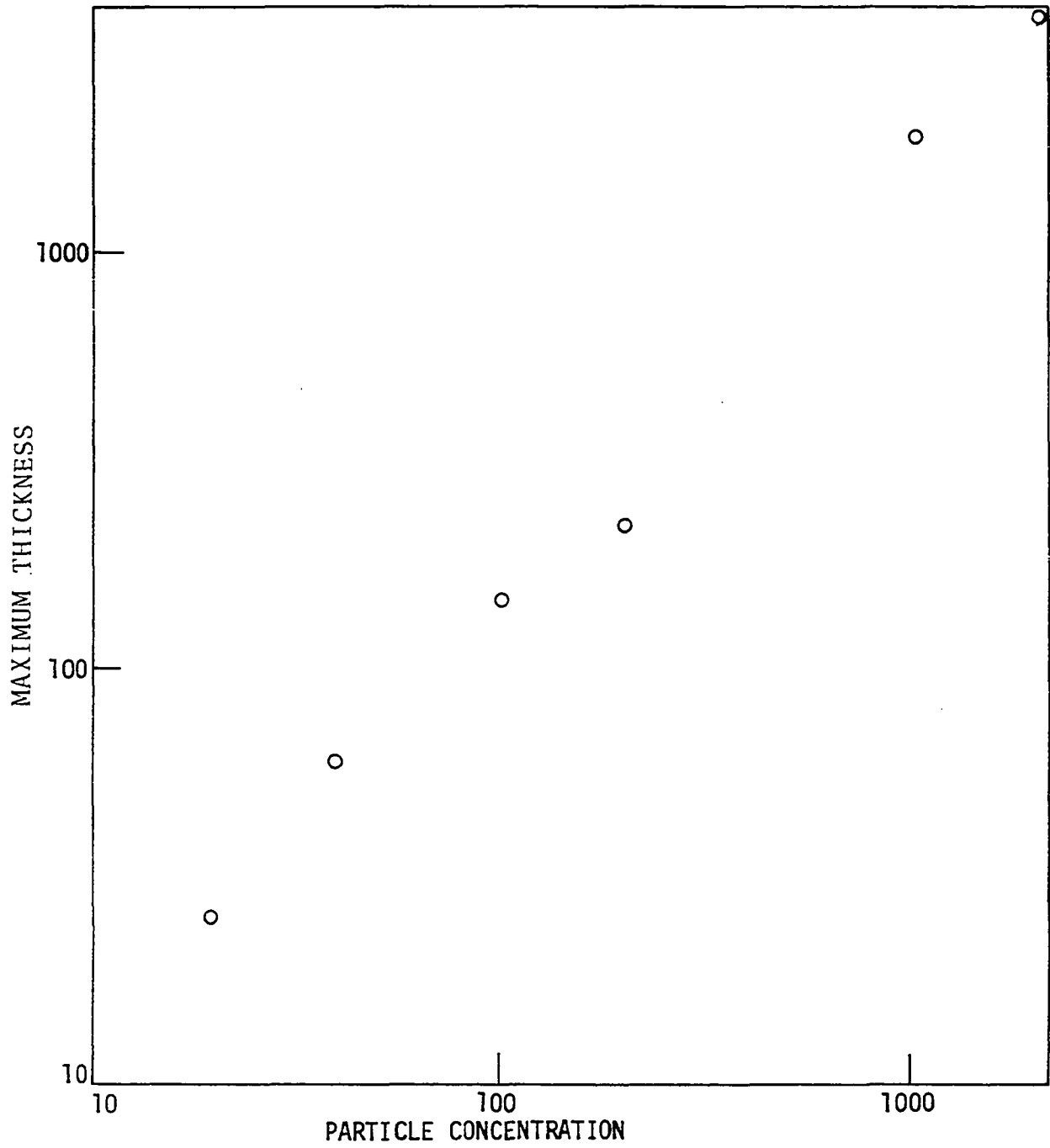
Figure 29. Log PC vs intercept for data shown in Figures
27 and 28
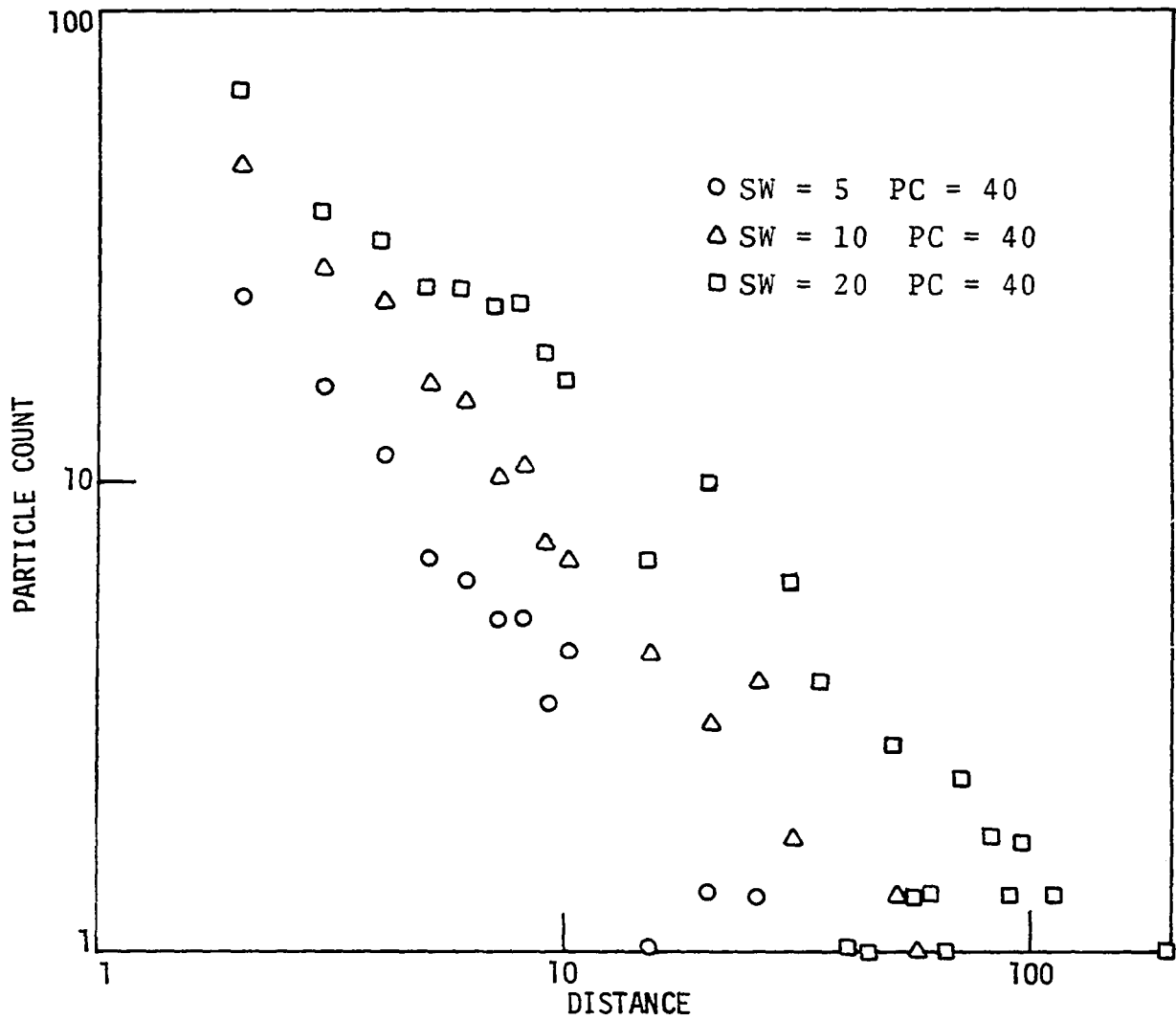
Figure 30. Log distance vs log particle count: Case I, SW = 5, 10 and 20, PC = 40
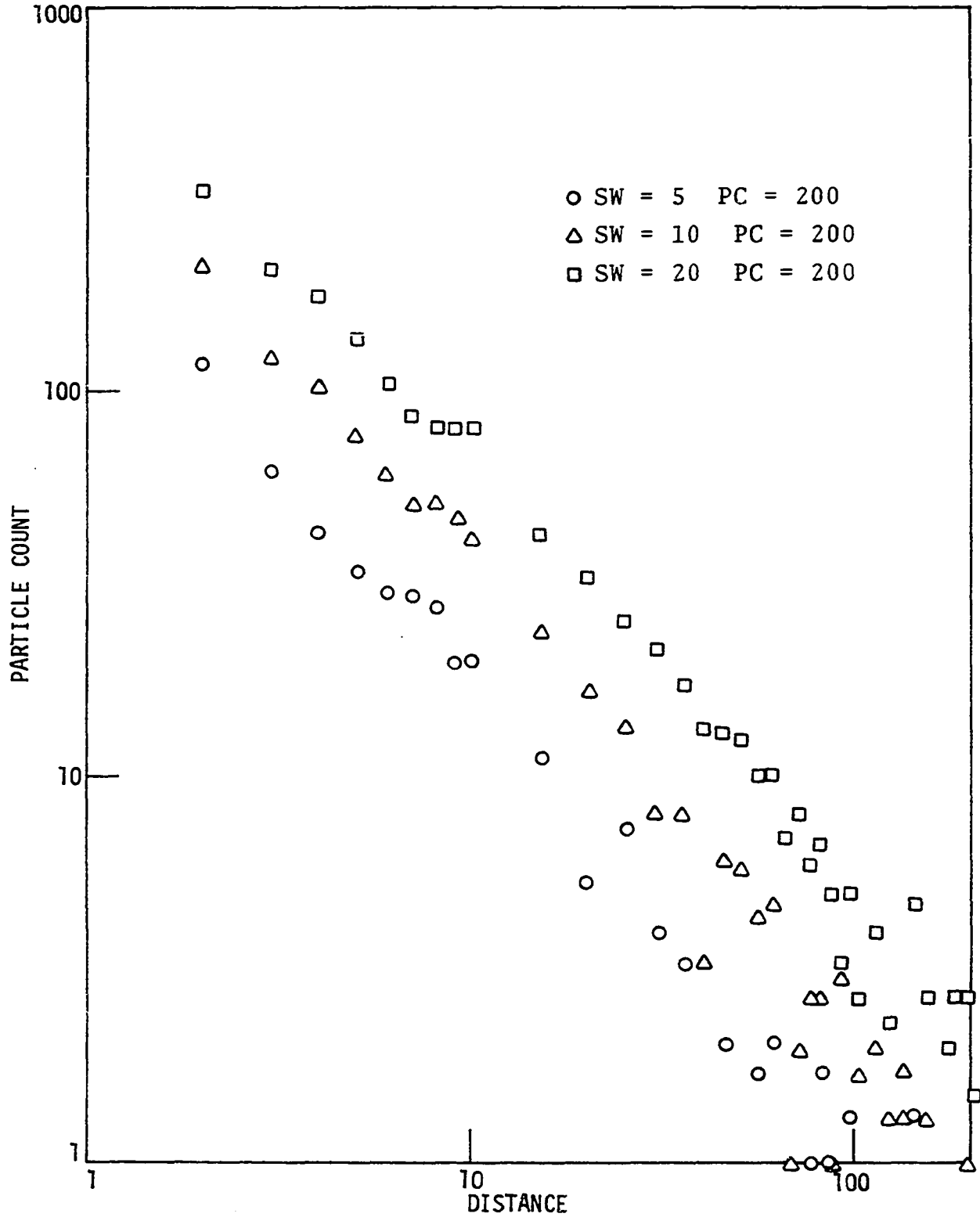
Figure 31. Log distance vs log particle count: Case I, SW = 5, 10 and 20, PC = 200
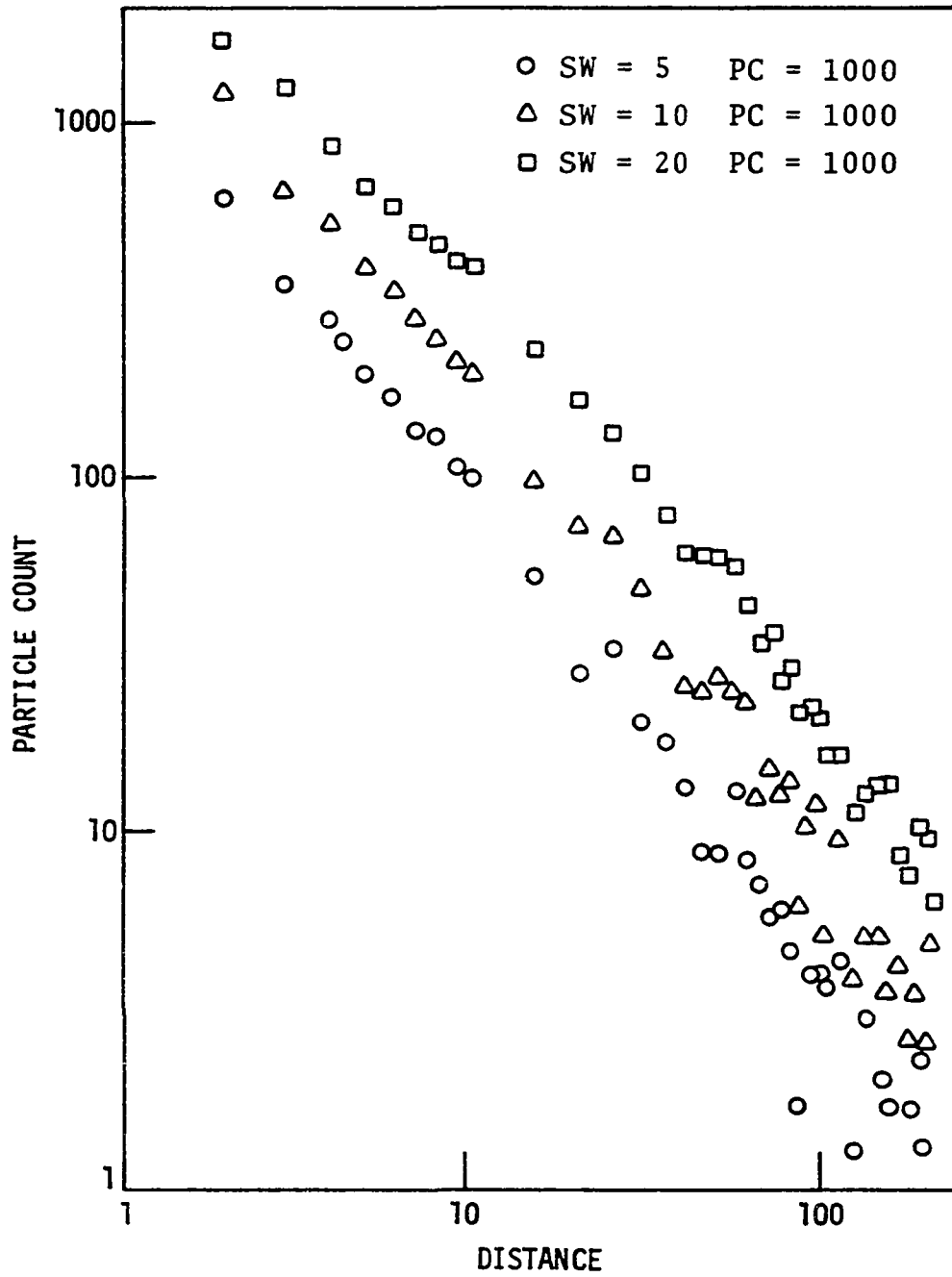
Figure 32. Log distance vs log particle count: Case I, SW = 5, 10 and 20, PC = 1000

now contribute more material. These graphs look somewhat different than those previously shown for constant source width in that maximum particle count is given by the widest source, a result of the increase in material. The rate of decrease of particle count, or slope decreases with increasing source width in two of the three sets as follows:

SW	PC	Slope	Intercept
5	40	-1.2913	1.7915
10	40	-1.1420	2.0087
20	40	-1.0620	2.1660
5	200	-1.1512	2.3540
10	200	-1.2647	2.7838
20	200	-1.1628	2.9684
5	1000	-1.3650	3.2782
10	1000	-1.3055	3.5278
20	1000	-1.2040	3.7142

This example might be considered comparable to stating that wind competence is sufficient to remove a uniform amount of material per unit source width and therefore the total amount of transported material is directly related to source width.

Source width may also be varied while maintaining a constant total amount of material. This is accomplished by varying particle concentration such that SW X PC is a constant. Results of a series of walks to illustrate this effect are shown in Figures 33, 34, and 35. In this case, the greatest particle count results from the narrowest source however the
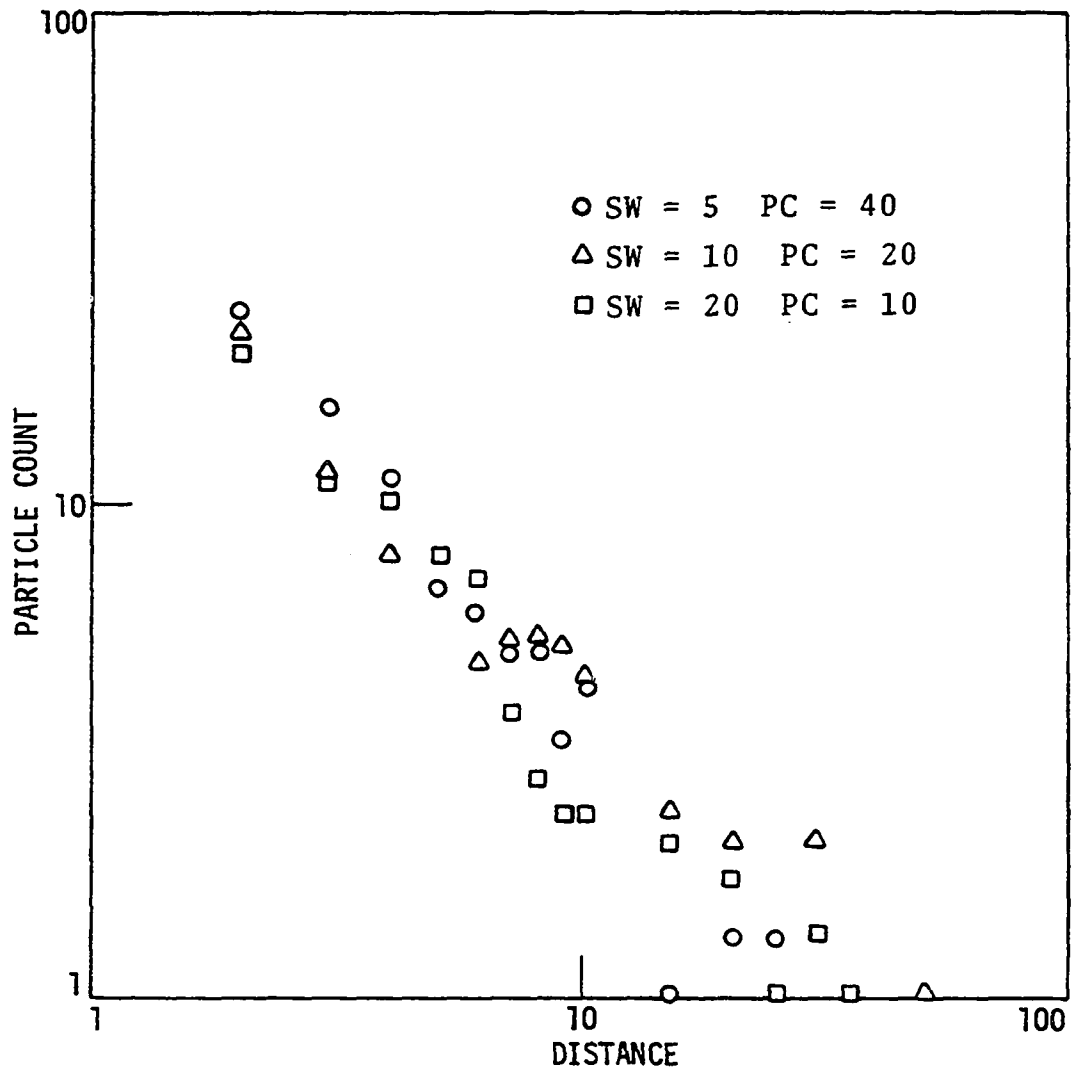
Figure 33. Log distance vs log particle count: Case I, SW = 5, 10 and 20, volume = 200
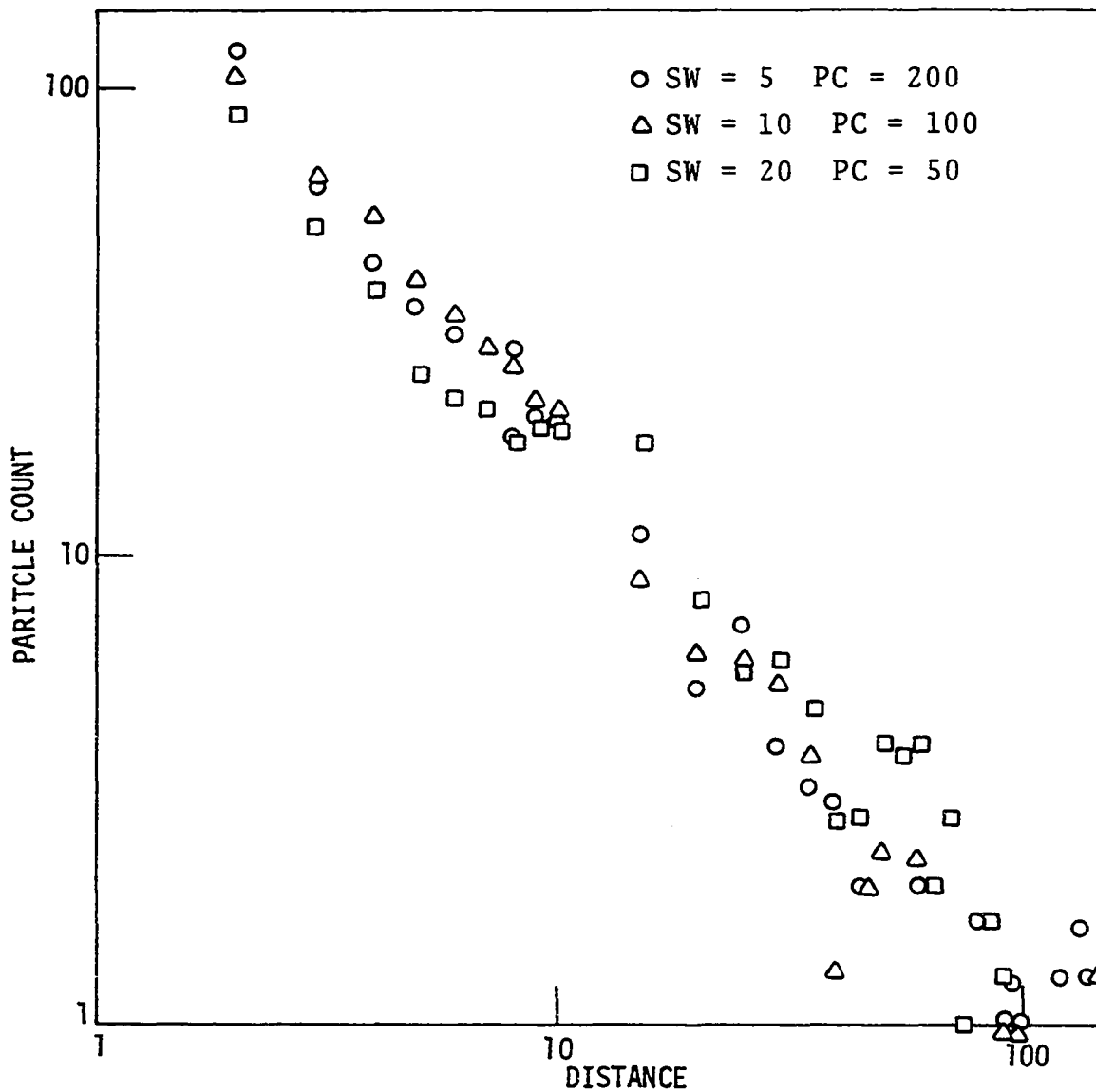
Figure 34.   Log distance vs log particle count: Case I,
              SW = 5, 10 and 20, volume = 1000
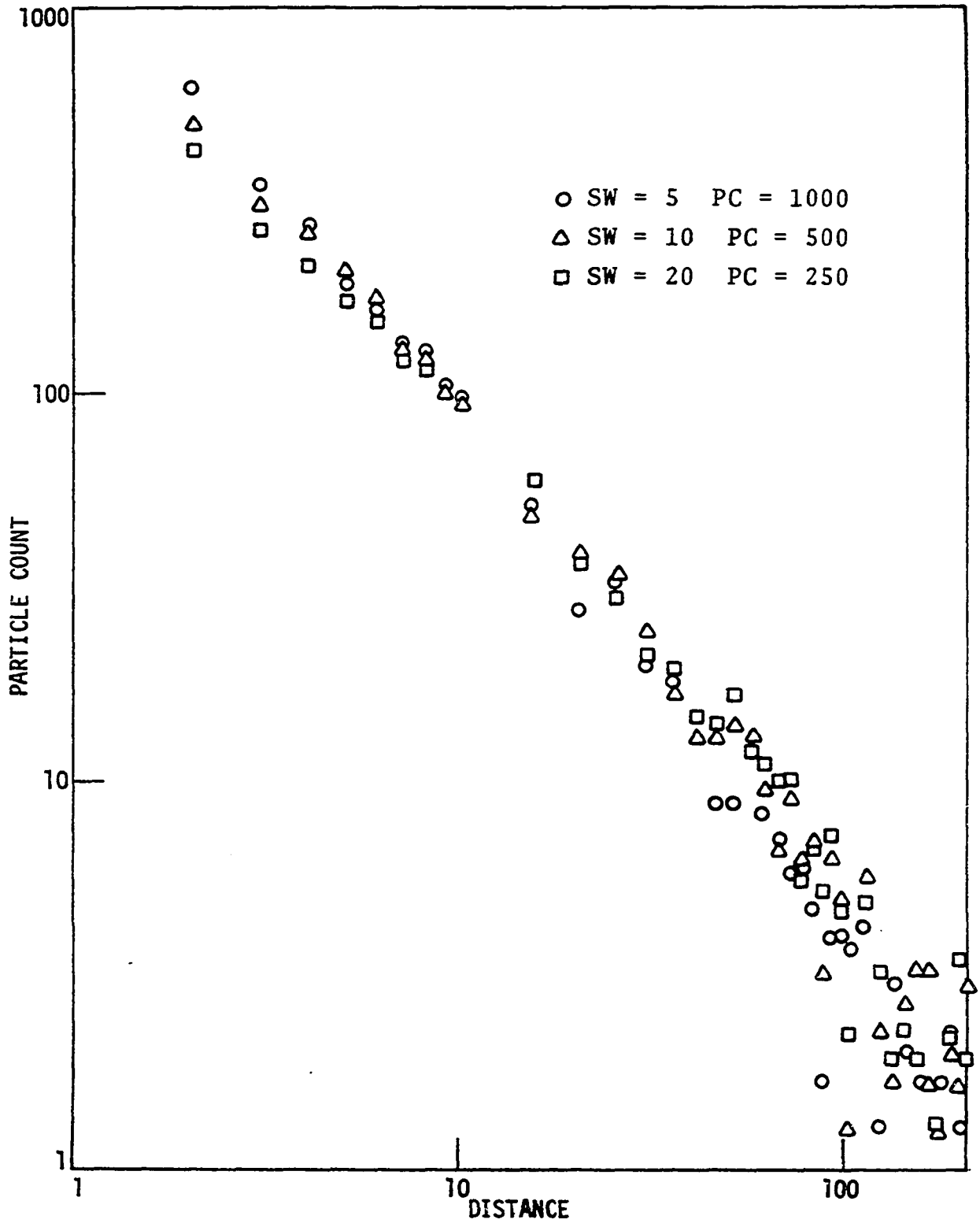
Figure 35. Log distance vs log particle count: Case I,
SW = 5, 10 and 20, volume = 5000

rate of decrease is still generally lower for wider sources.
Another interesting characteristic brought out in this series
of walks is the difference in the amount of material left
suspended in the air at the end of the deposition area.
Results indicate that a wider source leaves more particles
suspended considering constant total number of particles.
The mean percentage of particles in suspension at distance
200 for the data of Figures 33, 34 and 35 is given as:

SW	% Particles in Suspension
5	11.0
10	14.2
20	18.6

The reasoning for this increase may give new meaning to the
old adage "what can't get up, can't get out."

Wind oriented at any angle, α, to the source other than
perpendicular will have a two-fold effect, (1) effective
source width increases by $SW/\cos\alpha$ and as a result, (2) total
number of particles increases (assuming constant source point
particle concentration). Figures 36 and 37 represent walks
at various values of α, from 5 to 85° in 20 degree increments.
For a constant source width of 5 units and a constant source
point particle concentration of 100, effective source width,
ESW, and total volume of material change as follows:
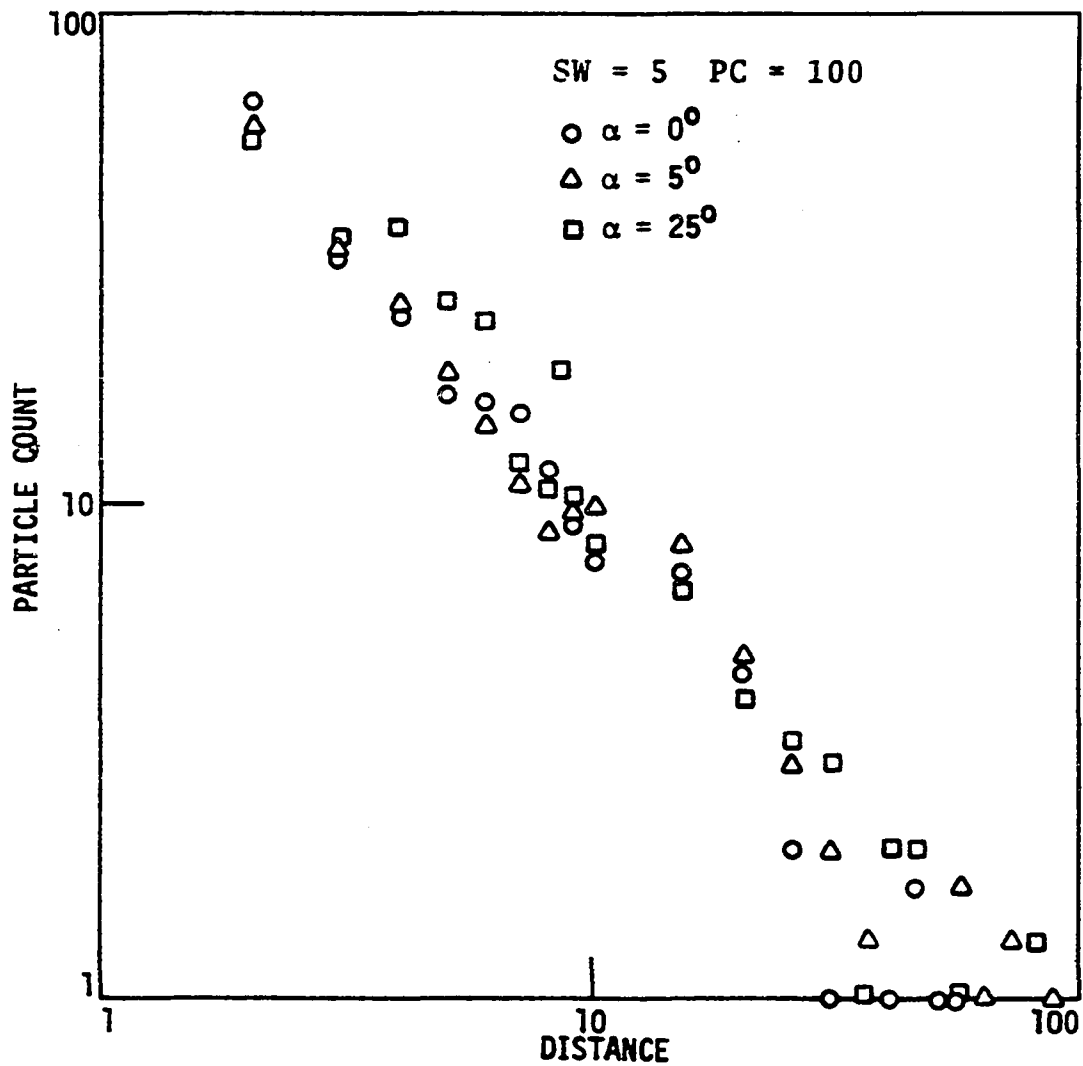
Figure 36. Log distance vs log particle count: SW = 5, PC = 100, α = 0°, 5° and 25°
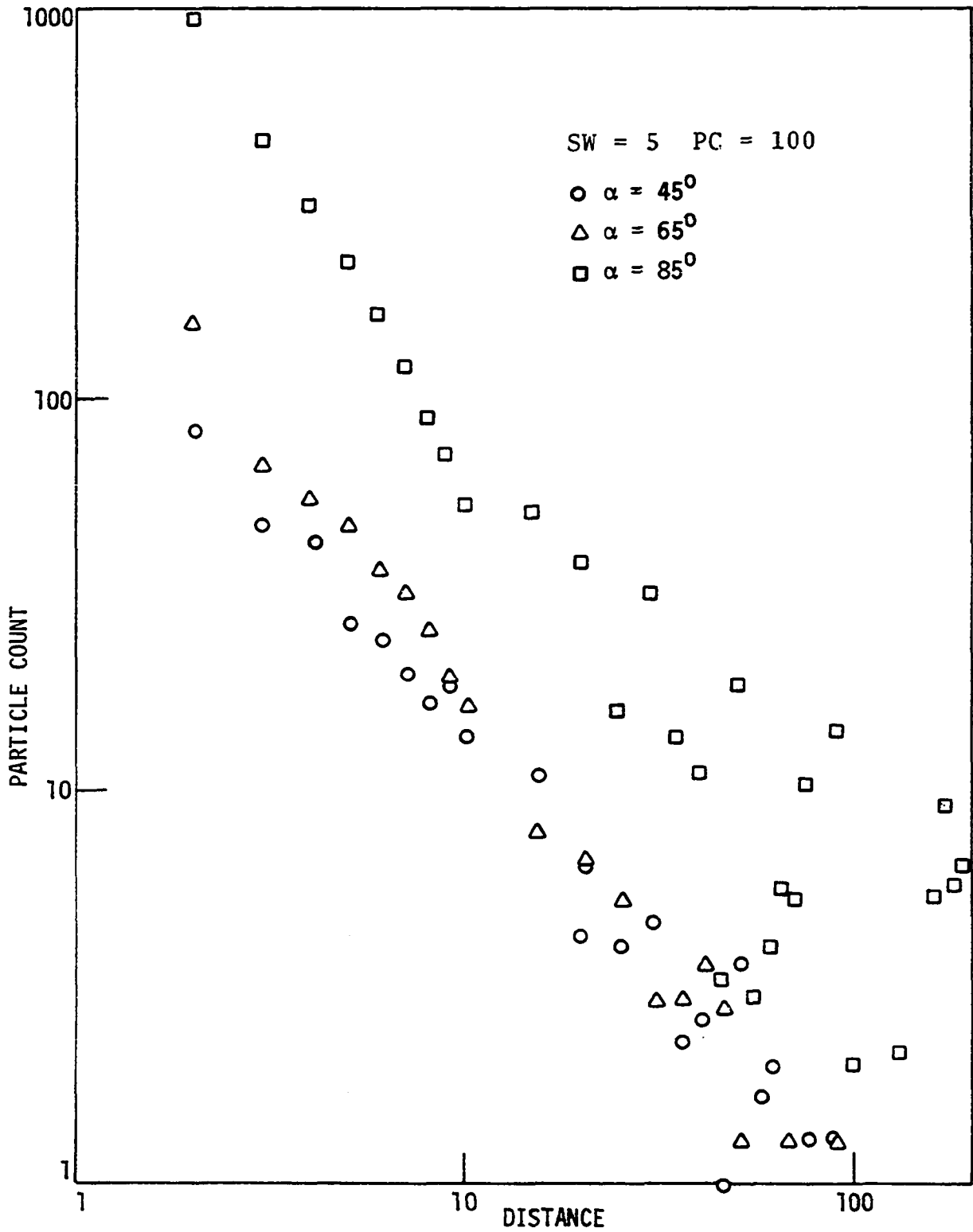
Figure 37. Log distance vs log particle count: SW = 5,
PC = 100, α = 45°, 65° and 85°

α	ESW	Volume
0°	5	500
5	5	500
25	6	600
45	7	700
65	12	1200
85	57	5700

At low angles, where source width is not appreciably increased, thickness-distance relations appear to be nearly identical to wind blowing normal to the source, Figure 27. In fact, because of the randomness of the system, these trends almost appear as one line. At larger angles this effect of increasing source width and particle number shows some interesting results much different than for small angles.

Maximum thickness is increased considerably, a result of the greater number of particles being transported, and in addition a definite change in slope occurs among the three positions shown in Figure 37. This also indicates that slope is a function of source width and, indirectly then, wind angle. The various positions of the wind also indicate that the value of α must be sufficiently large before any significant change occurs in the slope of the line. Note that maximum particle count or thickness increases with increasingly larger angles, however this is only related to source width through increased particle volume.

An advantage to using a numerical scheme for random-walk simulation is that any combination of variables may be input

to illustrate a particular case in question. As an example, consider a situation where a source 10 units in width only contributes material from one side, in effect an effective source width of 5 units. If the effective area were on the side closest to the deposition area, the resulting particle-count versus distance relationship would be identical to that already presented for similar conditions; i.e. 0° wind.

If the effective area were located on the opposite left side, with a 5 unit "gap" between the source and deposition area, particles which began walking out of the source would be required to step over this region. Comparing this case with the previous one, results indicate that fewer particles land at the beginning of the deposition area, and the rate of decrease is less when particles must travel the greater distance.

Case II: variable wind

Accumulations of particles where wind direction is rotated through one quadrant from 5 to 85 degrees in 10 degree increments are shown in Figures 38 and 39 for source widths of 5 and 10 units respectively. Since each direction is only walked through once, the probability for all directions is equal. As in the case of unidirectional wind, larger values of particle concentration, which represent greater quantities of material, result in greater thicknesses.
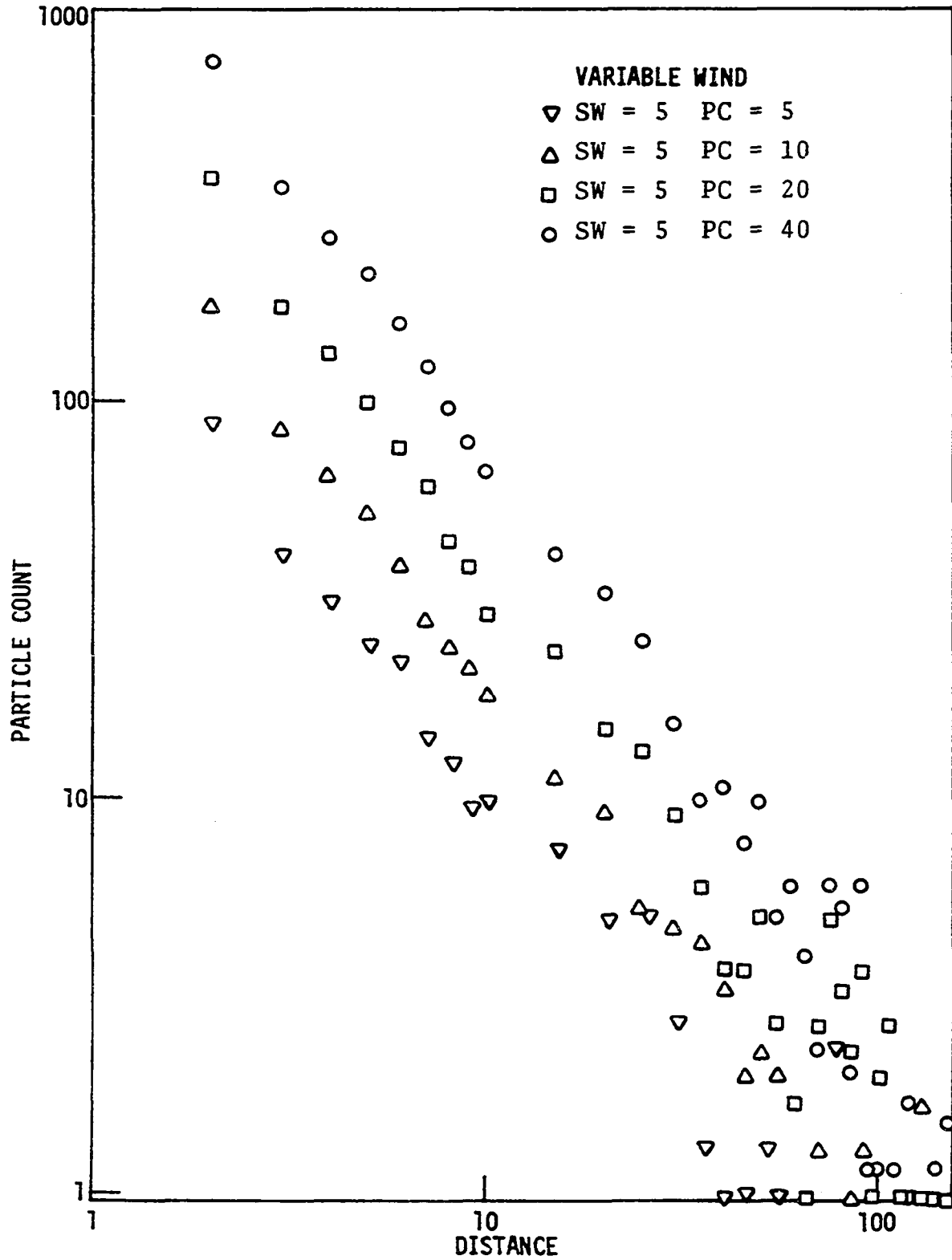
Figure 38. Log distance vs log particle count: Case II,
SW = 5, PC = 5, 10, 20 and 40
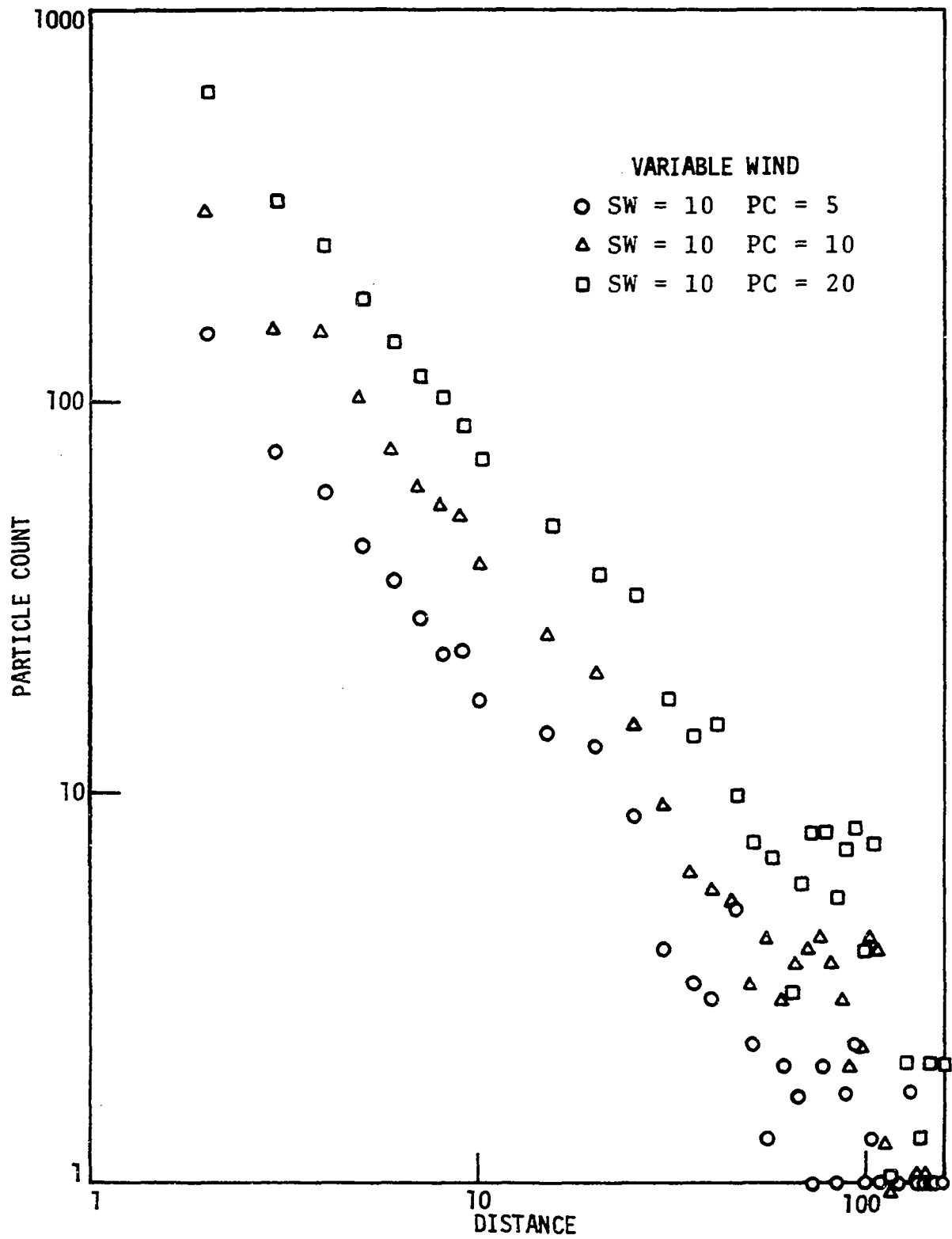
Figure 39. Log distance vs log particle count: Case II,
SW = 10, PC = 5, 10 and 20

Again, considerable scatter is shown at greater distance, and in many cases individual runs appear to overlap after a distance of about 100 units. These results are not surprising, considering that the variable wind model is simply a summation of a series of unidirectional wind walks. However, the data of Figures 38 and 39 indicate that slope of the log distance vs log particle count curve increases slightly with increasing particle concentration.

Case III: variable plus prevailing wind

In the variable wind model, the probability of wind blowing in any direction, P_{v_i}, was equal to 0.0278. This is calculated considering 36 equal 10 degree segments in 360°, with the sum of probabilities equal to one. By introducing a prevailing wind component, wind directional probabilities change, depending upon the strength of the prevailing wind. Strength of the prevailer is specified by allowing repeated walks in that direction. Considering the full sweep of directions (36), the probability of the prevailing wind, P_p, can be calculated in terms of the number of walks in that direction and is given as follows:

Number of prevailing walks	P_{v_i}	P_p
1	0.0278	0.0278
2	0.0270	0.0541
4	0.0256	0.1026
8	0.0233	0.1860
16	0.0196	0.3137
32	0.0154	0.4923

Figures 40 and 41 give results of trial walks with source width 5 and 10 units respectively, and corresponding particle concentrations specified as 10 and 5. The direction of the prevailing wind component varies from 25 to 65 degrees, while the strength remains constant at 2. No distinct trends could be established for either set of data as results of linear regressions indicate nearly identical values of slope and intercept within each group. Between groups, data from Figure 41 give a lower value of both slope and intercept.

The effect of prevailing wind strength within any prevailing wind direction is shown in Figures 42 and 43, where the number of prevailing repetitions increases from 1 to 32. The maximum particle count increases very systematically with increasing strength while the slope is not significantly affected until after 4 repetitions, corresponding to a prevailing strength probability of 0.1860. In other words, the prevailing wind must be in effect about 20 percent of the time to affect the shape of the particle count distance curve.

Considering the largest probability of prevailing wind strength 0.4923, corresponding to 32 repetitions, the effect of direction is shown in Figure 44 for a source of 5 units width, and a particle concentration of 10. Intercept increases with increasing angle and in addition, slope also
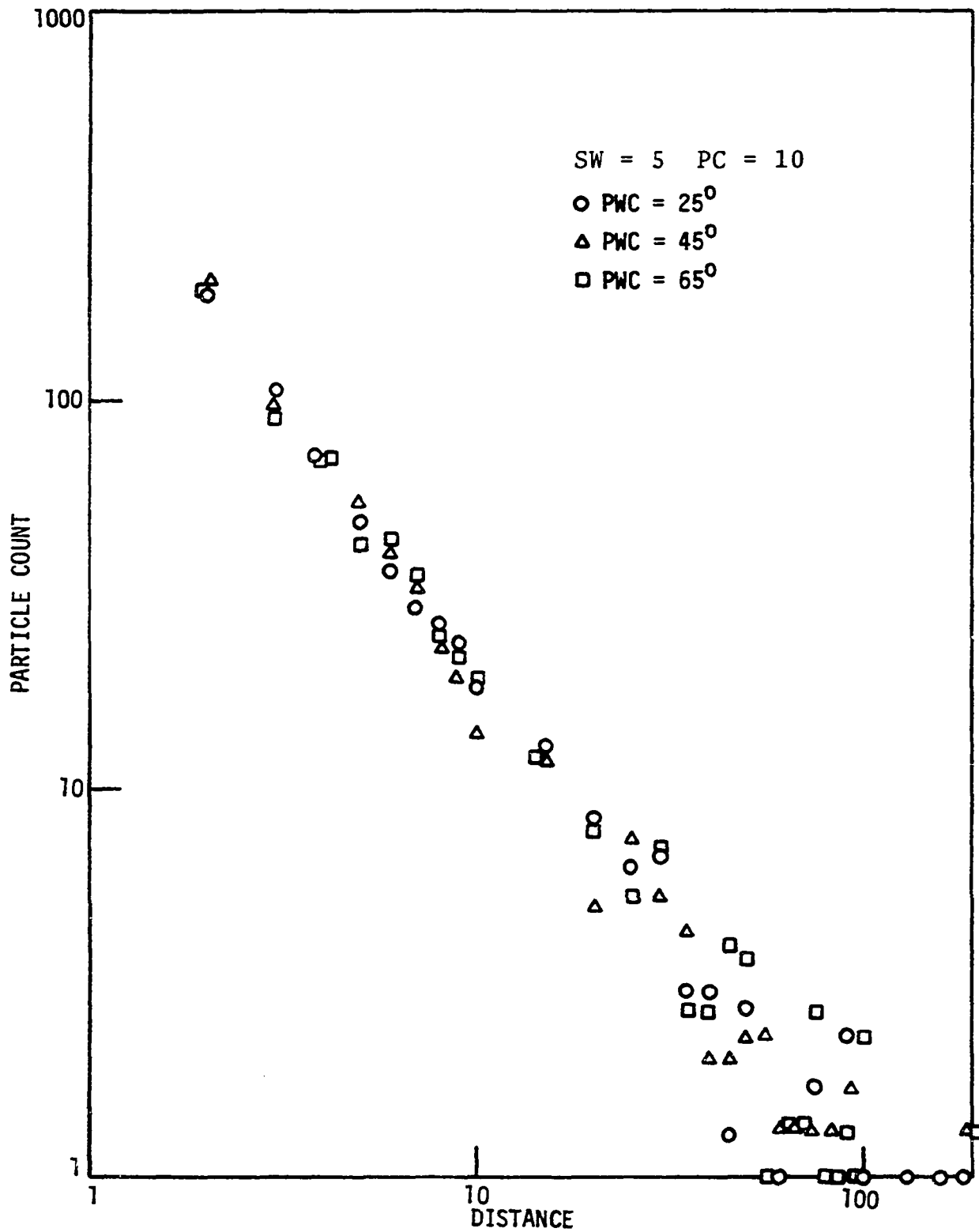
Figure 40. Log distance vs log particle count: Case III, SW = 5, PC = 10, PWC = 25°, 45° and 65°
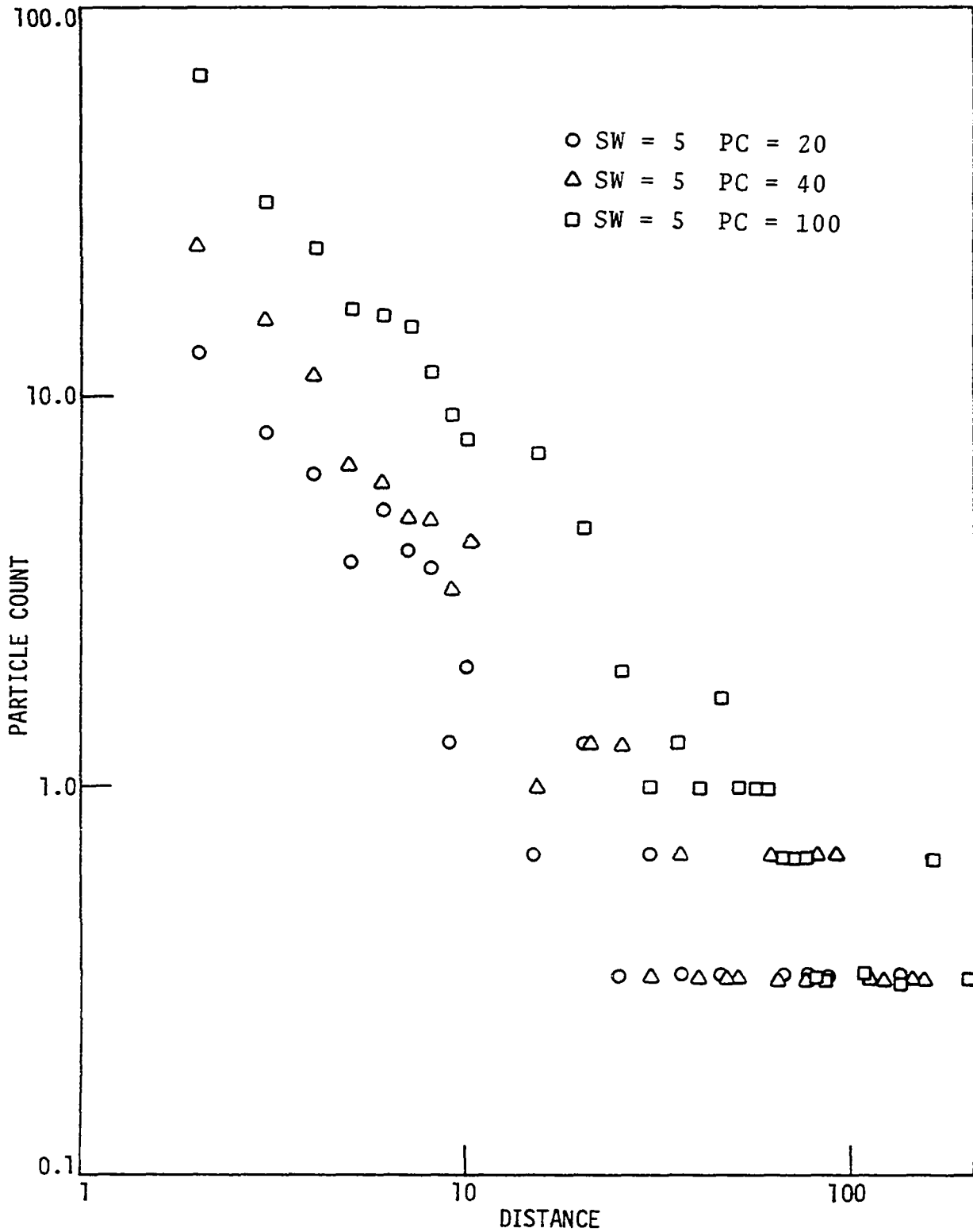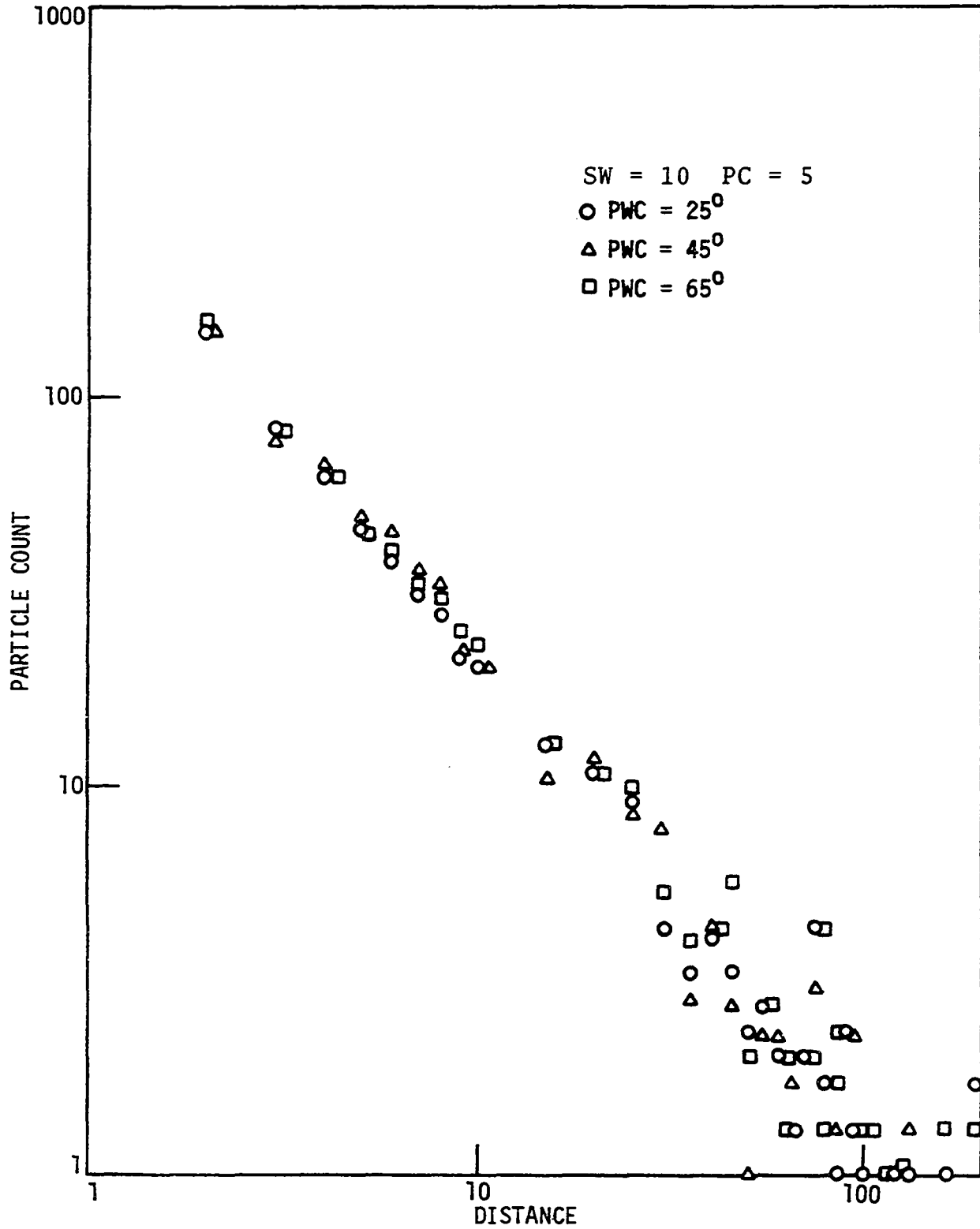
Figure 41. Log distance vs log particle count: Case III, SW = 10, PC = 5, PWC = 25°, 45° and 65°
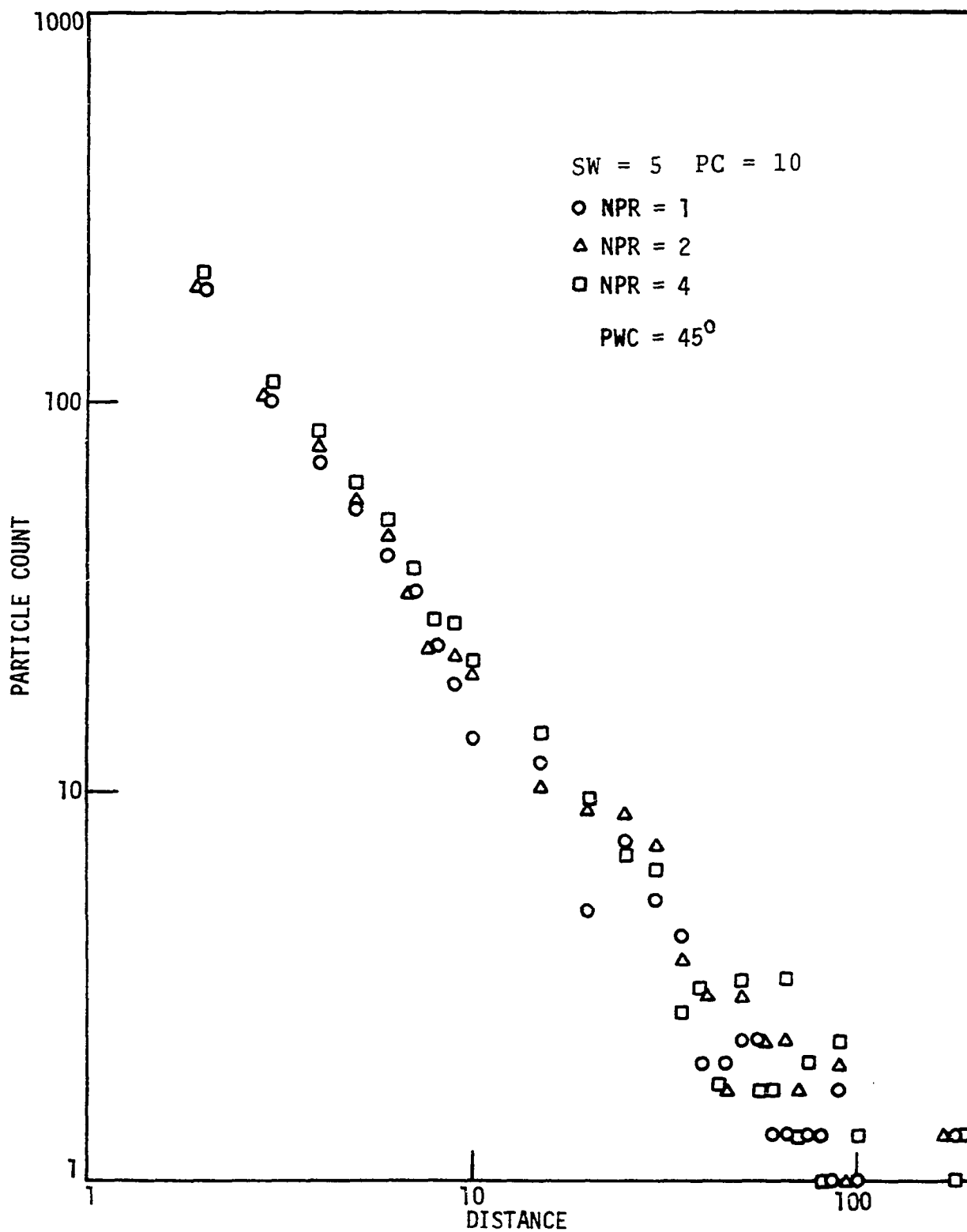
Figure 42. Log distance vs log particle count: Case III,
SW = 5, PC = 10, PWC = 45°, NPR = 1, 2 and 4
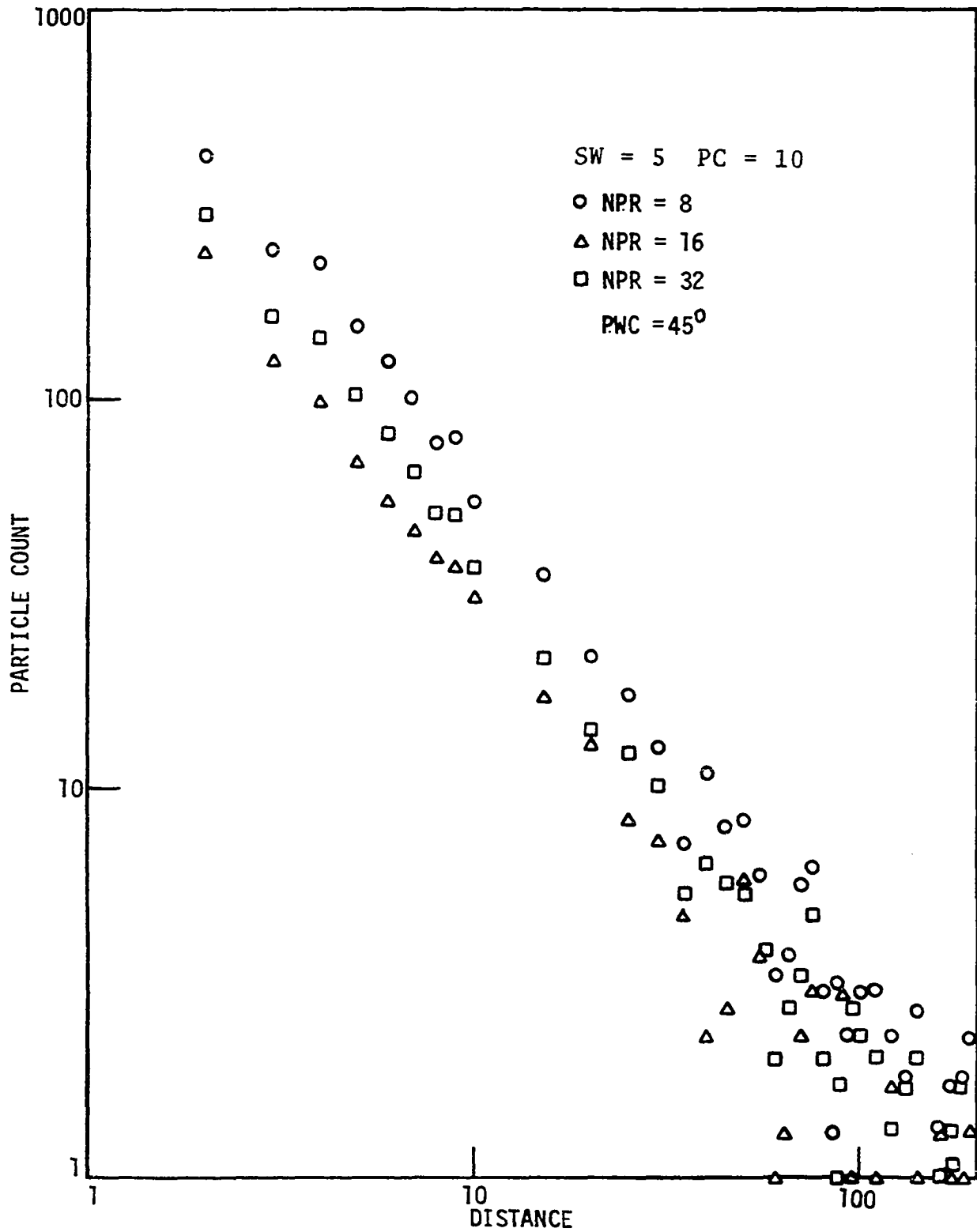
Figure 43. Log distance vs log particle count: Case III,
SW = 5, PC = 10, PWC = 45°, NPR = 8, 16 and 32
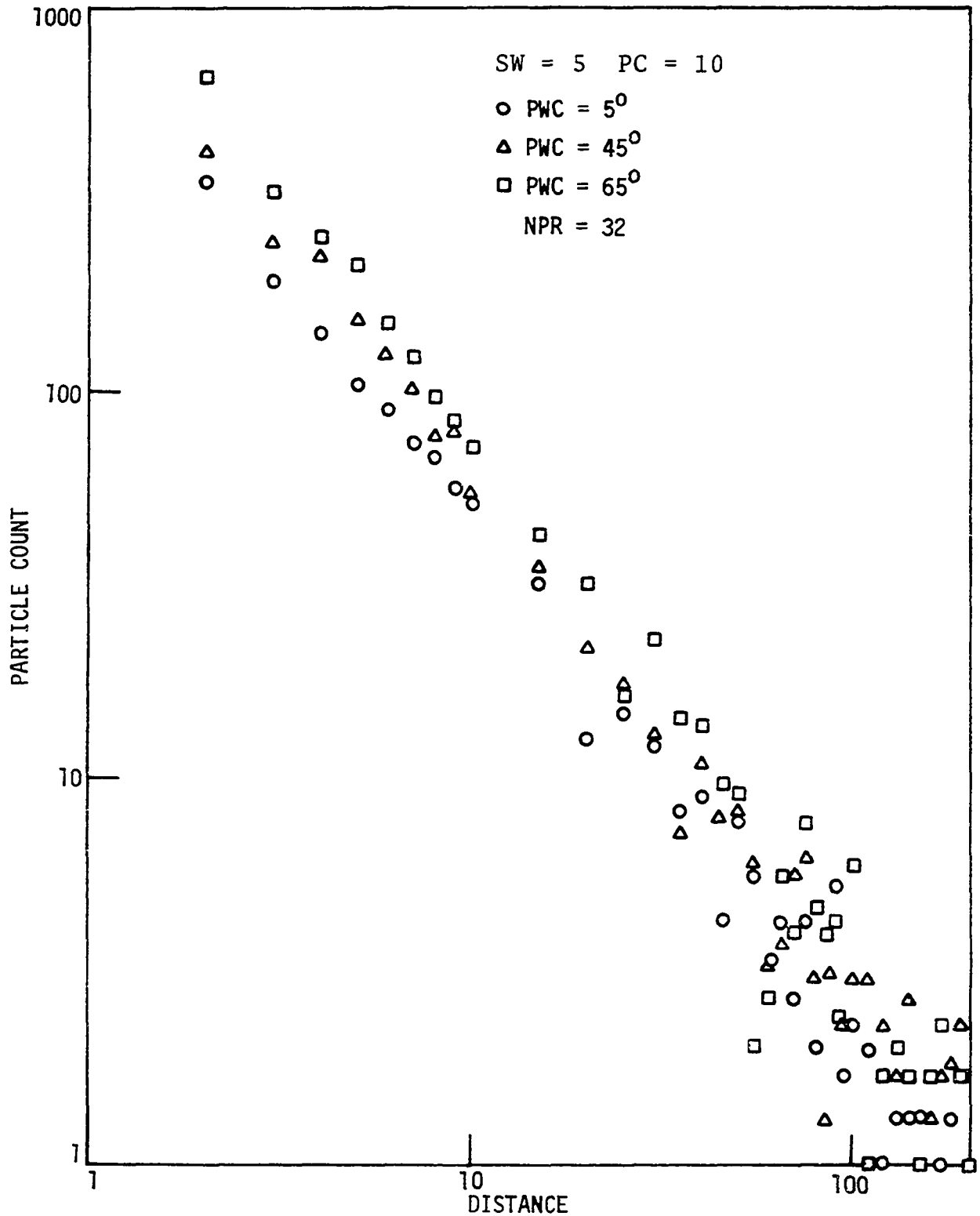
Figure 44.   Log distance vs log particle count: Case III, SW = 5, PC = 10, PWC = 5°, 45° and 65°, NPR = 32

increases somewhat. The effect of increased effective source width at larger angles of α appears to be overshadowed by the increased number of particles in transport.

Particle size

Probability adjustment   The probability of fall for heavier particles, as previously presented, may be taken into consideration by making adjustments to the model. Figures 45 thru 47 present results of a series of unidirectional walks where $\alpha = 0^\circ$ and source width and particle concentration have been held constant at 10 and 100 respectively, while fall probability changes from 0.500 to 0.700 in increments of 0.025.

As can be seen, higher probabilities result in more particles landing closer to the source, and linear regressions indicate that not only the maximum particle count increases, but the slope becomes steeper. Of equal importance is the fact that the maximum transport distance becomes less as fall probability increases. The following data display this characteristic:

P_f	X_m (maximum transport distance)
0.500	13.3% suspended at 200 units
0.525	5.8% " " " "
0.550	1.1% " " " "
0.575	190 units
0.600	120 "
0.625	80 "
0.650	55 "
0.675	55 "
0.700	45 "
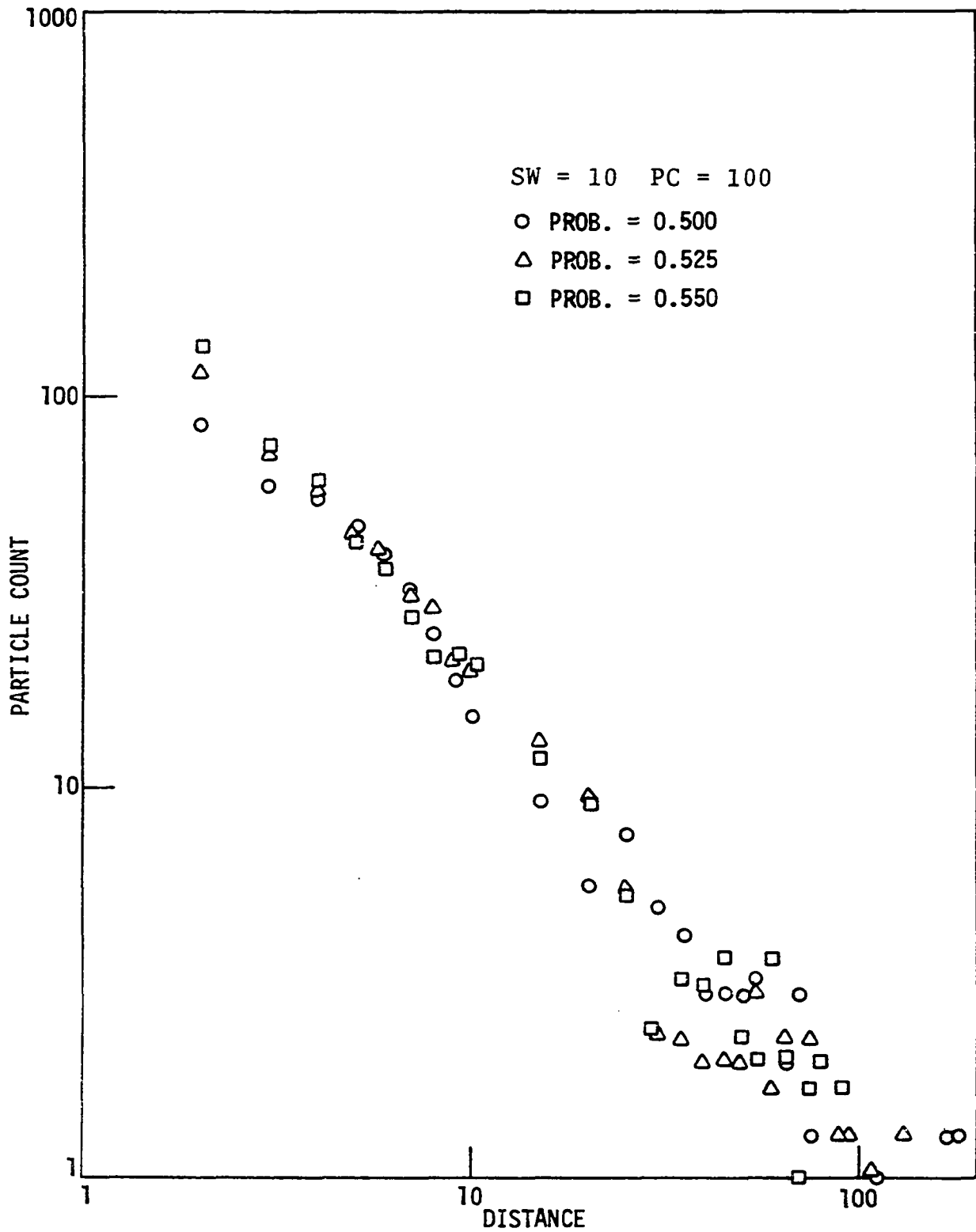
Figure 45. Log distance vs log particle count: Case I,
SW = 10, PC = 100, P_f = 0.500, 0.525 and 0.550
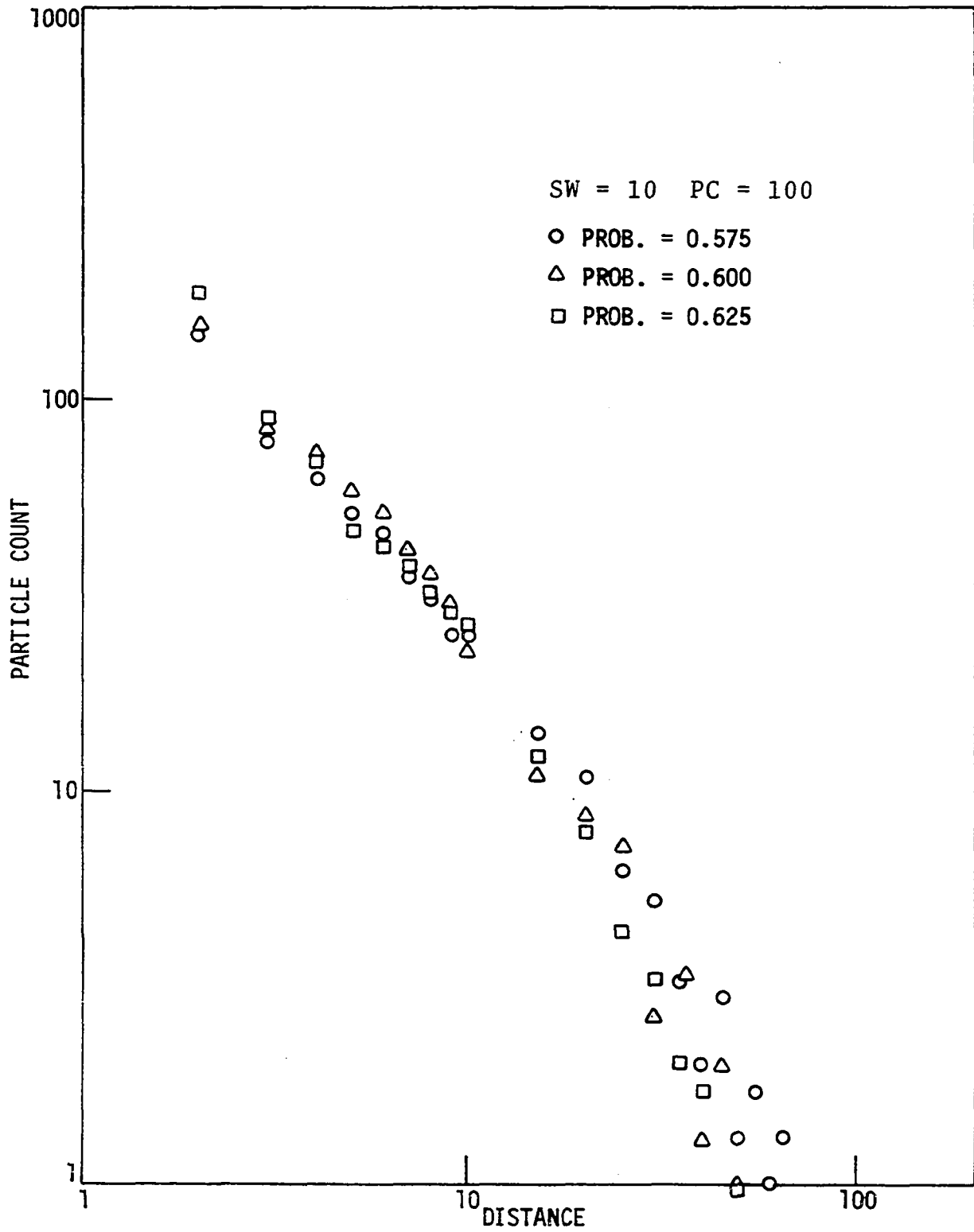
Figure 46. Log distance vs log particle count: Case I,
SW = 10, PC = 100, P_f = 0.575, 0.600 and 0.625
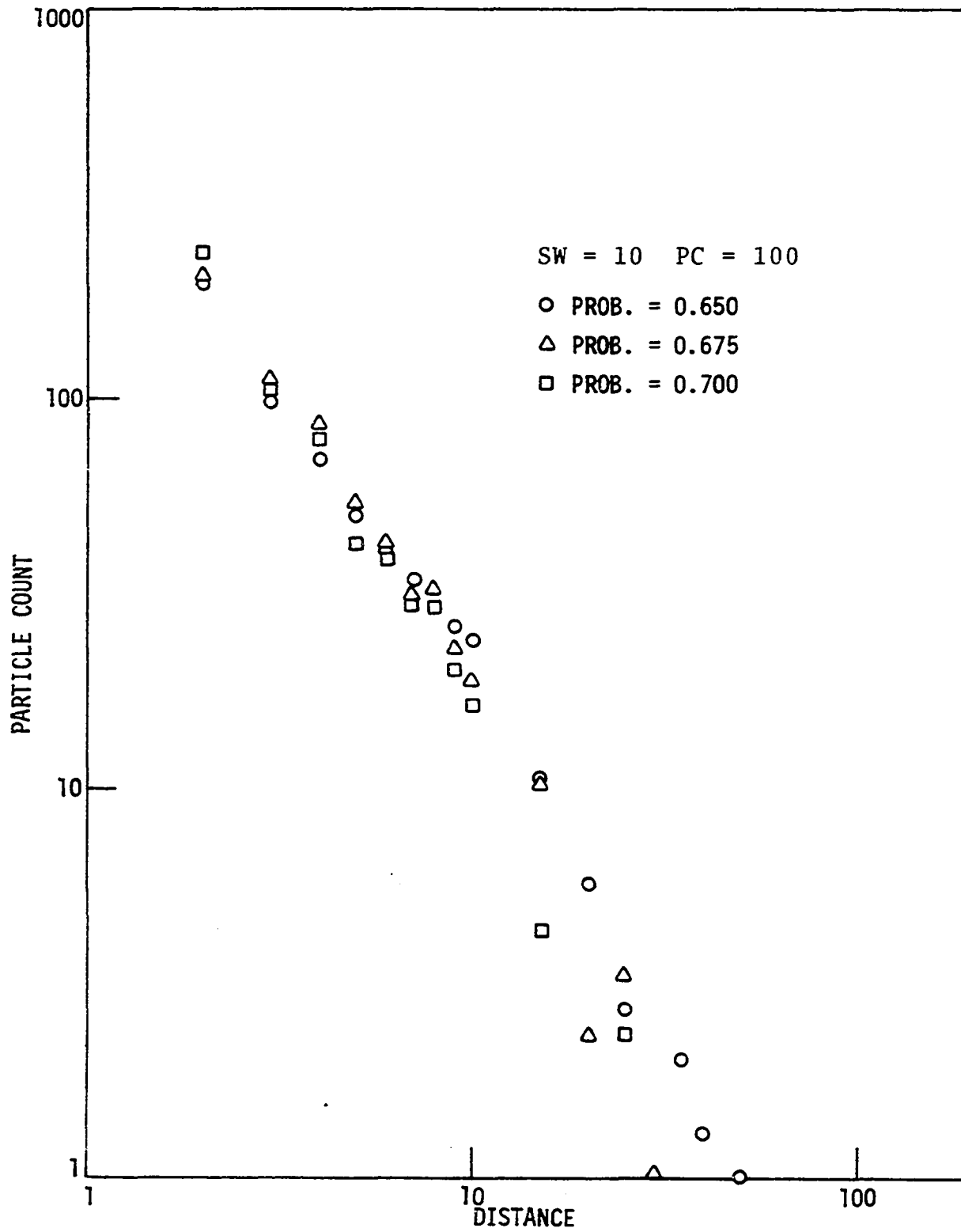
Figure 47. Log distance vs log particle count: Case I, SW = 10, PC = 100, P_f = 0.650, 0.675 and 0.700

A complete variable winds model, with a superimposed prevailing strength and fall probability adjustments is presented in Figure 48. Linear regressions give the following results:

P_f	Intercept	Slope	r
0.500	2.6143	-1.2556	0.9778
0.550	2.9438	-1.5645	0.9951
0.600	3.2073	-2.0123	0.9903
0.650	3.3204	-2.3220	0.9929

These results are very systematic and significant and show that higher fall probabilities and hence larger particles will be concentrated closer to the source and that the distribution decreases at a faster rate. As with the unidirectional case, this model also predicts that there is a maximum transport distance for various sizes.

Step length adjustment   Results of walks where the horizontal step length has been increased to simulate smaller particles being carried in turbulent diffusion indicate that larger steps, and hence smaller particles are transported greater distances. A completed model, with a mild prevailing wind is shown in Figure 49. Linear regressions give the following results:
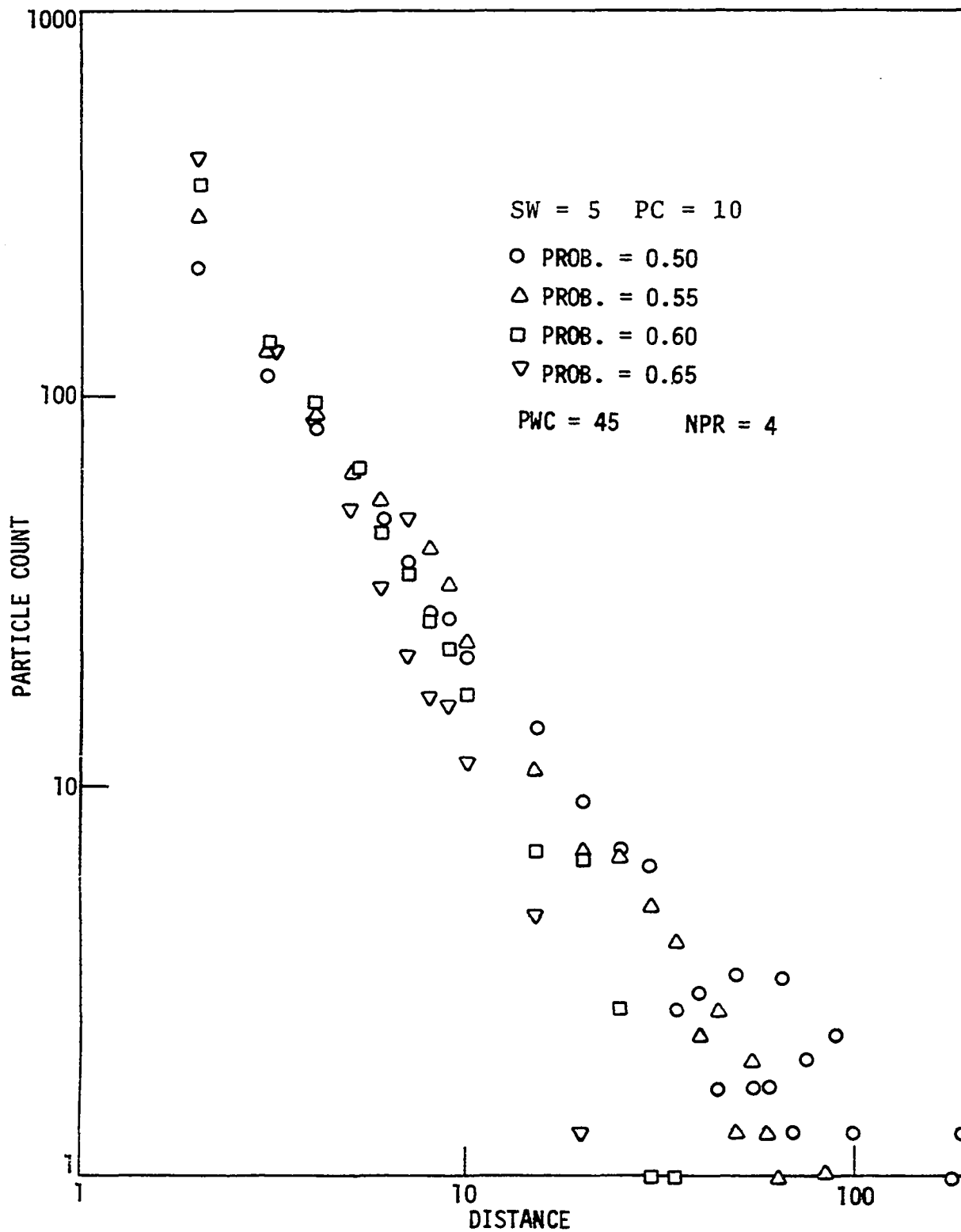
Figure 48. Log distance vs log particle count: Case III,
SW = 5, PC = 10, P_f = 0.50, 0.55, 0.60, 0.65,
PWC = 45°, NPR = 4
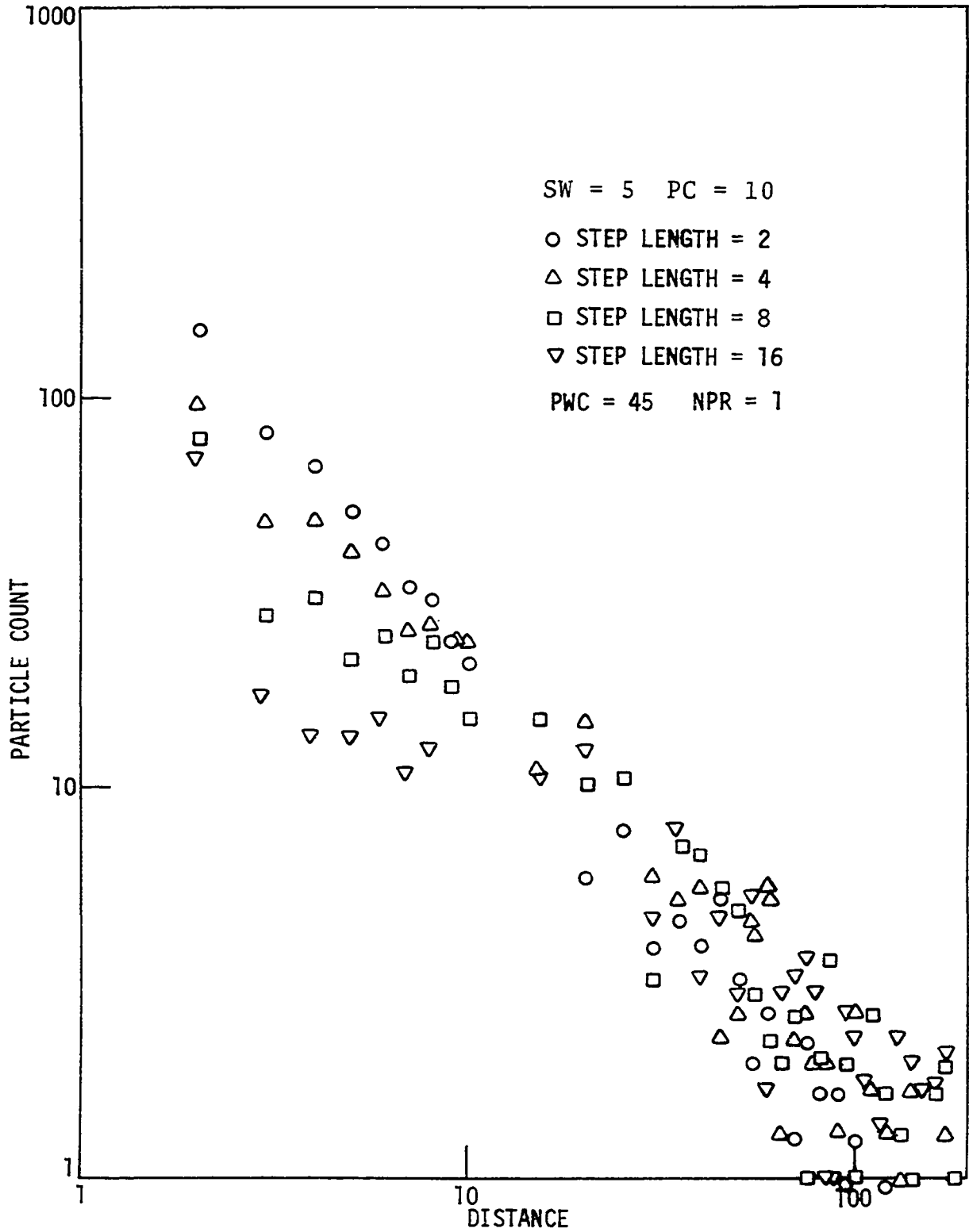
Figure 49. Log distance vs log particle count: Case III,
SW = 5, PC = 10, SL = 2, 4, 8, 16, PWC = 45°
NPR = 1

SL	Intercept	Slope	r
2	2.5453	-1.2253	0.9911
4	2.3144	-1.0329	0.9769
8	2.0857	-0.8975	0.9556
16	1.7942	-0.7270	0.9218

Note that these data show that as step length increases, and particle size becomes smaller, intercept decreases, and slope decreases. This is the same trend which was shown for the probability adjustment model previously presented. At the same time, as step length increases, the percentage of material left suspended in the air at the end of the deposition area increases:

SL	% Particles Still in Air
2	14.1
4	19.0
8	26.3
16	33.5

The use of either fall probability adjustment or step length adjustment gives the same trend in results. In effect, smaller particles are transported greater distances. The question then becomes which of these techniques is more realistic for describing the path of particles, particularly the fine fraction. The problem of clay deposition is still present and discussion will be made following presentation of dispersion study results.

Field and Laboratory Studies

Results of field and laboratory studies of thickness
and particle size used to test the random-walk model will
be presented from traverse studies in central Missouri and
east-central Iowa. Shear strength and density data
summaries will then be presented followed by results of clay
dispersion-aggregation investigations.

Missouri-West (MW)

Site information for the MW traverse with loess thick-
ness and distance from the valley wall is given in Table 4
along with a brief notation of the material immediately under-
lying the loess. Twelve sites were studied, six on each side
of the Missouri River. A maximum loess thickness of 446
inches (1132.8 cm) was measured at site 4-MW, located 0.9
miles (1.4 Km) south of the river. Note that this is consid-
erably less than measured at about the same distance in
western Iowa (80 , 171).

Figure 50 shows the overall thickness trends on both
sides of the river in relation to the present floodplain. A
general curvilinear trend is shown on both the north and
south sides of the floodplain; however, the thickness appears
to be much greater, at equal distances, on the south side.
Thickness-distance data are plotted on both semilogarithmic
and logarithmic scales and given in Figures 51 and 52 for
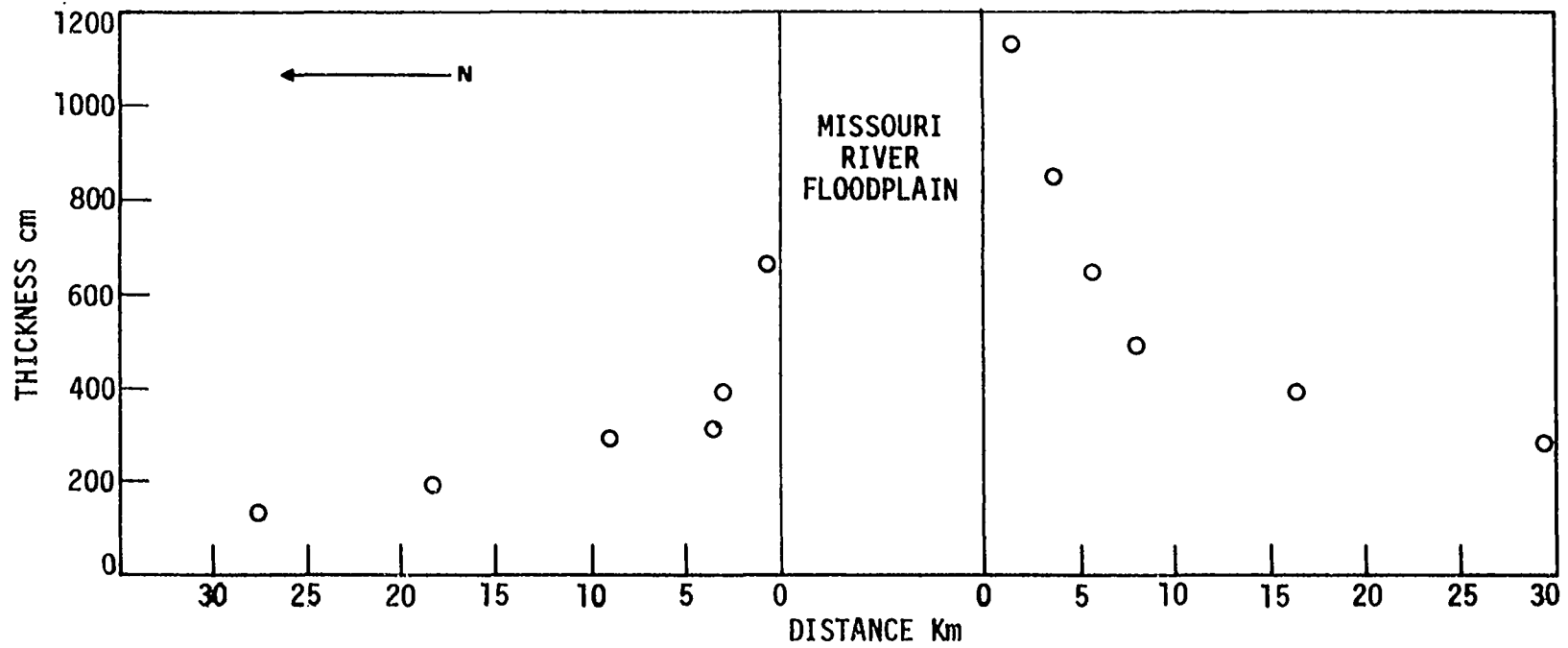
Figure 50. Distance vs thickness - Missouri West
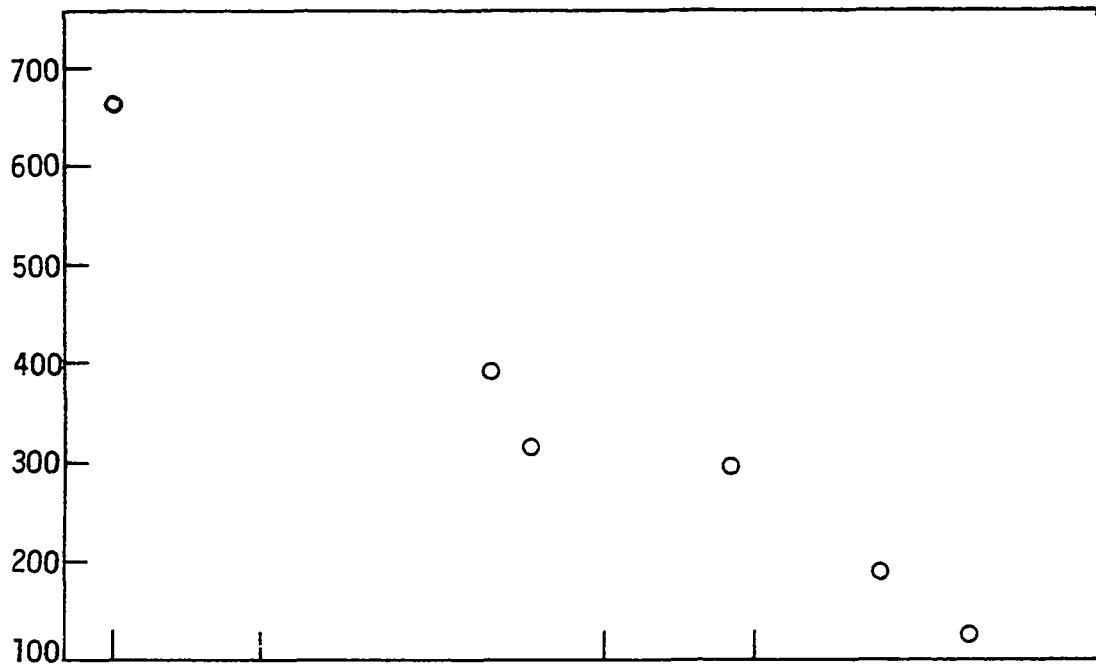
Figure 51a. Log distance vs thickness, north side - Missouri West
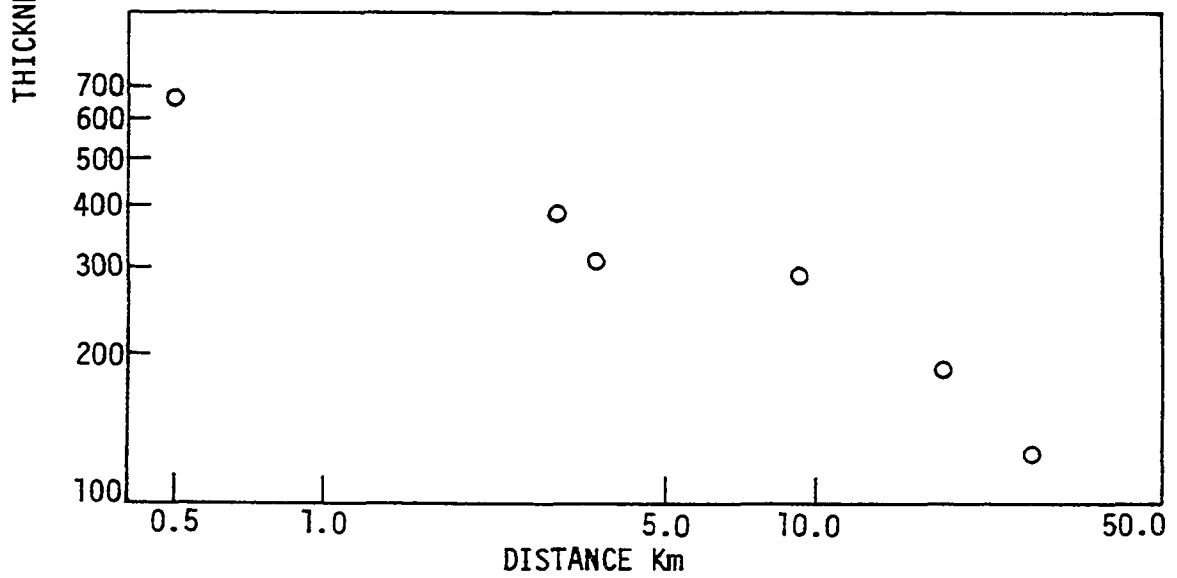
Figure 51b· Log distance vs log thickness, north side - Missouri West.
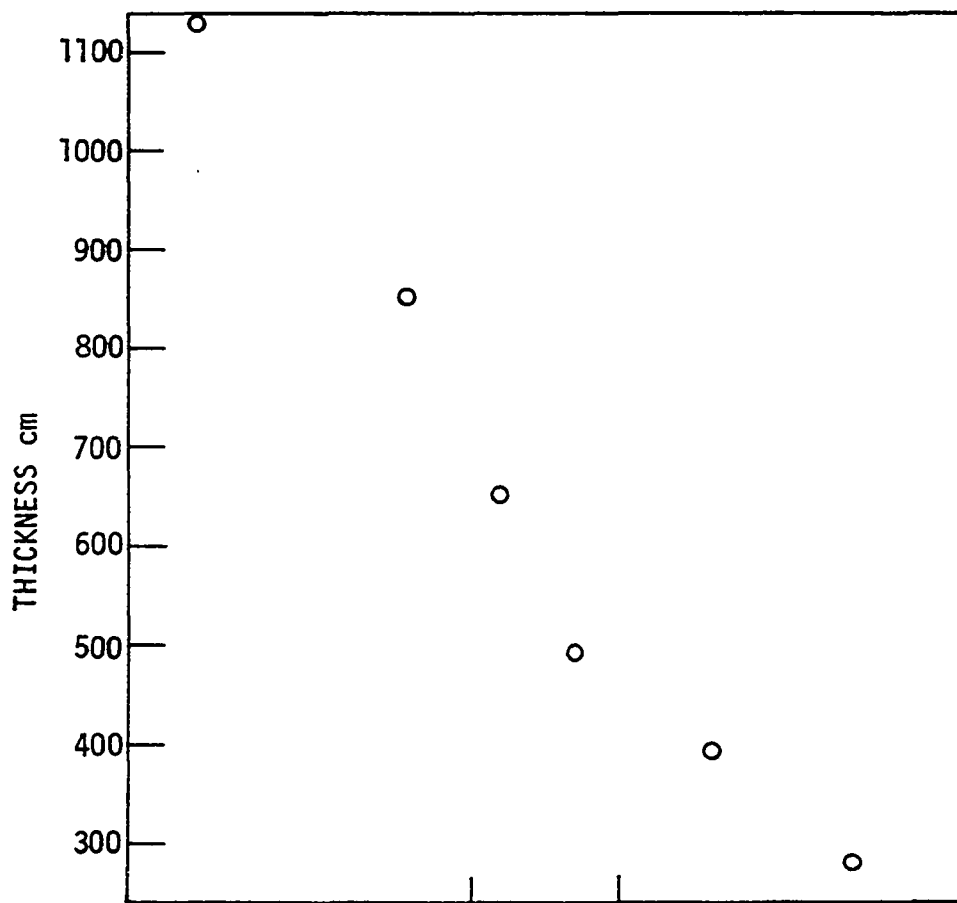
Figure 52a.   Log distance vs thickness, south side -
Missouri West
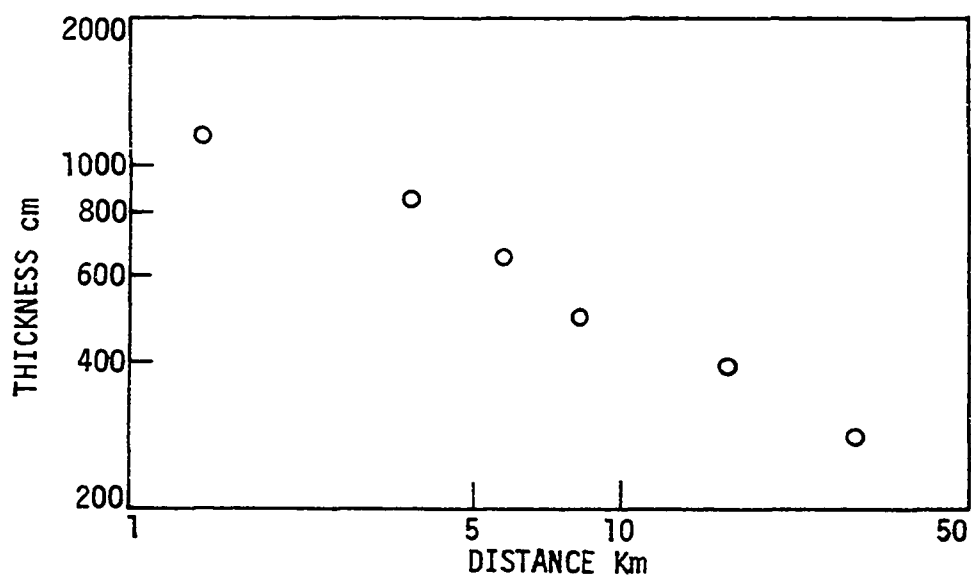
Figure 52b.   Log distance vs log thickness, south side -
Missouri West

locations north and south of the river respectively.

Linear regression of data north of the river, Figure 51, give the following empirical relations.

$$Y = 542.62 - 292.00 \log X \qquad r = 0.9805$$

$$\log Y = 2.74 - 0.38 \log X \qquad r = 0.9678$$

where

Y = thickness (cm)

X = distance (Km)

Statistically, a semilog relation gives a better fit to the data. It should be noted that site 7-MW was severely eroded, and eliminating this point gives slightly different relations:

$$Y = 561.00 - 299.02 \log X \qquad r = 0.9954$$

$$\log Y = 2.75 - 0.38 \log X \qquad r = 0.9691$$

The correlation coefficient of this modified semilog fit is considerably improved, while the log-log relationship has only slightly changed. It would appear that a log-linear relation best describes the loess thickness trend for the northern half of this traverse, however both equations are significant at 1%.

Plots of thickness versus distance for data south of the river, Figure 52, have been treated similarly and give the following linear equations:

Table 4. Site information - Missouri West.

Site		Distance Mi.	Km	Loess Thickness in.	cm	Notes
1-MW	S[a]	2.3	3.7	334	848.4	BWS(?) over YSP
2-MW	S	3.6	5.7	255	647.7	BWS or Loveland Loess (?)
3-MW	S	10.2	16.4	152	386.1	Swale or YSP (?)
4-MW	S	0.9	1.4	446	1132.8	BWS over Till Paleosol
5-MW	S	5.0	8.1	192	487.7	Sed. over Till Paleosol
6-MW	S	18.3	29.5	110	279.4	Swale
7-MW	N	2.2	3.6	124	315.0	Till Paleosol
8-MW	N	0.3	0.5	261	662.9	Loveland Loess (?)
9-MW	N	5.6	9.1	116	294.6	Sed.
10-MW	N	11.3	18.2	74	188.0	Sed. over Till Paleosol
11-MW	N	1.9	3.0	152	386.1	Till Paleosol
12-MW	N	17.1	27.5	50	127.0	Sed. over Till Paleosol

[a]S - site located south side of river.
   N - site located north side of river.

$$Y = 1189.58 - 662.68 \log X \qquad r = 0.9814$$
$$\log Y = 3.15 - 0.47 \log X \qquad r = 0.9909$$

In this case, a log-log form yields a better statistical fit as indicated by a higher correlation coefficient. However, as with equations presented for thickness north of the river, both functions are significant at the 1 percent level.

Changes in particle size composition of the "unweathered" portion below the soil profile are given in Table 5. Median particle size (size on the cumulative curve at which 50% is larger and 50% is finer) of each site is also presented. At sites 6-, 9-, 10-, and 12-MW, loess thickness was too thin to determine an accurate measure of unweathered particle size, thus these 4 sampling locations are not included in this analysis.

Figure 53 presents semilogarithmic plots of coarse and fine silt content versus distance for data on the south side of the river and linear regression of these data give the following expressions:

$$Y = 55.65 - 9.45 \log X \qquad r = 0.9866$$
$$Y = \% \text{ coarse silt} \quad X = \text{distance (Km)}$$
$$Y = 27.63 + 5.05 \log X \qquad r = .9381$$
$$Y = \% \text{ fine silt} \quad X = \text{distance (Km)}$$

Both equations are significant at 1 percent. These trends are similar in form to equations presented for a number of loess

Table 5. Area method particle size summary-Missouri West

Site	Sand >74μm	C. Silt 74-20μm	F. Silt 20-2μm	Clay <2μm	Median Size μm
1-MW	1.3	49.8	29.5	19.4	20.4
2-MW	1.1	48.2	32.5	18.2	19.5
3-MW	1.8	43.8	33.5	20.9	17.6
4-MW	1.5	54.4	28.5	15.6	22.0
5-MW	1.1	48.1	32.3	18.5	19.4
7-MW	1.9	46.6	31.7	19.8	19.0
8-MW	1.5	47.6	32.2	18.7	19.1
11-MW	2.1	45.1	32.7	20.1	18.3
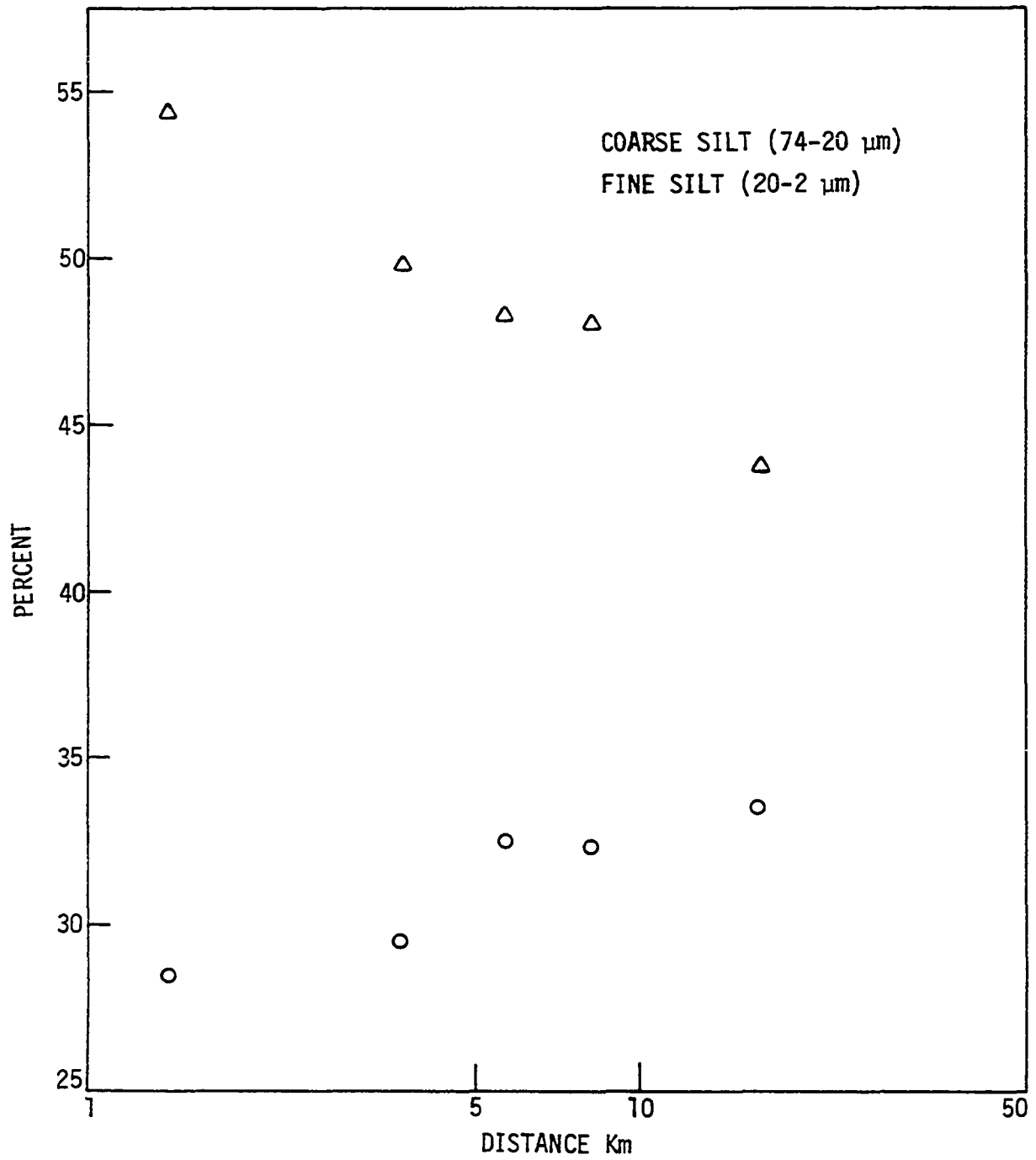
Figure 53. Log distance vs percent coarse and fine silt, south side - Missouri West

regions, as previously discussed.

Clay content and median particle size also change systematically with increasing distance from the river and are shown in Figure 54. These trends also appear to fit well with linear semilogarithmic expressions, and are given as:

$$Y = 15.45 + 4.27 \log X \qquad r = 0.8750$$

$$Y = \% \text{ clay}$$

$$Y = 22.65 - 3.99 \log x \qquad r = 0.9900$$

$$Y = \text{median particle size } (\mu m) \qquad X = \text{distance (Km)}$$

The equation for clay content is significant at 5 percent, while the expression for median size is significant at the 1 percent level.

Lack of sufficient data north of the river prohibits a full description of similar trends for particle size, however a few observations may be made. The general trends of decreasing coarse silt content and median particle size coupled with an increase in fine silt and clay content can be seen. These relations apply to both sides of the river, however not in the same magnitude. Note that site 4-MW located 0.9 miles (1.4 km) south is much more coarse textured than site 8-MW located at a distance of only 0.3 miles (0.5 km) north. Since the major difference appears in the amount of coarse silt, this may suggest that the sorting
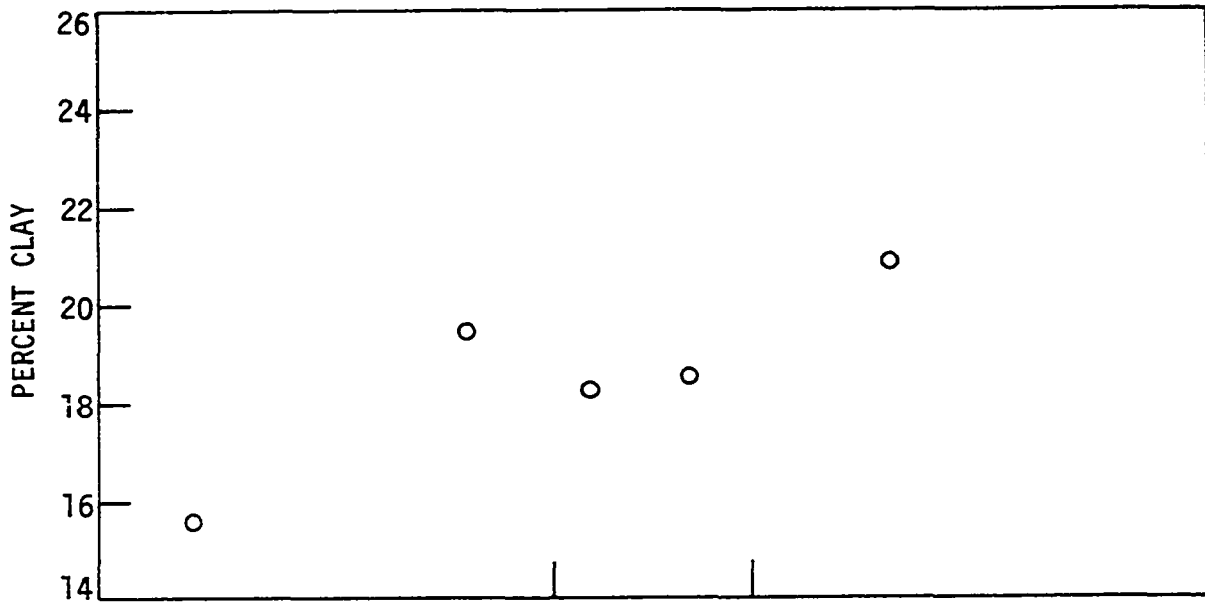
Figure 54a . Log distance vs percent clay, south side - Missouri West
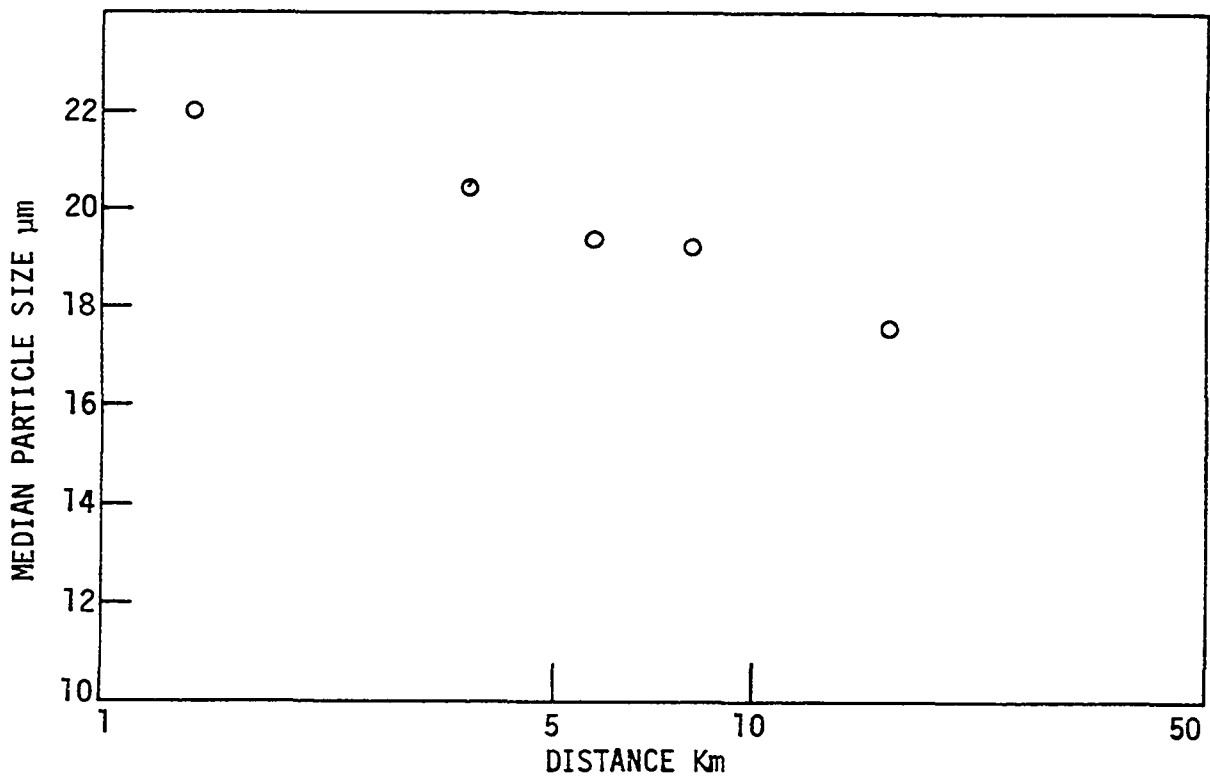
Figure 54b . Log distance vs median particle size, south side - Missouri West

mechanism is stronger in certain directions. One would

expect material even closer to the river on the south side

to be coarser still. This phenomenon is less pronounced

at greater distance as seen by examining particle size of

sites 1- and 7-MW, located at approximately the same

distance on opposite sides of the river. Differences in

each size fraction are less than those at shorter distances.

Missouri-East (ME)

Table 6 gives site information for ten sampling loca-

tions along the main eastern traverse, and in addition

similar data are presented for three supplemental sites,

7-, 8- and 13-ME. A graph of thickness versus distance for

the main traverse is shown in Figure 55. Data south of the

river show a curvilinear trend away from the river, while

the thickness trend north of the river is somewhat linear.

Difficulty in sampling on the north side of the river does

not provide enough data for complete analysis.

Semilogarithmic and logarithmic plots for data south

of the river are shown in Figure 56, and regressions of

these data give the following equations:

$$Y = 275.70 - 126.12 \log X \qquad r = 0.9786$$

$$\log Y = 2.39 - 0.25 \log X \qquad r = 0.9909$$

Again both functions are significant at 1 percent, however

the log-log form gives a higher correlation coefficient and

Table 6.   Site information - Missouri East transect

Site		Distance		Loess Thickness		Notes
		Mi.	Km	in.	cm	
1-ME	S[a]	2.7	4.4	75	190.5	Res. Paleosol over Bedrock
2-ME	S	6.7	10.8	48	121.9	Sed.
3-ME	S	13.2	21.2	42	106.7	Sed. over Bed-rock
4-ME	S	23.1	37.1	40	101.6	Sed. over Res. Paleosol
5-ME	S	19.8	31.9	41	104.1	Res. Paleosol over Bedrock
6-ME	S	1.2	1.9	80	203.2	Till Paleosol (?)
7-ME	E			78	198.1	Sed. over Till Paleosol
8-ME	E			42	106.7	LSP (?)
9-ME	N	8.4	13.6	24	61.0	Sed. over Till Paleosol
10-ME	N	6.6	10.7	38	96.5	Sed. over Res. Paleosol
11-ME	S	0.1	0.1	168	426.7	Loveland Loess (?) over Res. Paleosol
12-ME	N	2.0	3.2	58	147.3	Sed. over Res. Paleosol
13-ME	W			176	447.0	LSP (?)

[a]S - site located south side of river.
 E - site located east side of river.
 N - site located north side of river.
 W - site located west side of river.
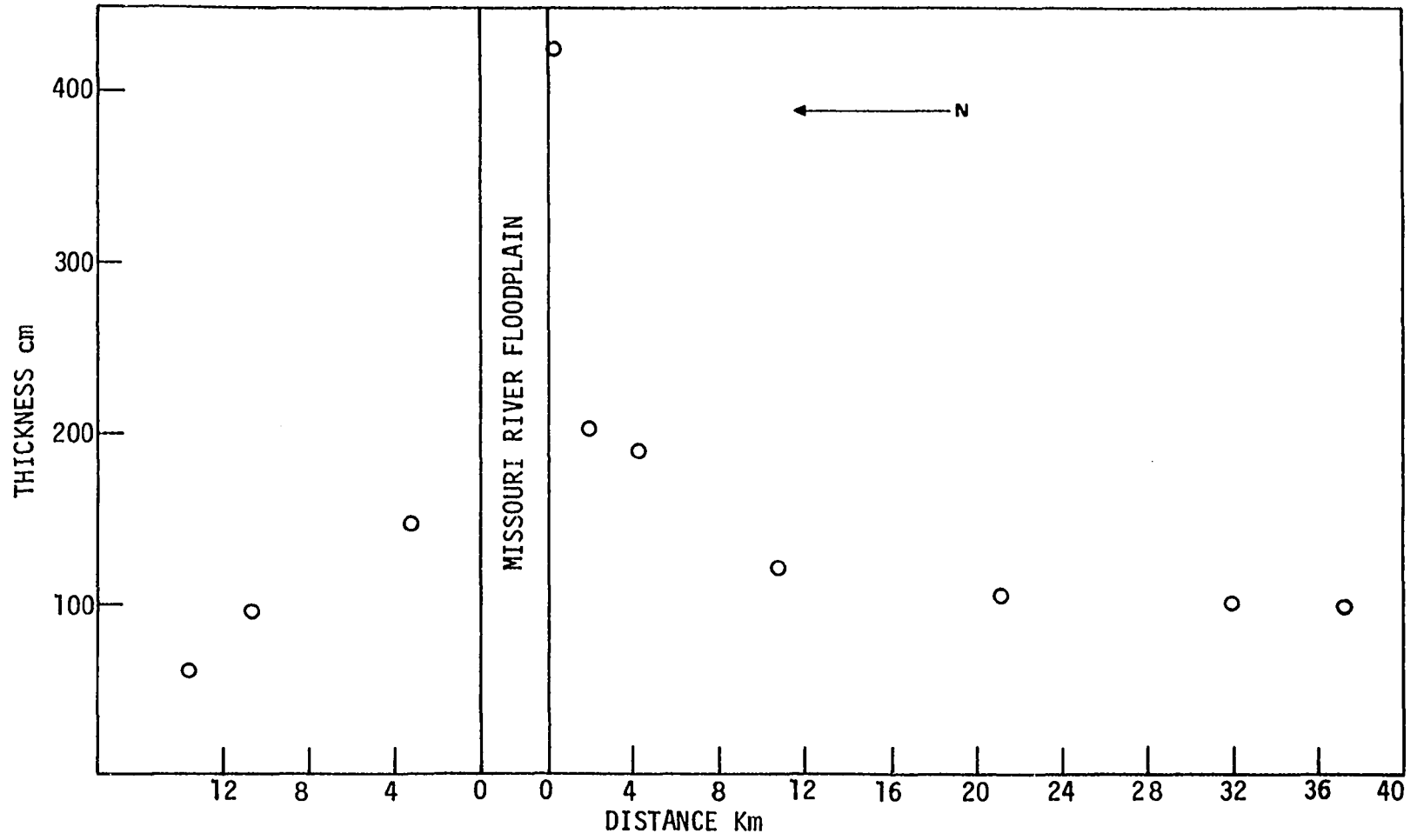
Figure 55. Distance vs thickness - Missouri East
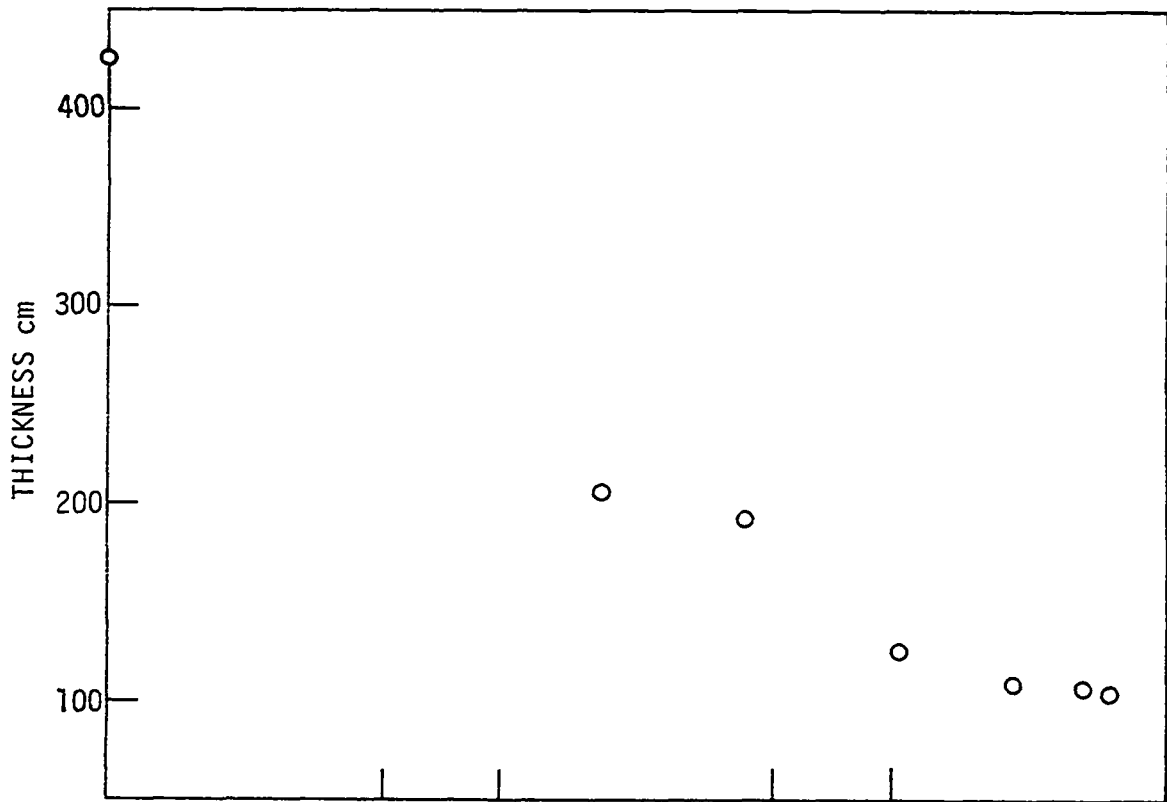
Figure 56a. Log distance vs thickness, south side -
Missouri East
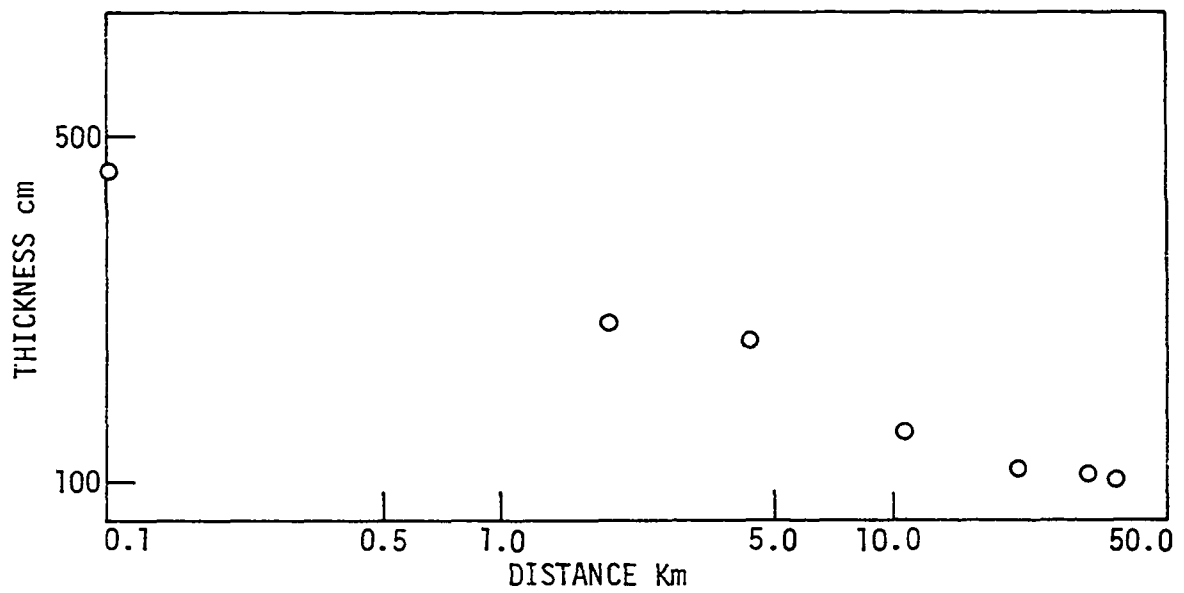
Figure 56b. Log distance vs log thickness, south side -
Missouri East

thus appears to give a better fit. This is probably be-
cause of the thickness close to the river; 168 inches
(426.7 cm).

Particle size data for this traverse are expressed on
a clay-free basis and are summarized in Table 7. Because
of the shallow depths of loess at the majority of sampling
locations, this technique was used to "normalize" the data
for analysis. As previously discussed, clay-free particle
size has been shown to be an effective means of interpreting
data in thin-loess areas. The data are presented graphi-
cally in Figure 57 for sites located south of the river.
As before, linear regressions of semilogarithmic plots give
expressions which are significant at 1 percent:

$$Y = 52.91 - 11.46 \log X \qquad r = 0.9683$$

$$Y = \% \text{ clay-free coarse silt}$$

$$Y = 43.80 + 10.64 \log X \qquad r = 0.9497$$

$$Y = \% \text{ clay-free fine silt}$$

Iowa River

Site information for loess sampling in east-central
Iowa is summarized in Table 8. Locations which were sampled
only for particle size analysis did not have complete sections
measured, therefore thickness data are incomplete. In those
cases, the maximum sampling depth is indicated. Sampling
north of the Iowa River was limited because of the close
proximity of Iowan Erosion Surface.

Table 7. Area method particle size summary-Missouri East[a]

Site	Sand >74 μm	C. Silt 74-20 μm	F. Silt 20-2 μm
1-ME	2.9	42.8	54.3
2-ME	3.6	36.3	60.1
3-ME	5.7	39.0	55.3
4-ME	3.5	36.8	59.7
5-ME	6.1	37.0	56.9
6-ME	2.2	52.1	45.7
7-ME	1.7	46.4	51.9
8-ME	12.8	41.8	45.4
9-ME	20.8	37.4	41.8
10-ME	2.0	59.5	38.5
11-ME	3.4	65.0	31.6
12-ME	0.8	40.2	59.0
13-ME	0.8	62.2	37.0

[a]Expressed as clay-free basis (2μm-2mm = 100%).
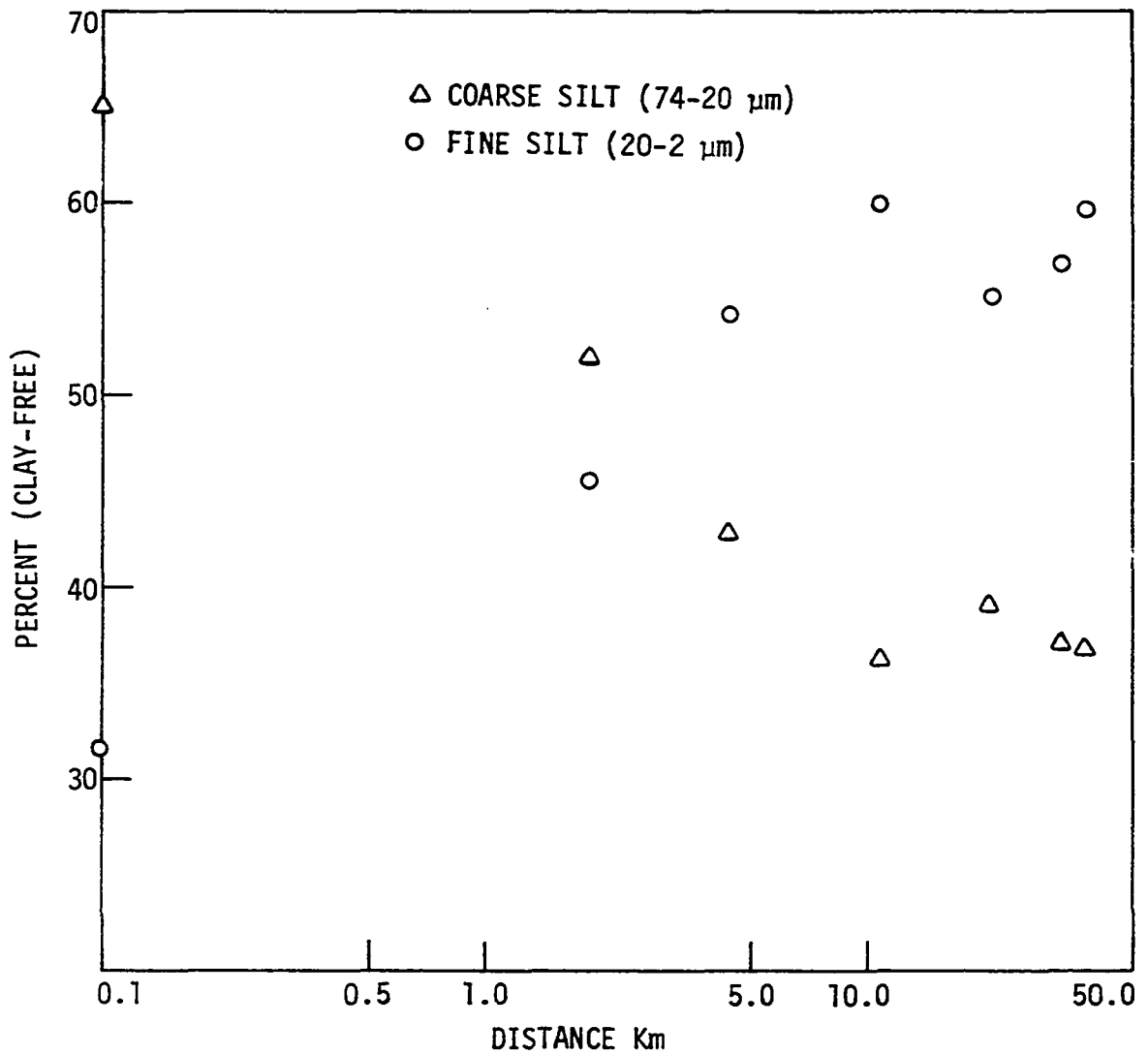
Figure 57. Log distance vs percent clay-free coarse and fine silt, south side - Missouri East

Table 8. Site information - Iowa River transect.

Site		Distance		Loess Thickness		Notes
		Mi.	Km	in.	cm	
1-LH	N[a]	2.2	3.5	207	525.8	BWS over YSP
2-LH	N	0.7	1.2	268	680.7	BWS over LSP
3-LH	S	5.3	8.6	202	513.1	YSP
4-LH	S	18.5	29.8	156	396.2	LSP
5-LH	S	11.2	18.0	164	416.6	BWS over YSP
6-LH	S	2.1	3.4	248	629.9	YSP
7-LH	S	29.9	48.1	138	350.5	YSP
8-LH	S	24.0	38.6	142	360.7	Swale over YSP
9-LH	S	1.2	1.9	238	604.5	BWS over LSP
10-LH	N	4.5	7.3	342+	868.7+	UU Loess
11-LH	S	0.6	1.0	418+	1061.7+	Sand interbeded w/loess
12-LH	S	2.0	3.3	249	632.5	BWS over YSP
14-LH	S	0.8	1.2	207+	525.8+	OU loess
15-LH	S	0.5	0.9	-	-	Thin loess over OU till
16-LH	N	0.1	0.2	252+	640.1+	LSP
17-LH	S	0.7	1.1	403	1023.6	BWS
18-LH	S	3.4	5.5	240	609.6	LSP

[a]N - site located north side of river.
S - site located south side of river.

Loess thickness in relation to the Iowa River and Iowan Erosion Surface is shown in Figure 58. Decreasing thickness away from both sides of the river is indicated, with a much greater thickness shown close to the river on the south side. Again a curvilinear decrease is indicated for changes in thickness on the south side. This decreasing thickness is shown on semilogarithmic and logarithmic plots in Figure 59 and can be expressed mathematically as:

$$Y = 893.30 - 354.49 \log X \qquad r = 0.9416$$
$$\log Y = 2.97 - 0.26 \log X \qquad r = 0.9839$$

The log-log fit produces a better fit of the data as indicated by a higher correlation coefficient however, as before, both functions are statistically significant at 1 percent. Note that the log-log form has been yielding a better fit to most of the thickness data presented. Thickness measurements north of the Iowa River taken on stable "preserved" landscape positions show a definite decrease away from the river however, the complexity of the Iowan Erosion Surface in this area produces many anomalies.

At site 10-LH, a minimum loess thickness of 342 inches (868.7 cm) was measured before drilling operations were stopped. As seen from the topographic sheet in Appendix B, this site is located directly on the classical Iowan border which stands prominantly above the "Iowan plain" to the north.
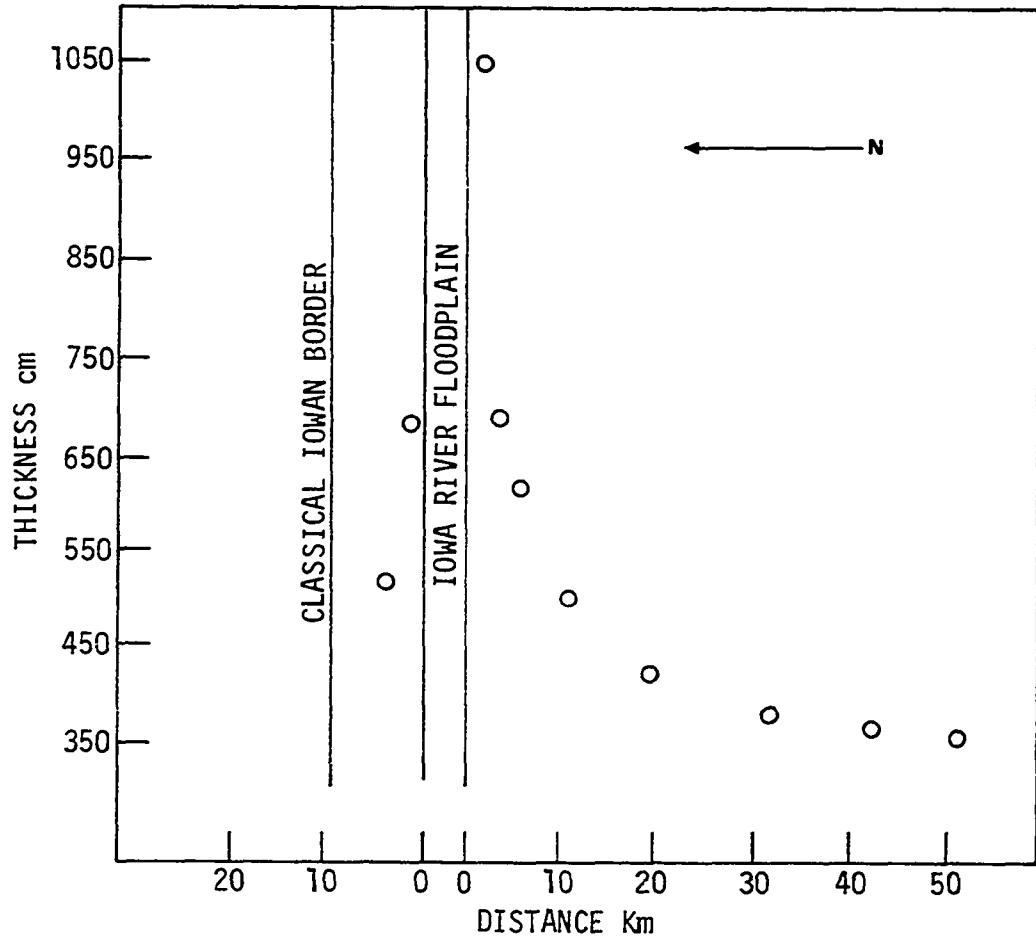
Figure 58. Distance vs thickness - Iowa River
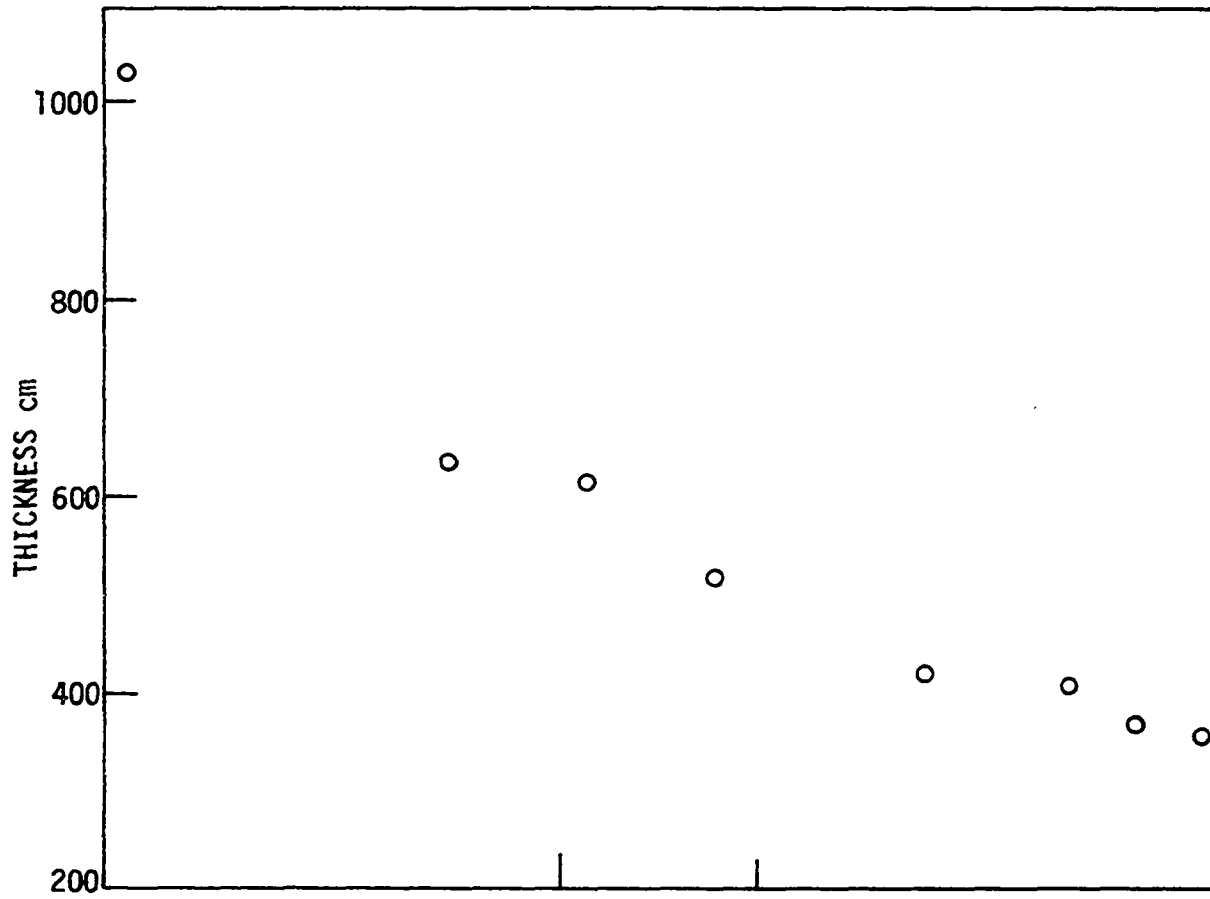
Figure 59a.   Log distance vs thickness, south side - Iowa River
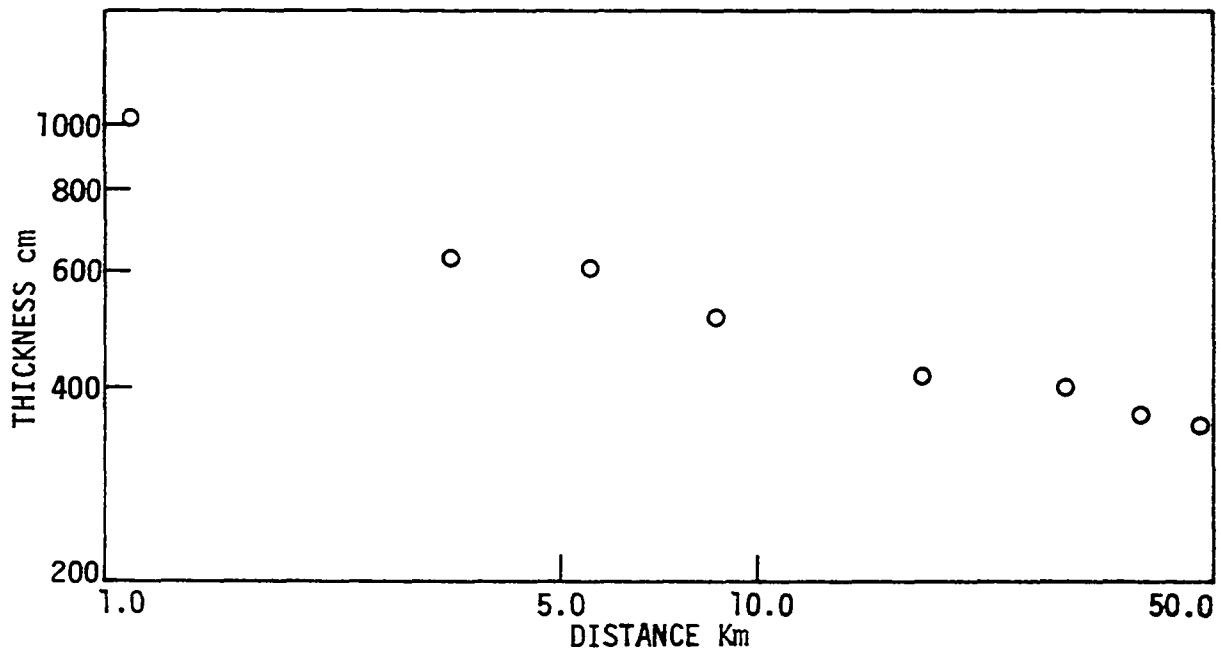
Figure 59b.   Log distance vs log thickness, south side - Iowa River

Loess thickness on the "Iowan" 0.1 miles (0.21 km) and 1.6 miles (2.63 km) directly north of site 10-LH was measured to be 88 inches (223.5 cm) and 78 inches (198.1 cm) respectively. Anomalous situations such as this cannot relate to any regional concept, and thus must be treated as local variations. Such variations also occur south of the river, as seen by examining site 11-LH which indicates a large amount of sand interbedded with only minor amounts of silt, Appendix D. Particle size analysis may help to reveal the source for such areas, and will be discussed in more detail.

A summary of the particle size analysis for individual sites is given in Table 9. Data for locations south of the river are presented graphically in Figures 60, 61, and 62. Changes in the silt fractions may be expressed in similar fashion to the Missouri data as:

$$Y = 55.67 - 15.85 \log X \qquad r = 0.9643$$

$$Y = \% \text{ coarse silt}$$

$$Y = 22.36 + 13.19 \log X \qquad r = 0.9046$$

$$Y = \% \text{ fine silt}$$

Although both equations are significant at 1 percent, much of the variation occurs from sites close to the river, where lateral changes occur. For example, sites 11-, 14- and 17-LH have large variations in sand content, from maximum to minimum respectively, which in turn affects the percentages

196

Table 9. Area method particle size summary - Iowa River

Site	Sand >74μm	C. Silt 74-20μm	F. Silt 20-2μm	Clay <2μm	Median Size μm
1-LH	1.3	44.1	32.0	22.6	16.8
2-LH	0.9	47.9	29.2	22.0	19.1
3-LH	1.5	38.8	37.3	22.4	14.6
4-LH	2.0	33.4	38.0	26.6	11.7
5-LH	1.4	33.0	40.2	25.4	11.4
6-LH	1.5	42.2	32.8	23.5	15.1
7-LH	1.1	30.3	43.1	25.5	9.6
8-LH	0.8	31.6	42.9	24.7	10.1
9-LH	0.9	49.5	31.4	18.2	20.1
12-LH	2.1	47.9	31.4	18.6	20.0
14-LH	15.9	55.5	15.7	12.9	37.7
16-LH	2.5	43.8	35.3	18.4	18.3
17-LH	6.3	58.1	20.2	15.4	31.5
18-LH	0.5	47.5	33.3	18.7	18.6
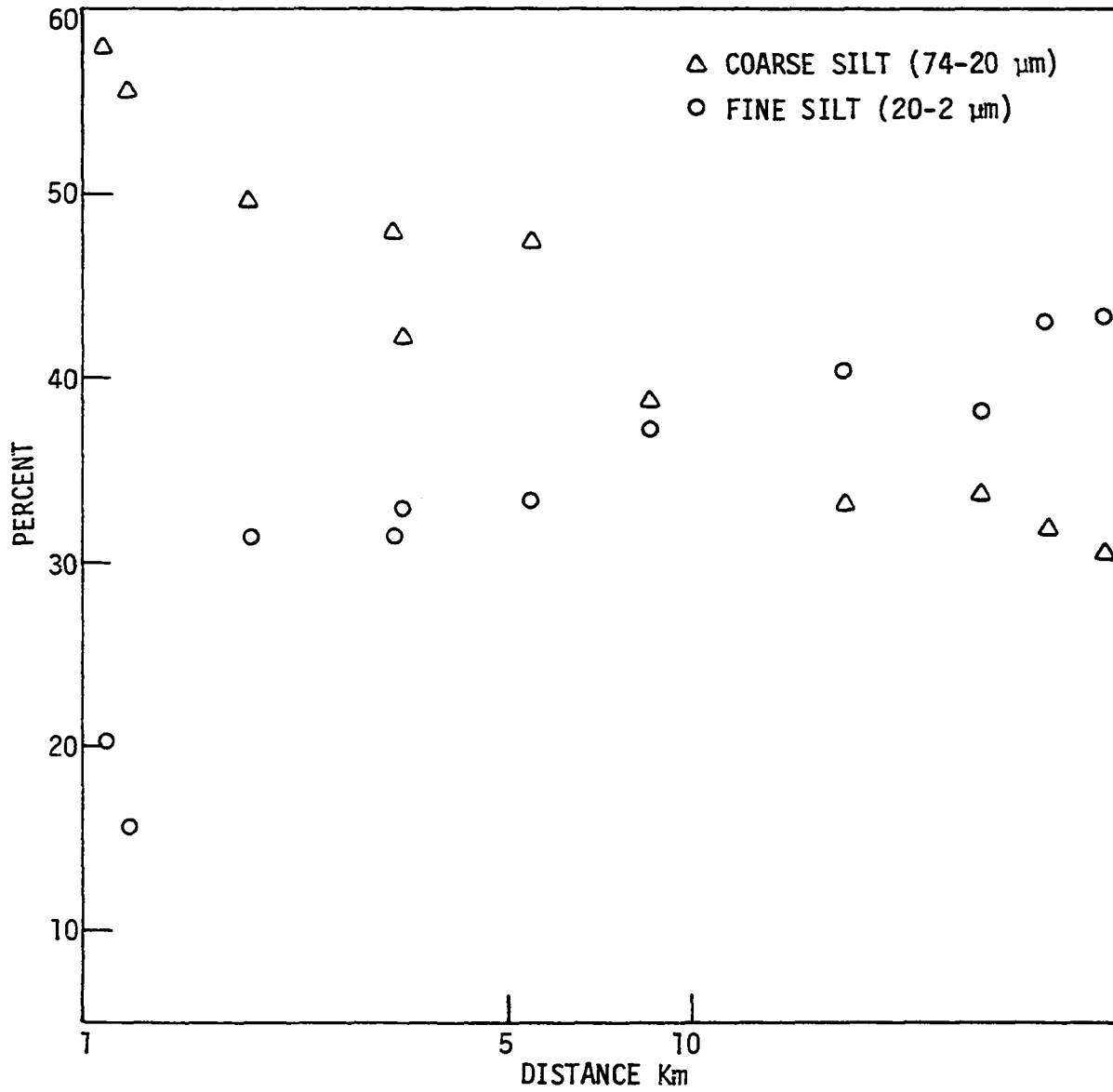
Figure 60. Log distance vs percent coarse and fine silt, south side - Iowa River

of other constituents.

Systematic changes in clay content south of the river
are shown in Figure 61 and may be expressed empirically as:

$$Y = 15.42 + 6.83 \log X \qquad r = 0.8956$$

$$Y = \% \text{ clay}$$

In addition, median particle size, Figure 62, changes accord-
ing to:

$$Y = 29.02 - 13.03 \log X \qquad r = 0.8647$$

$$Y = \text{median particle size in } \mu\text{m}$$

As with changes in silt content, the trends of increasing
clay content and decreasing median size are both significant
at 1 percent. North of the river, clay content increases
away from the river, while no specific trends are visible in
either silt content or median particle size. This is no
doubt partially a result of insufficient data.

In regard to previously mentioned local variations, or
anomalies, a few observations may be made concerning particle
size. At site 10-LH a stratigraphic change in gradation
occurs at approximately 151 inches (383.5 cm), as indicated
by particle size data given in Appendix C. The upper material
is finer textured, with the following values: 2.1% sand,
45.5% coarse silt, 26.5% fine silt, and 25.9% clay. In con-
trast to this, the lower portion of the section contains more
sand, 4.1%, considerably more coarse silt, 53.4%, and
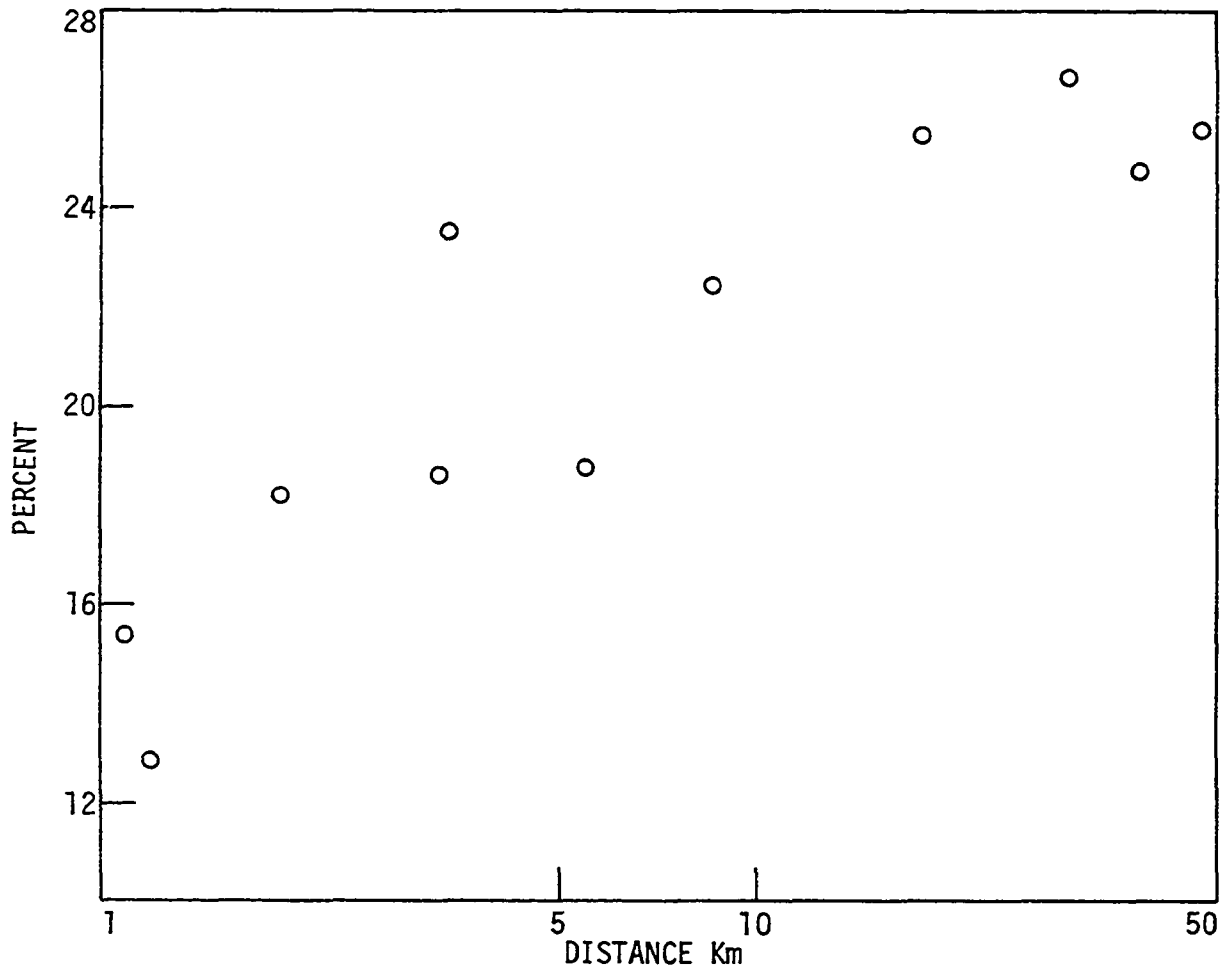
Figure 61. Log distance vs percent clay, south side - Iowa River
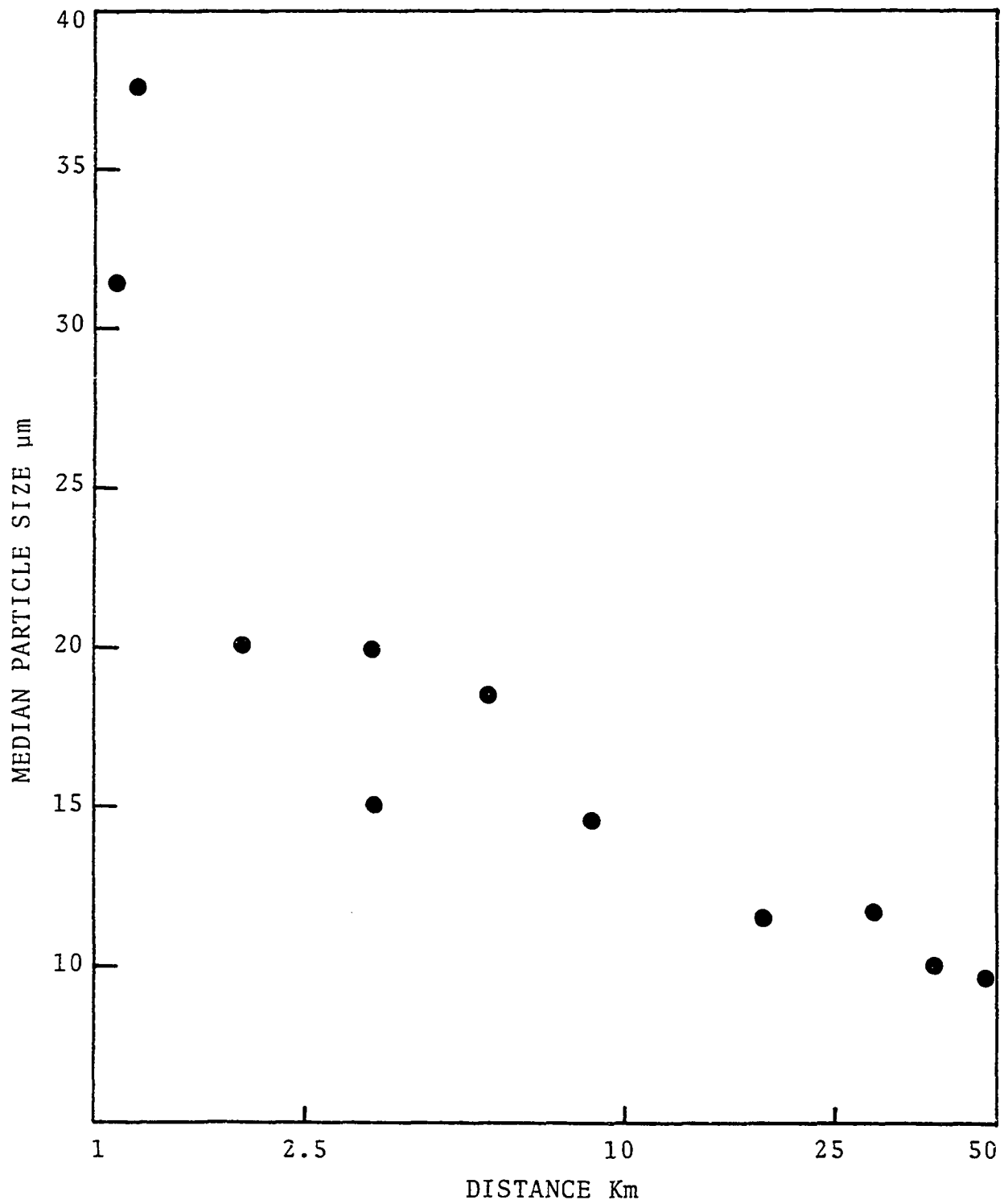
Figure 65. Log distance vs median particle size,
south side - Iowa River

considerably less clay, 17.4%. Fine silt content in the lower unit is about the same, averaging 25.1%. This dichotomy might suggest two sources; one close, relating to the lower increment of loess, and one at greater distance, relating to the uppermost increment.

Lateral sorting of material close to the source can be seen in samples taken at site 15-LH, located on the first, lowest Iowan Erosion Surface position adjacent to the flood-plain, Appendix B. Particle size analysis of samples from 3 sites, approximately 10 feet (3.05 m) apart, show that this "silty sand" becomes progressively finer over a very short distance (see Appendix C). Sand content decreases from 73.5 to 42.0%, while clay content increases from 7.8 to 15.3% away from the source. It is interesting to note that both coarse and fine silt fractions increase across the sampling set.

Density

Statistical analyses performed on bulk density data given in Appendix F, were conducted to substantiate any significant relationships between density, depth, and particle size. Multiple regressions were performed with bulk density as the dependent variable and depth, % coarse silt + sand, % fine silt, and % clay as independent variables. Regressions were performed in three manners; (1) combining all data, (2) subdividing data into weathering zones, i.e. oxidized, mottled, and deoxidized, disregarding location, and
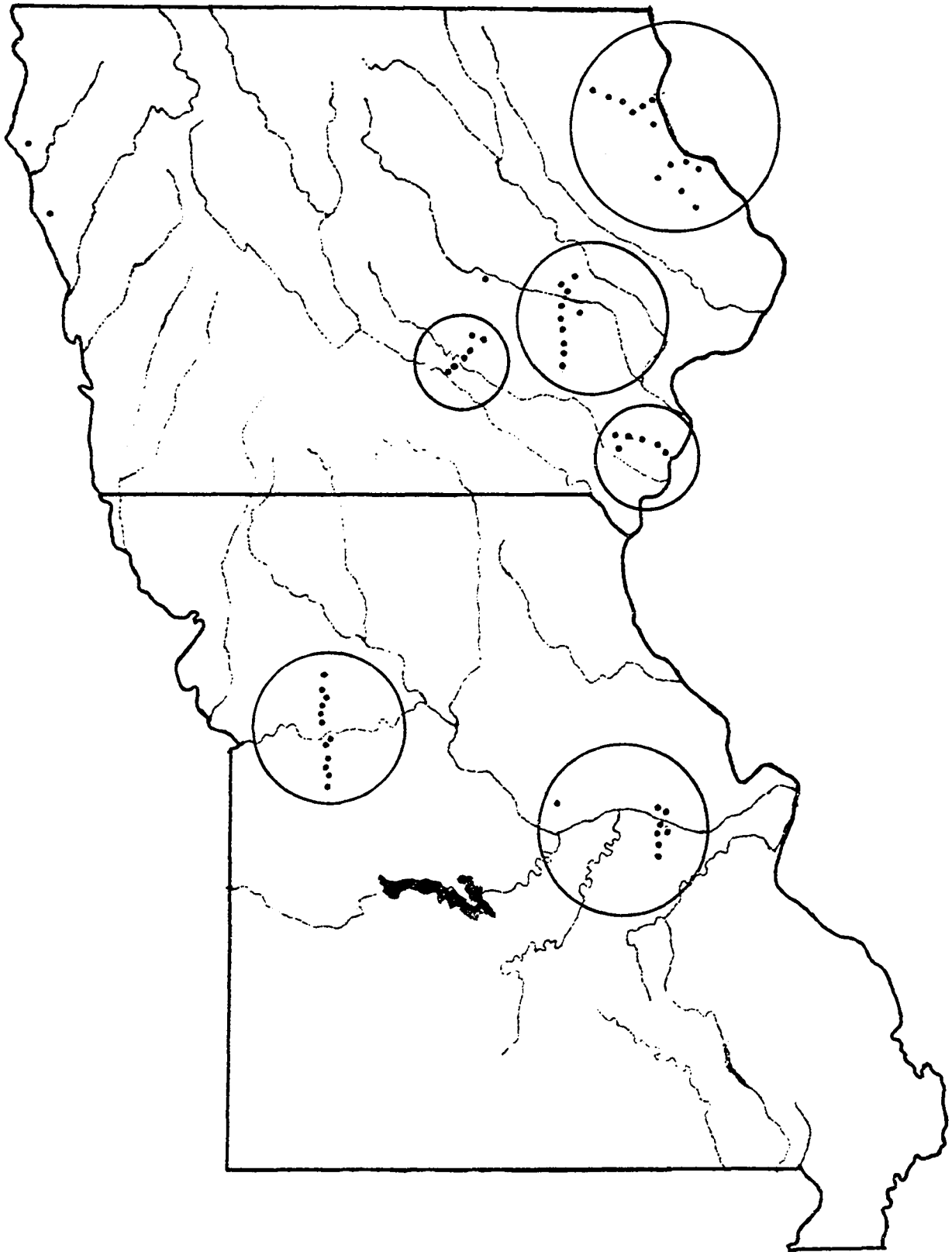
Figure 63. Location of density subgroups

(3) subdividing data into locations, shown in Figure 63,
disregarding weathering zones. Results of these analyses
are given in Appendix G.

Reasoning behind this break-down of analysis was to
investigate the influence of moisture, either as perched
water table, or rainfall. Figure 64 presents histograms of
percent saturation calculated for individual weathering
zones. These data indicate that weathering zone could be a
good indicator of seasonal moisture.

Equations for the best fit 1-variable, 2-variable, 3-
variable models are given in Table 10 from analyses of all
combined data. All three models are significant at 1%,
which indicates that certain variables do influence bulk
density. It should be noted however, that a large amount of
variation is present which is not explained by either particle
size or depth. Such variation is attributed to individual
site variables which are not constant throughout. Signifi-
cance testing is based on correlation coefficients and F-tests
for the model, and partial F-tests for individual variables.

Analyses of the data, subdivided into weathering zones
does not drastically affect the results and in fact produces
a much poorer fit for the deoxidized zone. Equations are
not given for these individual analyses, however, the effect
of weathering zones on density may be approached in another
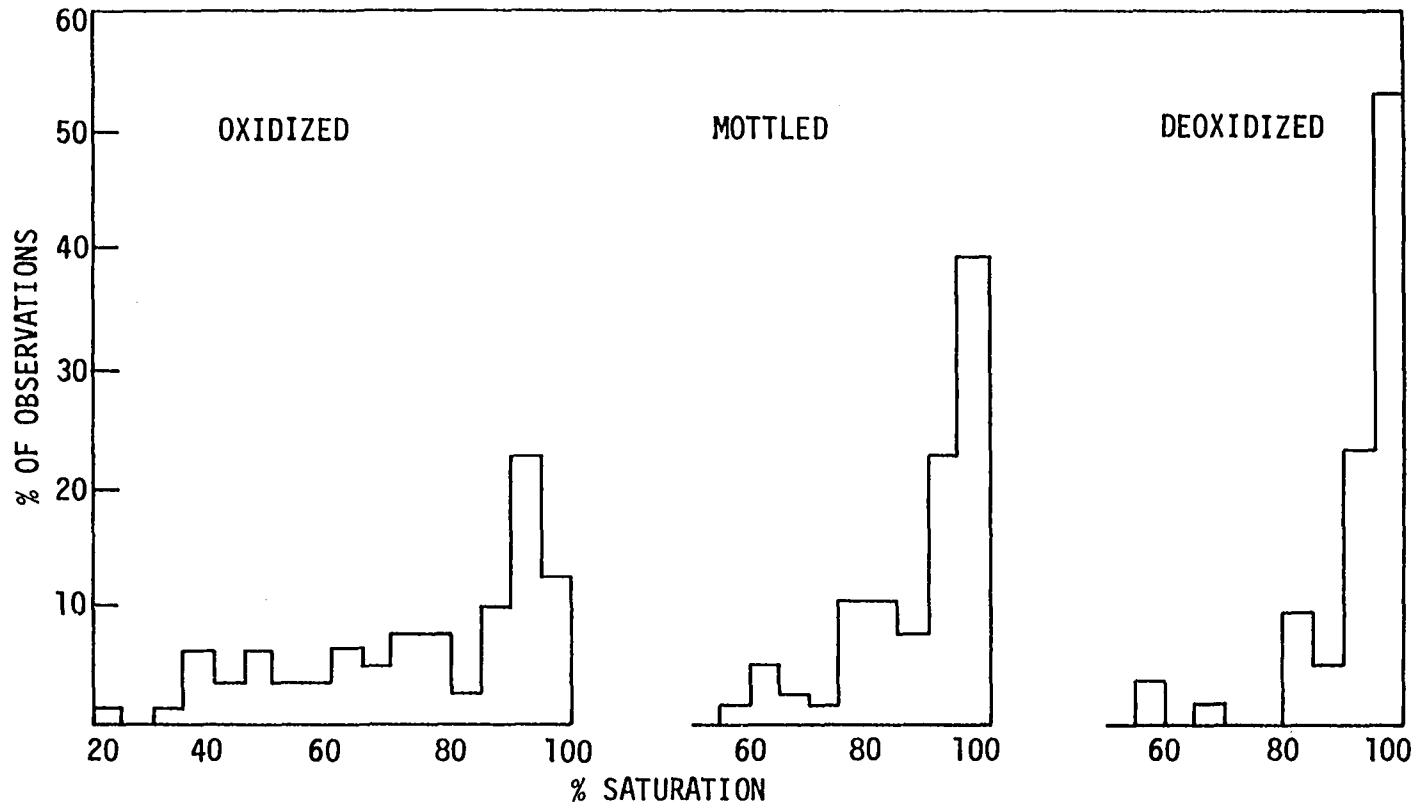
Figure 64. Histograms of percent saturation summarized by weathering zone

Table 10. Regression models for bulk density[a]

$Y = 1.34 + 0.005\ X3$

$r = 0.3489$

$F = 28.28$ significant @ 1%

$Y = 1.28 + 0.0001\ X1 + 0.005\ X3$

$r = 0.4223$

$F = 22.02$ significant @ 1%

$X1\ F = 13.97$ significant @ 1%

$X3\ F = 36.14$ significant @ 1%

$Y = 1.84 + 0.0001\ X1 - 0.005\ X2 - 0.006\ X4$

$r = 0.4258$

$F = 14.92$ significant @ 1%

$X1\ F = 8.47$ significant @ 1%

$X2\ F = 34.21$ significant @ 1%

$X4\ F = 12.67$ significant @ 1%

---

[a]Y = bulk density, gm/cm^3
$X1$ = depth, cm
$X2$ = % coarse silt + sand (2mm-2μm)
$X3$ = % fine silt (20-2μm)
$X4$ = % <2μm clay

manner. Consider the summary statistics presented in Table 11. The data have been divided into weathering zones and further subdivided into weathering zones within location areas. Disregarding measurements in the soil solum, for all areas with the exception of east-central Missouri, a progression of increasing bulk density occurs going from oxidized to mottled to deoxidized zones. This no doubt reflects the influence of moisture movement throughout the profile.

Regression analyses for individual sampling areas in some cases produce a much better fit to the data. This is particularly noticeable by examining the correlation coefficients for regression models of data in east-central Iowa, south-central Iowa, northeast Iowa, and east-central Missouri. Data for Iowa indicate that depth and fine silt content are the most significant variables, while clay content and fine silt appear more significant for east-central Missouri.

Shear strength

Regression analyses on BST data were conducted with friction angle, ϕ, and cohesion, c, as dependent variables, and depth, bulk density, moisture content, and clay content as independent variables. Further analyses were performed, combining bulk density and moisture content and calculating percent saturation. Results of all regression models are given in Appendix I. Regressions using percent saturation indicated that this variable was not statistically

Table 11. Density data summary

Location	Weathering Zone	Number of Observations	Mean gm/cc	Std. Deviation	Minimum Value	Maximum Value	Std Error of Mean	Variance	Coefficient of Variation
-	-	213	1.50	0.086	1.24	1.74	0.006	0.007	5.751
-	Solum	10	1.47	0.072	1.34	1.56	0.023	0.005	4.903
	Oxidized	69	1.46	0.085	1.24	1.67	0.010	0.007	5.808
	Mottled	78	1.50	0.074	1.35	1.67	0.008	0.005	4.922
	Deoxidized	53	1.55	0.075	1.36	1.74	0.010	0.006	4.810
	Unoxidized	3	1.63	0.097	1.55	1.74	0.056	0.009	5.946
East-Central Iowa	Oxidized	27	1.47	0.067	1.29	1.60	0.013	0.005	4.588
	Mottled	21	1.52	0.079	1.36	1.66	0.017	0.006	5.238
	Deoxidized	7	1.60	0.061	1.53	1.69	0.023	0.004	3.824
	Unoxidized	2	1.64	0.134	1.55	1.74	0.095	0.018	8.167
South-Central Iowa	Oxidized	8	1.44	0.035	1.39	1.50	0.012	0.001	2.444
	Mottled	15	1.51	0.031	1.46	1.56	0.008	0.001	2.048
	Deoxidized	6	1.56	0.057	1.47	1.63	0.023	0.003	3.640
Northeast Iowa	Oxidized	12	1.46	0.078	1.26	1.56	0.022	0.006	5.312
	Mottled	12	1.51	0.088	1.35	1.67	0.025	0.008	5.815
	Deoxidized	14	1.61	0.048	1.52	1.74	0.013	0.002	2.970
	Unoxidized	1	1.61	-	1.61	1.61	-	-	-

Table 11. continued

Location	Weathering Zone	Number of Observations	Mean gm/cc	Std. Deviation	Minimum Value	Maximum Value	Std. Error of Mean	Variance	Coefficient of Variation
Southeast Iowa	Solum	2	1.46	0.085	1.40	1.52	0.060	0.007	5.812
	Mottled	6	1.50	0.028	1.46	1.54	0.011	0.008	1.860
	Deoxidized	11	1.51	0.059	1.41	1.58	0.018	0.003	3.899
West-Central Missouri	Solum	2	1.38	0.049	1.34	1.41	0.035	0.002	3.600
	Oxidized	16	1.41	0.088	1.24	1.61	0.022	0.008	6.252
	Mottled	20	1.47	0.080	1.36	1.61	0.018	0.006	5.461
	Deoxidized	13	1.50	0.074	1.36	1.57	0.021	0.006	4.972
East-Central Missouri	Solum	6	1.50	0.049	1.42	1.56	0.020	0.002	3.277
	Oxidized	5	1.60	0.063	1.51	1.67	0.028	0.004	3.908
	Mottled	4	1.60	0.037	1.55	1.64	0.018	0.001	2.318
	Deoxidized	2	1.55	0.035	1.52	1.57	0.025	0.001	2.288

significant, and therefore these results have not been included.

Tables 12 and 13 present results of the best-fit models for friction angle and cohesion, respectively. One-variable models indicate that friction angle increases with depth and decreases with increasing clay content. Two-variable models for friction angle show that depth is the most important variable, and that neither moisture content nor clay content significantly add to the models. The 3-variable model does show some significance with depth, bulk density and moisture content; however, the last two variables are still not as important as depth.

Regression models for cohesion indicate some of the same significant variables as shown for friction angle. Cohesion decreases with increasing depth and increases with increasing clay content as given by 1-variable models. Results of the 2 and 3-variable models show a weakening of the fit, as indicated by lower significance of the model, and indicate that the addition of variables does not significantly add to the regression.

Clay aggregation-dispersion

Results of particle size analyses of profiles 1-, 3- and 8-LH using modified dispersion technique are given in Appendix E, and the summary particle size data are shown in Table 14. These samples were run using the standard

Table 12. Regression models for friction angle[a]

$Y1 = 23.90 + 0.04\ X1$

$r = 0.5353$

$F = 13.66$ significant @ 1%

$Y1 = 47.89 - 0.78\ X4$

$r = 0.3879$

$F = 6.55$ significant @ 5%

$Y1 = 32.15 + 0.04\ X1 - 0.36\ X3$

$r = 0.5746$

$F = 8.13$ significant @ 1%

$X1$ $F = 14.75$ significant @ 1%

$X3$ $F = 2.15$

$Y1 = 30.18 + 0.04\ X1 - 0.33\ X4$

$r = 0.5487$

$F = 7.75$ significant @ 1%

$X1$ $F = 7.39$ significant @ 1%

$X4$ $F = 1.04$

$Y1 = 67.10 + 0.05\ X1 - 22.83\ X2 - 0.45\ X3$

$r = 0.6231$

$F = 6.77$ significant @ 1%

$X1$ $F = 18.47$ significant @ 1%

$X2$ $F = 3.03$ significant @ 10%

$X3$ $F = 2.87$ significant @ 10%

---

[a] $Y1$ = friction angle, degrees
$X1$ = depth, cm
$X2$ = bulk density, gm/cm^3
$X3$ = moisture content, %
$X4$ = % <2µm clay

Table 13. Regression models for cohesion[a]

Y2 = 19.82 - 0.04 X1

r = 0.4094

F = 6.84   significant @ 5%

Y2 = 2.11 + 0.69 X4

r = 0.3181

F = 4.17   significant @ 5%

Y2 = 7.67 - 0.04 X1 + 19.09 X2

r = 0.4459

F = 4.09   significant @ 5%

X1   F = 8.07   significant @ 1%

X2   F = 1.29

Y2 = 12.46 - 0.03 X1 + 0.32 X4

r = 0.5487

F = 4.17   significant @ 5%

X1   F = 7.60   significant @ 1%

X4   F = 0.73

Y2 = -16.00 - 0.04 X1 + 19.07 X2 + 0.35 X4

r = 0.4671

F = 2.98   significant @ 10%

X1   F = 4.13   significant @ 10%

X2   F = 1.28

X4   F = 0.79

---

[a] Y2 = cohesion, KN/m^2
   X1 = depth, cm
   X2 = bulk density, gm/cm^3
   X3 = moisture content, %
   X4 = % <2 μm clay

technique, with the exception that dispersing agent was not added during dispersion. Figure 65 shows a comparison, for individual test data, between results of standard and modified procedure.

With the exception of two samples, in all cases coarse and fine silt content measured with the modified technique show a definite increase over the standard method. In addition, the clay content is correspondingly decreased compared to the standard analysis.

Table 14. Area method dispersion particle size summary

Site	Sand >74 μm	C. Silt 74-20 μm	F. Silt 20-2 μm	Clay <2 μm
1-LH	0.6	49.4	35.8	14.2
3-LH	1.4	44.0	44.2	10.4
8-LH	0.7	35.1	45.9	18.3

This would suggest that even after pulverization and agitation, a percentage of the clay fraction is still attached to or held as larger particles. The elimination of dispersing agent only accounts for about 58 percent of the clay-sized particles. Comparison of the summarized data in Table 14 with corresponding data of Table 9 simply indicates that the modified analyses yield a coarser sediment.
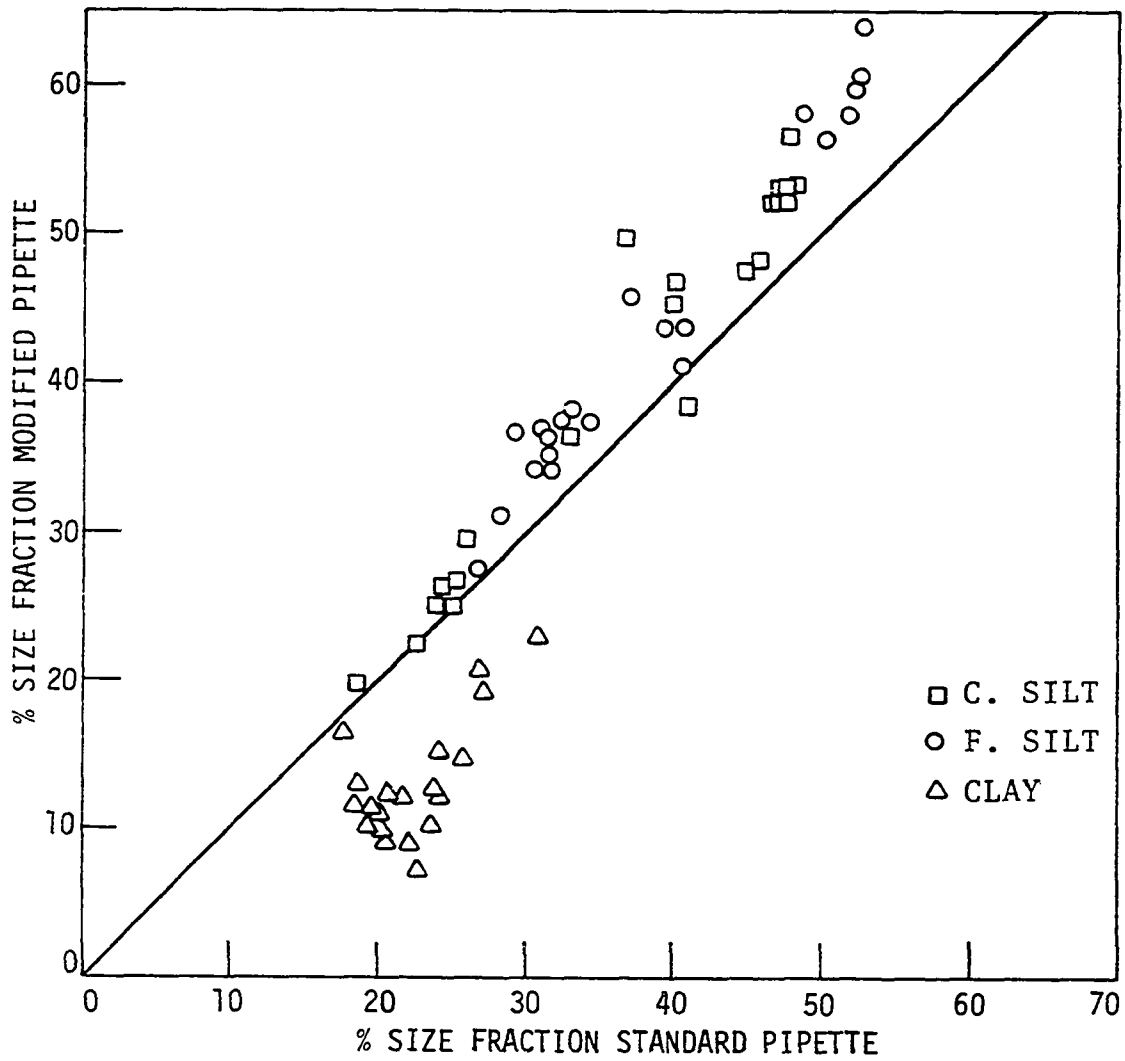
Figure 65. Modified vs standard pipette analyses

The effect of the turbulent dispersing action of the
air-jet apparatus was studied on two samples as previously
outlined. Figures 66 and 67 present the results of pipette
analyses with varying dispersion times. In both figures, an
increasing trend in both total clay and fine clay content
is shown with increasing dispersion time. However, at 5
minutes, the percent clay is still much less than that
obtained using standard analysis. This is in accordance with
previous results. Coarse silt content also shows a distinct
trend of decreasing percent with increasing time, however,
there is no definite trend shown in fine silt content.

Linear extrapolation of individual plots to zero dis-
persing time, gives the following results:

Sample	C. Silt	F. Silt	Clay	F. Clay
17-LH-9	66.9	27.4	2.9	2.1
4-LH-3	41.5	52.8	4.3	1.0

These data are drastically different from results using
standard procedures. Over a distance of 17.8 miles (28.7 m)
clay content only shows an increase of 1.4 percent, which
contrasts to an increase of 11.3 percent using the standard
dispersion method. Again this may suggest that the majority of
clay-sized particles and clay minerals are transported both
as silt-size aggregates and "piggy-back", being attached to
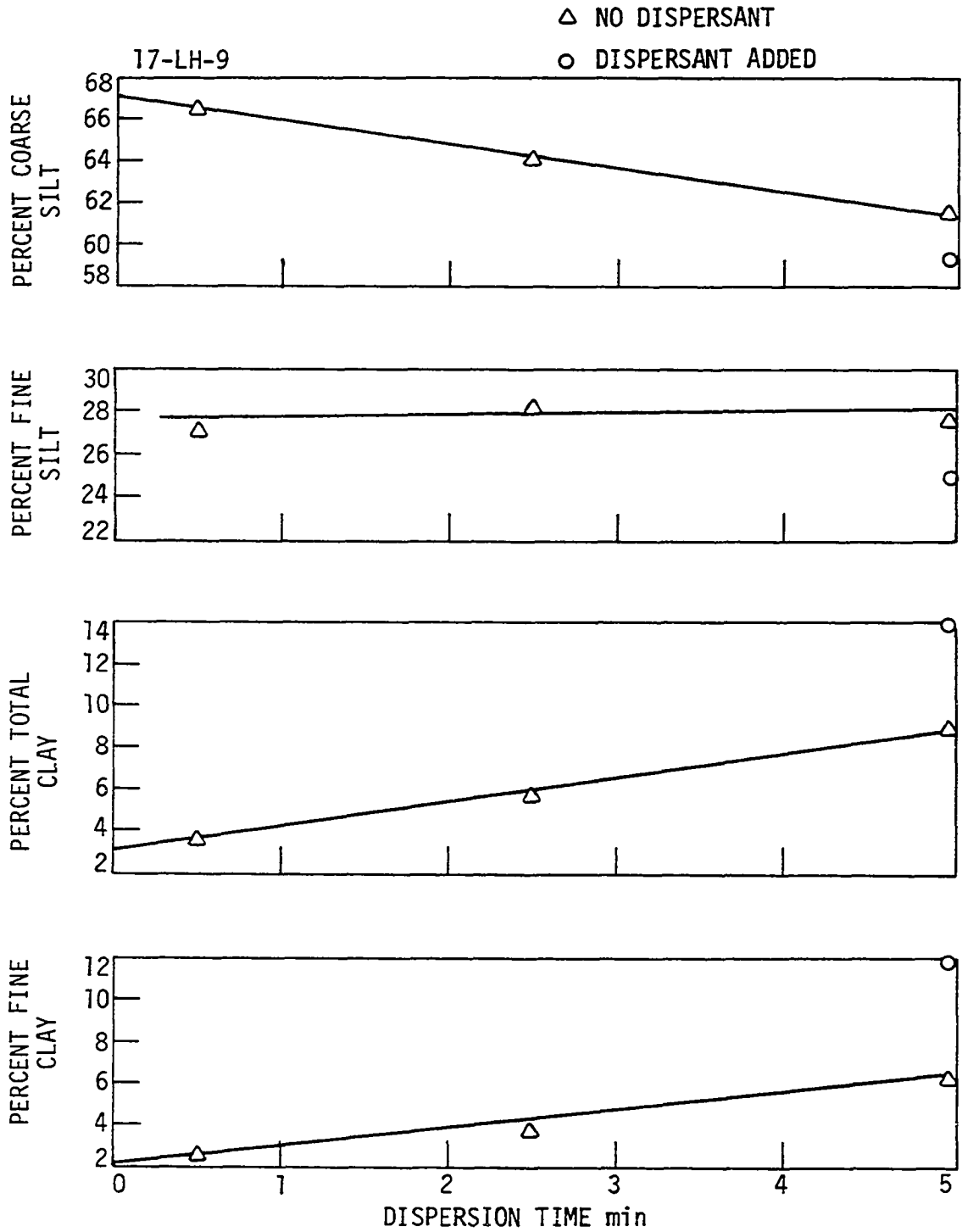
Figure 66. Dispersion time vs percent size fraction - 17-LH-9
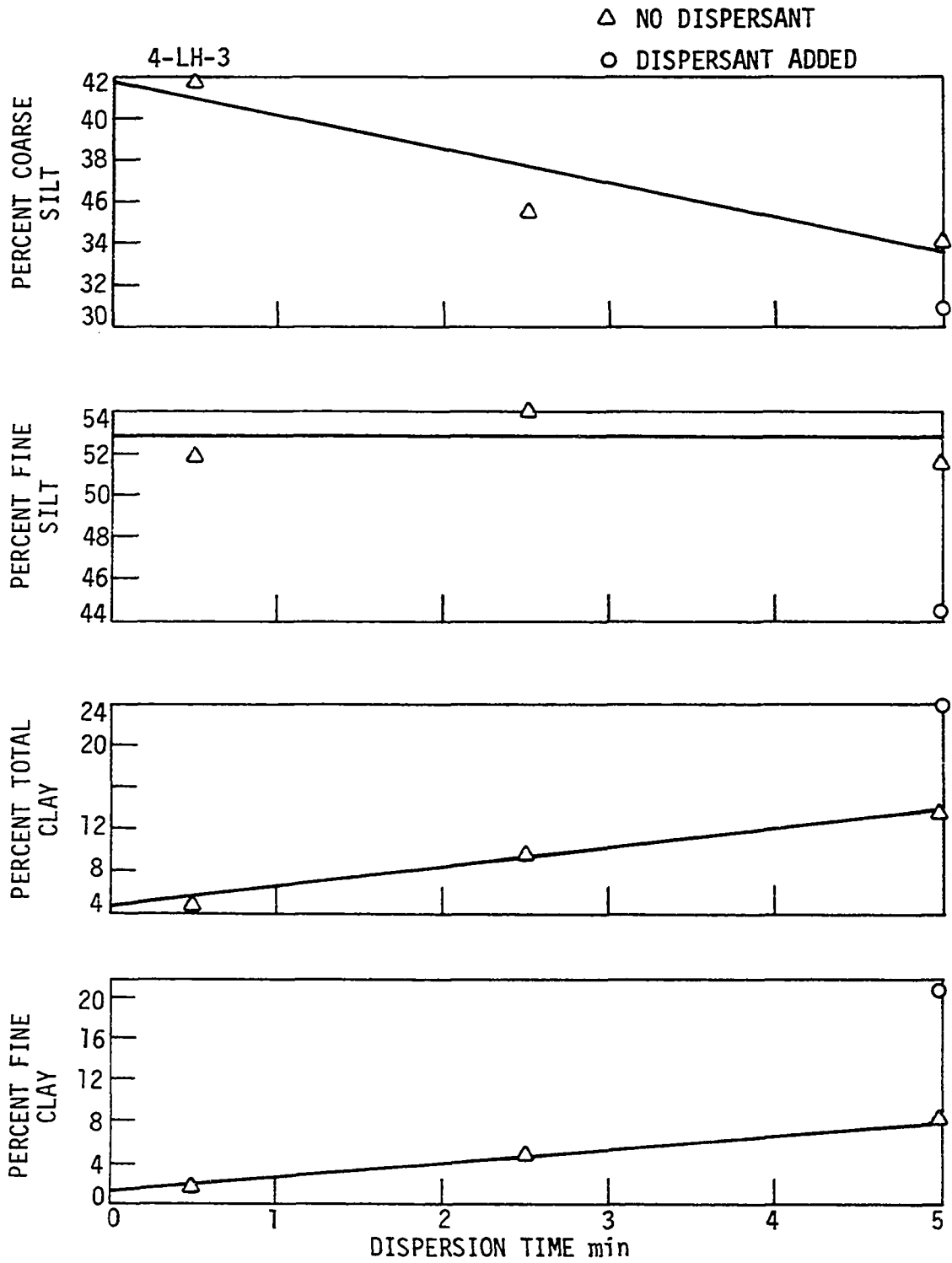
Figure 67. Dispersion time vs percent size fraction - 4-LH-3

host silt particles.

Scanning electron microscopy (SEM) was used to view selected samples from both Iowa and Missouri in order to observe the nature of individual particles. Micrographs are presented in Figures 68 thru 74 of samples 17-LH-12 and sample 1-MW-6.

The nature of undisturbed loess is shown in Figures 68a and 68b and is similar to photos presented by Badger (4) for western Iowa loess, and others (17, 59, 141) for loess throughout the world. The open structure is apparent from the extensive voids which are present. Both angular and rounded particles are present, and occur in various sizes. This sample was further processed by pulverization and sieving as previously outlined and will be shown in subsequent photos.

Figure 69a shows an example of material from Sample 17-LH-12 which was retained on a #200 sieve, and is therefore of sand size. The aggregated nature of the particle is evident, being composed of a large number of smaller particles. This same phenomena is also displayed in smaller fractions, Figure 69b. Although the number of individual particles which are aggregated together is smaller by comparison, the gross effect is the same.

Figure 70a shows material which is in the same size fraction as the aggregated particle of Figure 69b , however
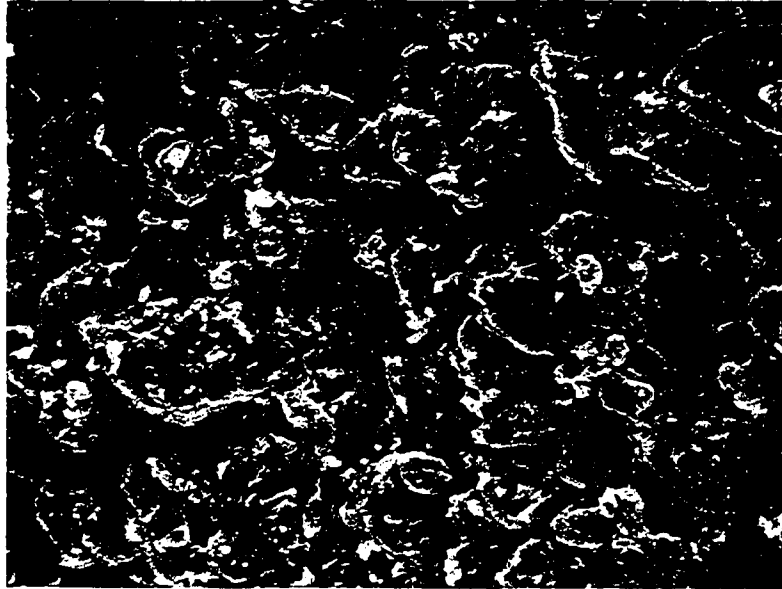
Figure 68a. SEM micrograph of undisturbed loess - sample 17-LH-12, magnification 300X
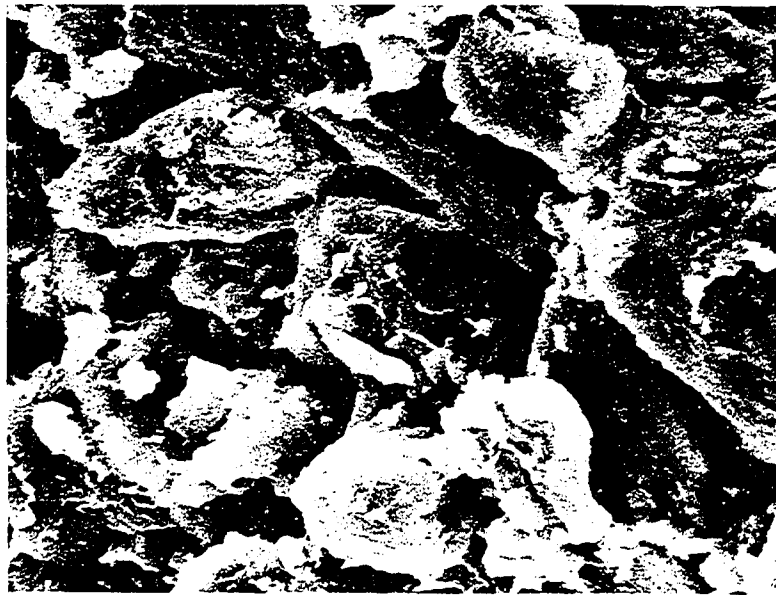
Figure 68b. SEM micrograph of undisturbed loess - sample 17-LH-12, magnification 1000X

Figure 69a. SEM micrograph: 17-LH-12 retained on #200
sieve, magnification 270X
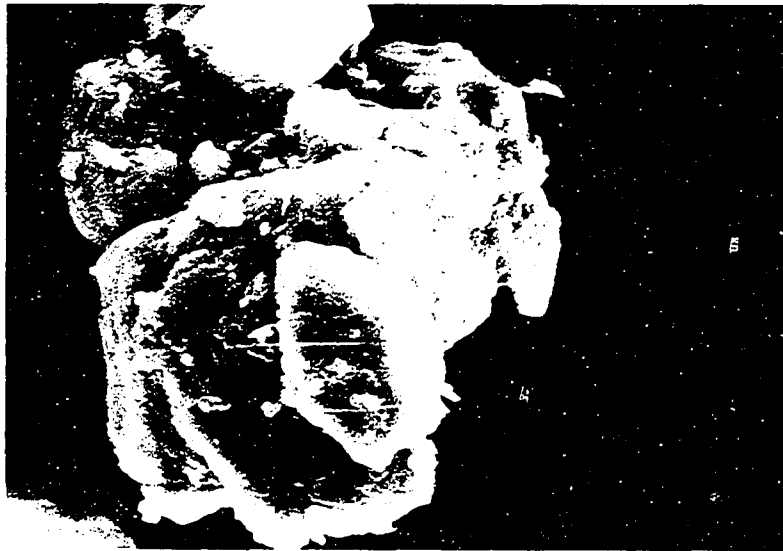
Figure 69b. SEM micrograph: 17-LH-12 retained on #325
sieve, magnification 1000X

Figure 70a. SEM micrograph: 17-LH-12 retained on #325 sieve, magnification 1000X

Figure 70b. SEM micrograph: 17-LH-12 passing #325 sieve, magnification 1000X

these particles appear much "cleaner." Basically, these
are individual silt particles with a minimal amount of
smaller particles attached. This is also the case with
material which passed a #325 sieve, finer than 44 μm, as
seen in Figure 70b.

Figure 71a and 71b show examples of aggregated parti-
cles from the sand fraction of sample 1-MW-6 which are very
similar in appearance to Figure 69a. Figure 72a and 72b
show material passing a #200 sieve but retained on a #325.
Again, both aggregated and "clean" particles are present as
previously shown in photos of the Iowa loess.

Figure 73a and 73b show an individual aggregated particle
from the same fraction as the previous photo set which appears
to have both clay-size quartz particles and clay mineral
flakes attached. The presence of both types of clay fraction
constitutents is seen further in Figure 74a and 74b for
material finer than 44 μm.
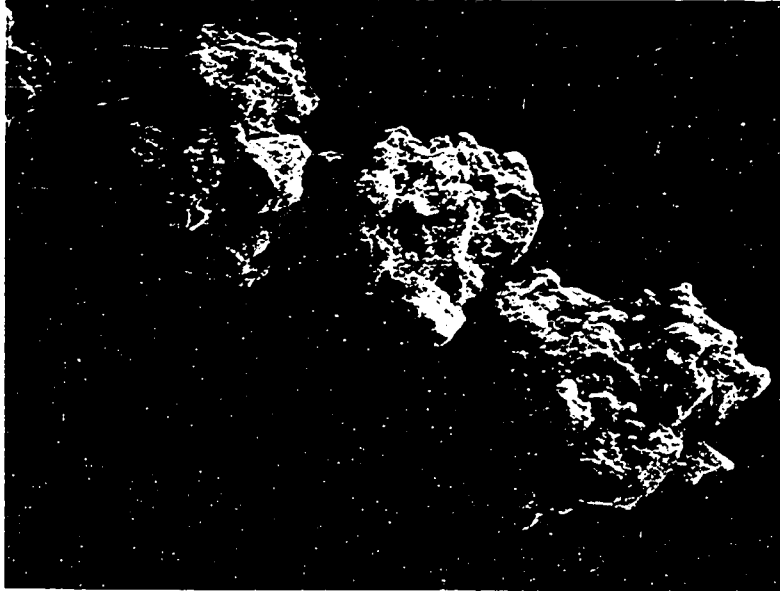
Figure 71a.   SEM micrograph: 1-MW-6 retained on #200 sieve,
magnification 185X

Figure 71b.   SEM micrograph: 1-MW-6 retained on #200 sieve,
magnification 1000X

Figure 72a. SEM micrograph: 1-MW-6 retained on #325 sieve,
magnification 300X
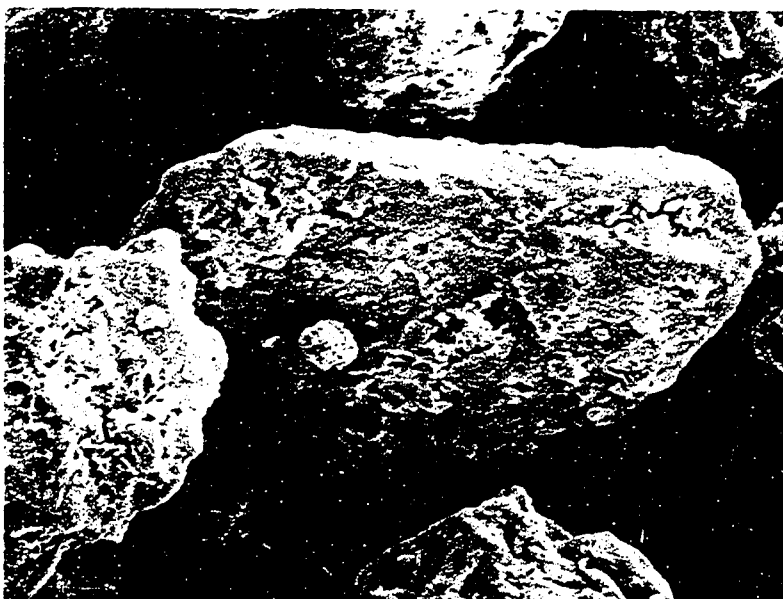
Figure 72b. SEM micrograph: 1-MW-6 retained on #325 sieve,
magnification 1000X
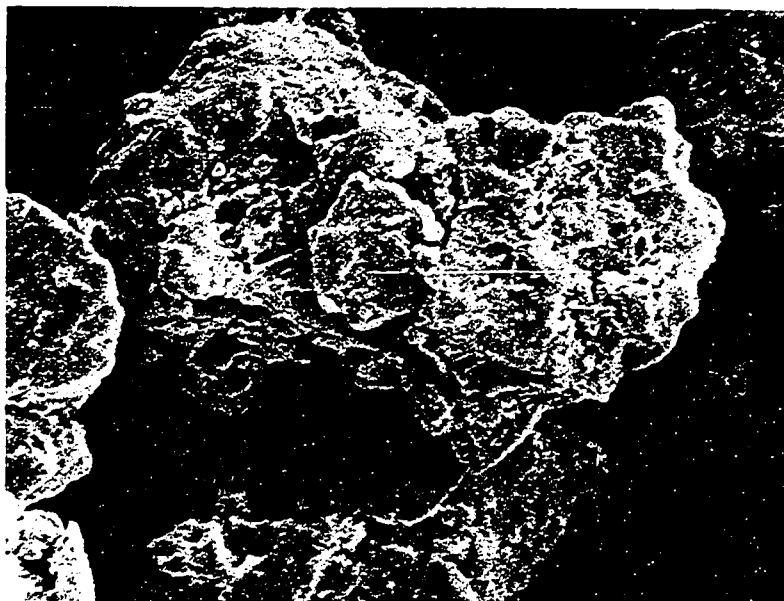
Figure 73a. SEM micrograph: 1-MW-6 retained on #325 sieve, magnification 1000X.
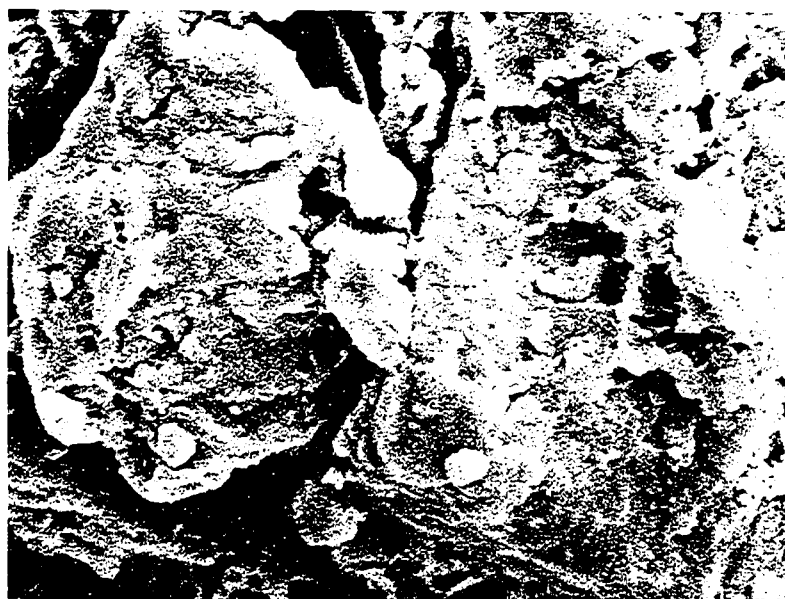
Figure 73b. SEM micrograph: 1-MW-6 retained on #325 sieve, magnification 3000X.
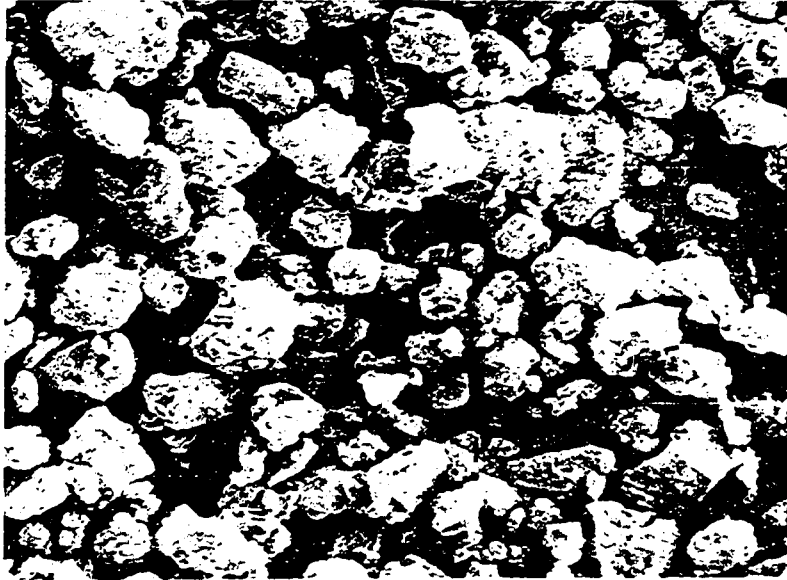
Figure 74a.   SEM micrograph: 1-MW-6 passing #325 sieve,
               magnification 300X

Figure 74b.   SEM micrograph: 1-MW-6 passing #325 sieve,
               magnification 1000X

DISCUSSION

The results of the variable-wind random walk model predict that the logarithm of particle count or thickness will decrease linearly with the logarithm of distance from the source. The shape of the curve, slope and intercept, is shown to be a function of source width, direction and strength of the prevailing wind, and amount of material in transport.

Waggoner and Bingham (165) previously developed a model based on turbulence, which showed that the logarithm of loess thickness should decrease with the logarithm of distance. Their verification was taken from Smith's traverses in Illinois, and Hutton's southwestern Iowa traverses, all of which displayed the log-log relationship. Wider sources were shown to have lower slopes, i.e. lower rates of decrease. However, both Smith (142) and Hutton (80) had published semi-logarithmic relationships for their work.

A review of previous studies indicates a deficiency of thickness measurements close to the source. This may account for the lack of logarithmic functions and the dominance of semi-logarithmic equations; the most important measurements are those close to the source, where thickness decreases most rapidly. With more complete sampling, data for traverses in Iowa and Missouri by the author indicate that

the full logarithmic functions may be applied.

In Illinois and Indiana, Frazee et al. (49) sampled six traverses on both "leeward" and "windward" sides of sources and applied an additive exponential model. Reevaluation of these data using log distance vs thickness gives significant linear regressions; however, in all cases two such functions must be used to completely describe the change. Within about the first 10 miles, or in the case of traverses 1 and 6 within the first mile, the rate of decrease in thickness is much greater than at farther distances.

By plotting the data on log-log scale, the following results of linear regression are obtained:

Traverse	Slope	Intercept	r
1	-0.3561	2.3893	0.9884
2	-0.2710	2.2857	0.9823
3	-0.4535	2.5960	0.9974
4	-0.4260	2.4333	0.9860
5	-0.3739	2.1029	0.9856
6	-0.3544	2.2114	0.9884

The form of $\log y = a \log x + b$, where y = thickness in inches, and x = distance from bluff in miles, shows excellent linearity, as shown by correlation coefficients all of which are significant at the 1% level. For paired observations, i.e. where data are available on both sides of the source, as with traverses 2 and 3, the slope of the log-log relation is steeper on the leeward side of the source and the intercept

is greater.

For observations in Alaska (158), thickness data may be represented by three straight-line segments if plotted as log distance versus thickness. However, converting to log-log scale, the data may also be significantly expressed by a singular linear function.

It appears then that in many cases, a log-log function to express the decrease in loess thickness with increasing distance from the source may be used with high statistical significance. Based on a random-walk scheme, a log-log relationship may be justified. The distance required to produce zero thickness is undefined, a result of particles continually "walking" and in fact accounts for the inability of some particles to land within a reasonable distance. The maximum thickness which should be measured immediately adjacent to the source at zero distance is also undefined, a result of continual pile-up of material. So even with minimal wind velocity, deposition occurs predominantly within a very short distance.

The variable-wind sedimentation model presented by Handy (67) required a maximum transport distance, and therefore winds blowing at an angle to the source would deposit thicker increments, considering an equal volume of material. However, this model, which sufficiently explained the log-linear

relationships, still did not account for zones of "extraordinary" thickness close to the source. Handy did note this, and in fact gave semilog fits for midwestern loess as both near-source and general equations. Such zones were considered to be a result of higher dust concentrations due to a still rising dust cloud close to the source. In light of the random-walk model, these zones are not particularly extraordinary.

Interpretive analyses inferred from the random-walk model presented indicate that wider sources will produce loess deposits which decrease in thickness at a slower rate than narrow sources. Comparison of Wisconsinan loess with older deposits, suggests that deposits such as Loveland in southwestern Iowa or Late Sangamon in western Illinois were derived from wider sources. For Smith's data in Illinois (142), linear regressions of both traverse 1 plus Cass County and Traverse 2 show that the slope of the log-log curve is steeper for Peorian loess compared with observations of Late Sangamon. In addition, greater amounts of Peorian were deposited, as indicated by a higher value of intercept. Semilogarithmic equations for Ruhe's (118) southwestern Iowa observations which were fitted by Handy (67) also show this relation. Referring to Table 1, this can also be seen in the case of the Farmdale loess of Illinois and Indiana and

in west Tennessee, the Roxana (Farmdale) loess also thins
at a much slower rate than the Peorian, and is essentially
a uniform blanket after about 6.2 miles (10 km) from the
source.

Data shown for central Missouri tend to contradict
results for changing source width, in that the rate of
change in loess thickness is much less for observations
south of the river for the ME (east) traverse. Here the
present floodplain width is about five times less than at the
MW traverse. One possible explanation for this conflict may
be related to the actual type of source. The Missouri River
in west-central Missouri is flowing in its own alluvial bed,
and therefore does constitute an actual floodplain. However
in the east-central portion of the state, flow has essential-
ly been controlled by bedrock restrictions on both sides,
and the river is deeply incised. There is no true floodplain,
and a shear vertical elevation difference of over 100 ft.
exists at the bluff. Because of these problems, this example
may not be representative of the model.

Changes in particle size with increasing distance from
the source are well-established, and generally conform to two
types of equations; semilogarithmic and linear. The fact
that the coarse fraction decreases and the finer size
fractions increase with increasing distance from the source

indicates that a sedimentation sorting must be in effect and that sorting is not random. Therefore, even with turbulent mixing en route, selective sedimentation must occur.

The random-walk model predicts that for a specific size, the logarithm of particle count versus the logarithm of distance, based on either fall probability or step length, approximates a straight line. Particle size analyses by pipette procedure gives the percentage of a fraction or a size range by weight and not total number of particles. Therefore, in order to compare results of the random-walk model with results of particle-size analyses, a conversion from particle number to weight percentage is required.

For the example presented in Figure 48 , individual particle sizes corresponding to fall probabilities, assuming a maximum size of 80 μm and a constant wind velocity, are calculated as:

P_f	Size (μm)
0.500	2
0.550	25
0.600	36
0.650	44

The weight of each individual particle may be calculated assuming a spherical shape as:

$$W = 4/3 \ \pi \ r^3 \ \gamma$$
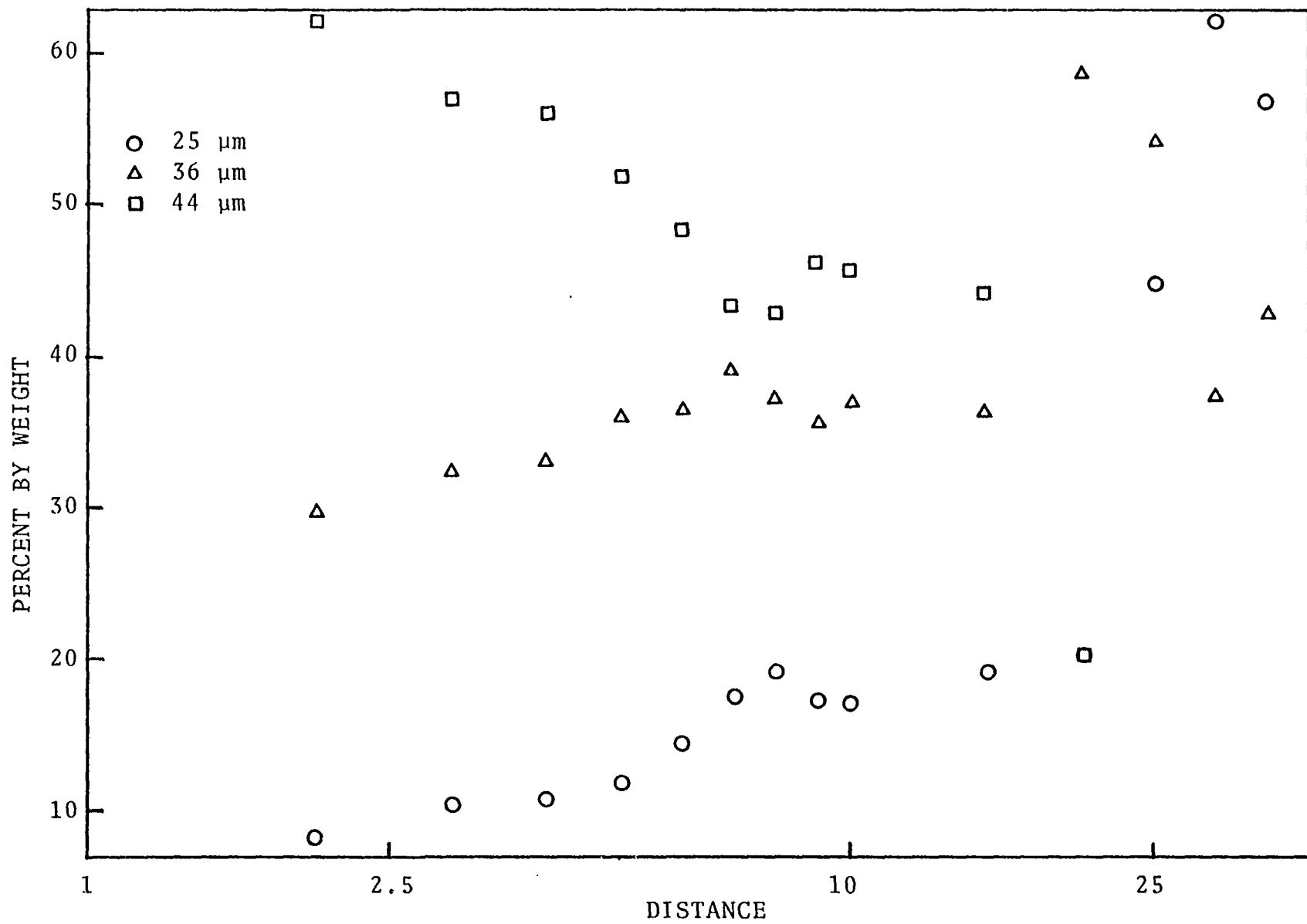
Figure 75. Particle size vs log distance, probability adjustment

where

r = radius

γ = specific gravity (2.65 for quartz)

in which case, the relative weights of individual sizes are calculated as:

Size (μm)	Weight (10^{-8} gm)
2	.00111
25	2.17
36	6.47
44	11.82

Figure 75 presents a plot of logarithim of distance versus percent of each fraction, exclusive of < 2μm.

Within about the first 15 units distance, a linear trend is seen, after which the data are sporadic. An increase in both the 25 and 36 μm size particles is indicated, along with a decrease in the 44 μm size. This is assuming that the same number of particles was initially available for all four particle count vs. distance curves. This would correspond to an initial size distribution of the dust cloud as; 57.8%-44 μm, 31.6%-36 μm, 10.6%-25 μm, 1%-2 μm. Recall that Chepil (21) found that silt of 20-50 μm diameter had no coherence and was most easily picked up by wind. Chepil (20) also performed particle size analyses on untreated samples of suspended dust and found that virtually all of the clay fraction was aggregated into particles greater than 50 μm.

Over 90% of suspended material was larger than 20 μm.

The log-linear trend shown in the initial portion of Figure 75 appears to conform to observed data, and problems associated with the latter portion can easily be explained. It will be recalled that adjustments to the model made for fall probabilities resulted in decreasing the transport distance of particles. Note that in Figure 75 after a distance of 20 units no material of 44 μm size is present. The lack of this fraction then dramatically affects the relative percentages of the remaining sizes and therefore the results become quite erratic.

Using the data of Figure 75, cumulative particle size curves were drawn and the median particle size was determined at various locations. These results are shown in Figure 76, and display the observed trend of linear decrease in median particle size with logarithm of distance. Comparing these data with data previously presented for observations in Iowa and Missouri reveals that for this trial, not only is the trend correct, but the range of particle sizes is very close.

Using step length adjustments and data from Figure 49, particle sizes may be calculated again assuming a maximum transport size of 80 μm;
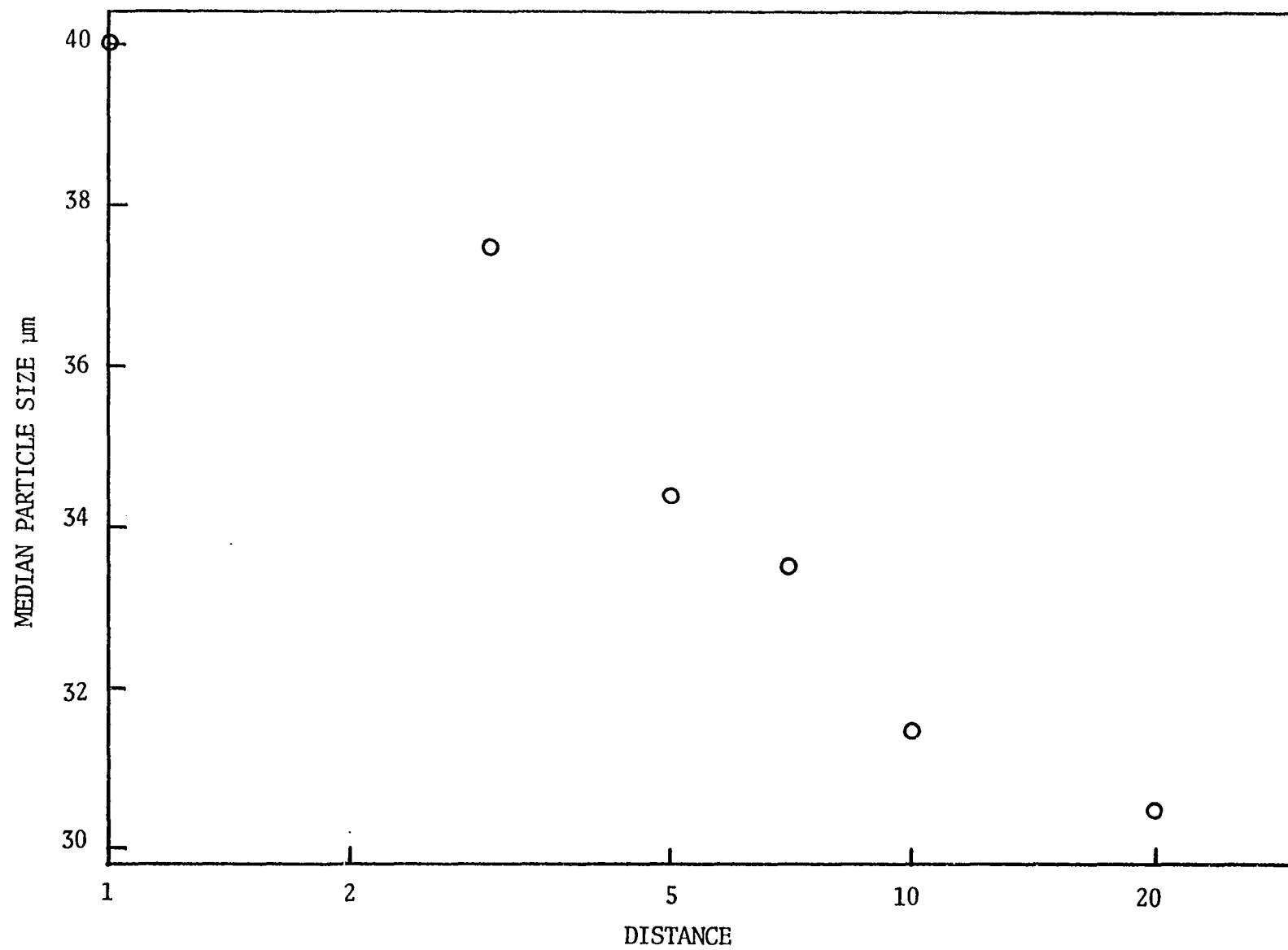
Figure 76. Median particle size versus log distance, data from Figure 75

SL	Size (μm)
1	80
2	57
4	40
8	28
16	20

The step length calculated for material of 2 μm size is 1432, much greater than the maximum deposition distance chosen and hence, no clay particles would be deposited. Corresponding weights for individual particles can be calculated as before:

Size (μm)	Weight ($\times 10^{-8}$ gm)
57	25.70
40	8.88
28	3.05
20	1.11

Figure 76 presents results of particle size trends, with weight percent of individual particle sizes plotted versus logarithm of distance.

As was the case in the probability adjustment model, there is a linear trend up to a distance of about 20 units for fractions smaller than 40 μm. The largest size, 57 μm, which comprised over 50 percent of the deposit, remained nearly uniform with increasing distance. This does not appear realistic, and it would seem that particle size may be explained better with a probability model.
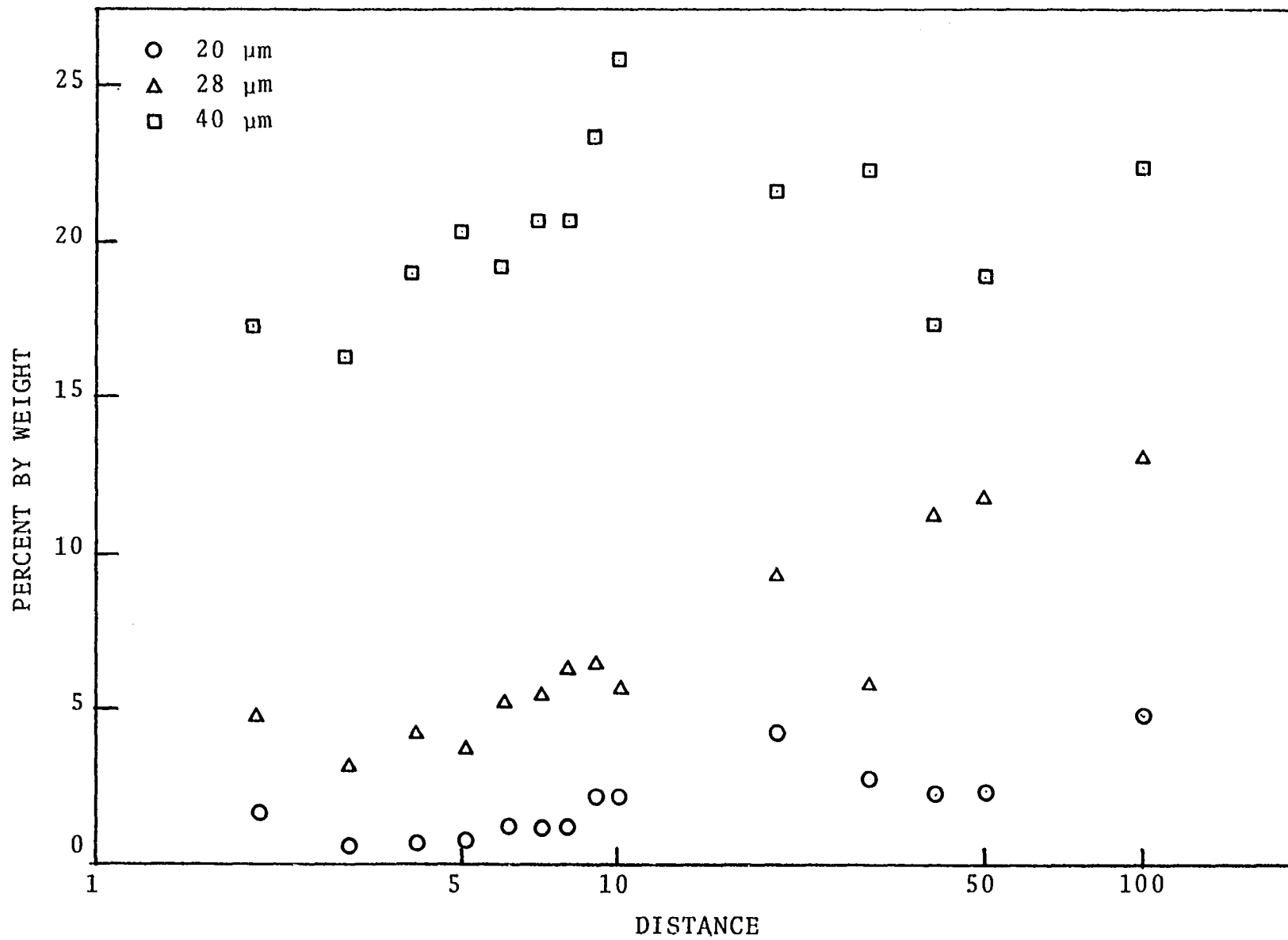
Figure 77. Particle size vs log distance, step length adjustment

A question still remains concerning the transport of the clay fraction. There is no doubt that in most cases, clay content increases with increasing distance from the source. Previous discussions have stated that clays are not easily wind eroded as individual particles however, they may be transported as aggregates. If attached to host grains, the clay would be more prone to travel with small silt particles, because of the larger surface area available. Although dispersion studies indicated that clays are attached to the coarse silt fraction, this could be accounted for considering postdepositional changes such as alternate wetting and drying cycles. Since coarse silt content decreases with increasing distance from the source, clay could not be attached during transport, and still show increasing amounts with increasing distance.

CONCLUSIONS

1. A random-walk variable wind model for loess deposition has been developed which predicts that the logarithm of thickness decreases linearly with the logarithm of distance from the source. Field evidence presented from east-central Iowa, west-central Missouri and east-central Missouri substantiate this model. Additional examples taken from the literature for observations in Alaska, Illinois and Indiana also provide supportive evidence for the model.

2. Variables which describe the nature of the deposit, i.e. maximum thickness adjacent to the source and rate of thickness decrease, are controlled by properties of the source and wind. Wider sources give greater thickness than narrower sources, assuming a constant particle concentration per unit of width. Considering an equal volume of material available for transport, narrower sources give a greater maximum thickness and the rate of thickness decrease is faster.

3. The effect of wind blowing at any angle, α, to the source is to increase the effective source width, however, the effects on the deposit are only noticeable when α is greater than about 65°. Wind blowing perpendicular to the source creates the thinnest deposits, while winds blowing just less than 90° to the source result in maximum thickness,

again assuming uniform particle concentration throughout the source.

4. In the case where no prevailing wind exists and the directions are completely variable, the resulting loess deposit will be symmetric about the source. The effect of a prevailing wind adds to the thickness only on the leeward side, while the distribution on the windward side remains the same as that produced by a completely variable wind. A mild prevailing wind does not noticeably affect the distribution, and as before, the effect is least when the wind direction is perpendicular to the source. A noticeable change in distribution occurs when probability of the prevailing wind is greater than about 0.20. Therefore, the surface winds need only be from a dominant direction 20 percent of the time to cause the distribution to deviate from symmetric.

5. Biasing the probability of fall to account for various particle sizes yields similar trends as seen from field evidence. Coarse fractions decrease linearly with the logarithm of distance while fine fractions (exclusive of clay size particles) increase linearly with logarithm of distance. These predictions, based on the random-walk model, explain the majority of particle size trends seen in most major loess deposits. Since clay particles are

significantly smaller than the rest of the constituents, the model does not sufficiently explain the systematic increases with increasing distance from the source.

6. Clay particles (both clay mineral flakes and clay-sized quartz particles) must be transported as aggregates in the size of fine silt, or ride attached to smaller silt size particles. This would explain similar increases in the clay and fine silt fractions with increasing distance from the source.

7. The complexity of loess deposits still persists, in that during the period of loess deposition, winds of varying velocity, duration and direction were present, and the resulting deposits which developed reflect those variations. This is best seen by examining the particle size distribution with depth at a particular site. Variations exist.

8. Engineering properties, specifically shear strength and in situ density are influenced by particle size variations and thickness of the deposit. Friction angle decreases with increasing clay content while cohesion increases. Therefore as clay content increases (increasing distance from the source) the material changes from a high friction angle-low cohesion shear strength (cohesionless) to a low friction angle-high cohesion shear strength (cohesive).

9. In situ density generally increases with depth; however, the effects of weathering zones should be considered

when examining these trends. A systematic increase in density may be seen going from oxidized to mottled to de-oxidized weathering zones. This trend reflects the fluctuation of a perched water table.

RECOMMENDATIONS FOR FURTHER STUDY

1. The application of the random-walk thickness and particle size models to specific locations where alluvial history is chronologically established should be studied. This would best be suited to areas where several sequences of loess are present, such as in Northern China, New Zealand or Central Europe.

2. The mechanics of modern accumulations of loess, for example in Alaska, should be studied to determine accurate measures of particle size characteristics of eolian dust and the transportation of the clay fraction.

3. Additional computer simulations should be initiated to study the effects of parallel sources, terminating sources, and intersecting sources such as the Mississippi and Ohio Rivers.

BIBLIOGRAPHY

1. Akiyama, F. N.   Shear strength properties of western Iowa loess.   Unpublished M.S. Thesis, Iowa State Univ., Ames, 1963.

2. Alden, W. C. and Leighton, M. M.   The Iowan drift, a review of the evidences of the Iowan stage of glaciation.   Iowa Geol. Survey Ann. Rept., 26 (1917), 49-212.

3. Anderson, K. W.   Prediction of Engineering Soil Properties by Quantitative Geomorphology.   Unpublished M.S. Thesis, Iowa State Univ., Ames, 1968.

4. Badger, W. W.   Structure of friable Iowa loess.   Unpublished Ph.D. Thesis, Iowa State University, Ames, 1972.

5. Bagnold, R. A.   The Physics of Blown Sand and Desert Dunes.   New York:Dover Publ., 1953.

6. Bagnold, R. A.   Deposition in the Process of Hydraulic Transport.   Sedimentology, 10 (1968), 45-56.

7. Bailey, N. T. J.   The Elements of Stochastic Processes.   New York:John Wiley & Sons, 1964.

8. Barber, M. N., and Ninham, B. W.   Random and Restricted Walks.   New York:Gordon and Breach, 1970.

9. Bariss, N.   A Comparative Landform Study of Selected Loess Areas in the Missouri River Basin (with Remarks on the Carpathian Basin in Eastern Europe).   in Loess and Related Eolian Deposits of the World, Lincoln:Univ. of Nebraska Press, 1968.

10. Beavers, A. H.   Source and Deposition of Clay Minerals in Peorian Loess.   Science, 126 (1957), 1285.

11. Bugliarello, G., and Jackson, E. D., III.   Random Walk Study of Convective Diffusion.   ASCE Proc., EM4 (1964), 49-78.

12. Buntley, G. J., Daniels, R. B., Gamble, E. E., and Brown, W. T. Fragipan Horizons in Soils of the Memphis-Loring-Grenada Sequence in West Tennessee. Soil Sci. Soc. Amer. Jour., 41 (1977), 400-407.

13. Caldwell, R. E. and White, J. L. A Study of the Origin and Distribution of Loess in Southern Indiana. Soil Sci. Soc. Amer. Proc., 20 (1956), 258-263.

14. Calvin, S. The Iowan drift. Journal of Geology, 19: 577-602, 1911.

15. Carey, J. B., Cunningham, R. L. and Williams, E. G. Loess Identification in Soils of Southeastern Pennsylvania. Soil Sci. Soc. Amer. Jour., 40 (1976), 745-750.

16. Caspall, F. A Note on the Origin of the Brady Paleosol in Northeastern Kansas. Proc. Assoc. Amer. Geographers, 4 (1972), 19-24.

17. Cegla, J., Buckley, T., and Smalley, I. J. Micro textures of Particles from some European Loess Deposits. Sedimentology, 17 (1971), 129-134.

18. Chamberlin, T. C. Supplementary Hypothesis Respecting the Origin of the Loess of the Mississippi Valley. Journal of Geology, 5 (1897), 795-802.

19. Chepil, W. S. Sedimentary Characteristics of Dust Storms: I. Sorting of Wind-Eroded Soil Material. Amer. Jour. Science, 255 (1957), 12-22.

20. Chepil, W. S. Sedimentary Characteristics of Dust Storms III. Composition of Suspended Dust. Amer. Jour. Science, 255 (1957), 206-213.

21. Chepil, W. S. Factors that Influence Clod Structure and Erodibility of Soil by Wind: IV. Sand, Silt and Clay. Soil Science, 80 (1955), 155-162.

22. Chepil, W. S. and Woodruff, N. P. Sedimentary Characteristics of Dust Storms: II. Visibility and Dust Concentration. Amer. Jour. Science, 255 (1957), 104-114.

23. Chiu, C. Stochastic Model of Motion of Solid Particles. ASCE Proc., HY5 (1967), 203-218.

24. Chu, T. Y. and Davidson, D. T. Simplified Air-Jet Dispersion Apparatus for Mechanical Analysis of Soils. Proc. Hwy. Res. Bd., 32 (1953), 541-547.

25. Coleman, R. Stochastic Processes. London:George Allen & Unwin Ltd., 1974.

26. Conover, W. J. and Matalas, N. C. A Statistical Model of Sediment Transport. USGS Prof. Paper 575 (1967), 60-61.

27. Cox, D. R., and Miller, H. D. The Theory of Stochastic Processes. New York:John Wiley & Sons, 1965.

28. Culling, W. E. H. Soil Creep and the Development of Hillside Slopes. Journal of Geology, 71 (1963), 127-161.

29. Dacey, M. F. Model of Recurring Random Walks for Sediment Transport. in Quantitative Studies in the Geological Sciences. E.H.T. Whitten ed., GSA Memorial 42, (1975), 105-119.

30. Daniels, R. B. and Young, K. K. Loess in South Central Louisiana. Southeastern Geology, 9 (1968), 9-20.

31a. Daniels, R. B., Handy, R. L. and Simonson, G. H. Dark-colored Bands in the Thick Loess of Western Iowa. Journal of Geology, 68 (1960), 450-458.

31b. Davidson, D. T. and Chu, T. Y. Dispersion of Loess for Mechanical Analysis. Hwy. Res. Bd. Proc., 30 (1951), 500-510.

32. Davidson, D. T. and Handy, R. L. Property Variations in the Peorian (Wisconsin) Loess of Southwestern Iowa. Ia. Acad. Sci. Proc., 59 (1952), 248-265.

33. Davidson, D. T. and Handy, R. L. Studies of the Clay Fraction of Southwestern Iowa Loess. Proc. 2nd National Conference on Clays and Clay Minerals, (1953), 190-208.

34a. Davidson, D. T. and Sheeler, J. B. Studies of the Clay Fraction in Engineering Soils: Influence of Amount of Clay on Engineering Properties. Hwy. Res. Bd. Proc., 31 (1952), 558-563.

34b. Davidson, D. T. and Sheeler, J. B. Cation Exchange Capacity of Loess and its Relation to Engineering Properties. ASTM Spec. Tech. Publ. 142 (1952), 1-19.

35. Davidson, D. T., Handy, R. L., and Chu, T. L. Depth Studies of the Wisconsin Loess in Southwestern Iowa: Particle Size and In-Place Density. Ia. Acad. Sci. Proc., 60 (1953), 333-353.

36. Davidson, D. T., and Associates. The Geology and Engineering Characteristics of Some Alaskan Soils. Iowa State University Engineering Experiment Station, Bulletin 186 (1959).

37. Eaton, G. P. Windborne Volcanic Ash: A Possible Index to Polar Wandering. Journal of Geology, 72 (1964), 1-35.

38. Fehrenbacher, J. B. Loess Stratigraphy, Distribution, and Time of Deposition in Illinois. Soil Science, 115 (1973), 176-182.

39. Fehrenbacher, J. B., White, J. L., Ulrich, H. P. and Odell, R. T. Loess Distribution in Southeastern Illinois and Southwestern Indiana. Soil Sci. Soc. Amer. Proc., 29 (1965), 566-572.

40. Feller, W. Probability Theory and its Applications I. New York:John Wiley & Sons, 1950.

41. Fisher, R. V. Textural Comparison of John Day Volcanic Siltstone with Loess and Volcanic Ash. Jour. Sedimentary Petrology, 36 (1966), 706-718.

42. Flemal, R. C., Odom, I. E., and Vail, R. G. Stratigraphy and Origin of the Paha Topography of Northwestern Illinois. Quaternary Research, 2 (1972), 232-243.

43. Flint, R. F. Glacial and Quaternary Geology. New York: John Wiley & Sons, 1971.

44. Foss, J. E., and Rust, R. H. Soil Development in Relation to Loessial Deposition in Southeastern Minnesota. Soil Sci. Soc. Amer. Proc., 26 (1962), 270-274.

45. Foss, J. E., Fanning, D. S., Miller, F. P., and Wagner. Loess Deposits of the Eastern Shore of Maryland. Soil Sci. Soc. Amer. Jour., 42 (1978), 329-334.

46. Fox, N. S., Lohnes, R. A., and Handy, R. L. Depth Studies of the Wisconsin Loess in Southwestern Iowa: IV Shear Strength. Iowa Acad. Sci. Proc., 73 (1966), 193-204.

47. Frankel, L. Relative Rates of Loess Deposition in Nebraska. Journal of Geology, 65 (1957), 649-652.

48. Franzmeier, D. P. Particle Size Sorting of Proglacial Eolian Materials. Soil Sci. Soc. Amer. Proc., 34 (1970) 920-924.

49. Frazee, C. J., Fehrenbacher, J. B., and Krumbein, W. C. Loess Distribution from a Source. Soil Sci. Soc. Amer. Proc., 34 (1970), 296-301.

50. Free, E. E. The Movement of Soil Material by the Wind. U.S.D.A. Bureau of Soils, Bulletin 68 (1911), 272.

51. Frye, J. C. and Leonard, A. B. Stratigraphy of the Late Pleistocene Loesses of Kansas. Journal of Geology, 59 (1951), 287-305.

52. Frye, J. C. and Willman, H. B. Wisconsinan Climatic History Interpreted from Lake Michigan Lobe Deposits and Soils. Geol. Soc. Amer. Memoir 136 (1973).

53. Frye, J. C., Glass, H. D., and William, H. B. Mineral Zonation of Woodfordian Loesses of Illinois. Illinois State Geological Survey, Circular 427, 1968.

54. Frye, J. C., Willman, H. B., and Glass, H. D. Correlation of Midwestern Loesses with the Glacial Succession. Loess and Related Eolian Deposits of the World. Lincoln:University Nebraska Press, 1965, 3-21.

55. Gibbs, H. J., Hilf, J. W., Holtz, W. G., and Walker, F. C. Shear Strength of Cohesive Soils: VI-B-1, Loessial Soils. Am. Soc.

56. Gillette, D. E., and Walker, T. R. Characteristics of Airborne Particles Produced by Wind Erosion of Sandy Soil, High Plains of West Texas. Soil Science, 123 (1977), 97-110.

57. Glass, H. D., Frye, J. C., and Willman, H. B. Record of Mississippi River Diversion in the Morton Loess of Illinois. Trans. Ill. Acad. Sci., 57 (1964), 24-27.

58. Glass, H. D., Frye, J. C., and William, H. B. Clay Mineral Composition; a Source Indicator of Midwest Loess. The Quaternary of Illinois. University of Illinois Spec. Publ. No. 14, 1968, 35-40.

59. Grabowska-Olszewska, B. SEM Analysis of Microstructures of Loess Deposits. Bull. Int. Assoc. Engr. Geology, 11 (1975), 45-48.

60. Hall, R. D. Sedimentation and Alteration of Loess in Southwestern Indiana. Unpublished Ph.D. Thesis, Indiana University, Bloomington, Indiana, 1973.

61. Hallberg, G. R. and Anderson, R. R. Relief Map of Iowa. Iowa Geological Survey, 1975.

62. Hallberg, G. R. Calibration of Cole-Calculated Engineering Data for Montmorillonite Soils, Agronomy Abstracts. Ann Meetings Soil Sci. Soc. Amer., (1978), 169.

63. Hallberg, G. R. Wind Aligned Drainage in Loess in Iowa. Ia. Acad. Sci. Proc., 86 (1979), 4-9.

64. Hallberg, G. R., Fenton, T. E., and Miller, G. A. Standard Weathering Zone Terminology for the Description of Quaternary Sediments in Iowa. Standard Procedures for Evaluation of Quaternary Materials in Iowa. Iowa Geological Survey Technical Information Series, 8, 1978.

65. Hallberg, G. R., Fenton, T. E., Miller, G. A., and Lutenegger, A. J. The Iowan Erosion Surface: An Old Story, An Important Lesson, and Some New Wrinkles. 42nd Annual Tri-State Geological Field Conference Guidebook (1978).

66. Handy, R. L. Collapsible Loess in Iowa. Soil Sci. Soc. Amer. Proc., 37 (1973), 281-284.

67. Handy, R. L. Loess Distribution by Variable Winds. Geol. Soc. Amer. Bull., 87 (1976), 915-927.

68. Handy, R. L., and Davidson, D. T. Evidence of Multiple Loess Deposition in Western Iowa. Ia. Acad. Sci. Proc., 63 (1956), 470-476.

69. Handy, R. L., and Fox, N. S. A Soil Bore-Hole Direct-Shear Test. Highway Research News, 27 (1967), 42-51.

70. Handy, R. L., Lyon, C. A., and Davidson, D. T. Analysis of Wind-Blown Silt - March, 1954. Proc. Ia. Acad. Sci., 61 (1954), 278-290.

71. Hanna, R. M. and O. W. Bidwell. The Relation of Certain Loessial Soils of Northeastern Kansas to the Texture of the Underlying Loess. Soil Sci. Soc. Proc., 20 (1955), 354-359.

72. Harlan, P. W. and Franzmeier, D. P. Soil Formation on Loess in Southwestern Indiana: I. Loess Stratigraphy and Soil Morphology. Soil Sci. Soc. Amer. Proc., 41 (1977), 93-98.

73. Hjulström, F. The Problem of the Geographic Location of Windblown Silt: An Attempt of Explanation. Geografiska Annaler, 37 (1955), 86-93.

74. Hogan, J. D. and Beatty, M. T. Age and Properties of Peorian Loess and Buried Paleosols in Southwestern Wisconsin. Soil Sci. Soc. Amer. Proc., 27 (1963), 345-349.

75. Holtz, W. G., and Gibbs, H. J. Consolidation and Related Properties of Loessial Soils. Am. Soc. Test. Mat. Spec. Tech. Publ., No. 126 (1951), 9-33.

76. Holtz, W. G., and Hilt, J. W. Settlement of Soil Foundations Due to Saturation. Proc. 5th Int. Conf. Soil Mech. Found. Engr., 1 (1961), 673-679.

77. Howe, W. B., and Heim, G. E., Jr. The Ferrelview Formation (Pleistocene) of Missouri. Missouri Geological Survey and Water Resources, Report of Investigation 42, (1968).

78. Huddleston, J. H., and Riecken, F. F. Local Soil-Landscape Relationships in Western Iowa: I. Distributions of Selected Chemical and Physical Properties. Soil Sci. Soc. Amer. Proc., 37 (1973), 264-270.

79. Hunter, R., Riecken, F. F., and McClelland, J. E. Profile Properties of Some Loess-Derived Brunizem Soils of Southeastern Iowa. Ia. Acad. Sci. Proc., 60 (1953), 380-389.

80. Hutton, C. E. Studies of Loess-Derived Soils in Southwestern Iowa. Soil Sci. Soc. Amer. Proc., 12 (1947), 424-431.

81. Inman, D. L. Measures for Describing the Size Distribution of Sediments. Journal Sedimentary Petrology, 22 (1952), 125-145.

82. Inman, D. L. Sorting of Sediments in the Light of Fluid Mechanics. Journal of Sedimentary Petrology, 19 (1949), 51-70.

83. Kalinske, A. A. Turbulence and the Transport of Sand and Silt by Wind. Annals New York Academy of Sciences, 44 (1943), 41-54.

84. Kay, G. F., and Graham, J. B. The Illinoian and Post-Illinoian Pleistocene Geology of Iowa. Iowa Geol. Survey Ann. Rept. 38, 1943, 1-262.

85. Kilmer, V. J. and Alexander, L. T. Methods of Making Mechanical Analysis of Soils. Soil Science, 68 (1949), 15-24.

86. Kleiss, H. J. Loess Distribution Along the Illinois Soil-Development Sequence. Soil Science, 115 (1973), 194-198.

87. Kleiss, H. J. and Fehrenbacher, J. B. Loess Distribution as Revealed by Mineral Variations. Soil Sci. Soc. Amer. Proc., 37 (1973), 291-295.

88. Kollmorgen, H. L. Isopachous Map and Study on Thickness of Peorian Loess in Nebraska. Soil Sci. Soc. Amer. Proc., 27 (1963), 445-448.

89. Krinsley, D. H., and Smalley, I. J. Shape and Nature of Small Sedimentary Quartz Particles. Science, 180 (1973), 1277-1279.

90. Krumbein, W. C. Sediments and Exponential Curves. Journal of Geology, 45 (1937), 577-601.

91. Krusekopf, H. H. Soils of Missouri - Genesis of Great Soil Groups. Soil Science, 85 (1958), 19-27.

92. Kuenen, P. H. Experimental Abrasion 4:Eolian Action. Journal of Geology, 68 (1960), 427-449.

93. Kuenen, P. H. Origin of Quartz Silt. Journal of Sedimentary Petrology, 39 (1969), 1631-1633.

94. Lamb, H. H. and Woodroffe, A. Atmospheric Circulation During the Last Ice Age. Quaternary Research, 1 (1970), 29-58.

95. Leighton, M. M. The Iowan Glaciation and the So-Called
     Iowan Loess Deposits. Iowa Acad. Sci. Proc., 24:
     87-92, 1917.

96. Leighton, M. M. and H. B. Willman. Loess Formations
     of the Mississippi Valley. Journal of Geology, 58
     (1950), 599-623.

97. Leopold, L. B., and Langbein, W. B. The Concept of
     Entropy in Landscape Evolution. U.S. Geol. Survey
     Prof. Paper 500-A, 1962.

98. Lewis, P. F. Linear Topography in the Southwestern
     Palouse, Washington-Oregon. Assoc. Am. Geogr. Ann.,
     50 (1960), 98-111.

99. Lohnes, R. A., and Handy, R. L. Slope Angles in
     Friable Loess. Journal of Geology, 76 (1968), 247-258.

100. Lugn, A. L. The Origin of Loesses and Their Relation
     to the Great Plains in North America. in Loess and Re-
     lated Eolian Deposits of the World: I. Univ. Nebraska
     Press, 1968.

101. Lutenegger, A. J., Remmes, B. D., and Handy, R. L.
     Borehole Shear Test for Stiff Soil. Proc. ASCE, GT11
     (1978), 1403-1407.

102. Lyon, C. A., Handy, R. L., and Davidson, D. T. Property
     Variations in the Wisconsin Loess of East-Central Iowa.
     Ia. Acad. Sci. Proc., 61 (1954), 291-312.

103. Maroney, D. and Swinehart, J.B. Middle Holocene Large-
     Scale Dune Formation in the Nebraska Sand Hills. Geol.
     Soc. Amer. Abstracts with Programs, 10 (1978), 450.

104. Matalucci, R. V., Abdel-Hady, M., and Shelton, J. W.
     Influence of Micro-Structure of Loess on Triaxial Shear
     Strength. Engineering Geology, 4 (1970), 341-351.

105. Miller, G. A. Soil Parent Material Stratigraphy and
     Soil Development, Cedar County, Iowa. Unpublished Ph.D.
     Dissertation, Iowa State University, Ames, Iowa (1974).

106. Nickling, W. G. Eolian Sediment Transport During Dust
     Storms: Slims River Valley, Yukon Territory. Canadian
     Journal of Earth Science, 15 (1978), 1069-1084.

107. Nieter, W. M., and Krinsley, D. H. The Production and
     Recognition of Aeolian Features on Sand Grains by Silt
     Abrasion. Sedimentology, 23 (1976), 713-720.

108. Olson, G. R. Direct Shear and Consolidation Tests of Undisturbed Loess. Unpublished M.S. Thesis, Iowa State University, Ames, (1958).

109. Pasquill, F. Atmospheric Diffusion. New York:John Wiley & Sons, 1974.

110. Pewe, T. An Observation of Wind-Blown Silt. Journal of Geology, 59 (1951), 399-401.

111. Pewe, T. The Origin of Upland Silts Near Fairbanks, Alaska. Geol. Soc. Amer. Bull., 66 (1955), 699-724.

112. Price, W. E. Simulation of Alluvial Fan Deposition by a Random Walk. Water Resources Research, 10 (1974), 263-274.

113. Pritchard, C. L. Petrology of Pleistocene Loess from Northwestern Missouri. Unpublished M.S. Thesis, University of Missouri, (1971).

114. Reed, E. C. Loess Deposition in Nebraska. in Loess and Related Eolian Deposits of the World. Lincoln: Univ. of Nebraska Press, 1968.

115. Reed, E. C., and Dreeszen, V. H. Revision of the Classification of the Pleistocene Deposits of Nebraska. Nebraska Geological Survey Bulletin 23, 1965.

116. Rieger, S., and Juve, R. L. Soil Development in Recent Loess in the Matanuska Valley, Alaska. Soil Sci. Soc. Amer. Proc., 25 (1961), 243-248.

117. Ritchie, A. Jr., Colby, W. G., Swanson, C. L. W., and Tamura, T. Characteristics of Eolian Influenced Soils in Connecticut: I. Physical Properties. Soil Sci. Soc. Amer. Proc., (1957), 428-432.

118. Ruhe, R. V. Quaternary Landscapes in Iowa. Iowa State University Press:Ames, Iowa, 1969.

119. Ruhe, R. V. Application of Pedology to Quarternary Research. in Pedology and Quaternary Research. University Alberta Print. Dept., Edmonton: 1969, 1-23.

120. Ruhe, R. V. Background of Model for Loess-Derived Soils in the Upper Mississippi River Basin. Soil Science, 115 (1973), 250-253.

121. Ruhe, R. V. Stratigraphy of Mid-Continent Loess, U.S.A. in Quaternary of North America. New York:Dowden, Hutchinson and Ross, 1976, 197-211.

122. Ruhe, R. V. A Bignell (?) Loess Section in Western Iowa. Ia. Acad. Sci. Proc., 56 (1949), 229-231.

123. Ruhe, R. V., Dietz, W. P., Fenton, T. E., and Hall, G. F. Iowan Drift Problem, Northeastern Iowa. Iowa Geol. Survey Rept. Inv. 7, 1968.

124. Ruhe, R. V., Miller, G. A., and Vreeken, W. J. Paleosols, Loess Sedimentation and Soil Stratigraphy. in Paleopedology - Origin, Nature and Dating of Paleosols, 1971.

125. Ruhe, R. V., and Olson, C. G. Loess Stratigraphy and Paleosols in Southwest Indiana. Guidebook 25th Midwest Friends of the Pleistocene Field Conference, 1978.

126. Ruhe, R. V., Prill, R. C., and Riecken, F. F. Profile Characteristics of Some Loess-Derived Soils and Soil Aeration. Soil Sci. Soc. Amer. Proc., 19 (1955), 345-347.

127. Rutledge, E. M., Holowaychuk, N., Hall, G. F., and Wilding, L. P. Loess in Ohio in Relation to Several Possible Source Areas: I. Physical and Chemical Properties. Soil Sci. Soc. Amer. Proc., 39 (1975), 1125-1132.

128. Scheidegger, A. E. On the Statistical Properties of Some Transport Equations. Canadian Jour. Physics, 39 (1961), 1573-1582.

129. Scheidegger, A. E. Statistical Hydrodynamics in Porous Media. Advances in Hydroscience, 1 (1964), 161-181.

130. Scheidegger, A. E. Theoretical Geomorphology. New York:Springer-Verlag, 1970.

131. Scheidegger, A. E., and Langbein, W. B. Probability Concepts in Geomorphology. U.S. Geol. Survey Prof. Paper 500-C, 1966.

132. Scheidegger, A. E., and Potter, P. E. Textural Studies
      of Grading:Volcanic Ash Falls. Sedimentology, 11
      (1968), 163-170.

133. Scholtes, W. H., and Smith, G. D. Some Observations of
      the Paha of Northeast Iowa. Ia. Acad. Sci. Proc., 57
      (1950), 283-291.

134. Shimik, B. Papers on the Loess. State University,
      Iowa Lab. Nat. Hist. Bull., 5 (1904), 298-381.

135. Shrader, W. D. Soil Association Areas of Northern
      Missouri. Soil Sci. Soc. Amer. Proc., 11 (1946),
      458-463.

136. Slaughter, M., and Hamil, M. Model for Deposition of
      Volcanic Ash and Resulting Bentonite. Geol. Soc. Amer.
      Bull., 81 (1970), 961-968.

137. Smalley, I. J. The Properties of Glacial Loess and
      the Formation of Loess Deposits. Journal of Sedimentary
      Petrology, 36 (1966), 669-676.

138. Smalley, I. J. Cohesion of Soil Particles and the
      Intrinsic Resistance of Simple Soil Systems to Wind
      Erosion. Journal of Soil Science, 21 (1970), 154-161.

139. Smalley, I. J., and Cabrera, J. G. The Shape and
      Surface Texture of Loess Particles. Geol. Soc. Amer.
      Bull., 81 (1970), 1591-1596.

140. Smalley, I. J., and Cabrera, J. G. The Shape and
      Surface Texture of Loess Particles: Reply. Geol. Soc.
      Amer. Bull., 82 (1971), 2361-2363.

141. Smalley, I. J., Krinsley, D. H., and Vita-Finzi, C.
      Observations on the Kaiserstuhl Loess. Geol. Mag.,
      110 (1971), 29-36.

142. Smith, G. D. Illinois Loess: Variations in Its Proper-
      ties and Distribution. University of Illinois
      Agricultural Experiment Station, Bull. 490, 1942.

143. Smith, R. M., Twiss, P- C., Krauss, R. K., and Brown,
      M. J. Dust Deposition in Relation to Site, Season,
      and Climatic Variables. Soil Sci. Soc. Amer. Proc.,
      34 (1970), 112-117.

144. Springer, M. E. The Composition of the Silt Fraction as Related to the Development of Soils from Loess. Soil Sci. Soc. Amer. Proc., 12 (1948), 461-467.

145. Stefanoff, G. and Ivanov, I. P. On the Evaluation of the Shear Strength of Loess. Proc. 4th Conf. on Soil Mechanics, Budapest, (1971), 315-324. (in German)

146. Sundborg, A. Meteorological and Climatological Conditions for the Genesis of Aeolian Sediments. Geografiska Annaler, 37 (1955), 94-111.

147. Sutton, O. G. A Theory of Eddy Diffusion in the Atmosphere. Proc. Royal Soc. London: A, 135 (1932), 143-165.

148. Sutton, O. G. The Application to Micrometeorology of the Theory of Turbulent Flow over Rough Surfaces. Quart. Jour. of the Royal Meteorological Society, 75 (1949), 342.

149. Sutton, O. G. Micrometeorology. New York:McGraw Hill Co., 1953.

150. Sutton, O. G. Atmospheric Turbulence. New York: John Wiley & Sons, Inc., 1955.

151. Swineford, A., and Frye, J. C. A Mechanical Analysis of Wind-Blown Dust Compared with Analysis of Loess. Am. Jour. Sci., 243 (1945), 249-255.

152. Swineford, A., and Frye, J. C. Petrography of the Peoria Loess in Kansas. Journal of Geology, 59 (1951), 306-322.

153. Syers, J. K., Jackson, M. L., Berkheiser, V. E., Clayton, R. N., and Rex, R. W. Eolian Sediment Influence on Pedogenesis During the Quaternary. Soil Science, 107 (1969), 421-427.

154. Tamura, T., Ritchie, A. Jr., Swanson, C. L. W., and Hanna, R. M. Characteristics of Eolian Influenced Soils in Connecticut: II. Chemical and Mineralogical Properties as Keys to Profile Mixing. Soil Sci. Soc. Amer. Proc., 21 (1957), 536-539.

155. Teller, J. T.   Aeolian Deposits of Clay Sand.   Journal of Sedimentary Petrology, 42 (1972), 684-686.

156. Theisen, A. A., and Knox, E. G.   Distribution and Characteristics of Loessial Soil Parent Material in Northwestern Oregon.   Soil Sci. Soc. Amer. Proc., 23 (1959), 385-388.

157. Thorp, J. and Smith, H. T. U.   Pleistocene Eolian Deposits of the United States, Alaska, and parts of Canada, and New York:Geol. Soc. Amer. Map, 1952.

158. Trainer, F. W.   Eolian Deposits of the Matanuska Valley Agricultural Area Alaska.   U.S. Geol. Survey Bulletin 1121-C, (1961).

159. Tuck, R.   The Loess of the Matanuska Valley, Alaska. Journal of Geology, 46 (1938), 647-653.

160. Turner, D. B.   Workbook of Atmospheric Dispersion Estimates.   U.S. Dept. of Health, Education, and Welfare, Public Health Service Publ. No. 999-AP-26, (1967).

161a. Udden, J. A.   The Mechanical Composition of Wind Deposits.   Augustana Library Publ., 1, 1898.

161b. Udden, J. A.   Erosion, Transportation, and Sedimentation Performed by the Atmosphere.   Journal of Geology, 2 (1894), 318-331.

162. Vita-Finzi, C., and Smalley, I. J.   Origin of Quartz Silt: Comments on a Note by Ph.H. Kuenen.   Journal Sedimentary Petrology, 40 (1970), 1367-1368.

163. Vreeken, W. J.   Quaternary Evolution in Tama County, Iowa.   Annals of the Assoc. of Amer. Geographers, 65 (1975), 283-296.

164. Walter, N. F., Hallberg, G. R. and Fenton, T. E. Particle-Size Analysis by the Iowa State University Soil Survey Laboratory in G. R. Hallberg ed., Standard Procedures for Evaluation of Quaternary Materials in Iowa. Iowa Geol. Survey, Tech. Inf. Series No. 8, 1978.

165. Waggoner, P. E., and Bingham, C.   Depth of Loess and Distance from Source.   Soil Science, 92 (1961), 396-401.

166. Warnke, D. A. The Shape and Surface Texture of Loess
     Particles: Discussion. Geol. Soc. Amer. Bull., 82
     (1971), 2357-2360.

167. Warren, A. Morphology and Sediments of the Nebraska
     Sand Hills in Relation to Pleistocene Winds and the
     Development of Aeolian Bedforms. Journal of Geology,
     84 (1976), 685-700.

168. West, L. T., Rutledge, E. M., and Barber, D. M. A
     Transect of Loess on Crowley's Ridge. Soil Sci. Soc.
     Amer. Proc., (1979), (in press).

169. Wickstrom, A. E., Riggs, K. A., Jr., and Davidson, D. T.
     Fine Sands in East-Central Iowa. Iowa Acad. Sci. Proc.,
     62 (1955), 298-317.

170. Wineland, J. D. Borehole Shear Device. In Situ
     Measurement of Soil Properties. ASCE, 2 (1976), 511-
     522.

171. Worcester, B. K. Soil Genesis on the Stable Primary
     Divides of the Southwestern Iowa Loess Province.
     Unpublished Ph.D. Thesis, Iowa State University, Ames,
     Iowa, (1973).

172. Zingg, A. W. Wind Tunnel Studies of the Movement
     of Sedimentary Materials. Bulletin 34, Proc. of the
     5th Hydraulics Conference, Iowa Institute of Hydraulics,
     Iowa City, Iowa, (1953), 111-135.

ACKNOWLEDGMENTS

The author cannot sufficiently express the respect and gratitude that is deserving of his major professor, Dr. Richard L. Handy. His patience allowed me to explore numerous channels which might have otherwise seemed closed. He endured when there appeared to be more projects than there were fund numbers. The hours of discussion with him on the topic contained in this manuscript and a myriad of others have truly been a delight. I have a feeling that working with Dr. Handy will make all the difference.

APPENDIX A: PROFILE DESCRIPTIONS

This appendix contains a listing of the terminology and abbreviations used in describing each profile. Profiles are listed in numerical order by traverse. Munsell notations are for moist colors. Weathering zones in loess are indicated using the terminology of Hallberg et al. (64) as follows:

First Symbol - color reference;

O - oxidized; 60% of matrix with hues of 2.5Y or redder, values of 3 or higher, and may have segregation of secondary iron compounds into mottles, tubules, or nodules.

D - deoxidized; 60% of matrix with hues of 10YR, 2.5Y and 5Y, values of 5 and 6, chromas of 1 and 2 with considerable segregation of iron (ferric oxides) into tubules (pipestems) or nodules.

U - unoxidized; matrix with hues of 5Y, 5GY, 5GB and 5G, values of 4, 5 and b, chromas of 1 or less (except 5Y 6/1 is deoxidized), with no segregation of iron into tubules or nodules. May include hues of N or values of 3 or less with the presence of zones with abundant organic matter.

Second Symbol - leached or unleached state;

L - leached; no carbonates detectable.

L2 - leached; primary carbonates absent in matrix, secondary carbonates present.

U - unleached; primary carbonates present.

Modifier Symbol - when used precedes first symbol;

    M - mottled; refers to zones containing 20-50%

       contrasting mottles.

Abbreviations used in descriptions are as follows:

abund	abundant	Mn	manganese
ang	angular	mot	mottles
blk	blocky	occ	occasional
BWS	Basal Wisconsin Soil	org	organic
calc	calcareous	Res	residual
carb	carbonates	sbk	subangular blocky
com	common	Sed	Sediment
concr	concretions	seg	segregation
Fe	iron	sl	slight
incr	increasing	vert	vertical
int	intercalated	vhvy	very heavy
LSP	Late Sangamon Paleosol	YSP	Yarmouth-Sangamon Paleosol

Site: 1-MW
Location: SE ¼ SE ¼ Sec. 21 T51N R25W
Sampled by: Lutenegger, Handy, Moldt

Depth in. (cm)	Zone	Description
0-60 (0-152.4)	Solum	
60-112 (152.4-284.5)	OL	10YR 5/4; loess
112-178 (284.5-452.1)	OL	10YR 5/4 com 5Y 7/2 tubules loess
178-208 (452.1-528.3)	DL	5Y 6/2 com 10YR 6/8 tubules loess
208-220 (528.3-558.8)	Ditch	
220-280 (558.8-711.2)	OL	10YR 6/4 few 10YR 5/8 mot; loess
280-305 (711.2-774.7)	DL	10YR 7/2; loess
305-307 (774.7-779.8)	Iron Band	10YR 7/8
307-319 (779.8-810.3)		10YR 7/4 abund Mn mot; loess
319-334 (810.3-848.4)		abund Mn tubules; loess
334-354 (848.4-899.2)	BWS	

Site: 2-MW
Location: SW cor. NE ¼ NE ¼ Sec. 33 T51N R25W
Sampled by: Lutenegger, Handy, Moldt

Depth	Zone	Description
0-60 (0-152.4)	Solum	
60-160 (152.4-406.4)	OL	10YR 5/4 few 10YR 7/2 mot; loess
160-193 (406.4-490.2)	DL	5Y 7/2 com 10YR 5/8 tubules; loess
193-194 (490.2-492.8)	Iron Band	

Depth in. (cm)	Zone	Description
194-255 (492.8-647.7)	DL	10YR 7/2 com 5YR 5/8-6/10 mot; loess
255-270 (647.7-685.8)	BWS	10YR 6/2 abund 5YR 4/8 mot; loess
270-300 (685.8-762.0)	Love-land(?)	10YR 8/2 com 5YR 6/10 mot; loess

Note: Semi-mush zone 204-215 (518.2-546.1).

Site: 3-MW
Location: SE ¼ SW ¼ Sec. 34 T50N R25W
Sampled by: Lutenegger, Handy, Moldt

Depth in. (cm)	Zone	Description
0-20 (0-50.8)	Ditch	
20-72 (50.8-182.9)	OL	Loess
72-91 (182.9-231.1)	MOL	abund Mn mot; loess
91-93 (231.1-236.2)	Iron Band	
93-152 (236.2-386.1)	DL	Loess
152-204 (386.1-518.2)	Swale fill	

Site: 4-MW
Location: NW cor. NE ¼ SE ¼ Sec. 16 T51N R25W
Sampled by: Lutenegger, Handy, Moldt

Depth in. (cm)	Zone	Description
0-56 (0-142.2)	Solum	
56-139 (142.2-353.1)	OL	10YR 6/4-4/4; loess
139-155 (353.1-393.7)	MOL	10YR 6/4 com 10YR 7/2 mot; loess
155-156 (393.7-396.2)	Iron Band	

Depth in. (cm)	Zone	Description
156-197 (396.2-500.4)	DL	5Y 8/2 few 5YR 5/8 tubules; loess
197-198 (500.4-502.9)	Iron Band	
198-264 (502.9-670.6)	DL	5Y 6/2 com 5YR 5/8 tubules; few Mn mot; loess
264-265 (670.6-673.1)	Iron Band	
265-280 (673.1-711.2)	DL	loess
280-281 (711.2-713.7)	Iron Band	
281-332 (713.7-843.3)	MOL	10YR 6/4-7/2 abund 5YR 5/10 mot; loess
332-377 (843.3-957.6)	DL	abund Fe & Mn stains few tubules; loess
377-446 (957.6-1132.8)	DL	loess
446-450 (1132.8-1143.0)	BWS	abund Fe seg; loess
450-454 (1143.0-1153.2)	LSP (?)	till paleosol slickenside

Note: Vertical joints prominant to 190 (482.6).

Site: 5-MW
Location: SE cor. NE ¼ SE ¼ Sec. 4 T50N R25W
Sampled by: Lutenegger, Handy, Moldt

0-60 (0-152.4)	Solum	
60-108 (152.4-274.3)	OL	10YR 6/4-5/4; loess
108-186 (274.3-472.4)	MOL	incr Mn with depth; loess

Depth in. (cm)	Zone	Description
186-208 (472.4-528.3)	Sed.	sl structure
208-230 (528.3-584.2)	Paleosol	abund clay skins & slickensides

Note: Add 6 in. (15.2 cm) to loess thickness for erosion.

Site: 6-MW
Location: SW ¼ SW ¼ Sec. 10 T48N R25W
Sampled by: Lutenegger, Handy, Moldt

0-58	(0-147.3)	Solum	
58-80	(147.3-203.2)	OL	loess
80-110	(203.2-279.4)	DL	loess
110-150	(279.4-381.0)	Swale	massive vhvy clay

Note: Standing water at 48 in. (121.9 cm).

Site: 7-MW
Location: NE ¼ SE ¼ Sec. 34 T53N R25W
Sampled by: Lutenegger, Handy, Moldt

0-60	(0-152.4)	Solum	
60-118	(152.4-299.7)	MOL	10YR 5/4 com 10YR 7/2 mot; loess
118-124	(299.7-315.0)	MOL	10YR 5/4 com 10YR 7/2 mot incr Mn; loess
124-147	(315.0-373.4)	Paleosol	5YR 4/6 few 10YR 6/2 mot slickensides

Note: Standing water at 140 in. (355.6 cm), mush zone 100-103 (254.0-261.6).

Depth in. (cm)	Zone	Description

Site: 8-MW
Location: NE ¼ SE ¼ Sec. 10 T52N R25W
Sampled by: Lutenegger, Handy, Moldt

Depth in. (cm)	Zone	Description
0-56 (0-142.2)	Solum	
56-143 (142.2-363.2)	OL	10YR 5/4; loess
143-195 (363.2-495.3)	OL	10YR 5/4 incr Mn stains; loess
195-198 (495.3-502.9)	OL	10YR 5/6; loess
198-226 (502.9-574.0)	OL	10YR 4/4; loess
226-257 (574.0-652.8)	MOL	10YR 6/4 com 10YR 6/2 mot; loess
257-280 (652.8-711.2)	BWS(?) Loveland (?)	loess paleosol 5YR 5/6 com 10YR 7/2 mot

Note: Add 4 in. (10.2 cm) to loess thickness for erosion, mush zone 83-145 (210.8-368.3), semi-mush 195-198 (495.3-502.9).

Site: 9-MW
Location: SW cor. NW ¼ SW ¼ Sec. 12 T53N R25W
Sampled by: Lutenegger, Handy, Moldt

Depth in. (cm)	Zone	Description
0-51 (0-129.5)	Solum	
51-75 (129.5-190.5)	MOL	5Y 6/2 com 5YR 5/8 mot some Fe seg; loess
75-77 (190.5-195.6)	Iron Band	
77-94 (195.6-238.8)	DL	5Y 7/2; loess
94-96 (238.8-243.8)	Iron Band	
116-130 (294.6-330.2)	Sed.	5Y 7/2 abund 5YR 5/8 mot

Depth in. (cm)	Zone	Description
130-144 (330.2-365.8)	Sed.	abund Mn concr
144-164 (365.8-416.6)	Sed.	com quartz pebbles sl structure

Note: Mush zone 72-73 (182.9-185.4) and 99-102 (251.5-259.1).

Site: 10-MW
Location: NW ¼ NW ¼ Sec. 13 T54N R25W
Sampled by: Lutenegger, Handy, Moldt

Depth	Zone	Description
0-56 (0-142.2)	Solum	
56-74 (142.2-188.0)	MOL	5YR 6/2 com 5YR 4/8 mot; loess
74-83 (188.0-210.8)	MOL	5YR 6/2 com 5YR 5/3 mot; loess
83-102 (210.8-259.1)	Paleosol	granular

Site: 11-MW
Location: NE ¼ NW ¼ Sec. 3 T52N R25W
Sampled by: Lutenegger, Handy, Moldt

Depth	Zone	Description
0-56 (0-142.2)	Solum	
56-62 (142.2-157.5)	MOL	5Y 7/2 abund 5YR 4/8 mot; loess
62-107 (157.5-271.8)	MOL	5Y 7/2 com 10YR 4/4 mot; loess
107-120 (271.8-304.8)	MOL	10YR 5/4 few 10YR 6/2 mot; loess
120-152 (304.8-386.1)	OL	10YR 5/6 incr Mn; loess
152-162 (386.1-411.5)	IIA_2	10YR 6/4 few 10YR 8/2 seg; paleosol

Depth in. (cm)	Zone	Description
162-165 (411.5-419.1)	IIB	5YR 4/6 com 5YR 7/2 mot; paleosol

Site: 12-MW
Location: SE cor. NE ¼ NE ¼ Sec. 14 T55N R25W
Sampled by: Lutenegger, Handy, Moldt

0-36 (0-91.4)	Solum	
36-47 (91.4-119.4)	MOL	5Y 6/2 com 10YR 5/6 mot; loess
47-56 (119.4-142.2)	Sed(?)	sl structure
56-63 (142.2-160.0)	IIA_2	10YR 4/2; paleosol
63-74 (160.0-188.0)	IIB	5YR 4/8 com 5Y 4/8 mot; paleosol

Note: Add 3 in. (7.6 cm) to loess thickness for erosion.

Site: 1-ME
Location: NE ¼ SE ¼ Sec. 11 T45N R5W
Sampled by: Lutenegger, Elsner, Carson

0-51 (0-129.5)	Solum	
51-54 (129.5-137.2)	DL	loess
54-58 (137.2-147.3)	MDL	10YR 6/2 abund 5YR 4/8 mot abund Fe; loess
58-75 (147.3-190.5)	DL	loess
75-80 (190.5-203.2)	IIA	res paleosol
80-99 (203.2-251.5)	IIB	10YR 6/2 ang blk; res paleosol
99- (251.5-	Bedrock	shale

Depth in. (cm)		Zone	Description

Site: 2-ME
Location: SW ¼ Sec. 35 T45N R5W
Sampled by: Lutenegger, Elsner, Carson

0-20	(0-50.8)	Solum	A horizon
20-26	(50.8-66.0)	Solum	10YR 5/6 com 10YR 7/2 stains; B_{12}
26-42	(66.0-106.7)	Solum	5Y 7/2 com 10YR 5/6-5-8 mot; B_{22}
42-51	(106.7-129.5)	MOL	loess
51-65	(129.5-165.1)	Sed	

Site: 3-ME
Location: NW ¼ NE ¼ Sec. 3 T43N R5W
Sampled by: Lutenegger, Elsner, Carson

0-9	(0-22.9)	Solum	A_p horizon
9-11	(22.9-27.9)	Solum	A_2 horizon
11-19	(27.9-48.3)	Solum	5YR 5/8-48; B_{12}
19-24	(48.3-61.0)	Solum	B_{22} horizon
24-38	(61.0-96.5)	OL	loess
38-50	(96.5-127.0)	Sed	

Site: 4-ME
Location: SE ¼ SW ¼ Sec. 22 T42N R5W
Sampled by: Lutenegger, Elsner, Carson

0-12	(0-30.5)	Solum	A_p horizon
12-16	(30.5-40.6)	Solum	A_2 horizon

Depth in. (cm)		Zone	Description
16-24	(40.6-61.0)	Solum	B_{12} horizon
24-32	(61.0-81.3)	Solum	B_{22} horizon
32-40	(81.3-101.6)	MOL	10YR 5/8 few 5Y 7/2 mot; loess
40-58	(101.6-147.3)	Sed	
58-89	(147.3-226.1)	Paleosol	5Y 5/2 com 5YR 5/6 mot

Site: 5-ME
Location: NE ¼ SW ¼ Sec. 3 T42N R5W
Sampled by: Lutenegger, Carson

0-41	(0-104.1)	Solum	loess
41-50	(104.1-127.0)	Res Paleosol	shale

Site: 6-ME
Location: SE ¼ SW ¼ Sec. 31 T46N R4W
Sampled by: Lutenegger, Elsner, Carson

0-6	(0-15.2)	Solum	A_p horizon
6-9	(15.2-22.9)	Solum	A_2 horizon
9-14	(22.9-35.6)	Solum	B_{12} sbk structure
14-23	(35.6-58.4)	Solum	B_{22} horizon
23-30	(58.4-76.2)	Solum	B_{32} hvy clay
30-80	(76.2-203.2)	OL	loess
80-95	(203.2-241.3)	Paleosol	

Depth in. (cm)		Zone	Description

Site: 7-ME
Location: SW ¼ NW ¼ Sec. 14 T46N R12W
Sampled by: Lutenegger, Elsner, Carson

0-7	(0-17.8)	Solum	A_p horizon
7-9	(17.8-22.9)	Solum	A_2 horizon
9-13	(22.9-33.0)	Solum	B_{12} horizon
13-23	(33.0-58.4)	Solum	B_{22} hvy clay
23-52	(58.4-132.1)	Solum	B_{32} horizon
52-61	(132.1-154.9)	OL	10YR 6/2; loess
61-78	(154.9-198.1)	MOL	loess
78-104	(198.1-264.2)	Sed	abund Fe along vert joints
104-134	(264.2-340.4)	Paleosol	5Y 7/2 com 5YR 6/8-6/10 mot
134-148	(340.4-375.9)	OL	10YR 6/6; till

Site: 8-ME
Location: SW ¼ SW ¼ Sec. 29 T48N R12W
Sampled by: Lutenegger, Elsner, Carson

0-41	(0-104.1)	Solum	loess
41-50	(104.1-127.0)	LSP(?)	

Site: 9-ME
Location: NE ¼ NW ¼ Sec. 11 T47N R5W
Sampled by: Lutenegger, Elsner, Carson

0-4	(0-10.2)	Solum	A_p horizon
4-14	(10.2-35.6)	Solum	5YR 5/6; B_{21}
14-17	(35.6-43.2)	Solum	ang blk; B_{22}
17-24	(43.2-61.0)	Solum	10YR 6/8; B_{32}

Depth in. (cm)		Zone	Description
24-32	(61.0-81.3)	Sed	abund Mn flecks
32-38	(81.3-96.5)	IIA	paleosol
38-59	(96.5-149.9)	IIB	5YR 5/8 few 10YR 6/4 mot; paleosol

Site: 10-ME
Location: SE ¼ Cor. SW ¼ SE ¼ Sec. 14 T47N R5W
Sampled by: Lutenegger, Elsner, Carson

0-8	(0-20.3)	Solum	A_p horizon
8-14	(20.3-35.6)	Solum	blk; B_{12}
14-28	(35.6-71.1)	Solum	hvy clay B_{22}
28-38	(71.1-96.5)	OL	loess
38-57	(96.5-144.8)	Sed	
57-71	(144.8-180.3)	Res Paleosol	

Site: 11-ME
Location: NE ¼ SE ¼ Sec. 25 T46N R5W
Sampled by: Lutenegger, Elsner, Carson

0-11	(0-27.9)	Solum	A_p horizon
11-14	(27.9-35.6)	Solum	A_2 horizon
14-24	(35.6-61.0)	Solum	B_{12} horizon
24-38	(61.0-96.5)	Solum	B_{22} horizon
38-58	(96.5-147.3)	Solum	B_{32} horizon
58-102	(147.3-259.1)	MOL	loess
102-138	(259.1-350.5)	OL	10YR 6/4; loess

Depth in. (cm)		Zone	Description
138-168	(350.5-426.7)	OL	10YR 5/6; loess
168-206	(426.7-523.2)	BWS(?) Love-land(?)	10YR 5/4; loess
206-208	(523.2-528.3)	Res Paleo-sol(?)	
208-	(528.3-	Bedrock	Siltstone(?)

Site: 12-ME
Location: NE ¼ SW ¼ Sec. 8 T46N R4W
Sampled by: Lutenegger, Elsner, Carson

0-10	(0-25.4)	Solum	A_p horizon
10-14	(25.4-35.6)	Solum	A_2 horizon
14-20	(35.6-50.8)	Solum .	B_{12}
20-28	(50.8-71.1)	Solum	hvy clay massive; B_{22}
28-36	(71.1-91.4)	MOL	loess
36-58	(91.4-147.3)	OL	loess
58-70	(147.3-177.8)	Sed	blk
70-76	(177.8-193.0)	Res Paleosol	

Site: 13-ME
Location: SE ¼ Cor. NE ¼ SW ¼ Sec. 25 T59N R6W
Sampled by: Lutenegger, Carson

0-60	(0-152.4)	Solum	
60-176	(152.4-447.0)	OU	abun $CaCO_3$ conc.; loess
176-182	(447.0-462.3)	Sed	

Depth in. (cm)		Zone	Description
182-212	(462.3-538.5)	LSP	
212-236	(538.5-599.4)	OL	till

Site: 1-LH
Location: NW ¼ SW ¼ Sec. 34 T82N R11W
Sampled by: Lutenegger, Handy

Depth in. (cm)		Zone	Description
0-60	(0-152.4)	Solum	
60-92	(152.4-233.7)	OL	loess
92-138	(233.7-350.5)	OU	10YR 5/6; loess
138-160	(350.5-406.4)	MOU	10YR 5/6 com Mn mot; loess
160-162	(406.4-411.5)	Iron Band	10YR 6/8
162-170	(411.5-431.8)	OU	loess
170-190	(431.8-482.6)	DU	5Y 6/2; loess
190-207	(482.6-525.8)	OL	10YR 4/4; loess
207-225	(525.8-571.5)	DL BWS(?)	10YR 6/2 few 10YR 6/8 mot; loess
225-248	(571.5-629.9)	LSP	till paleosol

Note: Standing water at 192 in. (487.7 cm), mush zone
125-150 (317.5-381.0).

Site: 2-LH
Location: NE ¼ Cor. NW ¼ Sec. 9 T81N R11W
Sampled by: Lutenegger, Handy

Depth in. (cm)		Zone	Description
0-60	(0-152.4)	Solum	
60-169	(152.4-259.1)	OL	loess
169-218	(259.1-553.7)	OU	10YR 6/2 few 5YR 5/8 mot; loess

Depth in. (cm)		Zone	Description
218-252	(553.7-640.1)	OU	10YR 5/2 few 5YR 5/8 mot; loess
252-262	(640.1-665.5)	OL	loess
262-269	(665.5-683.3)	BWS	loess
269-282	(683.3-716.3)	LSP	till paleosol

Note: Add 6 in. (15.2 cm) to loess thickness for erosion, semi-mush zone 210-223 (533.4-566.4).

Site: 3-LH
Location: NE ¼ NW ¼ Sec. 26 T80N R11W
Sampled by: Lutenegger, Handy

Depth in. (cm)		Zone	Description
0-60	(0-152.4)	Solum	
60-92	(152.4-233.7)	OL	loess
92-152	(233.7-386.1)	MOU	10YR 5/4 com 10YR 5/6 mot; loess
152-198	(386.1-502.9)	DU	5Y 6/2 few 10YR 5/6-5/8 mot; loess
198-202	(502.9-513.1)	DL	loess
202-205	(513.1-520.7)	YSP	till paleosol

Note: Semi-mush zone 116-120 (294.6-304.8).

Site: 4-LH
Location: NE ¼ NE ¼ Sec. 36 T78N R11W
Sampled by: Lutenegger, Handy

Depth in. (cm)		Zone	Description
0-56	(0-142.2)	Solum	
56-115	(142.2-292.1)	OL	loess
115-156	(292.1-396.2)	MOL	loess

Depth in. (cm)		Zone	Description
156-178	(396.2-452.1)	LSP	10YR 6/2 abund 5YR 5/10 mot; till paleosol

Site: 5-LH
Location: SE ¼ SE ¼ Sec. 23 T79N R11W
Sampled by: Lutenegger, Handy

Depth in. (cm)		Zone	Description
0-60	(0-152.4)	Solum	
60-78	(152.4-198.1)	OL	10YR 6/2 com 5YR 5/8; loess
78-112	(198.1-284.5)	OL	10YR 5/6; loess
112-130	(284.5-330.2)	OL	10YR 6/2; loess
130-132	(330.2-335.3)	Iron Band	10YR 5/8 abund Mn
132-146	(335.3-370.8)	MOU	10YR 5/4 abund 5YR 5/8 mot; loess
146-152	(370.8-386.1)	DU	10YR 5/2; loess
152-160	(386.1-406.4)	DU	5YR 4/2; loess
160-163	(406.4-414.0)	BWS	loess
163-180	(414.0-457.2)	YSP	till paleosol

Note: Add 4 in. (10.2 cm) to loess thickness for erosion, semi-mush zone 106-108 (269.2-274.3).

Site: 6-LH
Location: SE ¼ SW ¼ Sec. 3 T80N R11W
Sampled by: Lutenegger, Handy

Depth in. (cm)		Zone	Description
0-60	(0-152.4)	Solum	
60-110	(152.4-279.4)	OL	loess
110-164	(279.4-416.6)	MOL	loess

Depth in. (cm)		Zone	Description
164-248	(416.6-629.9)	OU	loess
248-249	(629.9-632.5)	LSP	till paleosol

Note: Mush zone 152-164 (386.1-416.6).

Site: 7-LH
Location: SW ¼ SE ¼ Sec. 29 T76N R10W
Sampled by: Lutenegger, Handfelt

0-60	(0-152.4)	Solum	
60-83	(152.4-210.8)	OL_2	loess
83-94	(210.8-238.8)	OU	loess
94-126	(238.8-320.0)	MDU	5Y 6/2-7/2 com 10YR 6/0 mot; loess
126-138	(320.0-350.5)	DL	5Y 4/2; loess
138-170	(350.5-431.8)	YSP	5Y 3/2 com 5YR 5/10 flecks; till paleosol

Note: Semi-mush zone 104-107 (264.2-271.8), standing water
at 80 in. (203.2 cm).

Site: 8-LH
Location: NE ¼ NW ¼ Sec. 31 T77N R10W
Sampled by: Lutenegger, Handfelt

0-60	(0-152.4)	Solum	
60-114	(152.4-289.6)	OL	loess
114-132	(289.6-335.3)	MOU	loess
132-142	(335.3-360.7)	DL	loess
142-183	(360.7-464.8)	Sed.	sandy, few quartz pebbles, charcoal flecks

Depth in. (cm)		Zone	Description
183-198	(464.8-502.9)	Swale fill	

Site: 9-LH
Location: Cen. NW ¼ SW ¼ Sec. 33 T81N R11W
Sampled by: Lutenegger, Hallberg, Kemmis

Depth		Zone	Description
0-37	(0-93.9)	Solum	
37-114	(93.9-289.6)	OL	loess
114-119	(289.6-302.3)	MOL	loess
119-126	(302.3-320.0)	OL	loess
126-191	(320.0-485.1)	OU	loess
191-199	(485.1-505.5)	MOU	weakly calc ; loess
199-238	(505.5-604.5)	MOL	Mn seg occ carb ; loess
238-246	(604.5-624.8)	BWS	org carbon, sbk; loess
246-249	(624.8-632.5)	Sed	A_2b platy; pedisediment
249-258	(632.5-655.3)	Sed	Bib; pedisediment
258-278	(655.3-706.1)	LSP	B_2b; till paleosol

Site: 10-LH
Location: NW ¼ NW ¼ Sec. 22 T82N R11W
Sampled by: Lutenegger, Hallberg, Kemmis

Depth		Zone	Description
0-160	(0-406.4)	OL	loess
160-164	(406.4-416.6)	OU	loess
164-184	(416.6-467.4)	MOU-MDU	loess
184-186	(467.4-472.4)	Iron Band (?)	Strong 7.5YR 5/6-5/8 Fe seg
186-226	(472.4-574.0)	DU	loess

Depth in. (cm)		Zone	Description
226-246	(574.0-624.8)	MOU-MDU	2.5Y 5/4 abund Fe & Mn seg; loess
246-252	(624.8-640.1)	DU	loess
252-282	(640.1-716.3)	MOU-MDU	2.5Y 5/4 com 2.5Y 5/1 mot; loess
282-294	(716.3-746.8)	UU	5Y 5/3-4/3 com 5GY 4/1 int; loess
294-300	(746.8-762.0)	UU	5Y 4/4 com 5GY 4/1 int; loess
300-342	(762.0-868.7)	UU	5GY 4/1 com org carbon; loess

Note: Mush zone 120-164 (304.8-416.6).

Site: 11-LH
Location: NE ¼ SE ¼ Sec. 23 T81N R12W
Sampled by: Lutenegger, Kemmis

0-229	(0-581.7)	OL	loess
229-379	(581.7-962.7)	O	sand
379-421	(962.7-1069.3)	OL	loess
421-	(1069.3-	O	sand

Site: 12-LH
Location: NW ¼ SW ¼ NW ¼ Sec. 31 T81N R11W
Sampled by: Lutenegger, Hallberg, Kemmis

0-46	(0-116.8)	Solum	
46-88	(116.8-223.5)	MDL	abund mot; loess
88-101	(223.5-256.5)	MDL	loess
101-114	(256.5-289.6)	MDL	few mot; loess

Depth in. (cm)		Zone	Description
114-124	(289.6-315.0)	MDL	loess
124-127	(315.0-322.6)	MDU	few snail shells; loess
127-128	(322.6-325.1)	Iron Band	
128-137	(325.1-348.0)	MDU	loess
137-141	(348.0-358.1)	MOU	abund Fe seg; loess
141-160	(358.1-406.4)	MDU	few mot & Fe seg; loess
160-168	(406.4-426.7)	Iron Band	
168-186	(426.7-472.4)	MDU	few Fe seg; loess
186-192	(472.4-487.7)	MDU	abund Fe seg; loess
192-198	(487.7-502.9)	MDU	few Fe seg; loess
198-209	(502.9-530.9)	UU	5GY 4/1 org flecks few snail shells; loess
209-211	(530.9-535.9)	Org Band	5Y 3/2
211-249	(535.9-632.5)	UU	loess
249-260	(632.5-660.4)	UL	5GY 4/1; few org carbon; loess
260-276	(660.4-701.0)	YSP	till paleosol

Note: Semi-mush zone 88-110 (223.5-279.4).

Site: 13-LH
Location: SW ¼ SE ¼ SW ¼ Sec. 19 T81N R11W
Sampled by: Lutenegger, Hallberg, Kemmis

| 0-42 | (--106.7) | Solum | ditch cut |
| 42-82 | (106.7-208.3) | MOL | loess |

Depth in. (cm)		Zone	Description
82-90	(208.3-228.6)	Sed	occ pebbles
90-126	(228.6-320.0)	OL	till

Site: 14-LH
Location: NE ¼ NW ¼ NW ¼ Sec. 34 T81N R11W
Sampled by: Lutenegger

0-50	(0-127.0)	Solum	
50-82	(127.0-208.3)	OL	loess
82-207	(208.3-525.8)	OU	loess

Site: 15-LH
Location: SE ¼ NE ¼ Sec. 30 T81N R11W
Sampled by: Lutenegger, Hallberg, Kemmis

Note: Roadcut samples "sandy loess" from first erosion
surface:

Sample 1 - North Side
Sample 2 - Middle
Sample 3 - South Side

Site: 16-LH
Location: NE ¼ SW ¼ Sec. 18 T81N R10W
Sampled by: Lutenegger, Hallberg, Kemmis

0-60	(0-152.4)	Solum	
60-96	(152.4-243.8)	OL	loess
96-204	(243.8-518.2)	OU	abund $CaCO_3$ conc; loess
204-228	(518.2-579.1)	MOU	loess
228-252	(579.1-640.1)	DU	loess

Depth in. (cm)		Zone	Description
252-	(640.1-	LSP	till paleosol

Site: 17-LH
Location: SE ¼ NE ¼ Sec. 2 T80N R10W
Sampled by: Lutenegger, Hallberg, Kemmis

0-36	(0-91.4)	Sand	
36-400	(91.4-1016.0)		loess
400-404	(1016.0-1026.2)	BWS	loess

Site: 18-LH
Location: SE ¼ NW ¼ Sec. 21 T80N R8W
Sampled by: Lutenegger, Wollenhaupt, Handfelt, Saye

0-54	(0-137.2)	solum	
54-84	(137.2-213.4)	OL	loess
84-214	(213.4-543.6)	OU	loess
214-240	(543.6-609.6)	BWS	loess
240-249	(609.6-632.5)	LSP	till paleosol

Note: Add 4 in. (10.2 cm) to loess thickness for erosion.

APPENDIX B: SAMPLING LOCATIONS

Locations of individual sampling sites are presented
on 7.5 minute topographic maps prepared by the United States
Department of Interior-Geological Survey. The following
scale and legends are used throughout:

SCALE 1:24 000

| 1000 | 0 | 1000 | 2000 | 3000 | 4000 | 5000 | 6000 | 7000 FEET |

1 KILOMETER

DATUM IS MEAN SEA LEVEL
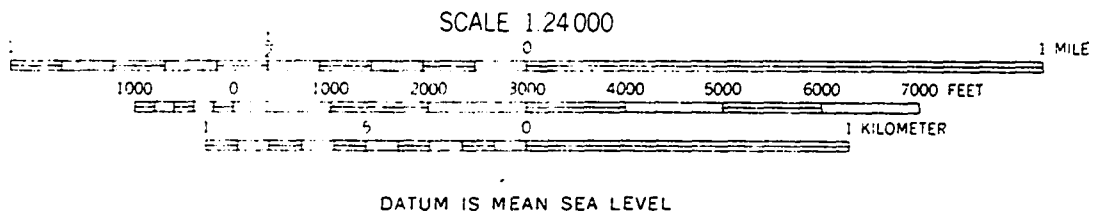
ROAD CLASSIFICATION

Primary highway, all weather,   Light-duty road, all weather,
hard surface   improved surface

Secondary highway, all weather,   Unimproved road, fair or dry
hard surface   weather

Interstate Route   U. S. Route   State Route

SITE: 1-MW,4-MW
QUADRANGLE: DOVER,MO.
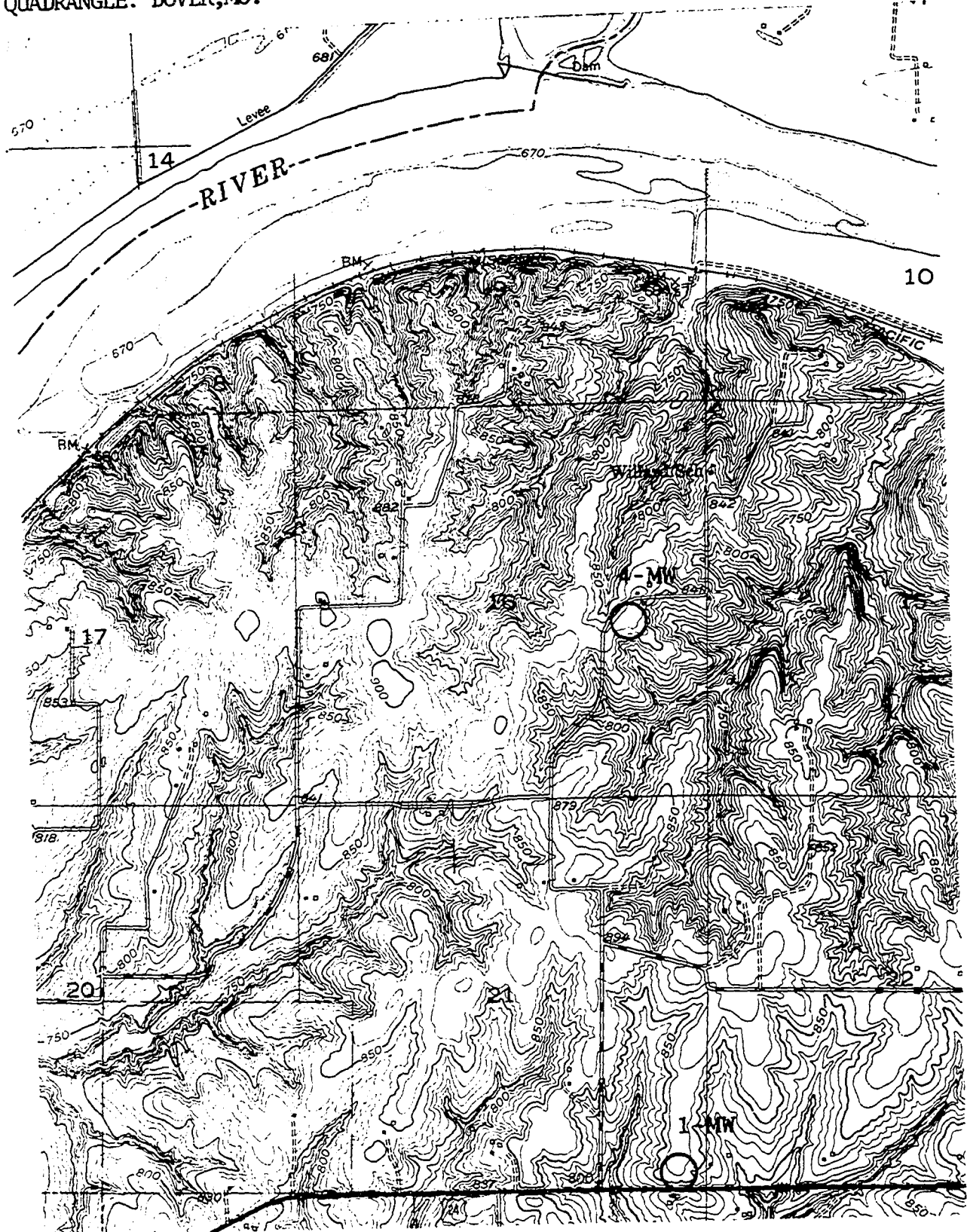
SITE: 2-MW,5-MW
QUADRANGLE: DOVER,MO.
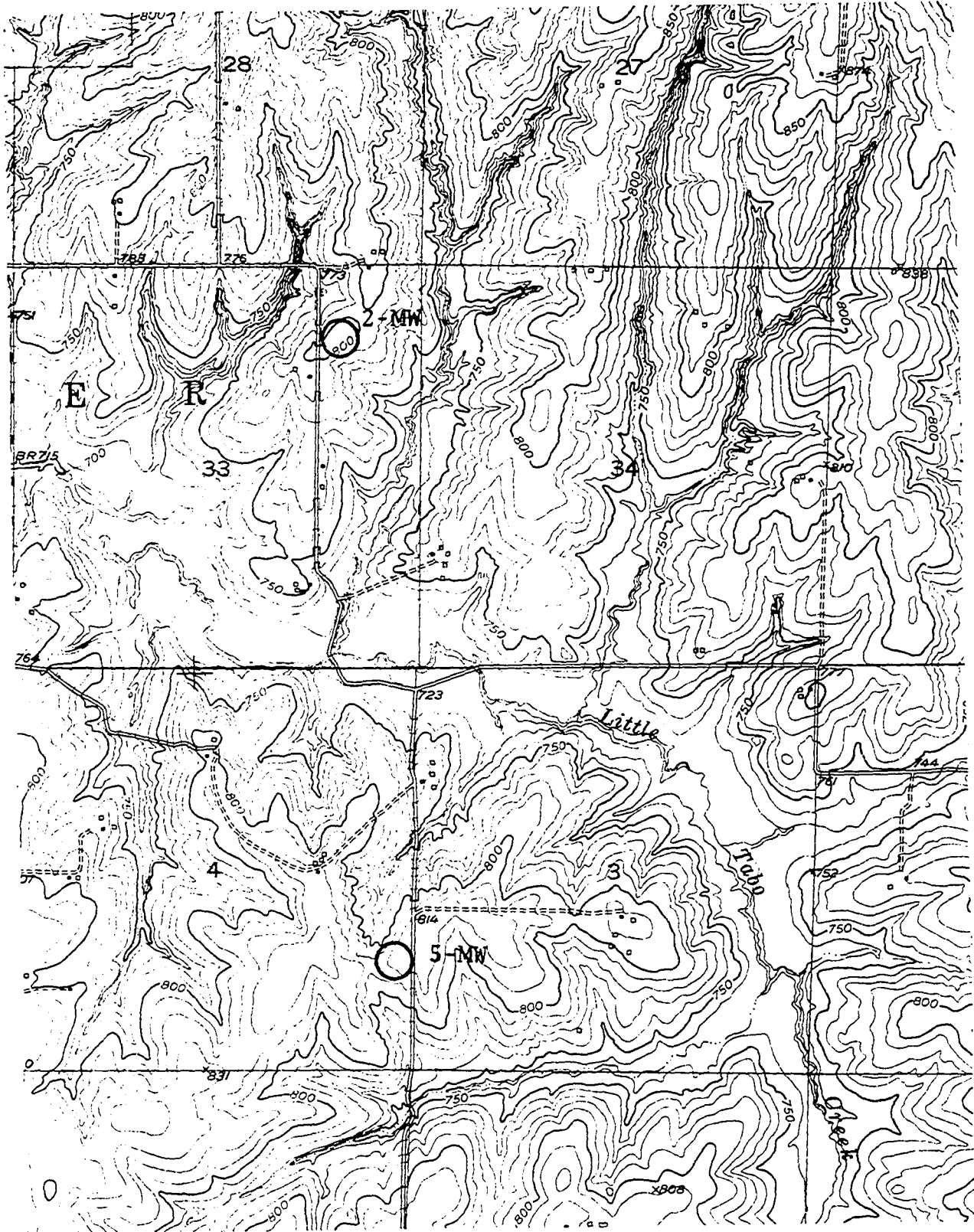
SITE: 3-MW
QUADRANGLE: HIGGINSVILLE, MO.
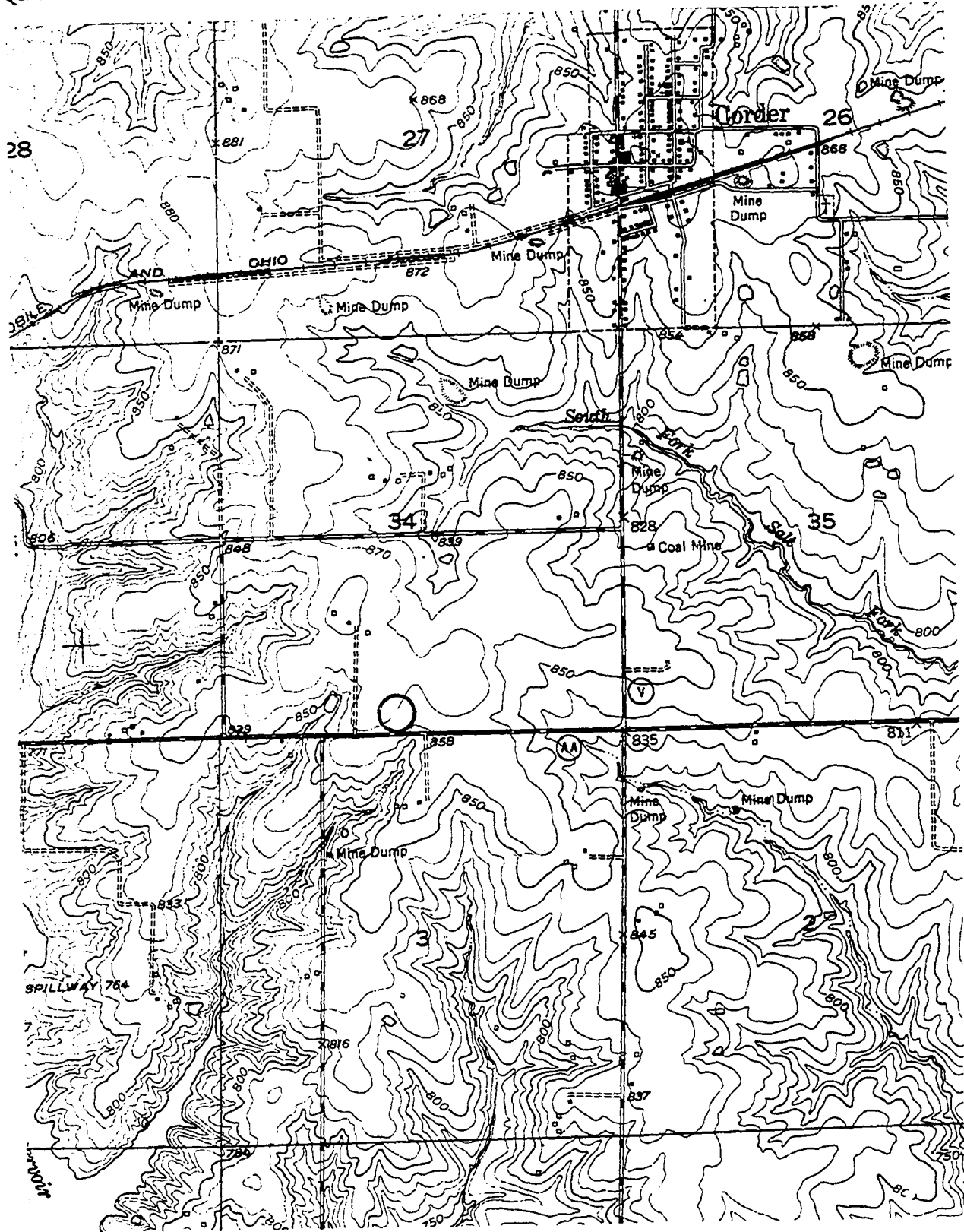
SITE: 6-MW
QUADRANGLE: KNOBNOSTER NW, MO.
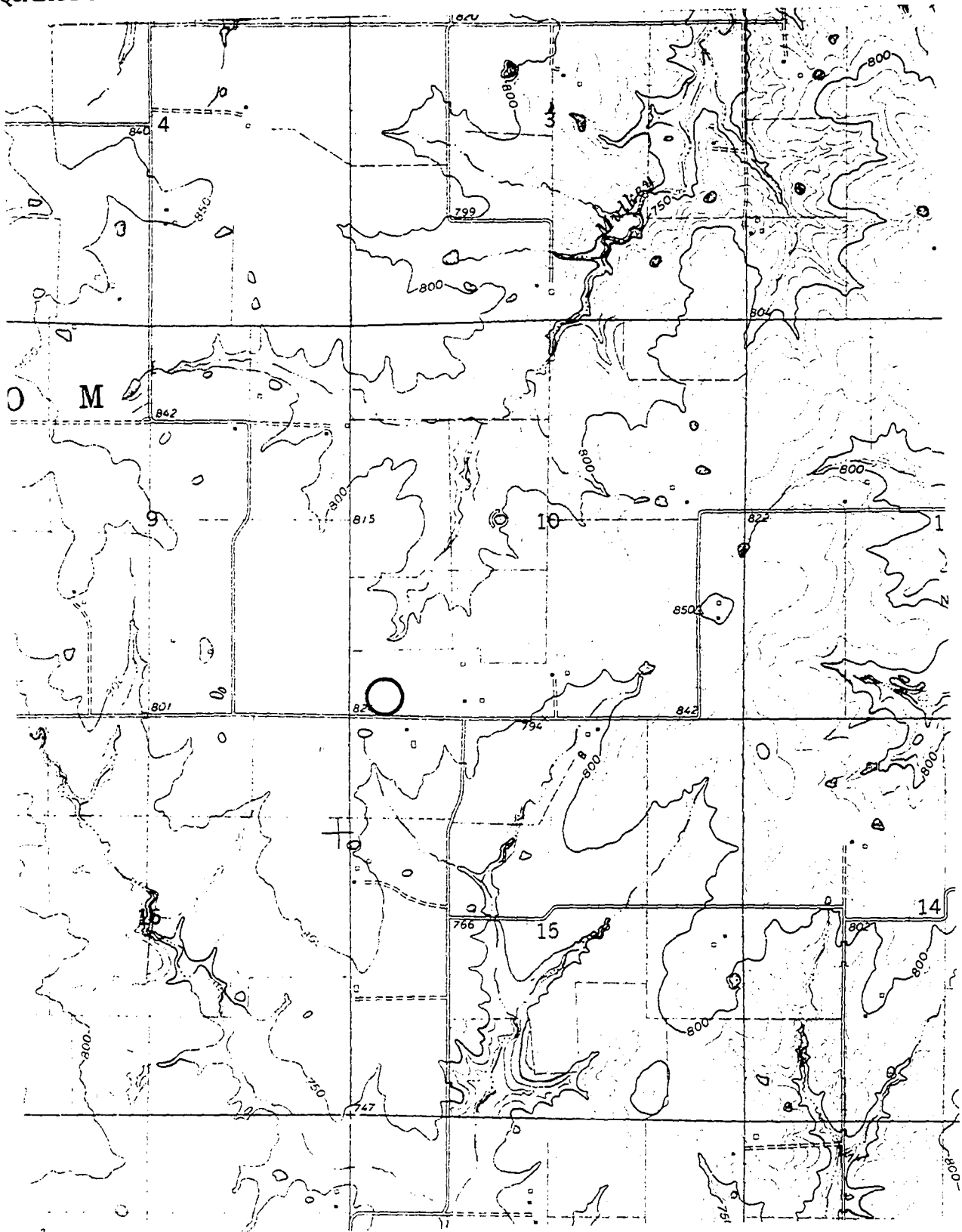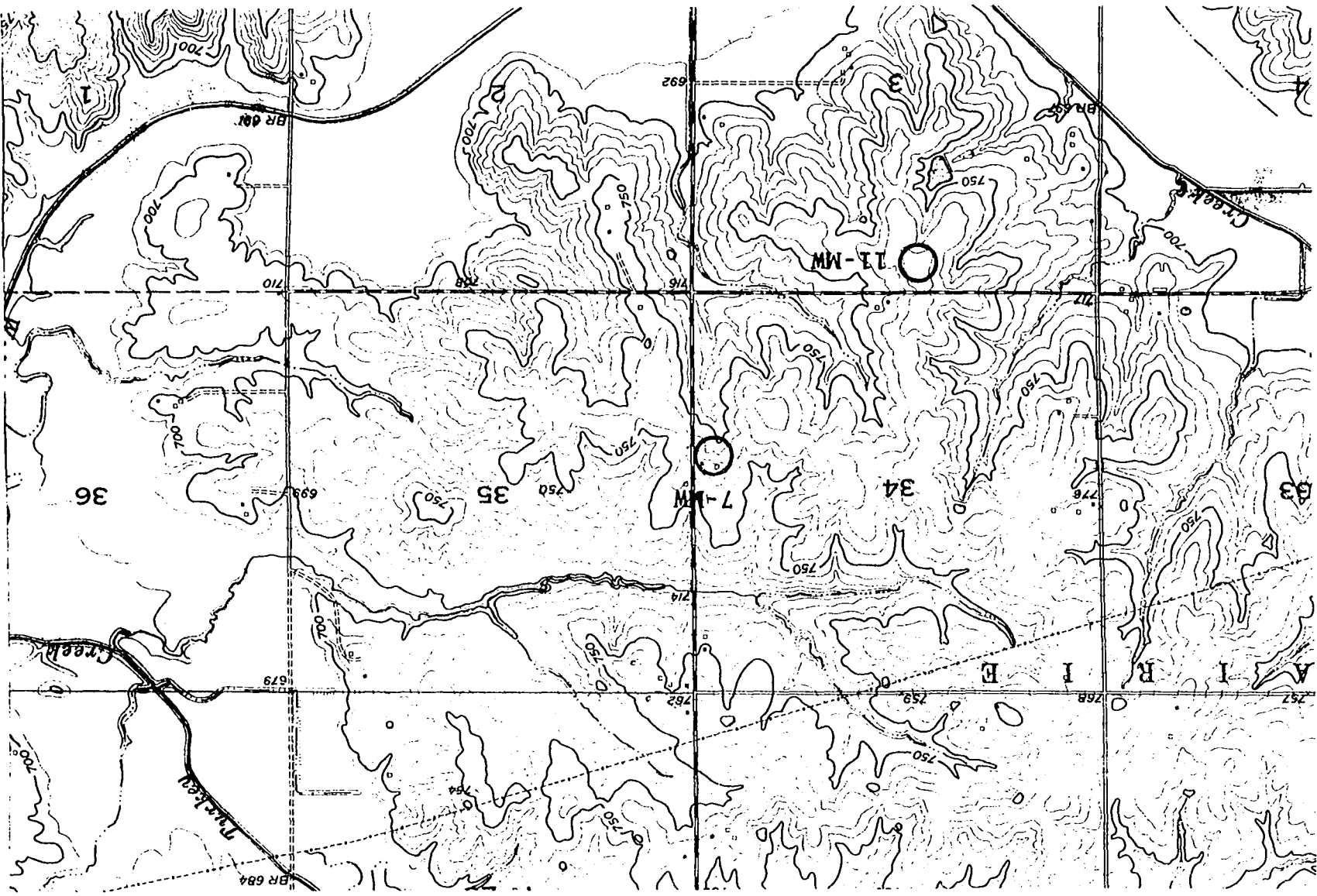
SITE: 7-MW,11-MW
QUADRANGLE: NORBORNE,MO.

SITE: 8-MW
QUADRANGLE: NORBORNE,MO.
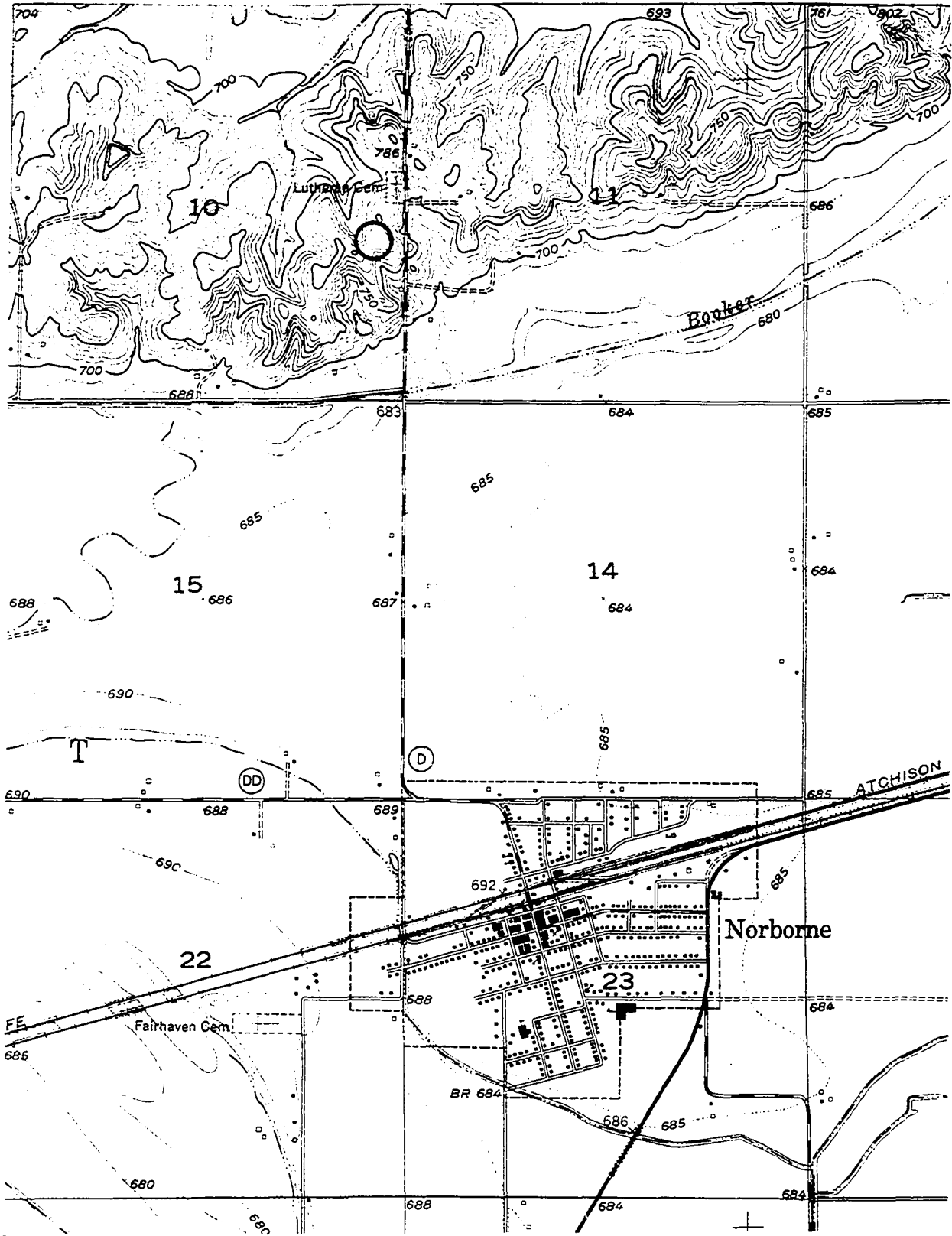
SITE: 9-MW
QUADRANGLE: ROADS,MO.
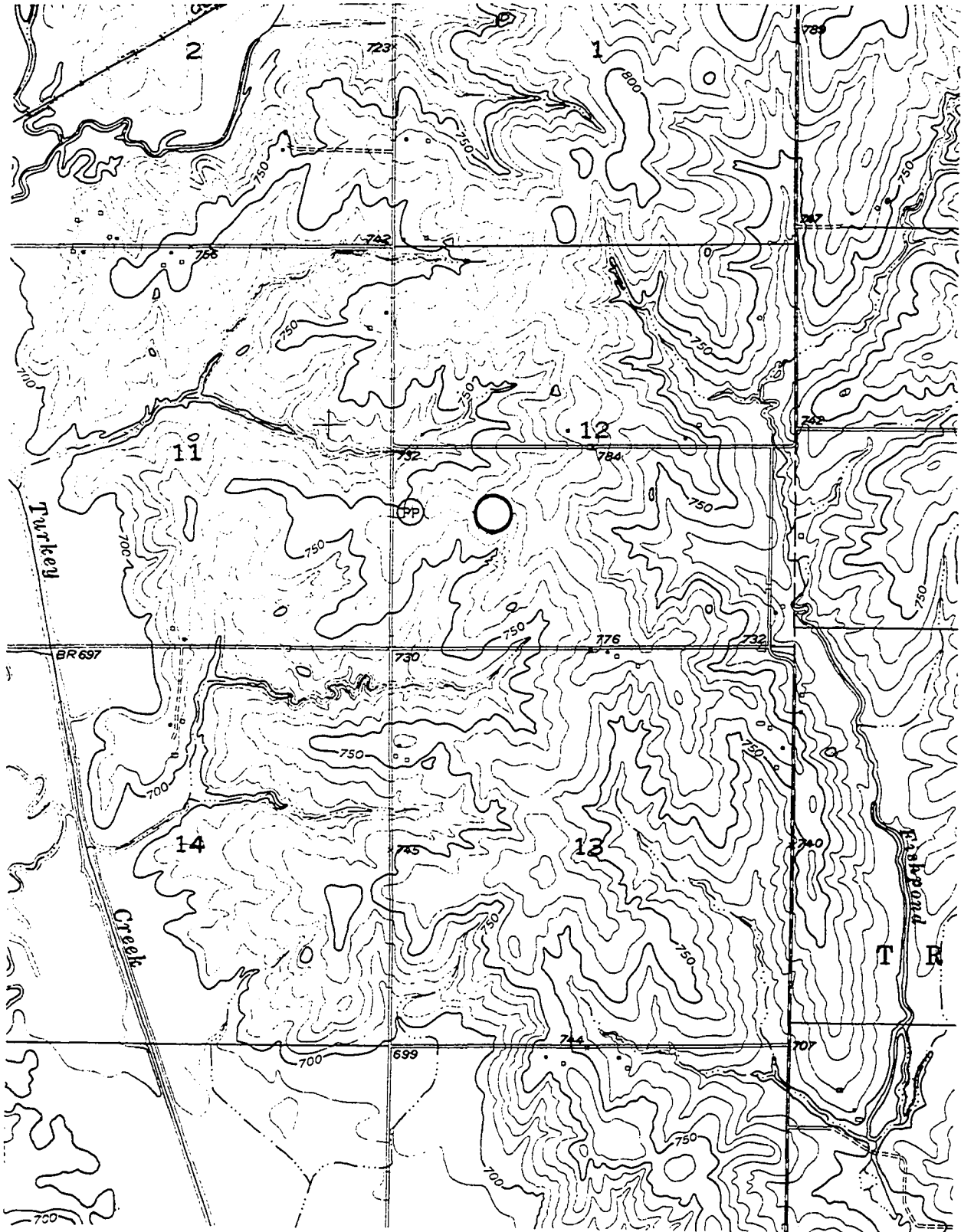
SITE: 10-MW
QUADRANGLE: ROADS,MO.
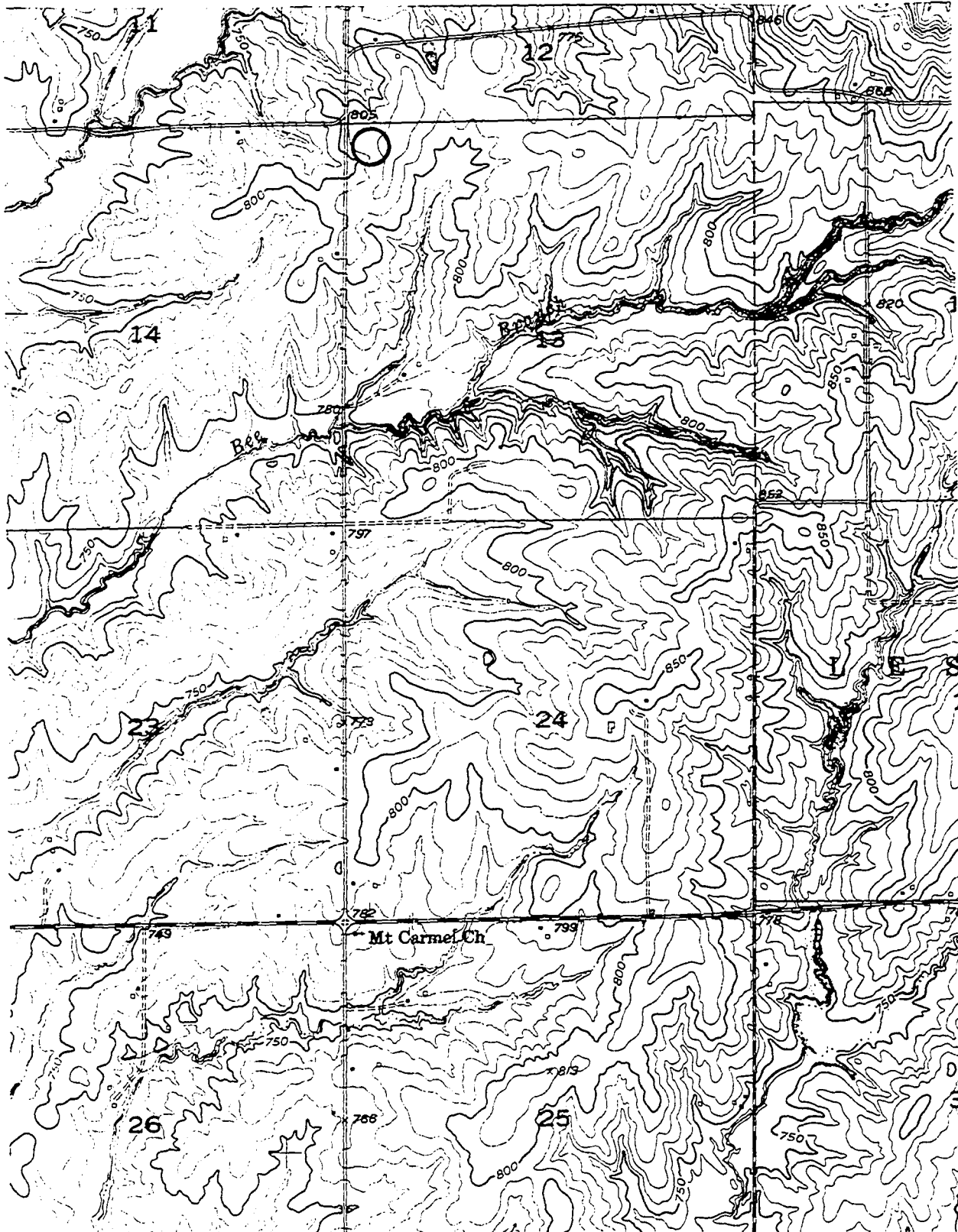
SITE: 12-MW
QUADRANGLE: PLYMOUTH, MO.
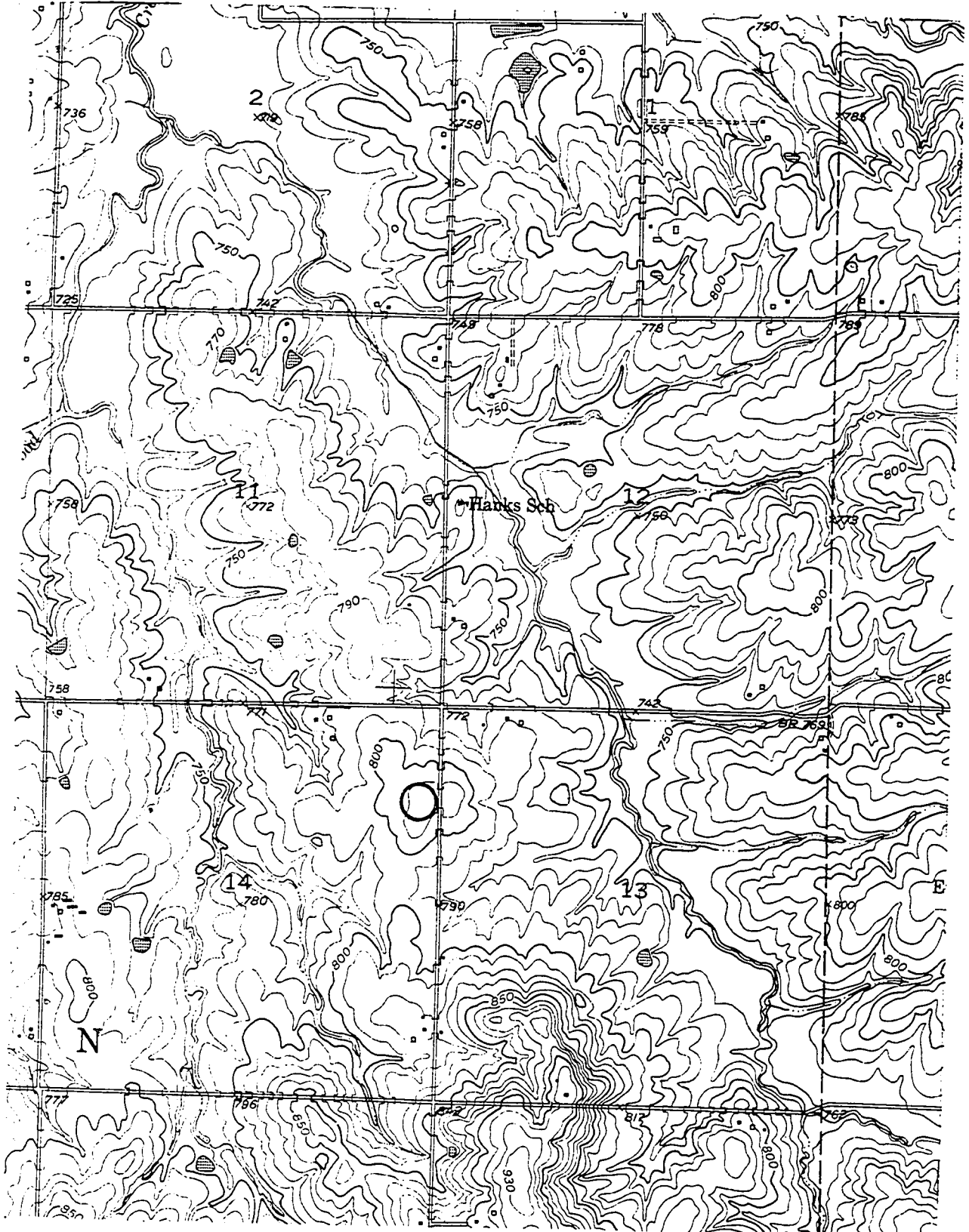
SITE: 1-ME
QUADRANGLE: HERMANN,MO.
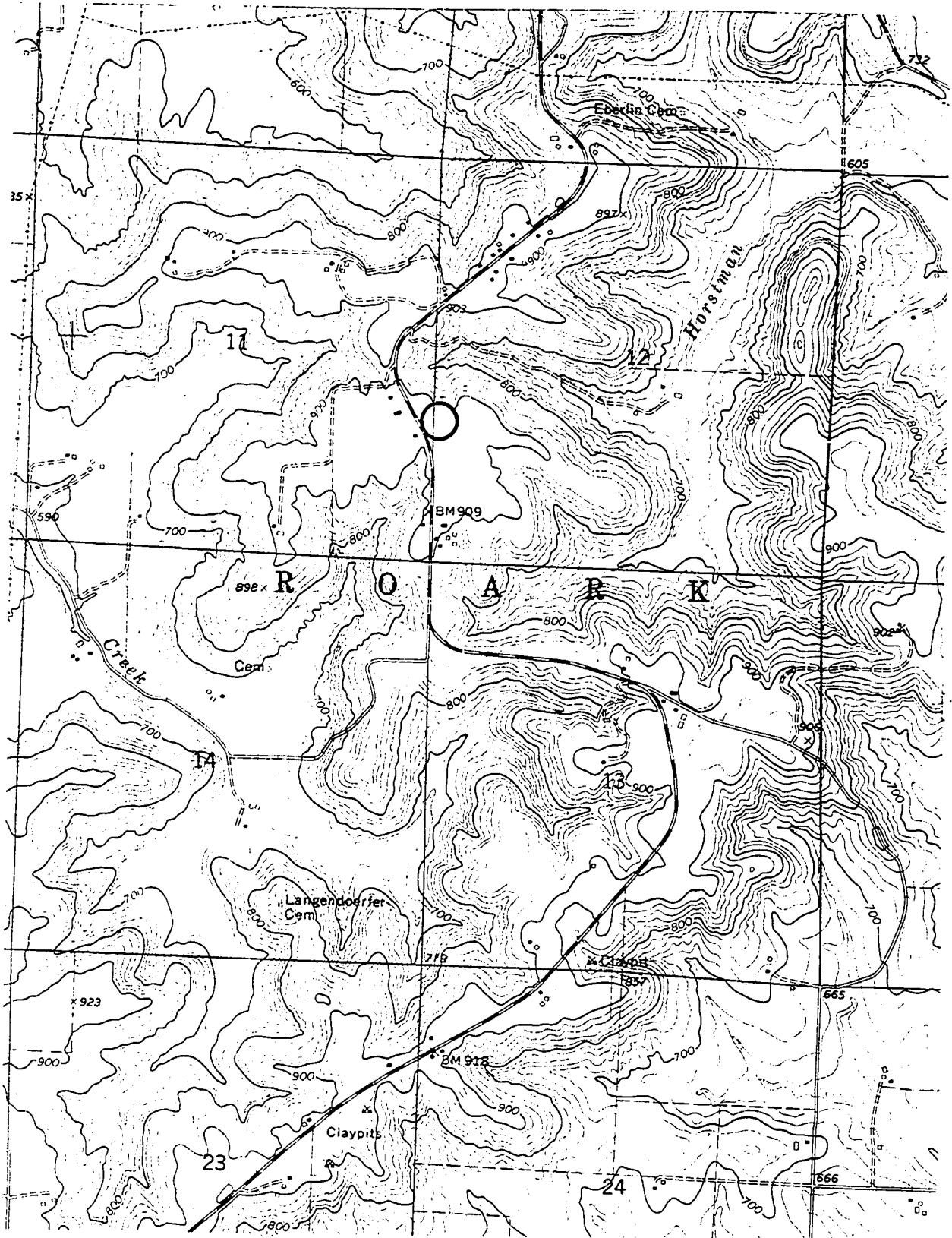
SITE: 2-ME
QUADRANGLE: SWISS,MO.

SITE: 3-ME
QUADRANGLE: SWISS, MO.

CLAYPITS

Substation   882   Bieber Cem   916   Claypits

816×   ×861   857   810

695

Puncheon   Creek

Claypits   860   35   Claypit   852

33   PIPELINE   34

Claypits

×942

BM   877

950   921×

Claypit   8

Drake
Lookout Tower

870   945

4   3   2

Claypits   (19)
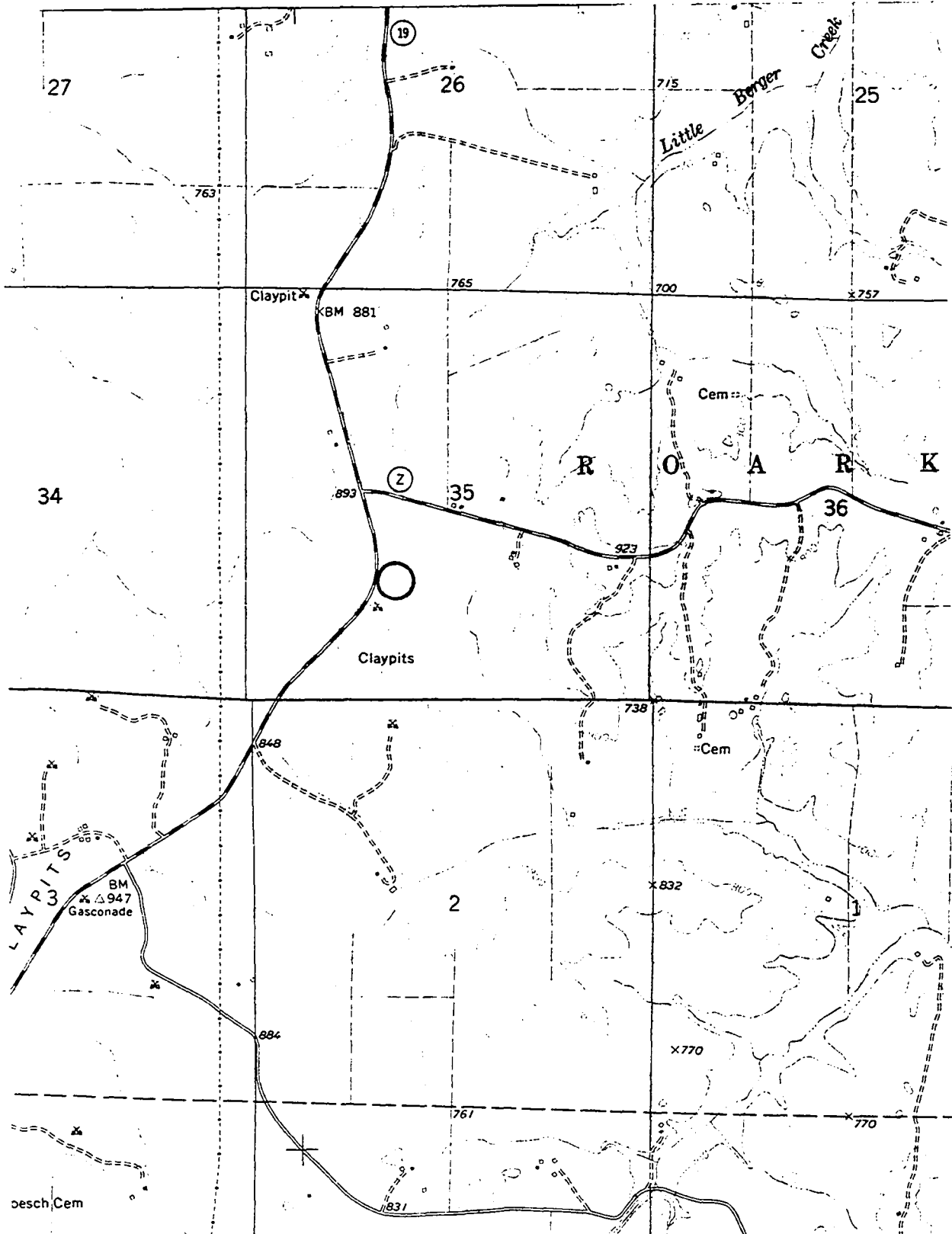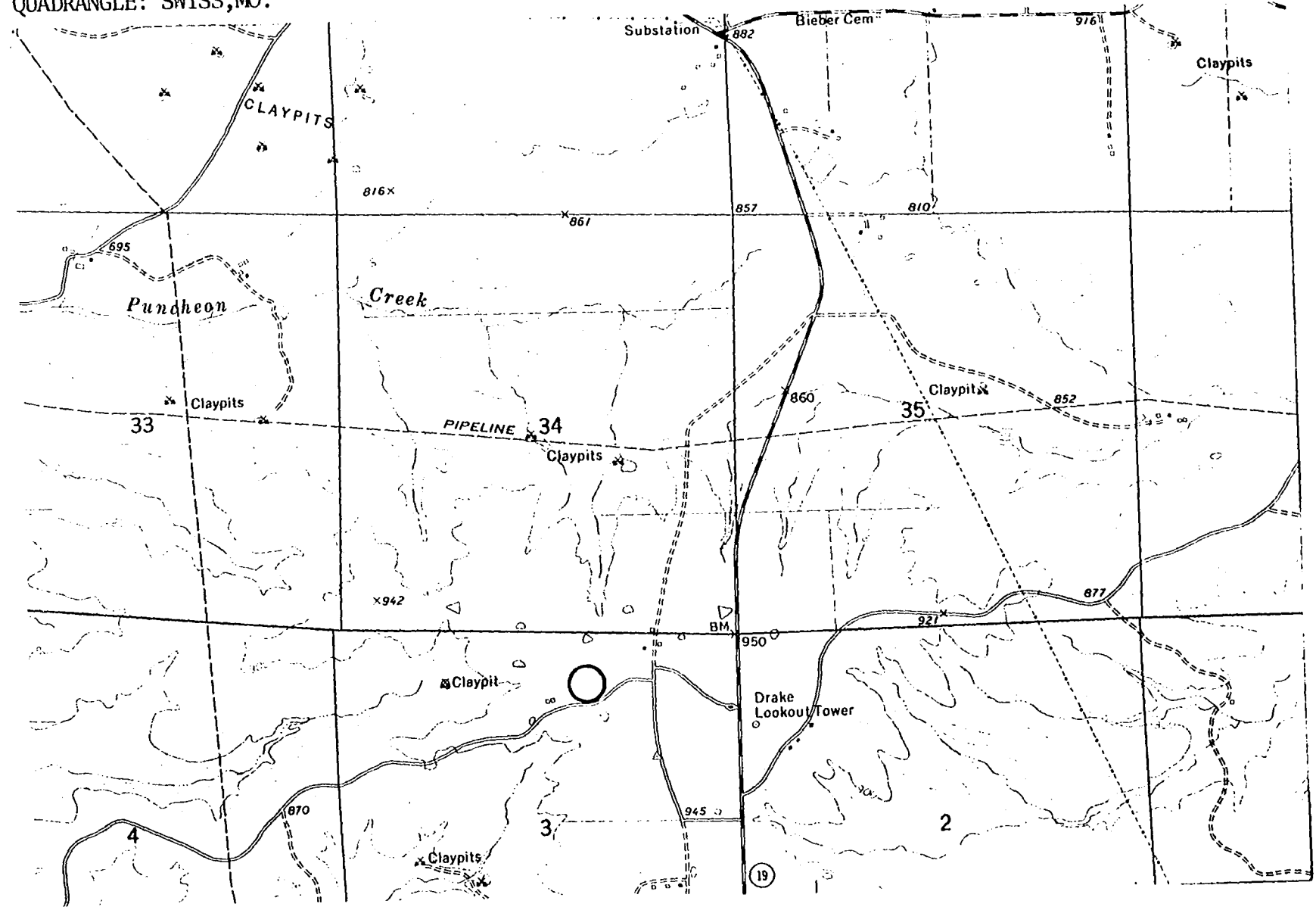
SITE: 4-ME
QUADRANGLE: OWENSVILLE EAST,MO.

299
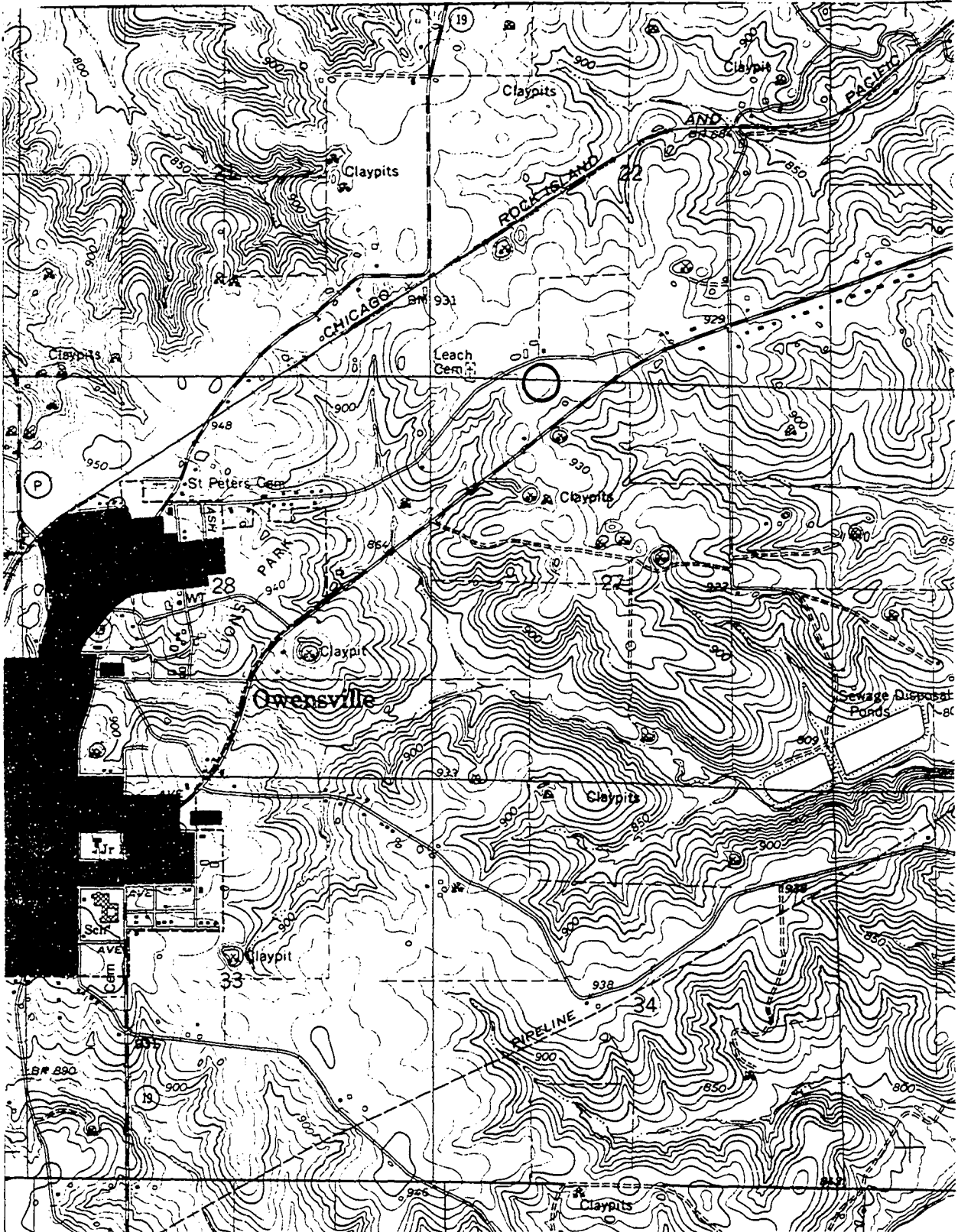
SITE: 5-ME
QUADRANGLE: ROSEBUD, MO.
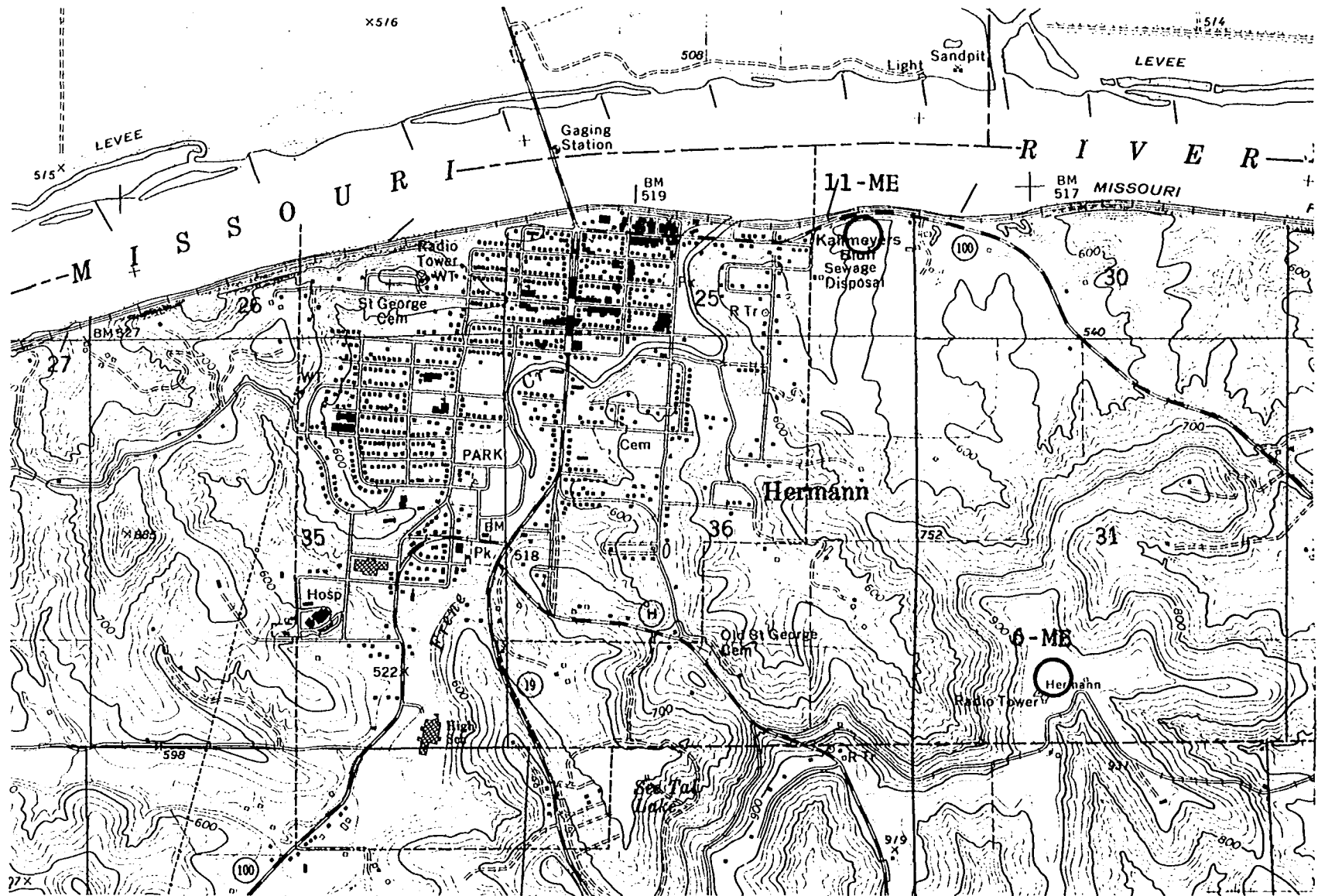
SITE: 7-ME
QUADRANGLE: ASHLAND, MO.

302
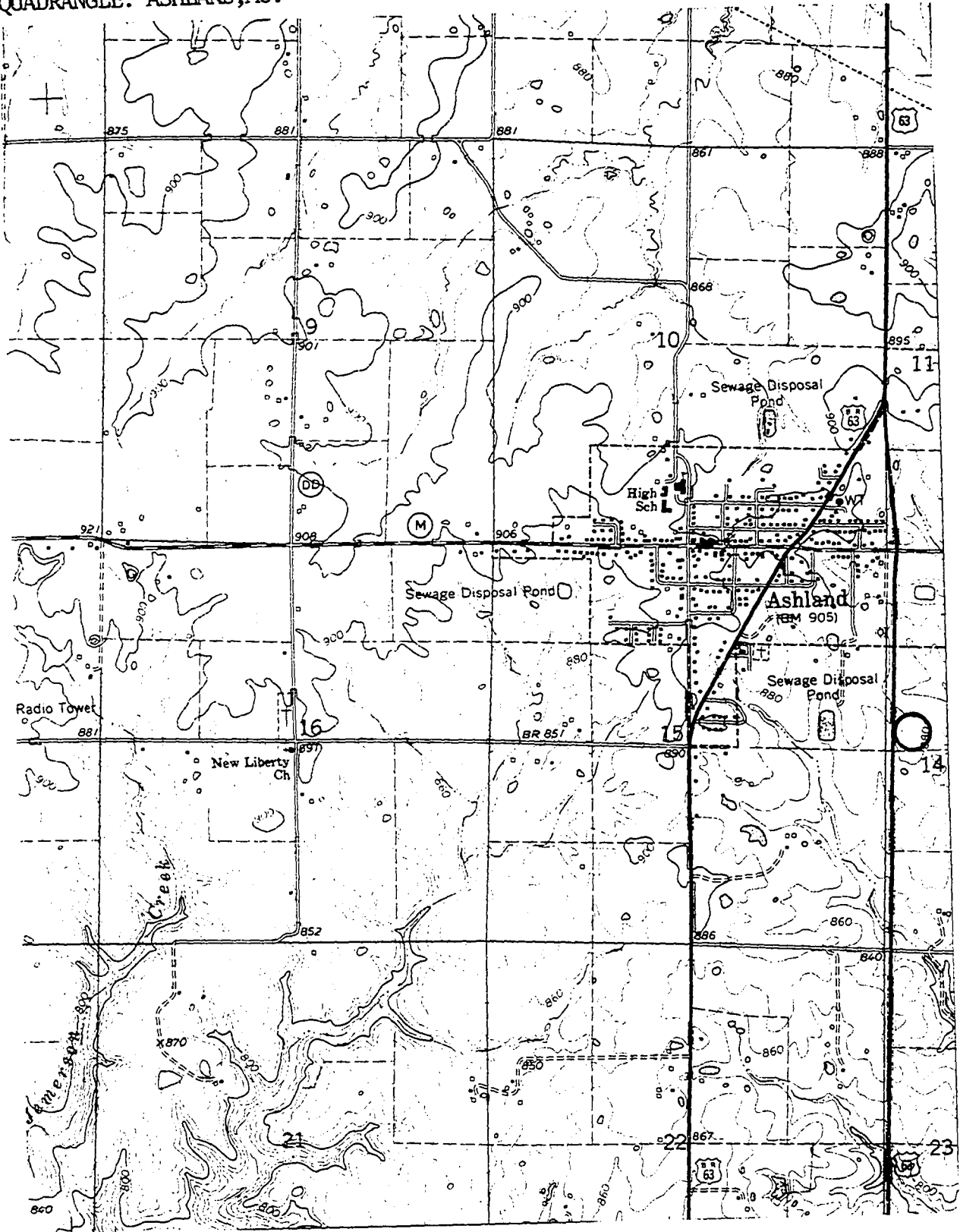
SITE: 8-ME
QUADRANGLE: COLUMBIA,MO.

SITE: 9-ME,10-ME
QUADRANGLE: PINNACLE LAKE,MO.
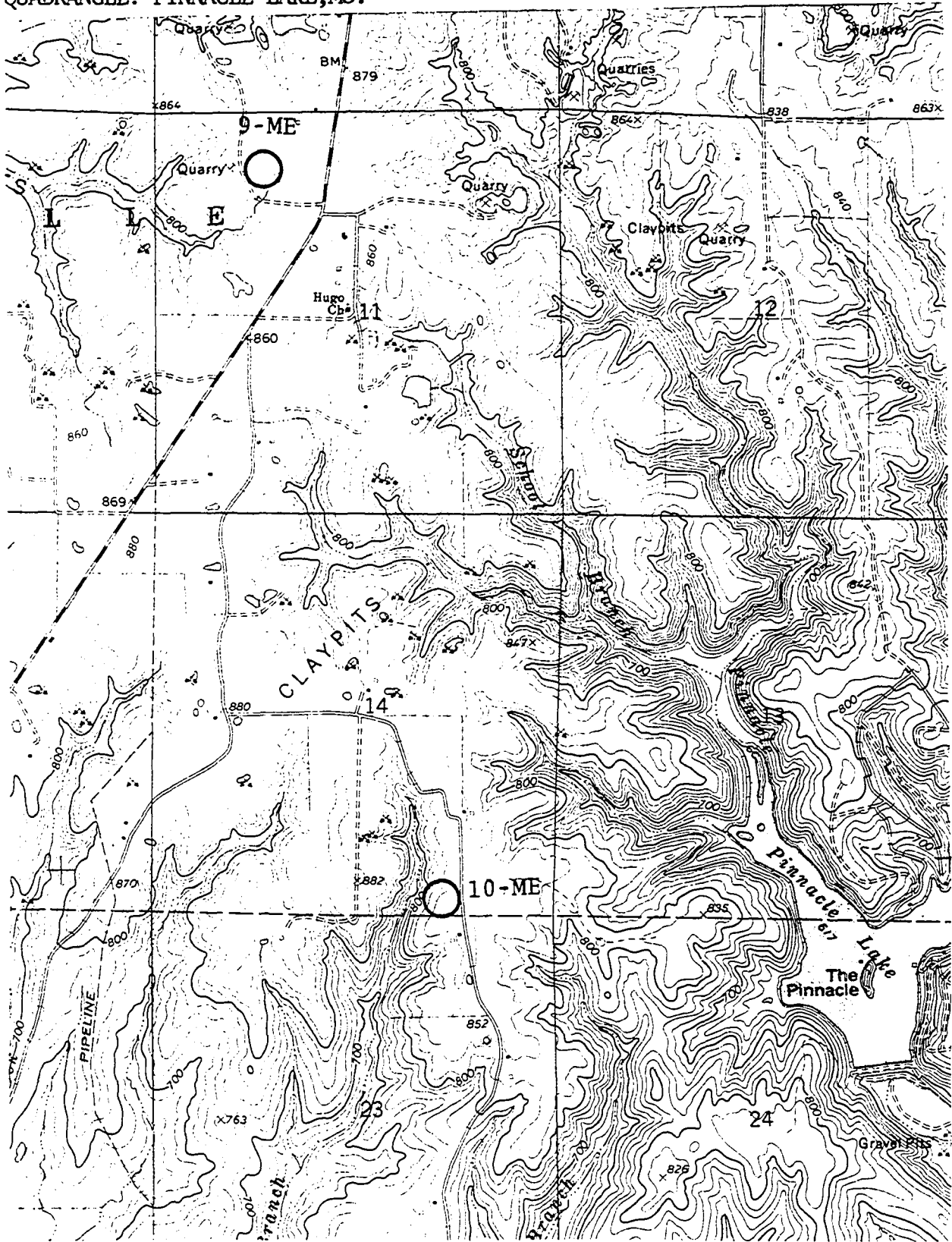
SITE: 12-ME
QUADRANGLE: PINNACLE LAKE,MO.
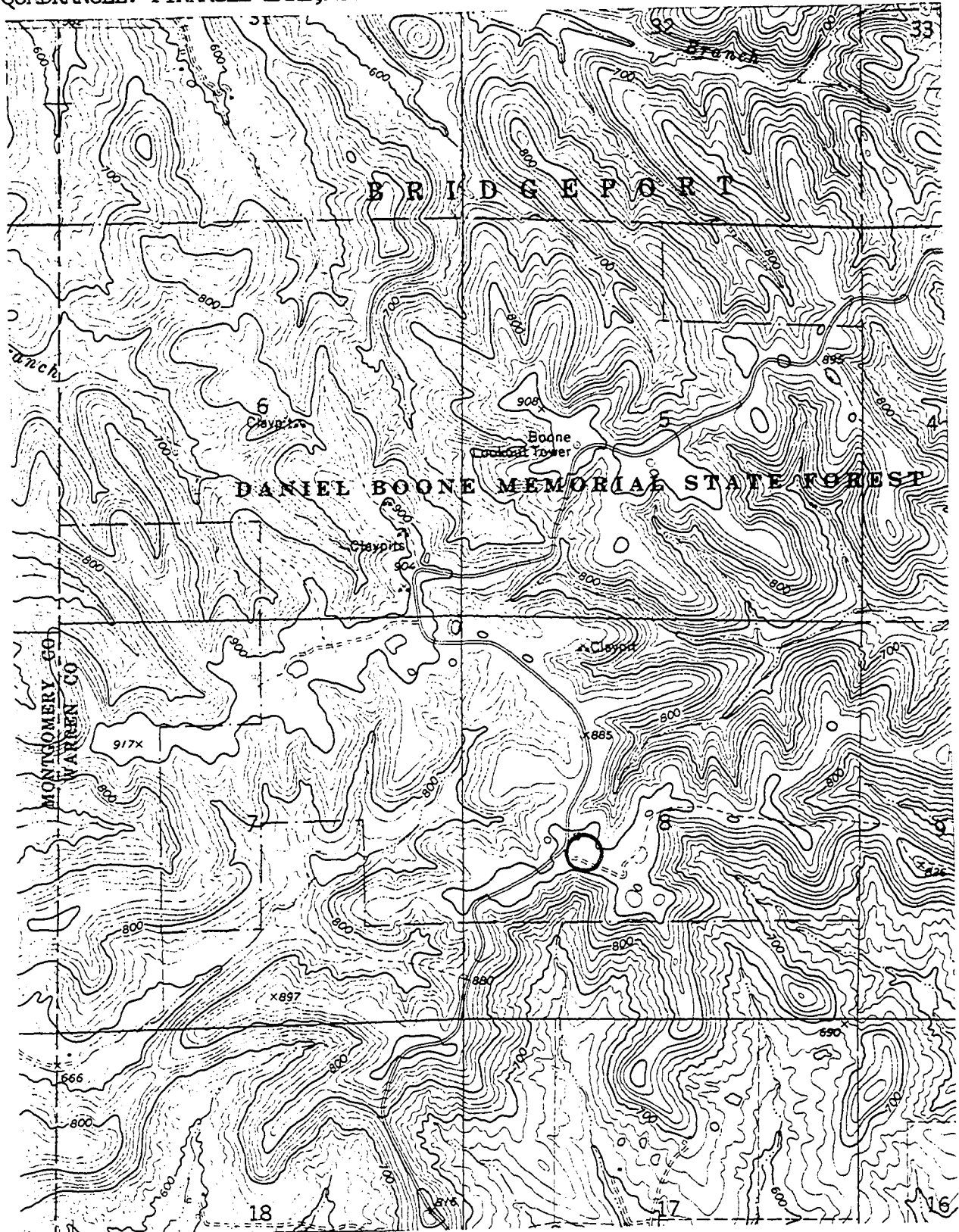
SITE: 13-ME
QUADRANGLE: MAYWOOD,MO.
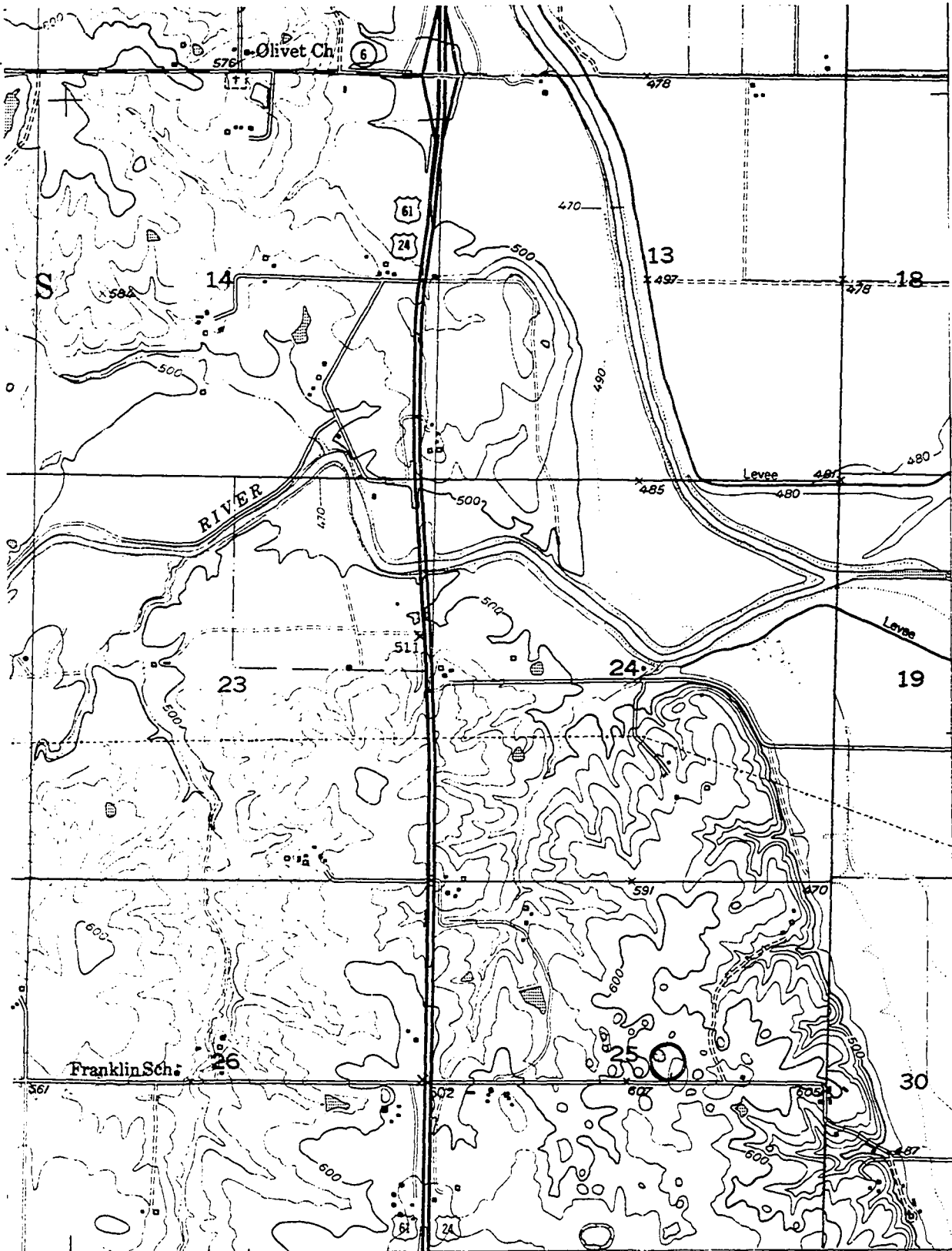
SITE: 1-LH
QUADRANGLE: MARENGO, IA.
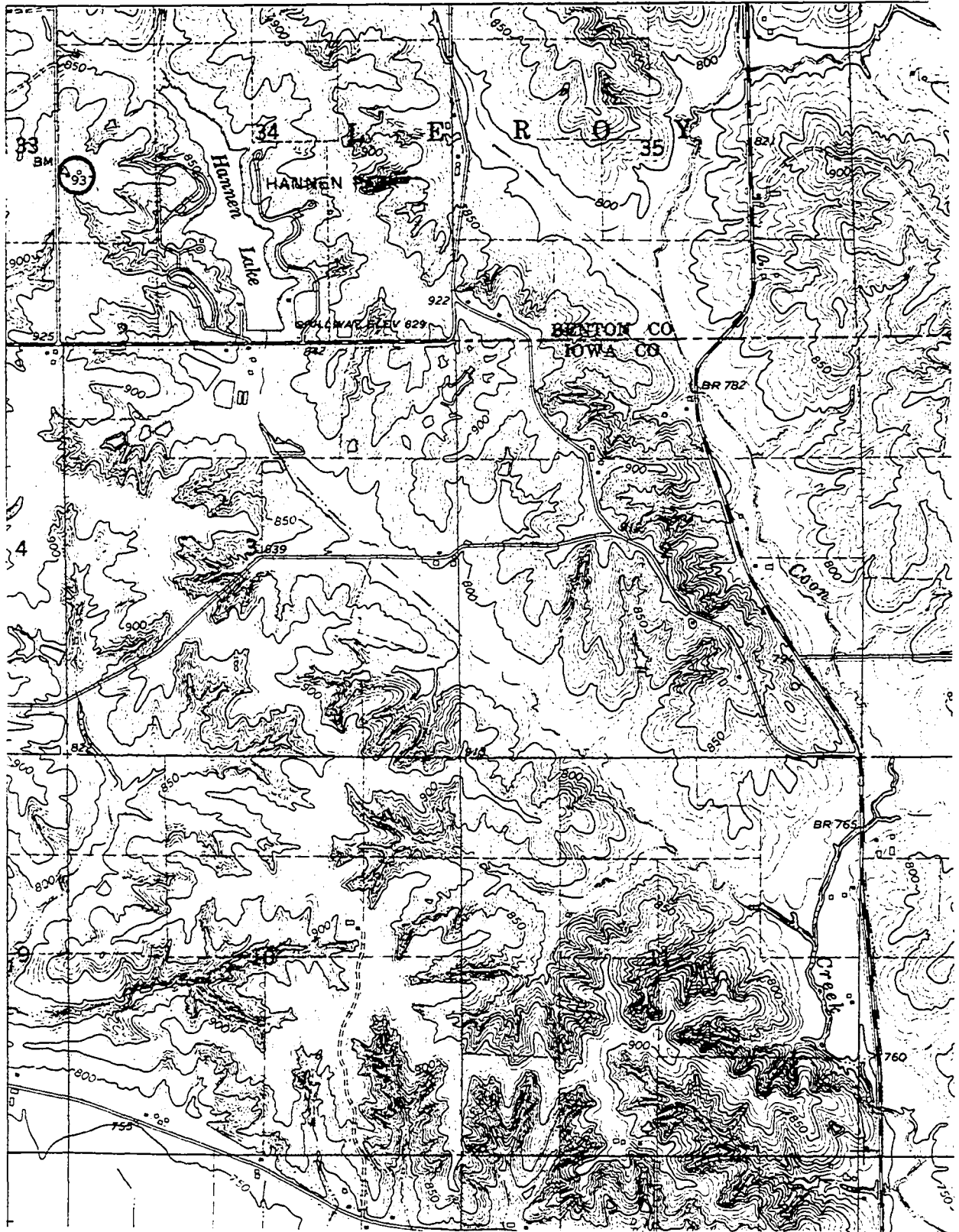
SITE: 2-LH
QUADRANGLE: LADORA, IA.
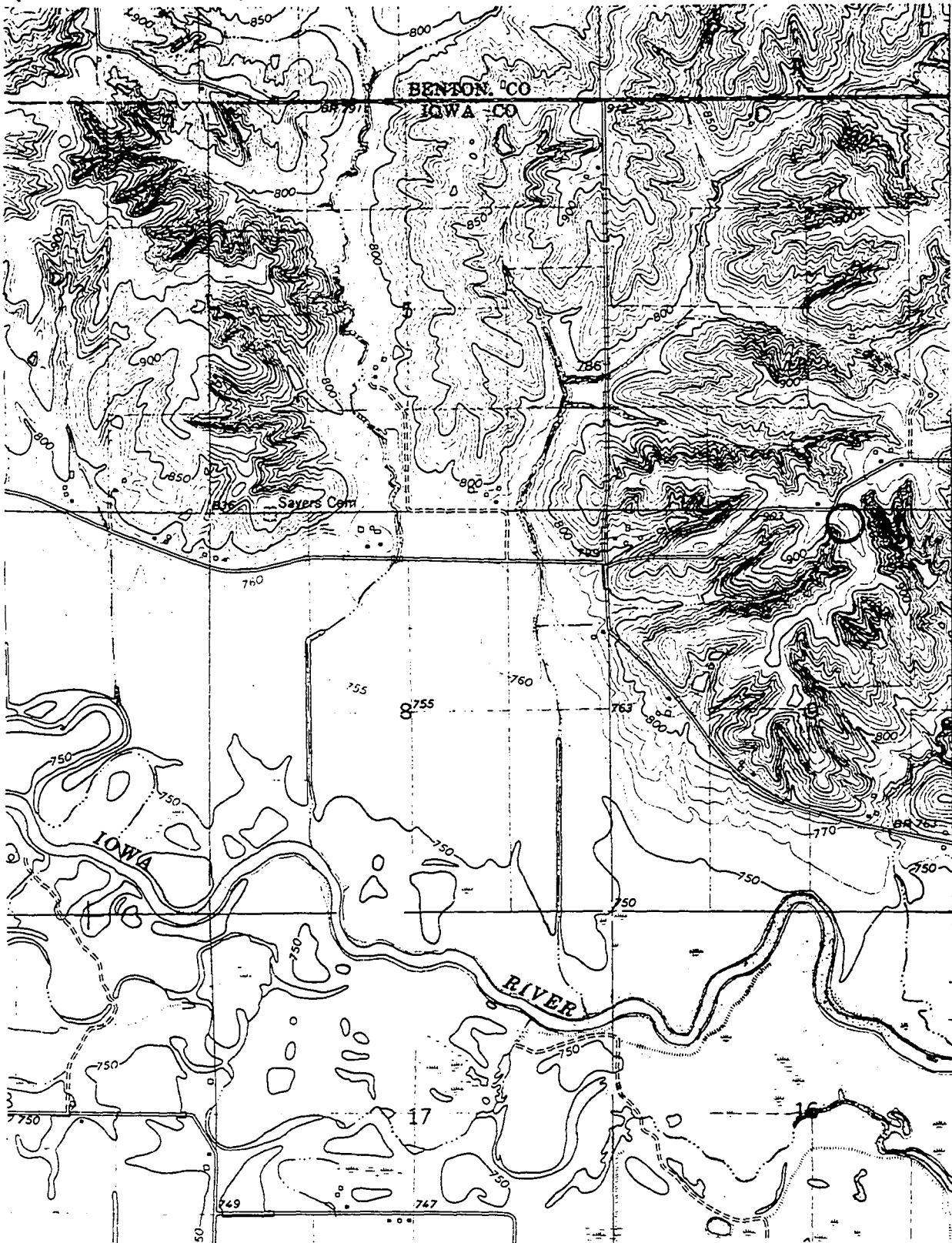
SITE: 3-LH
QUADRANGLE: WILLIAMSBURG, IA.
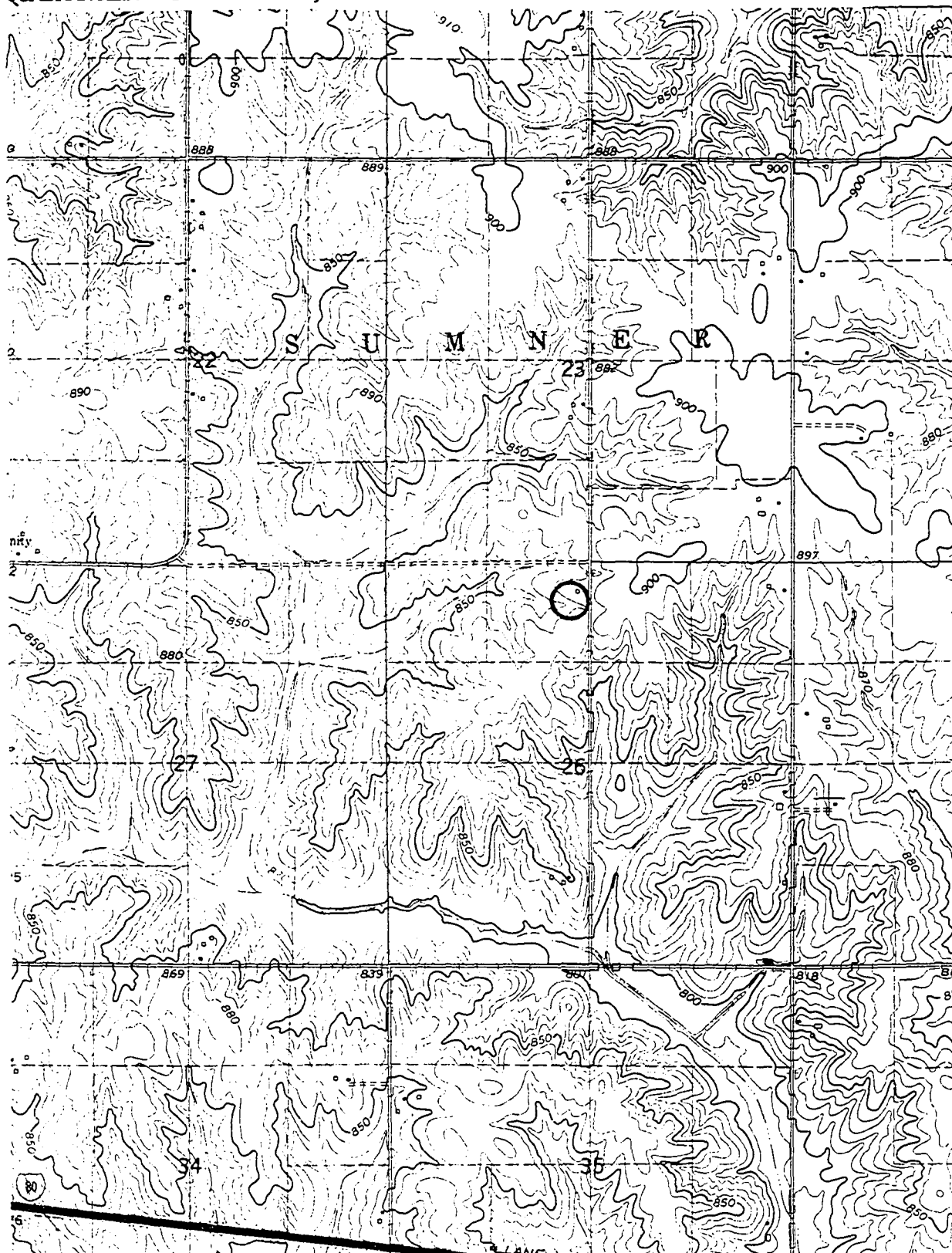
SITE: 4-LH
QUADRANGLE: NORTH ENGLISH, IA.
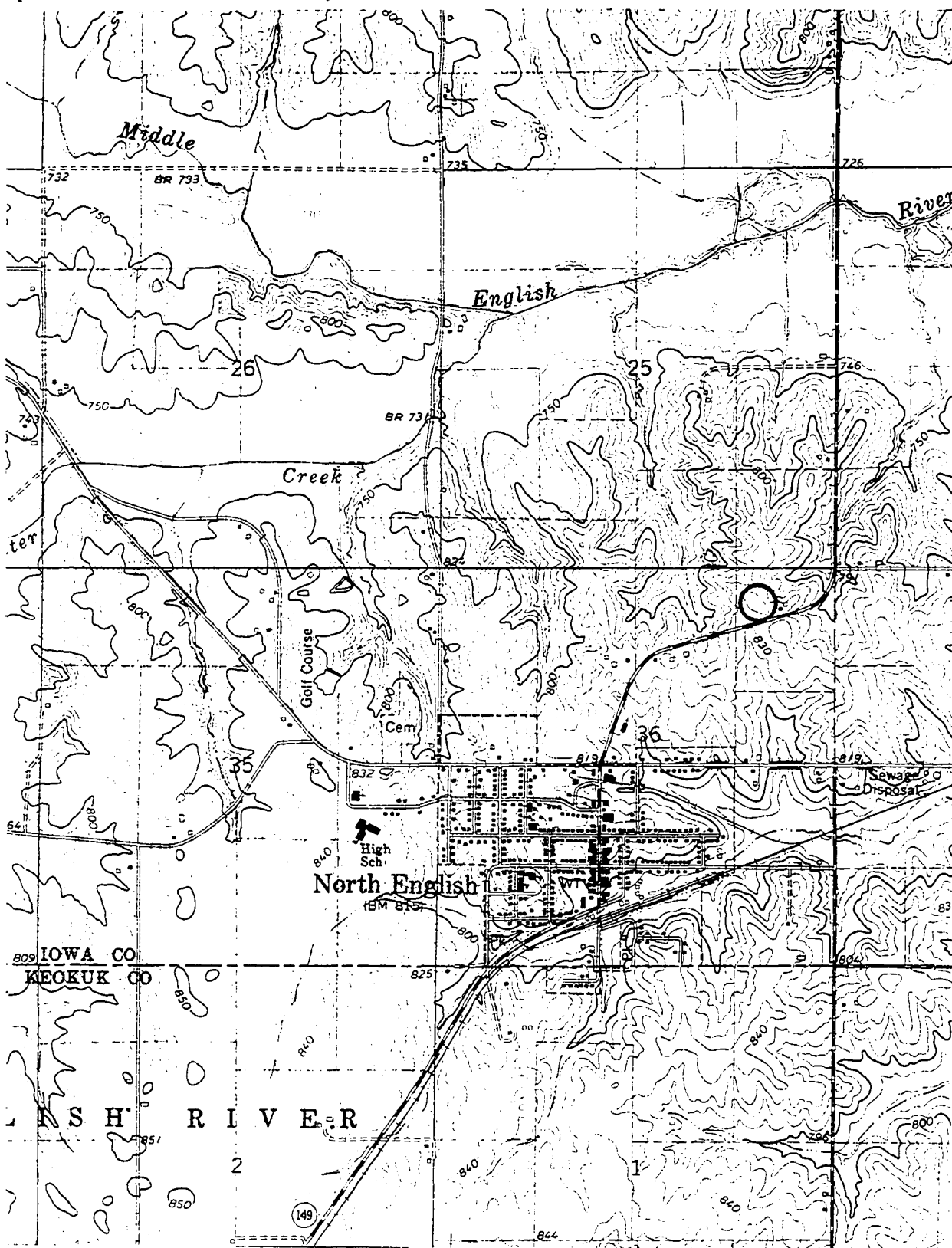
SITE: 5-LH
QUADRANGLE: WILLIAMSBURG, IA.

311
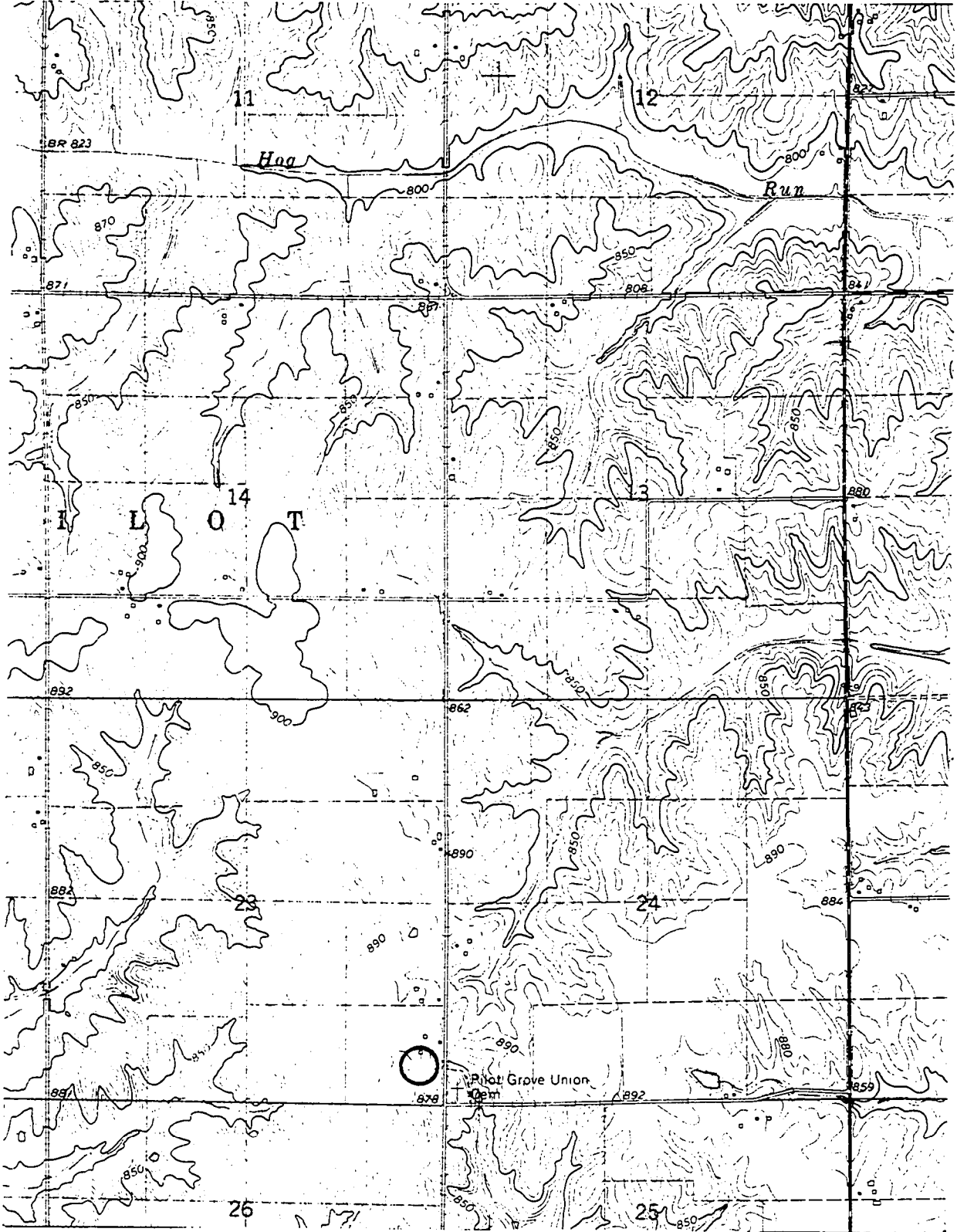
SITE: 6-LH
QUADRANGLE: MARENGO, IA.
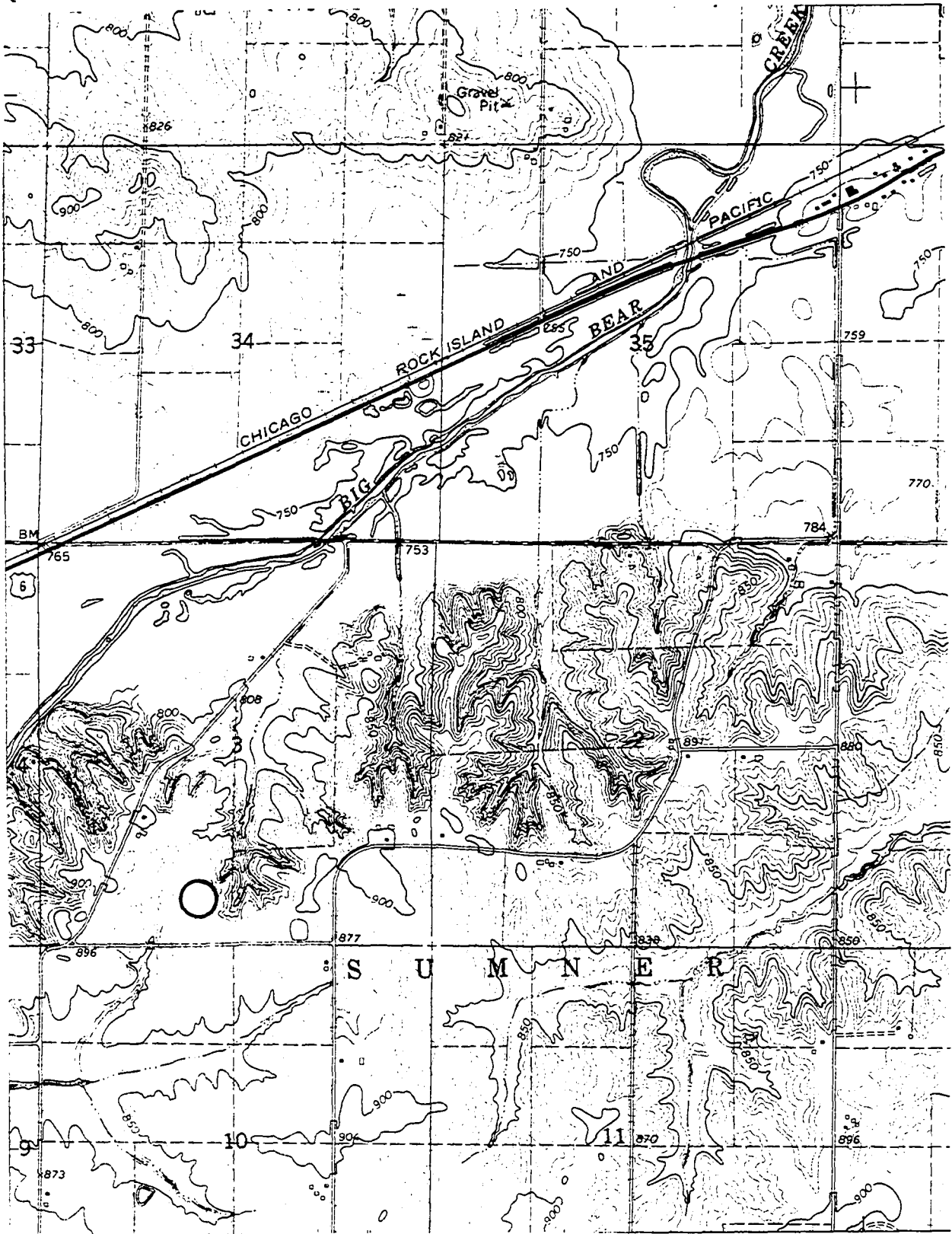
SITE: 7-LH
QUADRANGLE: HARPER, IA.
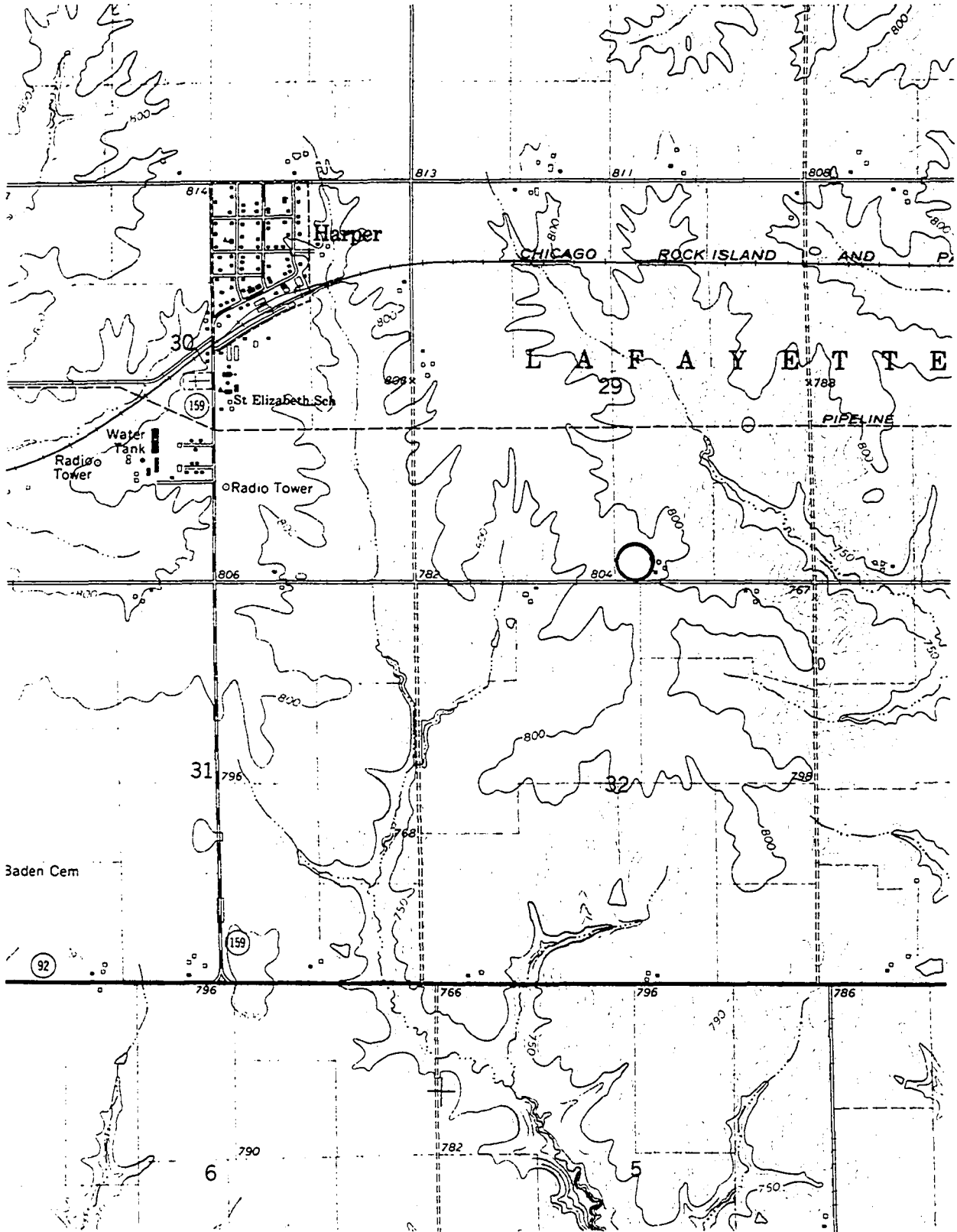
SITE: 8-LH
QUADRANGLE: SOUTH ENGLISH, IA.

314
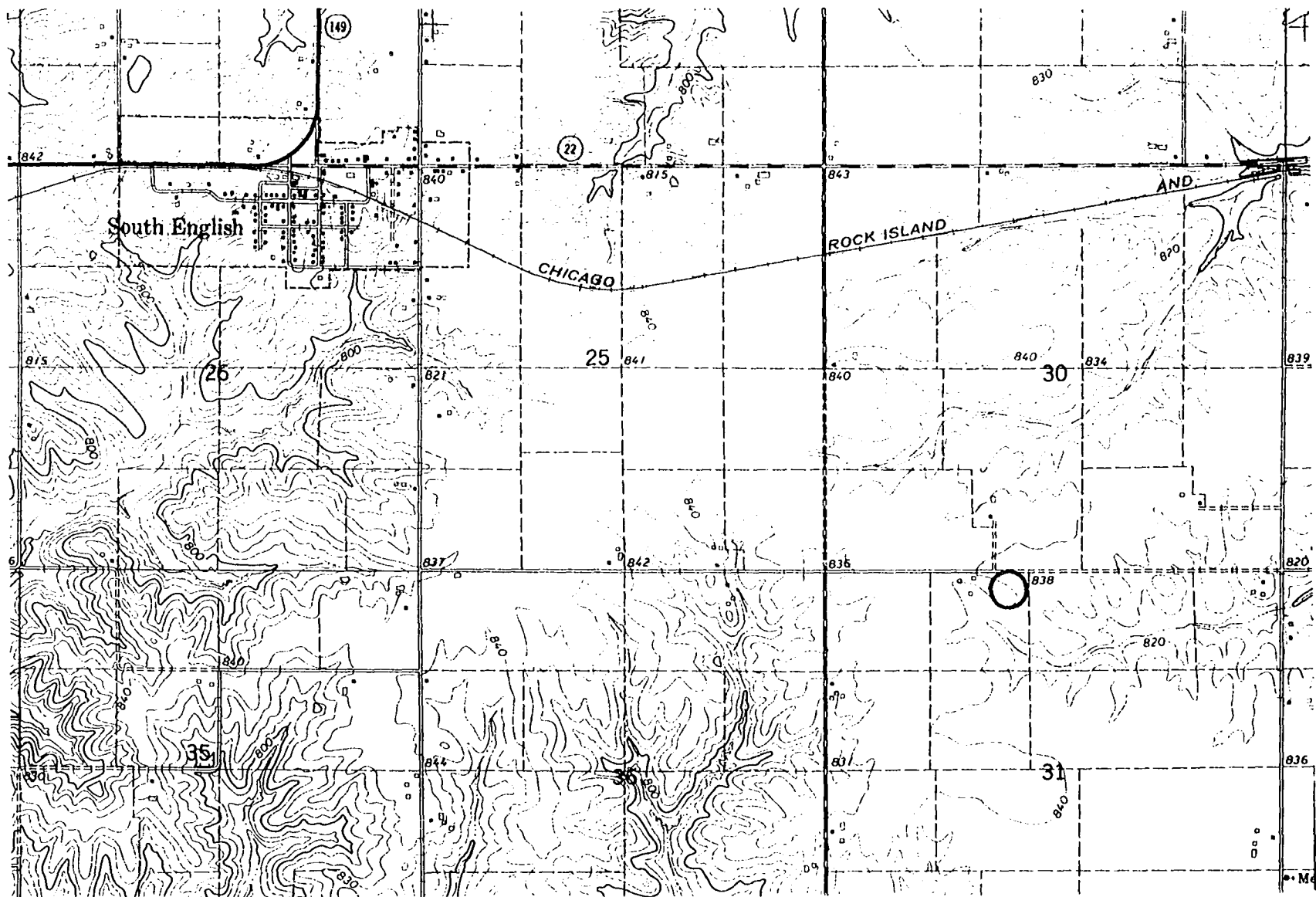
SITE: 9-LH
QUADRANGLE: LADORA, IA.
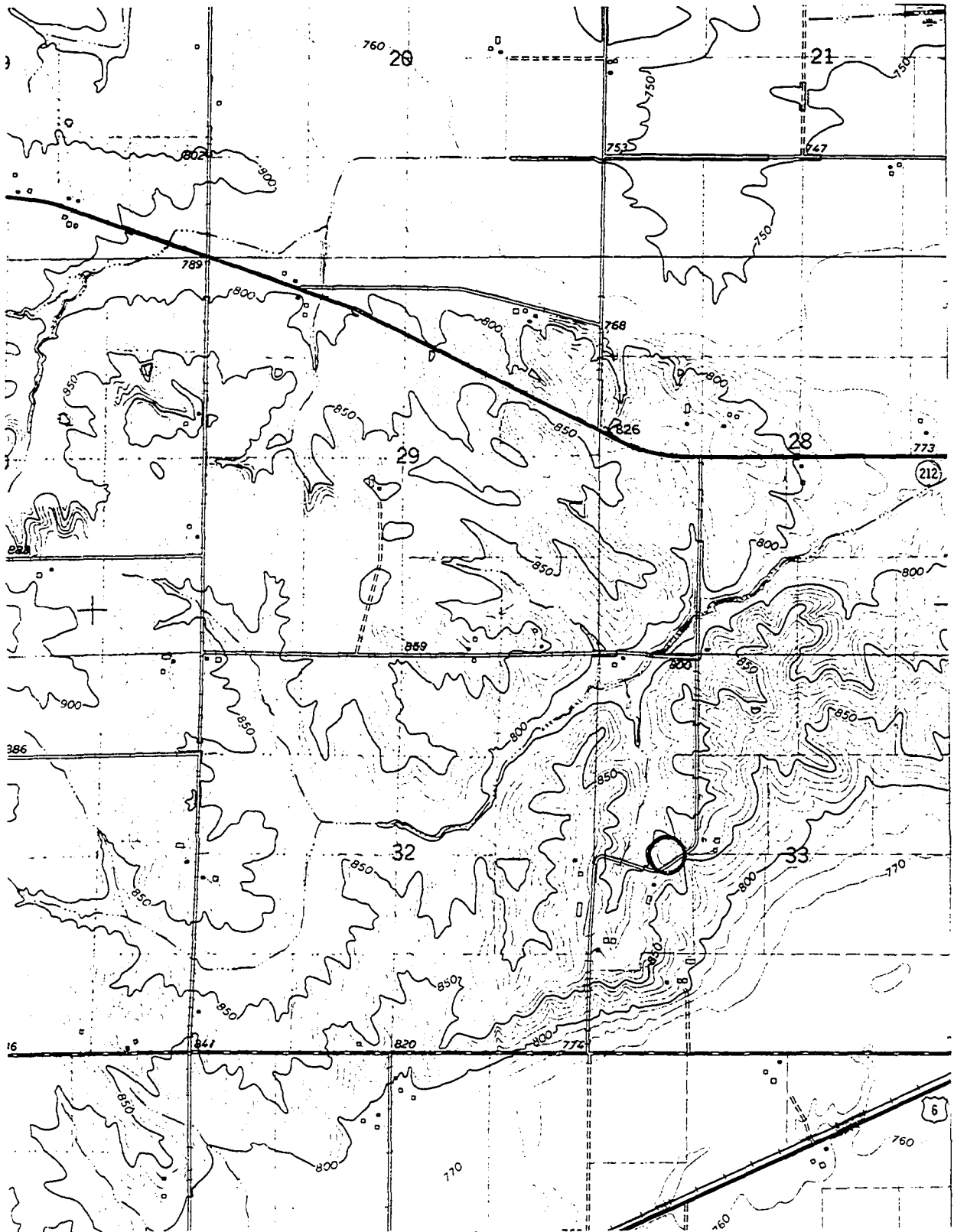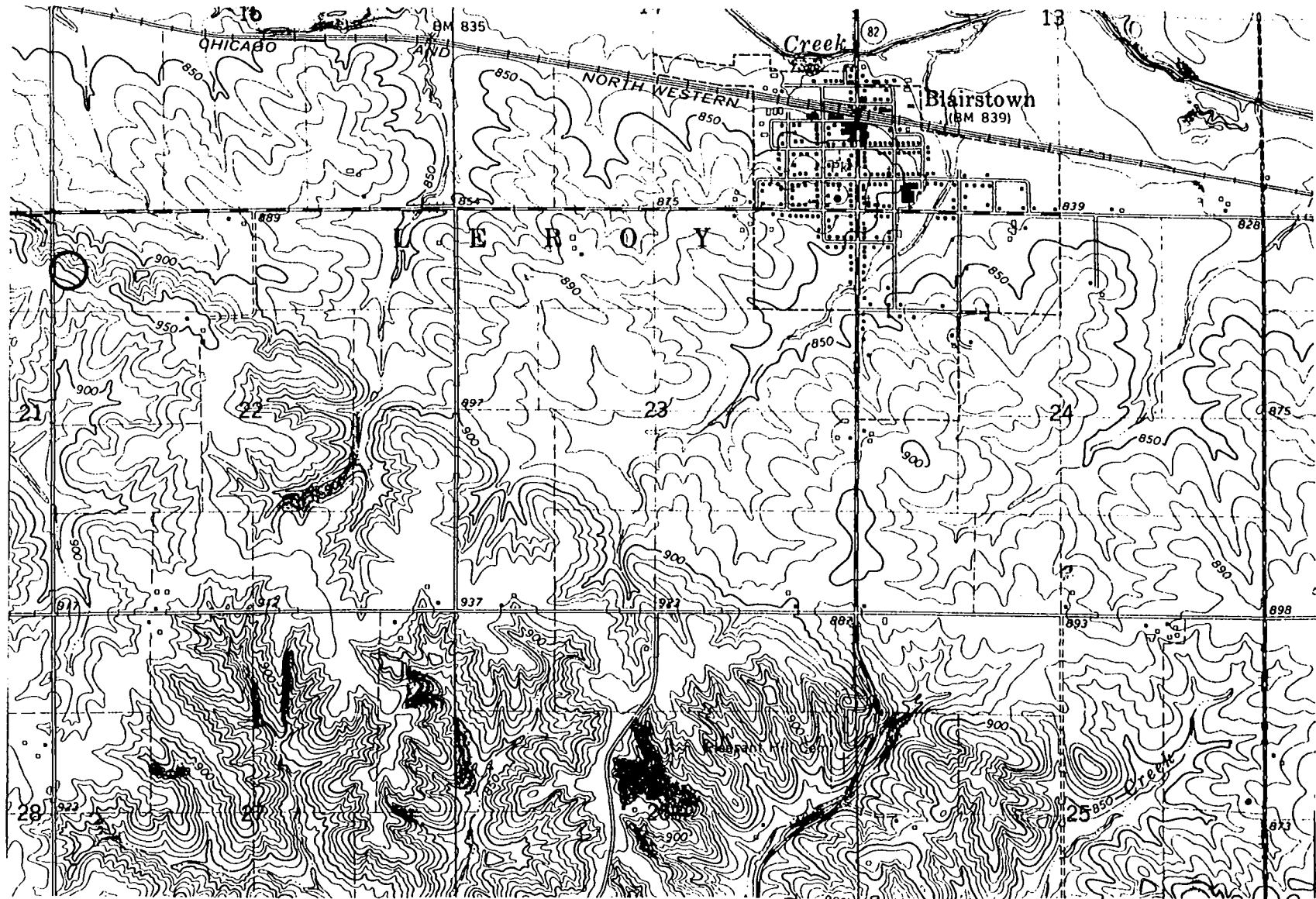
SITE: 11-LH
QUADRANGLE: LADORA, IA.
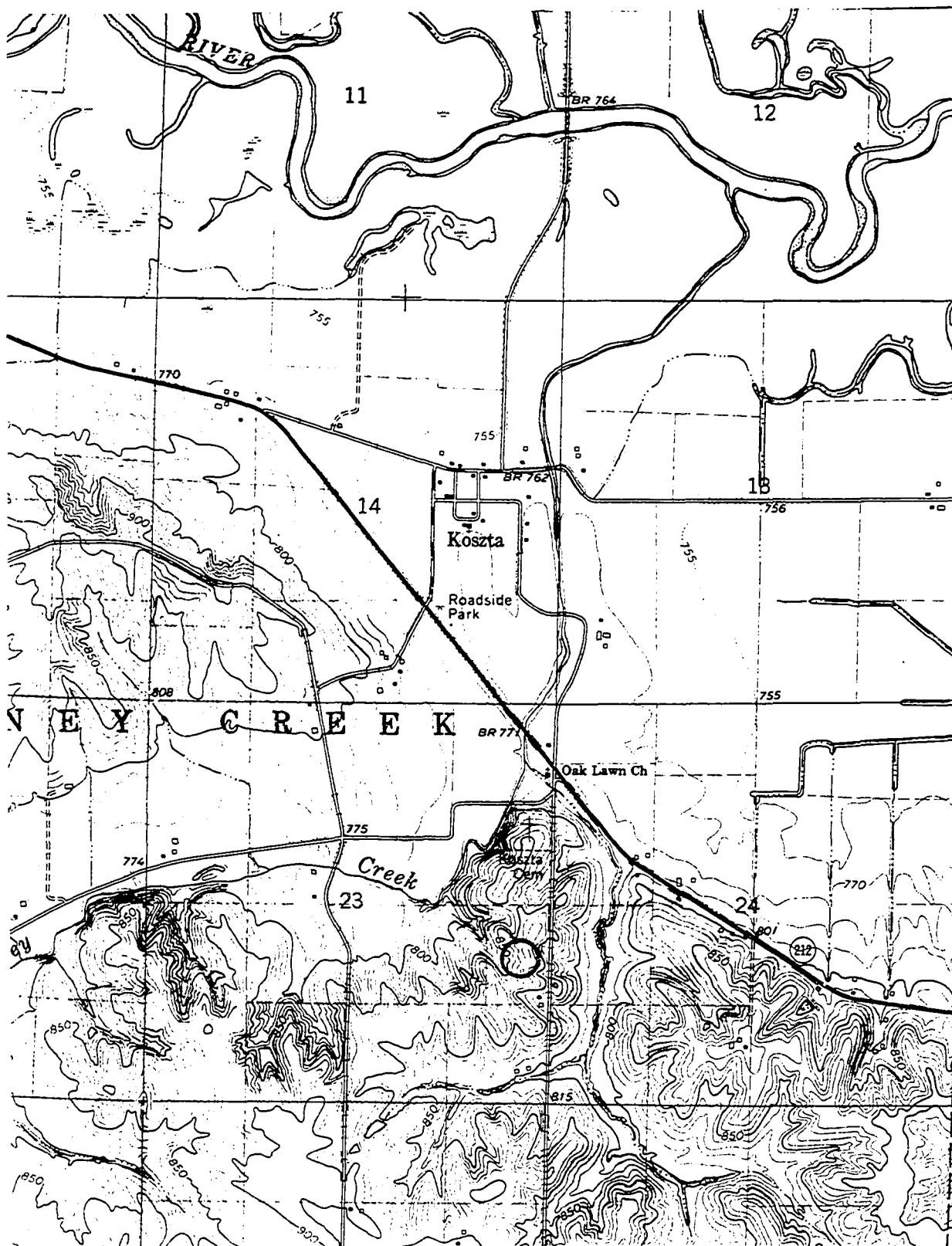
SITE: 12-LH
QUADRANGLE: LADORA, IA.
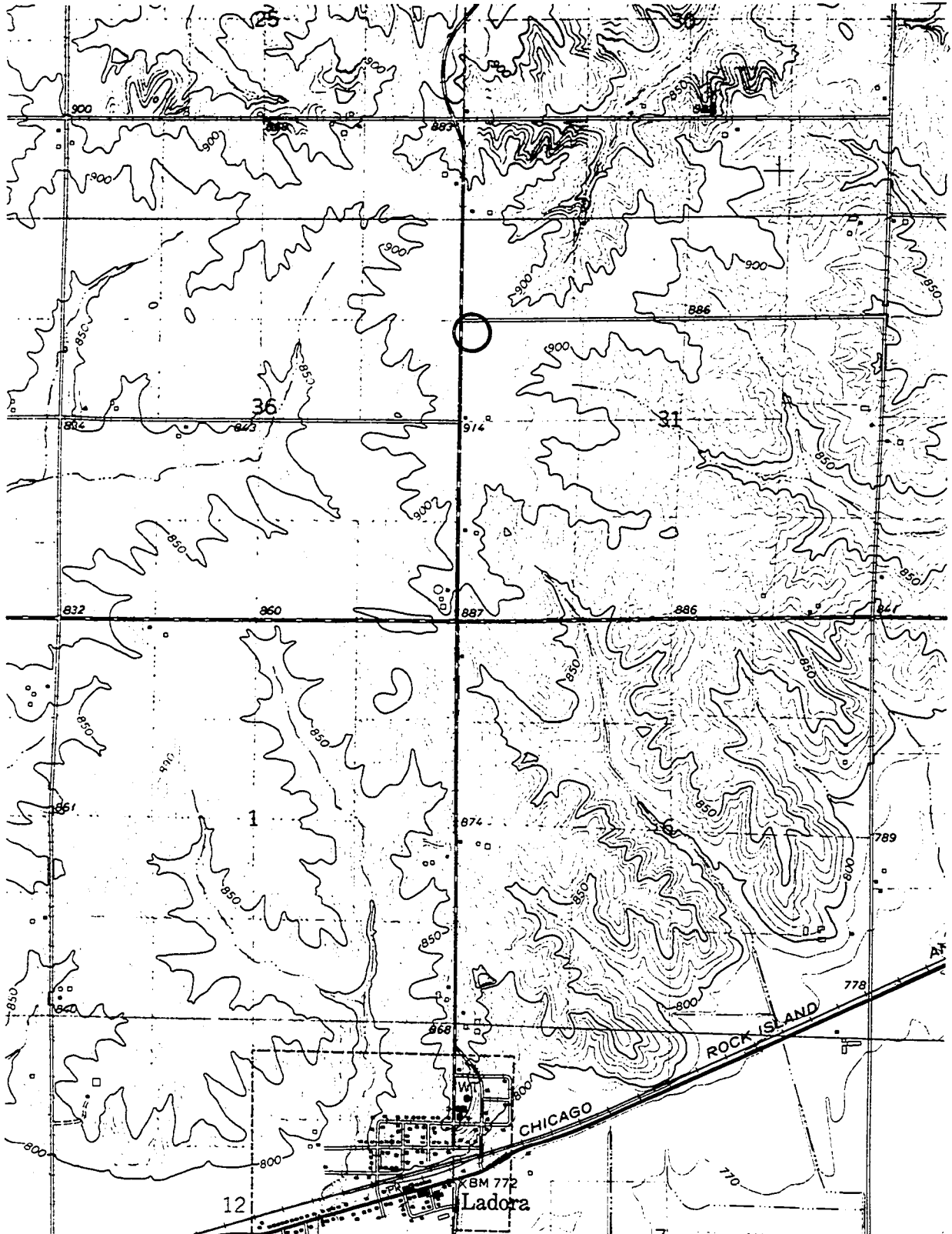
SITE: 14-LH
QUADRANGLE: MARENGO, IA.
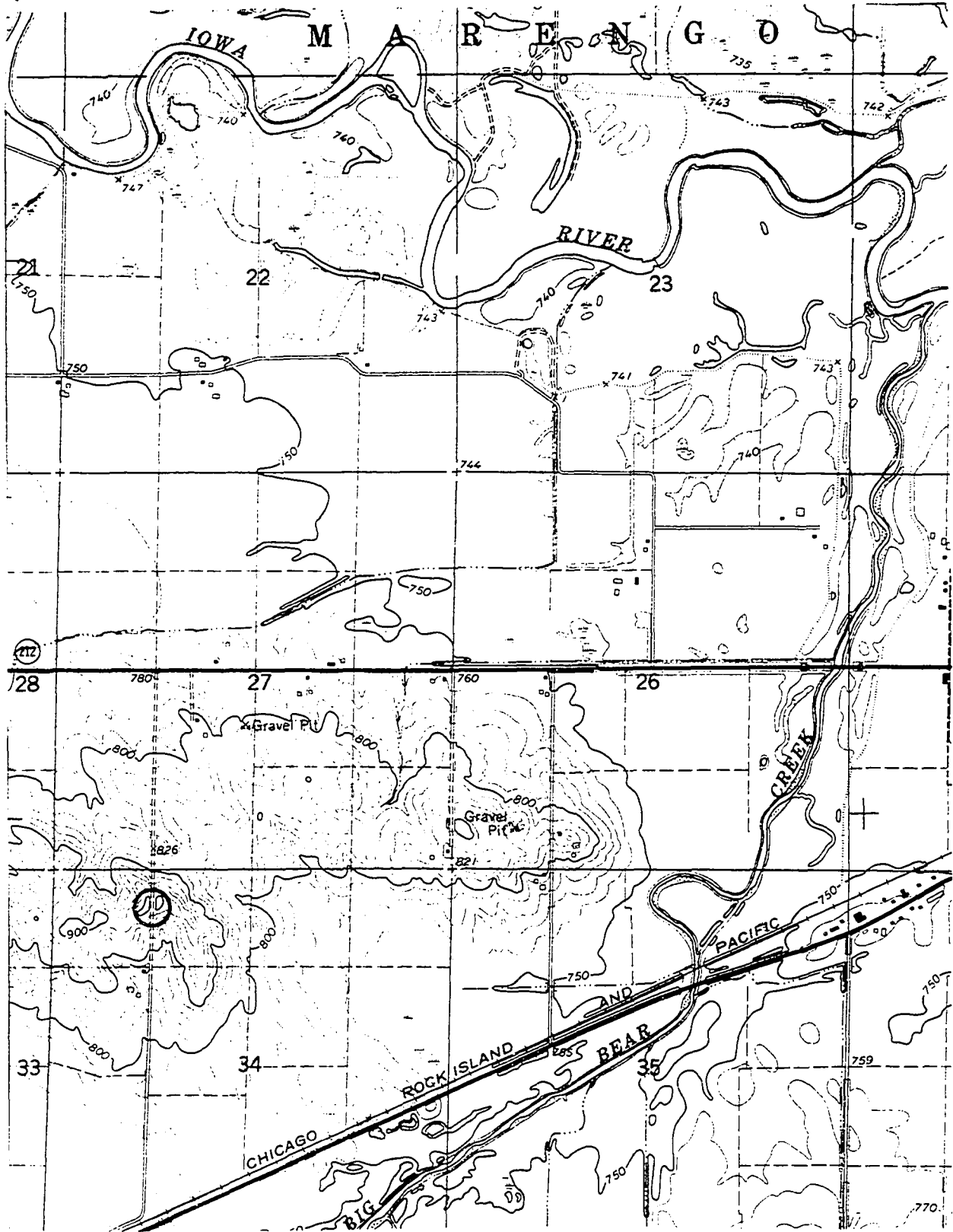
SITE: 15-LH
QUADRANGLE: LADORA, IA.

319
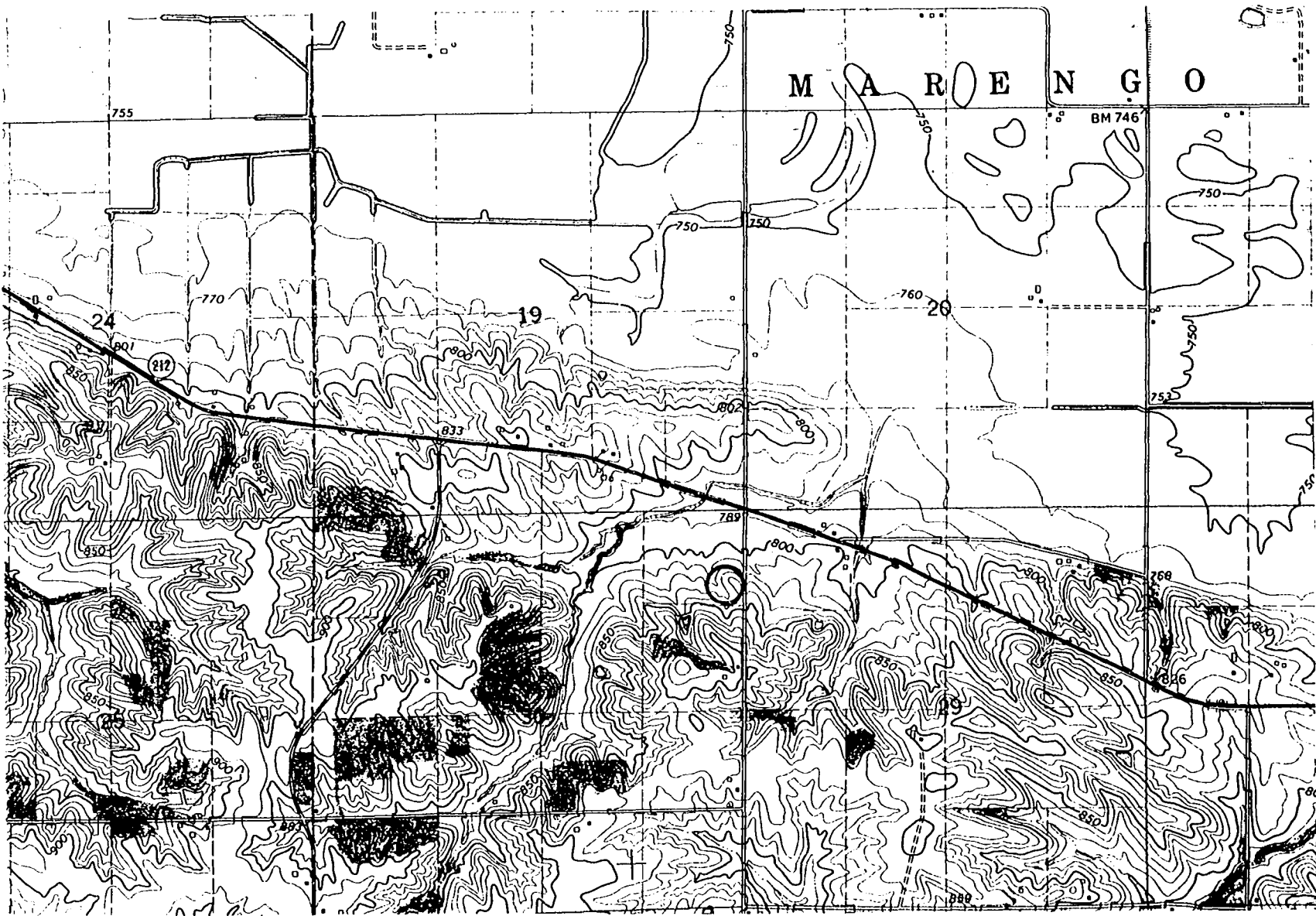
SITE: 16-LH
QUADRANGLE: MARENGO, IA.
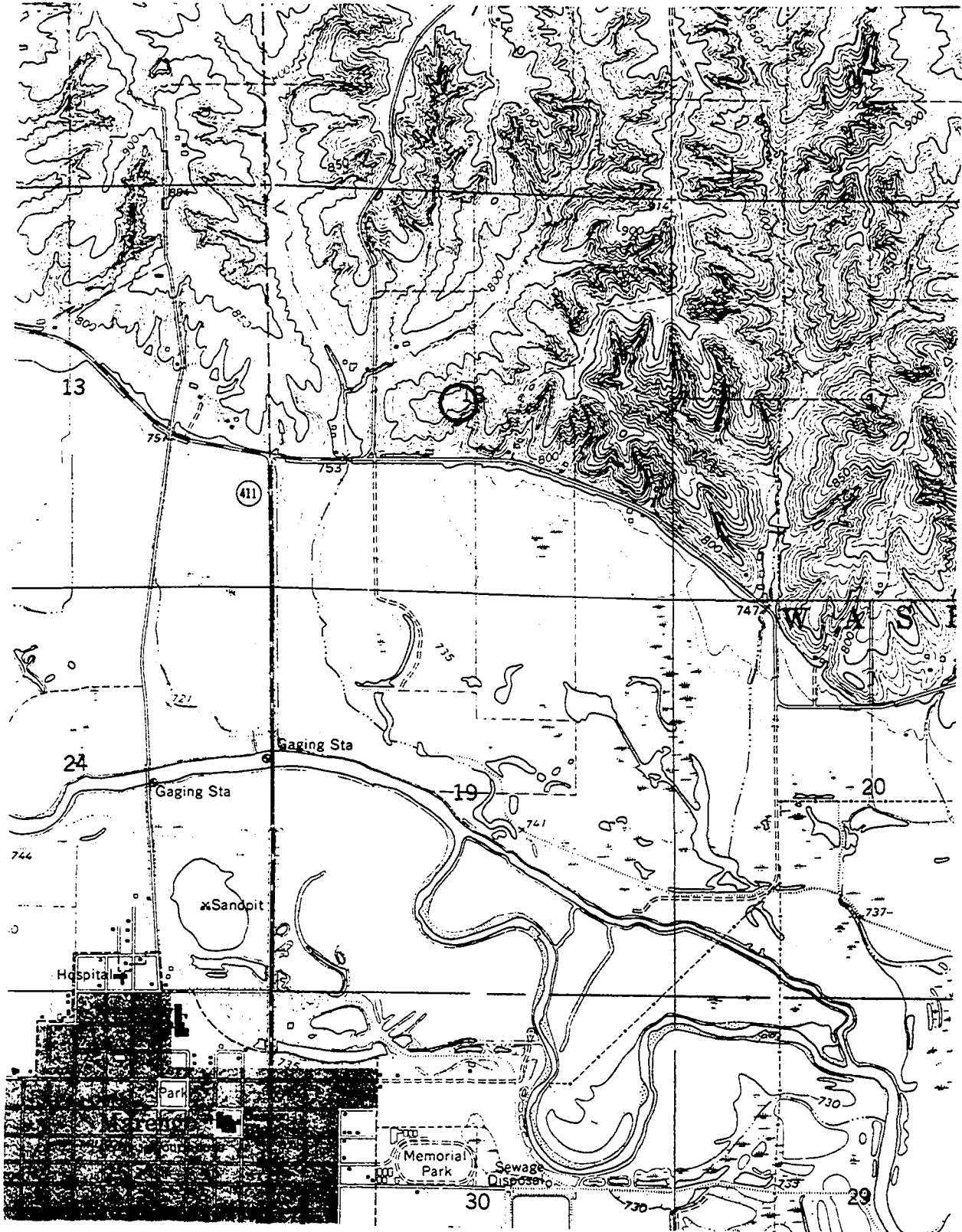
SITE: 17-LH
QUADRANGLE: MIDDLE AMANA, IA.
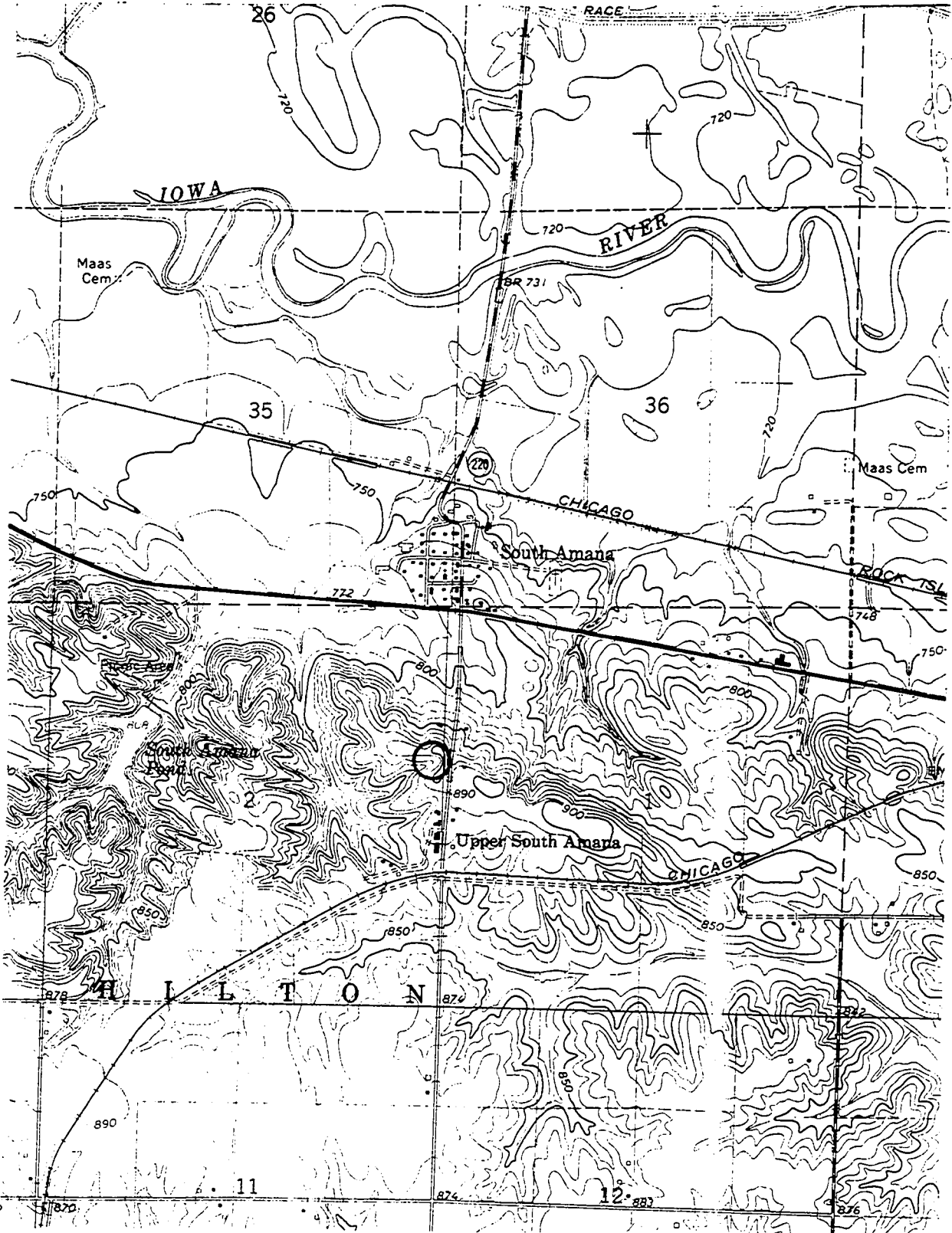
SITE: 18-LH
QUADRANGLE: OXFORD, IA.
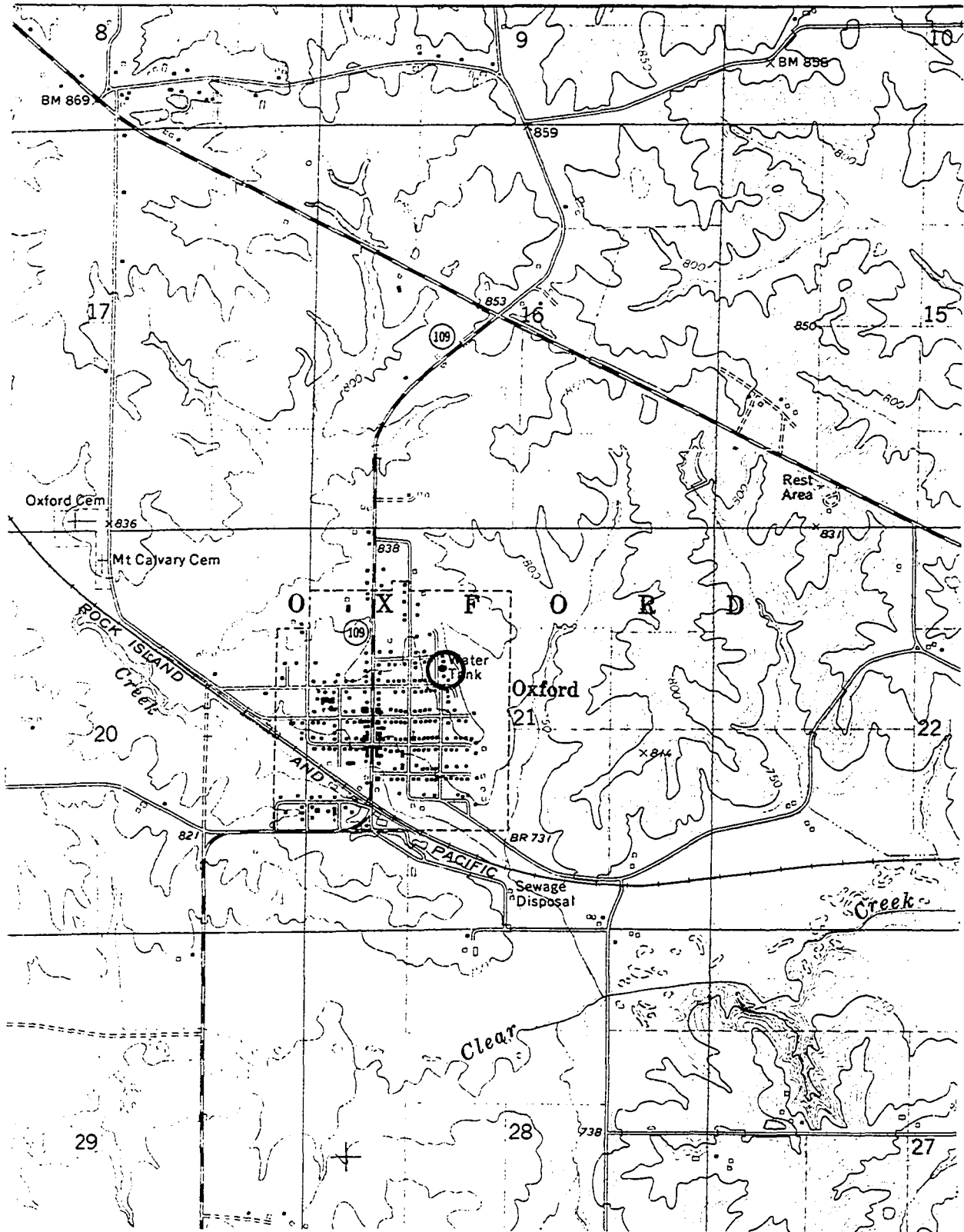
APPENDIX C: PARTICLE SIZE DATA

Sample	Depth		Particle Size Distribution (Percent)				
	in.	cm	>74 μm	74-20 μm	20-2 μm	<2 μm	<1 μm
1-MW-1	60	152.4	0.4	53.3	24.9	21.4	17.7
-2	78	198.1	1.4	53.4	28.1	17.1	14.4
-3	88	223.5	0.9	54.8	28.7	15.6	13.9
-4	110	279.4	0.4	51.2	29.7	18.7	16.3
-5	136	345.4	0.2	55.0	29.5	15.3	13.8
-6	160	406.4	0.3	51.3	28.9	19.5	17.6
-7	184	467.4	0.7	46.4	29.9	23.0	19.9
-8	210	533.4	0.4	47.3	32.5	19.8	17.9
-9	220	558.8	0.8	50.8	28.3	20.1	18.4
-10	244	619.8	0.4	47.9	33.3	18.4	16.3
-11	268	680.7	0.4	49.5	29.7	20.4	17.8
-12	288	731.5	0.3	43.0	33.3	23.4	20.5
-13	292	741.7	1.0	50.0	28.8	20.2	18.1
-14	316	802.6	2.3	52.7	27.4	17.6	15.3
-15	340	863.6	4.0	51.0	25.3	19.7	17.2
-16	364	924.6	4.2	36.3	20.9	38.6	38.6
-17	386	980.4	11.8	35.7	18.7	33.8	31.9
2-MW-1	60	152.4	0.4	44.7	31.4	23.5	20.4
-2	84	213.4	0.4	51.1	28.9	19.6	17.1
-3	108	274.3	0.3	41.8	37.2	20.7	17.8
-4	134	340.4	0.4	53.3	29.7	16.6	15.0
-5	168	426.7	0.5	47.8	35.3	16.4	15.2
-6	192	487.7	0.8	45.2	36.2	17.8	14.4
-7	218	553.7	0.6	53.9	27.6	17.9	15.1
-8	244	619.8	0.9	50.5	30.1	18.5	16.3
-9	254	645.2	1.3	50.7	26.6	21.4	18.9
-10	264	670.6	1.0	47.1	24.0	27.9	26.3

324

Sample	Depth		Particle Size Distribution (Percent)				
	in.	cm	>74 µm	74-20 µm	20-2 µm	<2 µm	<1 µm
2-MW-11	276	701.0	0.8	45.0	23.3	30.9	29.7
-12	288	731.5	0.8	42.8	24.8	31.6	29.5
3-MW-1	60	152.4	0.7	37.4	37.4	24.5	20.9
-2	84	213.4	0.7	43.9	34.8	20.6	18.7
-3	108	274.3	0.4	45.2	33.5	20.9	18.4
-4	132	335.3	2.1	46.2	32.6	19.1	16.5
-5	153	388.6	1.4	39.6	24.7	34.3	32.1
-6	166	421.6	1.5	35.2	22.1	41.2	40.0
-7	179	454.7	1.3	33.7	20.8	44.2	42.3
-8	198	502.9	1.5	35.1	24.5	38.9	36.3
4-MW-1	60	152.4	0.3	50.8	32.1	16.8	13.4
-2	84	213.4	2.1	55.9	27.7	14.3	10.1
-3	112	284.5	0.3	52.9	30.8	16.0	11.4
-4	136	345.4	0.6	51.7	32.0	15.7	13.4
-5	159	403.9	0.4	56.7	28.1	14.8	11.8
-6	185	469.9	0.3	57.3	29.1	13.3	11.6
-7	210	533.4	0.5	48.2	36.6	14.7	10.9
-8	234	594.4	0.4	51.3	31.2	17.1	14.9
-9	258	655.3	1.2	55.3	28.1	15.4	13.9
-10	282	716.3	0.4	57.7	27.8	14.1	13.5
-11	306	777.2	0.4	54.4	30.3	14.9	13.8
-12	330	838.2	0.5	59.4	25.1	15.0	12.0
-13	354	899.2	3.5	53.6	28.0	14.9	13.4
-14	376	955.0	0.9	56.0	26.6	16.5	14.1
-15	421	1069.3	3.4	56.4	24.6	15.6	13.0
-16	447	1135.4	8.0	44.6	19.1	28.3	26.2
-17	459	1165.9	9.5	29.6	15.0	45.9	44.2

Sample	Depth		Particle Size Distribution (Percent)				
	in.	cm	>74µm	74-20µm	20-2µm	<2µm	<1µm
5-MW-1	61	154.9	0.4	42.7	32.4	24.5	18.4
-2	86	218.4	0.4	48.7	33.7	17.2	15.3
-3	109	276.9	0.4	48.7	31.6	19.3	17.2
-4	136	345.4	0.6	48.8	32.6	18.0	15.9
-5	161	408.9	1.1	51.0	31.2	16.7	13.4
-6	170	431.8	1.4	53.9	29.3	15.4	12.5
-7	186	472.4	2.0	51.3	29.3	17.4	15.4
-8	198	502.9	1.4	48.4	25.9	24.3	20.6
-9	207	525.8	1.7	47.7	25.1	25.5	24.3
-10	220	558.8	0.7	35.2	17.0	47.1	46.4
6-MW-1	61	154.9	0.8	32.4	39.1	27.7	24.2
-2	89	226.1	0.9	34.2	39.3	25.6	21.6
-3	109	276.9	1.8	40.8	30.3	27.1	24.8
-4	110	279.4	0.2	35.6	24.5	39.7	37.9
-5	120	304.8	1.9	27.7	21.8	48.6	47.2
7-MW-1	61	154.9	0.6	40.4	36.1	22.9	19.6
-2	85	215.9	1.3	48.9	31.9	17.9	15.4
-3	102	259.1	1.8	49.3	32.6	16.3	13.2
-4	124	315.0	1.3	47.2	22.8	28.7	24.2
-5	132	335.3	1.0	37.1	17.4	44.5	43.4
-6	149	378.5	0.9	38.1	22.5	38.5	35.7
8-MW-1	60	152.4	0.3	36.5	38.7	24.5	19.7
-2	84	213.4	0.2	40.4	36.9	22.5	18.2
-3	108	274.3	0.3	45.1	35.4	19.2	16.0
-4	132	335.3	0.4	45.8	36.7	17.1	13.8
-5	144	365.8	0.4	45.7	35.3	18.6	15.6

Sample	Depth		Particle Size Distribution (Percent)				
	in.	cm	>74μm	74-20μm	20-2μm	<2μm	<1μm
8-MW-6	156	396.2	0.4	48.9	32.8	17.9	16.1
-7	180	457.2	0.8	55.5	27.0	16.7	15.3
-8	204	518.2	1.1	52.3	27.1	19.5	16.3
-9	228	579.1	2.1	53.0	28.6	16.3	13.7
-10	252	640.1	3.0	54.3	25.5	17.2	15.2
-11	260	660.4	1.9	45.3	22.7	30.1	28.8
-12	276	701.0	2.0	48.6	23.1	26.3	24.9
9-MW-1	56	142.2	0.5	28.8	37.1	33.6	30.4
-2	71	180.3	0.7	32.8	39.5	27.0	23.3
-3	95	241.3	9.0	41.6	29.8	19.6	16.0
-4	103	261.6	10.4	53.1	16.4	20.1	18.7
-5	121	307.3	11.0	39.8	25.9	23.3	19.0
-6	141	358.1	11.2	35.6	22.4	30.8	29.8
10-MW-1	46	116.8	1.6	30.3	38.5	29.6	26.6
-2	66	167.6	12.3	38.2	31.0	18.5	16.1
-3	82	208.3	19.1	38.0	25.9	17.0	15.4
-4	97	246.4	19.3	27.9	20.1	32.7	30.5
11-MW-1	60	154.4	0.8	41.5	32.6	25.1	21.9
-2	84	213.4	0.6	43.5	36.7	19.2	17.2
-3	108	274.3	1.5	51.7	29.6	17.2	15.4
-4	132	335.3	1.7	49.4	28.0	20.9	19.0
-5	156	396.2	1.9	53.4	27.6	17.1	14.9
-6	162	411.5	1.4	47.6	22.9	28.1	26.6
-7	165	419.1	0.7	37.1	15.5	46.7	44.5

327

Sample	Depth		Particle Size Distribution (Percent)				
	in.	cm	>74μm	74-20μm	20-2μm	<2μm	<1μm
12-MW-1	29	73.7	0.8	28.8	40.7	29.7	26.0
-2	37	93.9	0.7	26.6	44.9	27.8	23.6
-3	49	124.5	3.2	40.4	39.8	16.6	11.2
-4	66	167.6	1.4	18.4	30.6	49.6	45.8

Sample	Depth		Particle Size Distribution (Percent)				
	in.	cm	>74μm	74-20μm	20-2μm	<2μm	<1μm
1-ME-1	49	124.5	3.7	27.8	34.3	34.2	31.0
-2	57	144.8	4.4	25.8	38.7	31.1	27.7
-3	61	154.9	0.3	28.6	37.6	33.5	30.8
-4	69	175.3	0.4	32.2	36.4	31.0	28.8
-5	77	195.6	2.7	31.0	34.6	31.7	28.3
-6	80	203.2	2.3	30.8	31.6	35.3	32.2
-7	86	218.4	3.6	29.8	30.4	36.2	34.3
-8	97	246.4	6.6	30.4	28.7	34.3	32.3
-9	133	337.8	8.5	31.0	29.2	31.3	29.5
2-ME-1	20	50.8	2.9	35.4	40.8	20.9	16.5
-2	24	61.0	1.2	20.1	29.6	49.1	46.4
-3	27	68.6	0.9	18.8	32.3	48.0	44.7
-4	30	76.2	0.9	17.3	26.6	55.2	52.0
-5	36	91.4	2.0	23.5	40.6	33.9	30.2
-6	42	106.7	4.5	24.2	41.9	29.4	26.2
-7	48	121.9	10.3	27.5	38.7	23.5	20.5
-8	52	132.1	12.5	27.1	38.7	21.7	18.4
-9	56	142.2	17.4	26.6	34.2	21.8	17.7
-10	60	152.4	18.4	27.1	33.0	21.5	18.2
-11	64	162.6	17.8	27.1	31.9	23.2	19.8
3-ME-1	7	17.8	3.3	41.4	43.2	12.1	8.9
-2	12	30.5	2.1	30.3	38.0	29.6	26.3
-3	16	40.6	1.4	21.1	32.1	45.4	41.8
-4	24	61.0	1.3	21.2	33.5	44.0	41.4
-5	32	81.3	3.5	25.9	42.4	28.2	24.7
-6	42	106.7	10.0	36.2	38.6	15.2	12.6
-7	46	116.8	11.3	31.4	40.5	16.8	13.1
-8	50	127.0	12.9	34.5	36.4	16.2	13.2

Sample	Depth		Particle Size Distribution (Percent)				
	in.	cm	>74μm	74-20μm	20-2μm	<2μm	<1μm
4-ME-1	10	25.4	6.8	36.6	40.8	15.8	13.7
-2	16	40.6	1.2	16.1	27.2	55.5	52.1
-3	20	50.8	0.6	12.8	19.0	67.6	64.7
-4	24	61.0	0.5	10.8	27.0	61.7	58.9
-5	30	76.2	1.9	21.9	40.2	36.0	32.2
-6	36	91.4	4.6	27.5	40.9	27.0	24.5
-7	40	101.6	4.2	26.6	45.0	24.2	21.0
-8	48	121.9	7.8	34.3	42.3	15.6	12.5
-9	60	152.4	2.7	21.5	25.4	50.4	48.4
-10	64	162.6	2.1	17.3	16.7	63.9	62.2
-11	70	177.8	3.7	17.1	17.4	61.8	61.8
-12	76	193.0	4.2	13.3	17.5	65.0	64.5
-13	82	208.3	6.3	18.8	22.5	52.4	51.7
-14	88	223.5	8.4	20.0	24.7	46.9	44.4
5-ME-1	16	40.6	2.7	27.7	34.8	34.8	31.9
-2	20	50.8	1.8	19.3	34.4	44.5	40.3
-3	28	71.1	3.2	20.1	40.3	36.4	32.0
-4	34	86.4	5.7	28.2	42.2	23.9	19.5
-5	40	101.6	6.2	24.2	38.7	30.9	26.3
-6	42	106.7	1.8	3.0	12.4	82.8	77.3
-7	48	121.9	1.3	5.8	16.8	76.1	71.4
-8	54	137.2	1.3	0.9	8.8	89.0	83.6
6-ME-1	12	30.5	2.4	35.6	33.2	28.8	24.8
-2	20	50.8	1.3	25.0	30.3	43.4	38.8
-3	32	81.3	1.1	30.6	31.6	36.7	33.8
-4	40	101.6	1.4	31.8	36.9	29.9	27.5

Sample	Depth		Particle Size Distribution (Percent)				
	in.	cm	>74μm	74-20μm	20-2μm	<2μm	<1μm
6-ME-5	48	121.9	1.1	37.5	38.7	22.7	19.3
-6	60	152.4	2.0	43.2	37.4	17.4	14.5
-7	72	182.9	3.3	54.1	24.2	18.4	16.2
-8	76	193.0	3.3	45.8	32.3	18.6	15.7
-9	82	208.3	1.5	30.5	25.8	42.2	40.2
-10	84	213.4	1.6	29.3	21.2	47.9	46.3
-11	88	223.5	1.4	23.1	16.7	58.8	57.3
-12	94	238.8	1.1	21.8	18.0	59.1	58.1
7-ME-1	4	10.2	2.9	49.0	34.5	13.6	12.9
-2	12	30.5	1.4	25.3	26.4	46.9	42.5
-3	18	45.7	1.1	27.7	31.4	39.8	35.8
-4	24	61.0	0.8	30.3	32.7	36.2	32.5
-5	42	106.7	0.4	33.2	37.0	29.4	25.9
-6	60	152.4	0.5	33.2	42.0	24.3	21.4
-7	69	175.3	2.3	34.2	38.6	24.9	21.3
-8	72	182.9	5.2	38.0	35.9	20.9	17.9
-9	78	198.1	8.0	41.1	31.8	19.1	16.2
-10	96	243.8	9.4	37.7	28.3	24.6	23.7
-11	106	269.2	8.3	34.4	23.4	33.9	32.0
-12	114	239.6	10.2	33.6	30.1	26.1	17.5
-13	124	315.0	10.6	22.7	20.4	46.3	45.8
-14	132	335.3	21.4	21.6	19.2	37.8	34.9
-15	140	355.6	21.5	20.1	19.2	39.2	36.4
-16	148	375.9	21.9	21.3	19.3	37.5	35.3

Sample	Depth		Particle Size Distribution (Percent)				
	in.	cm	>74 μm	74-20 μm	20-2 μm	<2 μm	<1 μm
8-ME-1	10	25.4	0.7	24.1	33.1	42.1	38.1
-2	28	71.1	7.1	30.8	36.7	25.4	21.6
-3	40	101.6	20.3	32.6	28.4	18.7	14.8
-4	51	129.5	30.0	18.6	16.7	34.7	31.1
-5	58	147.3	27.1	16.2	18.4	38.3	34.2
-6	69	175.3	28.6	17.3	19.4	34.7	31.7
-7	99	251.5	24.0	23.4	26.1	26.5	22.4
-8	-	-	14.5	20.2	36.2	29.1	24.6
-9	-	-	25.6	24.2	28.3	21.9	17.2
9-ME-1	4	10.2	12.7	31.3	40.0	16.0	12.6
-2	12	30.5	14.1	25.2	26.7	34.0	32.2
-3	22	55.9	14.2	24.7	26.2	34.9	31.9
-4	26	66.0	17.7	26.7	26.3	29.3	26.5
-5	34	86.4	16.0	26.4	21.8	35.8	32.5
-6	41	104.1	13.3	21.5	19.7	45.5	42.7
-7	48	121.9	14.1	19.0	17.3	49.6	47.2
-8	56	142.2	15.7	17.2	18.6	48.5	45.0
-9	75	190.5	20.4	24.0	24.9	30.7	26.5
10-ME-1	4	10.2	5.3	32.9	42.5	19.3	15.6
-2	12	30.5	1.7	27.1	40.5	30.7	27.6
-3	18	45.7	0.4	19.4	29.8	50.4	46.6
-4	28	71.1	0.5	19.6	35.3	44.6	41.0
-5	32	81.3	1.2	21.9	40.8	36.1	33.2
-6	36	91.4	1.6	24.1	42.8	31.5	27.4
-7	44	111.8	4.4	32.4	43.1	20.1	17.1
-8	64	162.6	2.1	17.4	16.8	63.7	62.1

Sample	Depth		Particle Size Distribution (Percent)				
	in.	cm	>74μm	74-20μm	20-2μm	<2μm	<1μm
11-ME-1	8	20.3	2.2	57.4	24.8	15.6	13.0
-2	22	55.9	1.9	43.2	21.1	33.8	30.4
-3	36	91.4	1.8	45.4	22.3	30.5	28.3
-4	50	127.0	1.8	45.4	25.9	26.9	26.0
-5	60	152.4	1.9	46.9	26.8	24.4	22.3
-6	69	175.3	2.7	50.4	26.1	20.8	19.5
-7	78	198.1	2.3	58.3	20.9	18.5	15.7
-8	96	243.8	3.7	54.6	24.2	17.5	15.8
-9	114	289.6	3.8	52.4	28.9	14.9	13.4
-10	132	335.3	3.2	51.1	27.0	18.7	16.8
-11	150	381.0	4.1	56.0	24.2	15.7	14.3
-12	168	426.7	3.3	54.3	23.4	19.0	17.5
-13	176	447.0	2.6	52.0	23.0	22.4	20.5
-14	186	472.4	3.3	53.3	23.5	19.9	17.9
-15	194	492.8	3.1	52.5	21.4	23.0	21.0
-16	200	508.0	3.0	47.6	24.1	25.3	22.4
-17	208	528.3	1.7	28.2	26.7	43.4	37.7
12-ME-1	22	55.9	0.6	15.7	25.1	58.6	56.3
-2	36	91.4	0.6	23.2	44.4	31.8	28.0
-3	48	121.9	1.6	29.9	43.6	23.9	20.6
-4	56	142.2	2.5	38.5	38.6	20.4	18.2
-5	64	162.6	3.1	37.0	37.1	22.8	19.8
-6	76	193.0	3.1	29.3	23.2	44.4	41.4
13-ME-1	60	152.4	0.5	61.4	26.8	11.3	11.2
-2	84	213.4	1.7	63.8	26.2	8.3	8.2
-3	108	274.3	0.9	67.6	21.8	9.7	9.6
-4	132	335.3	0.3	49.4	38.4	11.9	11.8

Sample	Depth		Particle Size Distribution (Percent)				
	in.	cm	>74μm	74-20μm	20-2μm	<2μm	<1μm
13-ME-5	156	396.2	0.8	40.1	40.8	18.3	16.4
-6	179	454.7	30.7	22.5	25.9	20.9	18.0
-7	188	477.5	23.6	13.0	11.4	52.0	50.3
-8	194	492.8	19.8	18.6	12.7	48.9	47.5
-9	204	518.2	28.7	16.1	14.6	40.6	38.1
-10	212	538.5	25.8	23.6	16.6	34.0	31.6

Sample	Depth		Particle Size Distribution (Percent)				
	in.	cm	>74 μm	74-20 μm	20-2 μm	<2 μm	<1 μm
1-LH-1	77	195.6	0.3	44.7	28.3	26.7	23.8
-2	107	271.8	1.2	47.9	26.8	24.1	21.1
-3	130	330.2	0.6	47.2	30.6	21.6	17.8
-4	138	350.5	0.4	47.8	31.5	20.3	17.2
-5	148	375.9	0.3	48.5	31.8	19.4	16.2
-6	160	406.4	1.0	45.9	34.2	18.9	15.2
-7	173	439.4	0.5	49.4	31.6	18.5	16.8
-8	207	525.8	0.4	26.9	48.7	24.0	19.5
-9	225	571.5	2.3	16.6	41.8	39.2	35.7
-10	227	576.6	1.7	15.9	35.1	47.3	41.5
-11	236	599.4	1.5	9.6	18.7	70.2	64.8
2-LH-1	73	185.4	0.4	42.4	28.1	29.1	25.4
-2	83	210.8	0.4	37.9	34.0	27.7	24.1
-3	96	243.8	0.3	41.4	29.3	29.0	26.0
-4	122	309.8	0.6	47.7	29.9	21.8	20.4
-5	140	355.6	0.7	51.5	24.4	23.4	22.4
-6	163	414.0	0.6	52.9	26.4	20.1	19.4
-7	198	502.9	0.5	55.4	25.5	18.6	15.4
-8	208	528.3	0.5	54.8	26.9	17.8	16.1
-9	219	556.2	0.4	60.6	19.7	19.3	18.4
-10	238	604.5	0.3	40.8	39.2	19.7	17.4
-11	268	680.7	2.0	16.2	52.8	29.0	25.0
-12	277	703.5	15.3	18.7	34.4	31.6	27.4
-13	287	728.9	12.9	5.8	12.7	68.6	59.1

Sample	Depth		Particle Size Distribution (Percent)				
	in.	cm	>74 μm	74-20 μm	20-2 μm	<2 μm	<1 μm
3-LH-1	64	162.6	0.6	40.2	33.1	26.1	22.7
-2	88	223.5	0.8	46.2	29.2	23.8	20.6
-3	110	274.4	0.8	47.9	31.2	20.1	17.3
-4	133	337.8	0.4	46.9	32.5	20.2	17.2
-5	158	401.3	0.4	39.9	36.9	22.8	19.6
-6	180	457.2	0.9	22.6	52.6	23.9	21.0
-7	186	472.4	2.9	24.0	52.6	20.5	15.8
-8	190	482.6	3.2	23.8	52.4	20.6	15.9
-9	195	495.3	3.4	25.1	51.7	19.8	15.9
4-LH-1	76	193.0	0.6	37.8	33.9	27.7	24.2
-2	101	256.5	0.6	41.9	33.4	24.1	21.3
-3	128	325.1	0.5	30.3	43.4	25.8	21.6
-4	151	383.5	5.4	20.8	43.7	30.1	24.9
-5	158	401.3	3.4	14.5	29.8	52.2	42.9
5-LH-1	76	193.0	0.2	35.6	37.4	26.8	24.4
-2	100	254.0	0.3	41.3	33.7	24.7	20.1
-3	124	315.0	0.3	36.2	40.0	23.5	18.8
-4	148	376.0	2.7	21.2	49.5	26.6	22.4
-5	166	421.7	1.9	20.8	42.7	34.6	28.4
-6	174	442.0	1.5	15.0	30.0	54.6	49.2
6-LH-1	72	182.9	0.5	39.2	30.2	30.1	25.6
-2	96	243.8	0.5	44.2	29.7	25.6	21.9
-3	120	304.8	1.4	49.0	28.0	21.6	19.4
-4	144	365.8	1.2	44.5	31.3	23.0	18.8
-5	166	421.6	1.4	44.6	32.9	19.7	18.1
-6	193	490.2	0.5	55.1	25.0	14.4	17.1
-7	205	520.7	0.5	44.7	32.5	22.3	18.5

Sample	Depth		Particle Size Distribution (Percent)				
	in.	cm	>74μm	74-20μm	20-2μm	<2μm	<1μm
6-LH-8	228	579.1	0.5	29.0	46.7	23.8	19.0
-9	240	609.6	1.0	25.4	48.7	24.9	21.4
-10	249	632.5	4.6	19.7	38.3	37.3	31.5
7-LH-1	75	190.5	0.2	35.9	40.4	23.5	19.1
-2	103	261.6	0.4	35.6	40.9	23.1	19.4
-3	125	317.5	2.0	19.8	46.6	31.6	26.2
-4	139	353.1	1.0	18.7	41.2	39.1	24.9
-5	156	296.2	1.8	14.1	28.5	55.6	48.2
8-LH-1	70	177.8	0.7	32.6	39.5	27.2	23.6
-2	92	233.7	0.6	41.0	40.8	17.6	11.7
-3	112	284.5	0.2	36.7	41.1	22.0	19.4
-4	126	320.0	0.7	18.5	50.2	30.6	26.1
-5	142	360.7	4.0	17.0	36.9	42.0	36.2
-6	150	381.0	3.0	19.3	37.5	40.1	35.4
-7	162	411.5	2.5	17.3	41.4	38.9	32.1
-8	172	436.9	2.3	15.6	39.0	43.1	39.2
-9	184	467.4	2.6	16.4	34.3	46.6	43.1
-10	196	497.8	6.0	14.4	31.0	48.6	45.6
9-LH-1	60	152.4	0.4	45.1	28.0	26.5	24.6
-2	72	182.9	0.4	45.3	29.4	24.9	22.8
-3	96	243.8	0.4	52.4	28.9	18.3	15.5
-4	120	304.8	0.4	55.9	29.0	14.7	12.2
-5	144	365.8	0.6	54.2	29.2	16.0	14.5
-6	168	426.7	0.5	54.2	30.1	15.2	13.5
-7	192	487.7	0.4	57.3	27.5	14.8	13.2
-8	216	548.6	0.4	43.0	30.5	20.1	19.3

Sample	Depth		Particle Size Distribution (Percent)				
	in.	cm	>74 μm	74-20 μm	20-2 μm	<2 μm	<1 μm
9-LH-9	230	584.2	0.5	27.1	50.0	22.4	20.2
-10	233	591.8	0.4	29.5	51.9	18.2	16.4
-11	241	612.1	3.1	19.0	53.5	24.1	21.2
-12	248	628.6	14.9	21.7	41.8	21.6	16.9
-13	256	643.9	19.5	20.3	41.2	19.0	14.7
-14	272	690.9	22.3	13.3	11.3	53.1	51.1
10-LH-1	77	195.6	0.5	39.7	29.9	29.9	26.7
-2	106	269.2	2.0	49.2	25.2	23.6	21.3
-3	113	287.0	0.9	45.1	26.9	27.1	24.5
-4	123	312.4	1.3	52.5	23.6	22.6	20.5
-5	142	360.7	1.7	52.3	23.3	22.7	20.6
-6	160	406.4	1.9	55.9	23.2	19.0	16.8
-7	170	431.8	2.6	61.0	21.3	15.1	13.1
-8	190	482.6	2.8	47.6	31.2	18.4	16.5
-9	220	558.8	6.5	52.5	23.6	17.4	15.8
-10	246	624.8	4.9	55.1	23.0	17.0	15.4
-11	260	660.4	6.3	57.1	20.7	15.9	14.7
-12	286	727.4	4.2	52.1	25.3	18.4	17.1
-13	310	787.4	3.4	50.2	27.6	18.8	16.7
-14	325	825.5	2.2	57.3	24.8	15.7	14.8
11-LH-1	180	457.2	3.0	53.8	27.2	16.0	13.0
-2	198	502.9	0.5	40.7	30.3	28.5	25.7
-3	222	563.9	0.8	46.0	28.8	24.4	22.7
-4	229	581.7	22.1	38.0	17.7	22.2	20.1
-5	288	731.5	86.3	5.1	1.5	7.1	6.6
-6	312	792.5	80.9	6.4	0.8	11.9	11.4
-7	318	807.7	21.0	46.4	16.5	16.1	14.9
-8	342	868.7	1.8	52.2	33.6	12.4	9.0
-9	352	894.1	13.2	47.5	26.1	13.2	10.0

| Sample | Depth | | Particle Size Distribution (Percent) | | | | |
	in.	cm	>74μm	74-20μm	20-2μm	<2μm	<1μm
12-LH-1	30	76.2	1.7	33.2	29.1	36.0	33.0
-2	42	106.7	1.2	48.3	27.5	23.0	20.5
-3	53	134.6	1.5	39.6	30.5	28.4	25.8
-4	68	172.7	0.6	45.2	29.4	24.8	23.0
-5	83	210.8	0.7	51.7	26.0	21.6	19.5
-6	95	241.3	1.3	51.5	25.3	21.9	19.7
-7	114	289.6	1.5	56.8	25.8	15.9	14.0
-8	139	353.1	0.5	52.7	31.0	15.8	15.0
-9	160	406.4	0.9	53.3	27.5	18.3	18.1
-10	163	414.0	0.8	55.1	27.8	16.3	14.3
-11	180	457.2	0.8	55.6	26.9	16.7	15.1
-12	190	482.6	1.2	51.7	28.3	18.8	17.2
-13	195	495.3	0.3	50.2	30.4	19.1	17.2
-14	203	515.6	4.7	40.3	37.8	17.2	15.9
-15	249	632.5	4.3	26.9	48.3	20.5	16.7
-16	252	640.1	4.1	28.9	47.7	19.3	15.4
-17	262	665.5	2.1	22.1	40.1	35.7	31.7
-18	275	698.5	2.5	17.5	22.5	57.5	56.1
14-LH-1	28	71.1	2.7	46.7	25.8	24.8	23.3
-2	48	50.5	9.3	53.3	21.7	15.7	14.4
-3	60	152.4	11.9	55.1	18.0	15.0	12.8
-4	80	203.2	15.0	57.0	15.7	12.3	9.1
-5	96	243.8	18.0	53.8	16.2	12.0	11.1
-6	120	304.8	13.3	54.3	15.8	16.6	14.8
-7	150	381.0	21.3	53.2	13.8	11.7	10.7
-8	180	457.2	11.1	63.3	13.6	12.1	12.0

Sample	Depth		Particle Size Distribution (Percent)				
	in.	cm	<74 μm	74-20 μm	20-2 μm	<2 μm	<1 μm
15-LH-1	-	-	73.5	14.9	3.8	7.8	5.1
-2	-	-	52.0	30.6	6.9	10.5	10.3
-3	-	-	42.0	32.4	10.3	15.3	14.2
16-LH-1	60	152.4	0.6	47.8	26.1	25.5	25.1
-2	84	213.4	0.6	45.3	31.5	22.6	20.1
-3	108	274.3	0.8	55.0	27.3	16.9	15.3
-4	132	335.3	0.6	53.3	29.0	17.1	15.4
-5	156	396.2	0.4	51.1	31.0	17.5	17.2
-6	180	457.2	0.4	34.1	45.2	20.3	18.2
-7	204	518.2	1.4	25.7	52.6	20.3	17.5
-8	228	579.1	0.5	52.9	29.3	17.3	16.6
-9	252	640.1	0.4	45.3	34.2	20.1	17.8
17-LH-1	30	76.2	83.9	6.8	4.8	4.5	4.1
-2	57	144.8	30.7	30.7	18.0	20.6	18.6
-3	75	190.5	3.3	51.8	23.2	21.7	20.1
-4	93	236.2	4.0	52.0	24.4	19.6	17.7
-5	111	281.9	4.2	53.1	25.3	17.4	15.5
-6	129	327.7	2.9	58.9	20.7	17.5	15.6
-7	146	370.8	1.9	58.1	23.8	16.2	14.1
-8	164	416.6	2.5	56.8	24.2	16.5	14.1
-9	214	543.6	2.7	58.1	24.7	14.5	12.7
-10	264	670.6	7.9	59.0	19.6	13.5	13.3
-11	276	701.0	7.7	59.0	19.2	14.1	12.4
-12	287	729.0	5.9	60.9	19.2	14.0	12.9
-13	299	759.5	10.2	69.7	15.8	13.3	12.5
-14	312	792.5	8.8	60.5	18.0	12.7	11.7
-15	324	823.0	12.4	58.3	15.9	13.4	12.2
-16	364	924.6	6.5	62.5	16.8	14.2	13.7

Sample	Depth		Particle Size Distribution (Percent)				
	in.	cm	>74μm	74-20μm	20-2μm	<2μm	<1μm
17-LH-17	383	972.8	10.8	59.8	15.8	13.6	13.1
-18	393	998.2	4.9	62.4	17.6	15.1	14.4
-19	403	1023.6	6.5	61.6	16.9	15.0	14.2
18-LH-1	70	177.8	0.3	45.2	28.1	26.4	22.9
-2	90	228.6	0.6	50.3	31.4	17.7	15.6
-3	106	269.2	0.4	50.2	31.7	17.7	15.0
-4	113	287.0	0.5	51.3	32.0	16.2	14.0
-5	135	342.9	0.5	49.8	33.2	16.5	14.9
-6	155	393.7	0.5	52.2	30.9	16.4	14.3
-7	175	444.5	0.6	54.5	27.6	17.3	15.6
-8	214	543.6	0.5	34.0	45.6	19.9	17.2
-9	248	629.9	9.5	10.8	19.6	60.1	53.1

Sample	Depth		Particle Size Distribution (Percent)				
	in.	cm	>74 µm	74-20 µm	20-2 µm	<2 µm	<1 µm
1-DM-1	60	152.4	0.3	33.4	34.1	32.2	28.7
-2	84	213.4	0.1	41.6	33.5	24.8	22.1
-3	108	274.3	0.3	45.1	33.2	21.4	19.1
-4	132	335.3	0.9	19.6	52.3	27.2	22.8
-5	142	360.7	2.7	22.7	45.5	29.1	25.4
-6	160	406.4	4.1	22.7	32.7	40.5	36.5
-7	166	421.6	4.0	22.3	31.1	42.6	38.8
2-DM-1	60	152.4	0.2	34.5	38.5	26.8	23.1
-2	84	213.4	0.4	35.7	38.8	25.1	19.7
-3	108	274.3	0.3	36.5	38.9	24.3	21.5
-4	132	335.3	0.2	31.9	43.8	24.1	21.6
-5	156	396.2	2.6	22.2	36.9	38.3	35.3
-6	160	406.4	2.1	24.3	34.0	39.6	36.8
3-DM-1	60	152.4	0.3	36.2	33.6	29.9	26.8
-2	84	213.4	0.6	28.5	43.1	27.8	24.9
-3	108	274.3	0.1	31.2	41.6	27.1	24.1
-4	129	327.7	0.9	17.5	47.1	34.5	30.1
-5	132	335.3	1.3	20.6	42.4	35.7	31.5
-6	156	396.2	4.3	14.9	30.2	50.6	47.5
4-DM-1	60	152.4	0.9	40.2	29.9	29.0	26.3
-2	84	213.4	0.2	42.6	33.3	23.9	21.4
-3	108	274.3	0.4	42.6	35.8	21.2	18.7
-4	132	335.3	0.3	42.9	35.3	21.5	19.5
-5	156	396.2	0.2	29.6	42.6	27.6	23.7
-6	180	457.2	3.3	23.5	41.8	31.4	28.3
-7	183	464.8	2.2	18.4	35.5	43.9	41.1

Sample	Depth		Particle Size Distribution (Percent)				
	in.	cm	>74μm	74-20μm	20-2μm	<2μm	<1μm
5-DM-1	60	152.4	0.8	33.1	30.5	35.6	32.0
-2	84	213.4	0.5	34.6	34.6	30.3	27.1
-3	108	274.3	0.7	35.7	34.9	28.7	25.0
-4	132	335.3	0.3	42.1	33.3	24.3	21.6
-5	147	337.4	4.0	20.8	39.8	35.4	31.4
-6	154	391.2	3.9	22.4	38.5	35.2	31.9
-7	182	462.3	3.3	19.1	33.3	44.3	40.5
6-DM-1	8	20.3	1.8	35.0	36.1	27.1	22.5
-2	24	61.0	1.7	31.4	31.7	35.2	31.7
-3	42	106.7	0.8	32.1	32.1	35.0	30.9
-4	56	142.2	0.6	35.9	30.4	33.1	29.6
-5	72	182.9	0.2	40.8	32.2	26.8	23.8
-6	94	238.8	0.3	44.1	33.6	22.0	18.7
-7	106	269.2	0.3	42.2	34.3	23.2	20.1
-8	111	281.9	0.3	36.9	37.6	25.2	22.6
-9	127	322.6	0.2	45.2	35.1	19.5	15.7
-10	155	393.7	0.1	24.8	47.2	27.9	25.3
-11	169	429.3	3.7	21.9	34.5	39.9	36.9
7-DM-1	80	203.2	0.3	37.3	36.3	26.1	22.6
-2	107	271.8	0.3	42.1	34.6	23.0	20.8
-3	138	350.5	0.3	31.3	41.0	27.4	24.1

343

Sample	Depth		Particle Size Distribution (Percent)				
	in.	cm	>74 μm	74-20 μm	20-2 μm	<2 μm	<1 μm
8-DM-1	69	175.3	0.4	35.6	35.4	28.6	25.6
-2	136	345.4	0.2	28.7	46.1	25.0	21.2
9-DM-1	106	269.2	0.4	35.5	40.2	23.9	21.1
-2	144	365.8	0.4	44.7	36.3	18.6	16.0
-3	170	431.8	0.3	29.7	48.9	21.1	18.2
10-DM-1	39	99.1	0.3	35.9	34.0	29.8	25.9
-2	86	218.4	0.2	27.3	45.6	26.9	23.5
-3	136	345.4	0.3	40.0	37.4	22.3	19.4
11-DM-1	66	167.6	0.4	34.1	35.2	30.3	26.8
-2	122	309.7	0.2	32.4	42.2	25.2	22.6
12-DM-1	62	157.5	0.2	32.9	37.3	29.6	26.6
-2	95	241.3	0.3	28.0	44.1	27.6	23.8

Site	Depth		Particle Size Distribution (Percent)		
	in.	cm	>20μm	20-2μm	<2μm
2-1	88	223.5	52.4	30.4	17.2
	106	269.2	54.0	33.4	12.6
2-4	63	160.0	47.1	30.8	22.1
	76	193.0	50.0	31.3	18.7
	120	304.8	49.6	36.7	13.7
2-6	106	269.2	47.1	30.8	22.1
	140	355.6	52.0	32.8	15.2
	170	431.8	53.2	31.8	15.0
2-8	95	241.3	49.7	30.1	20.2
	138	350.5	58.8	26.2	15.0
	170	431.8	50.9	31.9	17.2
2-10	131	332.7	66.0	18.2	15.8
	202	513.1	62.1	23.4	14.5
	280	711.2	60.6	25.5	13.9
2-11	91	231.1	46.2	32.4	21.4
	117	297.2	51.4	31.4	17.2
	130	330.2	51.6	32.9	15.5
	166	421.6	53.1	32.2	14.7
	180	457.2	55.5	29.2	15.3

Site	Depth		Particle Size Distribution (Percent)		
	in.	cm	>20μm	20-2μm	<2μm
2-12	84	213.4	49.3	38.2	12.5
	128	325.1	49.9	35.6	14.5
2-14	78	198.1	47.1	30.0	22.9
	124	315.0	46.7	37.3	16.0
2-15	63	160.0	45.3	32.9	21.8
	106	269.2	47.0	33.4	19.6
	136	345.4	47.5	35.4	17.1
	171	434.3	47.7	37.3	15.0
	185	469.9	50.4	33.3	16.3
	211	535.9	50.3	34.2	15.5
2-16	75	190.5	46.8	33.7	19.5
	95	241.3	52.8	29.7	17.5
2-17	67	170.2	45.2	29.1	25.7
	97	246.4	47.6	31.1	21.3
2-18	62	157.5	46.9	28.4	24.7
	83	210.8	51.8	27.3	20.9
	99	251.5	50.6	29.6	19.8
	118	299.7	49.6	31.3	19.1
	124	315.0	46.9	34.7	18.4
14-BHS-1[1]	80	203.2	-	-	21.2
1-3	70	177.8	47.5	29.5	23.0

[1] Data courtesy of G.R. Hallberg.

Site	Depth		Particle Size Distribution (Percent)		
	in.	cm	>20μm	20-2μm	<2μm
23-120[a]	84	213.4	-	-	17.8
	90	228.6	-	-	14.7
29-4-280[a]	50	127.0	-	-	29.3
	60	152.4	-	-	29.3
29-NW-1[a]	72	182.9	-	-	26.1
29-WH-5[a]	90	228.6	39.9	45.0	15.1
42-163[a]	72	182.9	-	-	-
	94	238.8	-	-	20.7
44-H-2	35	88.9	28.8	38.0	33.2
	45	114.3	32.2	38.5	29.3
	75	190.5	38.7	40.8	20.5
	92	233.7	31.9	46.4	21.7
	101	256.5	23.4	54.4	22.2
44-L-1	39	99.1	28.4	38.1	33.5
	47	119.4	30.6	40.8	28.6
	68	172.7	29.9	44.4	25.7
	74	188.0	28.7	45.7	25.6
	84	213.4	20.6	49.4	30.0
44-L-2	66	167.6	37.8	37.9	24.3
	70	177.8	38.2	36.7	25.1
	75	190.5	38.4	36.1	25.5

Site	Depth		Particle Size Distribution (Percent)		
	in.	cm	>20 μm	20-2 μm	<2 μm
44-L-3	50	127.0	29.9	42.3	27.8
	54	137.2	30.7	41.6	27.7
	58	147.3	31.9	43.1	25.0
64-LH-1	66	167.6	46.3	30.7	23.0
	97	261.9	45.2	33.4	21.4
HF-1	132	335.3	-	-	-
	252	640.1	-	-	-
T-1	-	-	65.6	22.6	11.8
T-2	39	99.1	61.9	23.9	14.2

APPENDIX D: PARTICLE SIZE CONTROL DATA

	Particle Size Distribution (Percent)				
	>74μm	74-20μm	20-2μm	<2μm	<1μm

Pipette Standard 1

	>74μm	74-20μm	20-2μm	<2μm	<1μm
1	0.6	32.1	35.9	31.4	23.9
2	0.5	35.1	32.3	32.1	26.8
3	0.7	35.2	32.9	31.2	26.3
4	0.5	33.0	32.9	33.6	28.3
5	0.5	32.5	33.4	33.6	27.9
6	0.5	32.5	32.2	34.8	29.8
7	0.5	32.3	32.6	34.6	29.6
8	0.5	35.7	29.7	34.1	31.1
9	0.4	36.2	32.5	30.9	25.6

Pipette Standard 2

	>74μm	74-20μm	20-2μm	<2μm	<1μm
1	0.7	36.7	30.0	32.6	30.3
2	0.7	41.9	24.8	32.6	28.9
3	0.9	35.6	32.6	30.9	26.0
4	0.7	38.7	30.0	30.6	27.5
5	0.7	38.3	30.1	30.9	26.1
6	1.1	36.6	30.6	31.7	27.4
7	0.9	35.7	31.6	31.8	27.7
8	0.7	37.8	29.4	32.1	29.7
9	1.1	37.9	29.9	31.1	27.0
10	0.8	38.9	29.8	30.5	26.3
11	0.9	37.9	30.6	30.6	26.6
12	0.8	39.6	28.7	30.9	27.2
13	1.0	32.7	32.3	34.0	29.6
14	0.8	34.7	31.2	33.3	31.8

	Particle Size Distribution (Percent)				
	>74μm	74-20μm	20-2μm	<2μm	<1μm
15	0.8	34.5	31.6	33.1	29.4
16	0.9	33.7	32.0	33.4	29.1
17	0.9	33.2	32.0	33.9	30.2
18	1.0	34.9	30.7	33.4	29.3
19	0.9	36.2	29.7	33.2	30.1
20	0.9	35.3	31.3	32.5	28.6
21	0.9	37.3	30.8	31.0	26.7
22	0.7	34.0	31.3	34.0	29.4
23	0.8	37.0	31.1	31.1	27.4
24	0.9	34.6	31.5	33.0	28.9
25	0.8	35.4	31.5	32.3	28.2
26	0.9	37.1	30.3	31.7	27.6
27	0.8	33.3	32.3	33.6	29.7
28	0.8	35.9	30.9	32.4	28.1
29	0.8	36.1	31.4	31.7	27.7
30	0.7	39.1	30.2	30.0	28.3

APPENDIX E:

CLAY AGGREGATION-DISPERSION PARTICLE SIZE DATA

Sample	Depth		Particle Size Distribution (Percent)				
	in.	cm	>74 μm	74-20 μm	20-2 μm	<2 μm	<1 μm
1-LH-1	77	195.6	0.5	47.6	31.1	20.8	14.6
-2	107	271.8	0.6	56.7	27.5	15.2	10.9
-3	130	330.2	0.5	53.1	34.3	12.1	7.7
-4	138	350.5	0.5	53.2	35.5	10.8	6.6
-5	148	375.9	0.6	53.7	35.4	10.3	6.6
-6	160	406.4	1.1	48.2	37.5	13.2	8.2
-7	173	439.4	0.4	53.7	34.3	11.6	8.5
-8	207	525.8	0.5	29.5	57.9	12.1	7.2
3-LH-1	64	162.6	0.3	46.7	38.4	14.6	9.3
-2	88	223.5	0.7	52.1	36.7	10.5	4.8
-3	110	274.4	0.6	52.3	37.2	9.9	6.3
-4	133	337.8	0.6	52.0	37.6	9.8	6.1
-5	158	401.3	1.3	45.4	46.2	7.1	3.0
-6	180	457.3	1.0	22.0	64.2	12.8	6.9
-7	186	472.4	3.6	26.4	60.7	9.3	4.4
-8	190	482.6	2.8	25.1	59.8	12.3	4.8
-9	195	495.3	3.3	26.8	58.4	11.5	5.2
8-LH-1	70	177.8	0.3	36.8	43.7	19.2	13.7
-2	92	233.7	0.9	38.6	44.0	16.5	12.1
-3	112	284.5	0.2	49.9	40.8	9.1	5.6
-4	126	320.0	0.9	19.6	56.5	23.0	15.3

	Dispersion Time Min.	Particle Size Distribution (Percent)				
		>74 µm	74-20 µm	20-2 µm	<2 µm	<1 µm
17-LH-9						
1-A	0.5	3.1	66.8	26.8	3.3	2.7
1-B	0.5	2.7	64.2	29.0	4.1	2.8
1-C	0.5	2.4	68.2	25.6	3.4	2.7
2-A	2.5	2.5	64.4	27.1	6.0	3.6
2-B	2.5	2.0	63.9	29.3	4.8	3.4
2-C	2.5	2.3	63.3	28.1	6.3	4.3
3-A	5.0	2.2	60.5	28.1	9.2	6.5
3-B	5.0	2.0	60.6	29.0	8.4	6.0
3-C	5.0	2.2	63.1	25.6	9.1	6.4
4-A[1]	5.0	1.9	59.4	25.4	13.3	10.1
4-B[1]	5.0	1.7	59.9	24.6	13.8	12.6
4-C[1]	5.0	2.7	58.1	24.7	14.5	12.7
4-LH-3						
1-A	0.5	1.3	37.7	55.2	5.8	2.3
1-B	0.5	1.5	47.7	46.4	4.4	1.4
1-C	0.5	1.3	40.0	54.1	4.6	1.4
2-A	2.5	0.7	34.7	54.5	10.1	5.0
2-B	2.5	0.7	35.9	53.5	9.9	4.8
2-C	2.5	0.7	36.0	54.1	9.2	4.6
3-A	5.0	0.6	34.6	51.4	13.4	8.1
3-B	5.0	0.6	33.8	51.6	14.0	8.3
3-C	5.0	0.6	34.3	51.8	13.3	8.4
4-A[1]	5.0	0.5	30.3	43.4	25.8	21.6
4-B[1]	5.0	0.5	32.9	44.1	22.5	19.5
4-C[1]	5.0	0.5	29.9	45.9	23.7	20.5

[1]Dispersing agent added.

APPENDIX F: BULK DENSITY DATA

Site	Depth in.	cm	W. Zone	M %	Dbm gm/cc	Dbd gm/cc	S %
1-MW	72	182.9	OL	17.5	1.61	1.37	48.7
	106	269.2	OL	24.0	1.72	1.39	68.0
	130	330.2	OL	26.8	1.78	1.40	78.9
	167	424.2	MOL	29.9	1.84	1.42	88.6
from base of cut							
	25	63.5	OL	33.1	1.81	1.36	90.7
	47	119.4	OL	29.6	1.89	1.46	93.6
	73	185.4	DL	27.3	1.95	1.53	96.9
	98	248.9	DL	25.2	1.97	1.57	95.6
	120	304.8	DL	24.0	1.93	1.56	87.6
2-MW	73	185.4	OL	17.6	1.63	1.39	49.5
	99	251.5	OL	23.3	1.80	1.46	74.0
	127	322.6	MOL	28.2	1.78	1.39	80.4
	162	411.5	DL	30.0	1.87	1.44	92.1
	194	492.8	DL	26.1	1.95	1.55	93.9
	233	591.8	DL	23.2	1.91	1.55	84.5
	256	650.2	BWS	22.5	1.93	1.58	-
3-MW	77	195.6	MOL	32.0	1.85	1.40	93.5
	99	251.5	DL	29.3	1.90	1.47	94.4
	125	317.5	DL	24.0	1.95	1.57	90.8
	149	378.5	DL	28.0	1.97	1.54	100.0
4-MW	74	188.0	OL	16.3	1.51	1.30	40.5
	91	231.1	OL	24.0	1.64	1.32	62.6
	121	307.3	OL	21.3	1.69	1.39	61.8
	146	370.8	OL	19.8	1.48	1.24	44.4
	167	424.2	DL	20.4	1.64	1.36	56.4

| Site | Depth | | W. | M | Dbm | Dbd | S |
	in.	cm	Zone	%	gm/cc	gm/cc	%
4-MW	176	447.0	DL	20.4	1.64	1.36	56.4
	222	563.0	OL	21.6	1.64	1.35	58.0
	243	617.2	MOL	20.5	1.67	1.39	57.7
	290	736.6	MOL	26.2	1.77	1.40	76.8
	310	787.4	MOL	24.5	1.69	1.36	66.5
	332	843.3	MOL	20.8	1.74	1.44	64.3
	358	909.3	DL	20.5	1.76	1.46	65.3
	426	1082.0	MOL	20.4	1.92	1.59	80.3
5-MW	70	177.8	OL	27.6	1.84	1.44	85.7
	91	231.1	OL	28.5	1.89	1.47	92.2
	124	315.0	MOL	30.0	1.87	1.44	92.1
	156	396.2	MOL	24.5	1.99	1.60	95.7
	188	477.5	MOL	23.2	1.84	1.49	78.1
6-MW	94	238.8	DL	29.3	1.91	1.48	95.2
7-MW	55	139.7	OL	31.4	1.86	1.42	92.8
	94	238.8	MOL	27.7	1.91	1.50	92.3
	122	309.9	MOL	22.3	1.97	1.61	89.2
8-MW	151	383.5	OL	27.5	1.93	1.51	95.3
	215	546.1	OL	25.1	1.84	1.47	81.2
	246	624.8	MOL	22.2	1.89	1.55	79.8
	269	683.3	BWS	23.2	1.99	1.62	-
9-MW	62	157.5	MOL	32.8	1.85	1.39	94.8
	82	208.3	MOL	29.1	1.91	1.48	95.2
	94	238.8	MOL	28.1	1.92	1.50	94.5

Site	Depth in.	cm	W. Zone	M %	Dbm gm/cc	Dbd gm/cc	S %
10-MW	52	132.1	S	30.4	1.84	1.41	90.0
11-MW	119	302.3	MOL	23.5	1.90	1.54	83.8
	150	381.0	OL	22.3	1.97	1.61	89.2
12-MW	36	91.4	S	22.7	1.64	1.34	59.6

| Site | Depth | | W. | M | Dbm | Dbd | S |
	in.	cm	Zone	%	gm/cc	gm/cc	%
1-ME	52	137.2	DL	23.3	1.94	1.57	88.4
	64	162.6	DL	26.7	1.92	1.52	91.5
2-ME	27	68.6	S	32.7	1.89	1.42	99.1
	32	81.3	S	26.3	1.97	1.56	97.1
	42	106.7	MOL	23.6	1.98	1.60	93.3
3-ME	36	91.4	OL	22.4	2.00	1.63	93.4
	41	104.1	OL	20.9	1.97	1.63	85.8
4-ME	36	91.4	S	24.9	1.92	1.54	88.4
6-ME	40	101.6	OL	24.7	1.96	1.57	93.2
7-ME	69	175.3	MDL	21.2	1.88	1.55	77.5
	72	182.9	MOL	19.9	1.91	1.59	77.8
	78	198.1	MOL	19.4	1.96	1.64	81.5
10-ME	28	71.1	S	30.0	1.93	1.48	99.6
	32	81.3	S	28.9	1.94	1.51	97.6
	36	91.4	OL	25.5	1.90	1.51	88.5
12-ME	36	91.4	S	27.1	1.92	1.51	93.0
	52	132.1	OL	22.7	2.06	1.67	100.0

Site	Depth in.	cm	W. Zone	M %	Dbm gm/cc	Dbd gm/cc	S %
1-LH	92	233.7	OL	25.9	1.84	1.46	82.7
	187	475.0	DU	26.1	1.97	1.56	97.1
	198	502.9	OL	25.6	2.01	1.60	100.0
	204	518.2	OL2	26.3	1.98	1.57	98.0
	213	541.0	DL	26.3	1.94	1.54	93.1
	224	569.0	DL	27.5	1.95	1.53	96.9
2-LH	80	203.2	OL	23.6	1.76	1.42	71.7
	102	259.1	OL	25.0	1.74	1.39	72.1
	135	342.9	OL	22.1	1.71	1.40	64.4
	169	429.3	OU	24.8	1.94	1.55	91.6
	192	487.7	OU	26.2	1.94	1.54	93.1
	223	566.4	OU	28.1	1.92	1.50	94.5
	240	609.6	OU	28.2	1.90	1.48	93.0
3-LH	102	259.1	MOU	27.4	1.95	1.53	96.9
	140	355.6	MOU	24.0	2.01	1.62	97.5
	159	403.9	DU	24.3	2.02	1.62	100.0
	166	421.6	DU	23.7	2.00	1.62	95.0
	199	505.5	DL	21.0	2.05	1.69	96.2
4-LH	81	205.7	OL	16.1	1.65	1.42	48.5
	116	294.6	MOL	24.2	1.87	1.50	83.2
	135	342.9	MOL	20.7	2.00	1.66	88.3
	146	370.8	MOL	25.2	1.94	1.55	91.6

Site	Depth		W.	M	Dbm	Dbd	S
	in.	cm	Zone	%	gm/cc	gm/cc	%
5-LH	93	236.2	OL	29.6	1.84	1.42	88.6
	130	330.2	MOU	24.4	2.01	1.61	99.1
	156	396.2	DU	22.3	2.03	1.66	96.1
6-LH	83	210.8	OL	26.5	1.87	1.48	86.3
	112	284.5	MOL	26.2	1.83	1.45	82.1
	134	340.4	MOL	27.8	1.89	1.48	90.7
7-LH	85	215.9	OU	26.0	1.93	1.53	92.3
	95	241.3	MOU	25.9	1.95	1.55	93.9
	113	287.0	MOU	26.3	1.96	1.55	96.3
8-LH	115	292.1	MOU	26.7	1.98	1.56	99.5
9-LH	77	195.6	OL	11.6	1.60	1.43	36.1
	132	335.3	OU	11.2	1.58	1.42	33.8
	157	398.8	OU	12.8	1.73	1.53	46.2
	185	469.9	OU	14.1	1.73	1.52	48.1
	190	482.6	OU	15.9	1.79	1.54	58.2
	208	528.3	MOL	22.2	1.89	1.55	79.8
10-LH	73	185.4	OL	23.5	1.81	1.47	74.6
	81	205.7	OL	21.5	1.76	1.45	67.0
	103	261.6	OL	30.9	1.89	1.44	96.4
	109	276.9	OL	30.0	1.87	1.44	92.1

| Site | Depth | | W. | M | Dbm | Dbd | S |
	in.	cm	Zone	%	gm/cc	gm/cc	%
12-LH	53	134.6	MDL	33.0	1.86	1.40	95.5
	82	208.3	MDL	29.9	1.89	1.45	95.0
	95	241.3	MDL	32.5	1.86	1.40	95.5
	114	289.6	MDL	29.5	1.97	1.52	100.0
	180	457.2	MDU	23.6	2.02	1.64	96.8
	249	632.5	UU	19.8	2.09	1.74	98.4
	252	640.1	UL	27.8	1.98	1.55	100.0
18-LH	92	233.7	OL	18.0	1.52	1.29	44.0
	113	287.0	OU	19.4	1.66	1.39	55.6
	135	342.9	OU	20.6	1.76	1.46	65.3
	153	388.6	OU	23.3	1.82	1.47	76.8
	175	444.5	MOU	21.2	1.82	1.50	72.0
	206	523.2	MOU	25.5	1.91	1.52	89.2

Site	Depth in.	cm	W. Zone	M %	Dbm gm/cc	Dbd gm/cc	S %
1-DM	66	167.6	OL	27.8	1.89	1.47	92.2
	99	251.5	MOU	28.1	1.93	1.51	95.3
	117	297.2	MOL	29.3	1.93	1.49	98.2
	130	330.2	DL	29.6	1.90	1.47	94.4
2-DM	66	167.6	OL2	27.8	1.86	1.46	87.1
	85	215.9	MOL2	28.6	1.92	1.49	96.0
	124	315.0	MOL2	29.8	1.91	1.47	96.6
	143	363.2	DL	27.1	1.96	1.54	97.8
	152	386.1	DL	26.4	1.96	1.55	96.3
3-DM	62	157.5	OL	32.2	1.86	1.41	94.2
	96	243.8	MOU	27.7	1.98	1.55	100.0
	119	302.3	DL	25.3	2.02	1.61	100.0
	138	350.5	DL	26.6	1.96	1.55	96.3
4-DM	71	180.3	OL	30.5	1.88	1.44	94.3
	111	281.9	OL2	27.0	1.90	1.50	90.0
	119	302.3	MOL2	27.5	1.93	1.51	95.3
	136	345.4	MOU	26.6	1.95	1.54	95.4
	147	373.4	MOU	26.9	1.98	1.56	100.0
	174	442.0	DL	23.1	2.01	1.63	95.9
5-DM	71	180.3	OL	31.7	1.83	1.39	90.7
	88	223.5	OL	31.2	1.89	1.44	96.4
	101	256.5	MOL	30.2	1.93	1.48	99.6
	124	315.0	MOL	27.4	1.98	1.55	100.0
	167	424.2	MOL	29.7	1.94	1.50	99.0

| Site | Depth | | W | M | Dbm | Dbd | S |
	in.	cm	Zone	%	gm/cc	gm/cc	%
5-DM	71	180.3	OL	31.7	1.83	1.39	90.7
	88	223.5	OL	31.2	1.89	1.44	96.4
	101	256.5	MOL	30.2	1.93	1.48	99.6
	124	315.0	MOL	27.4	1.98	1.55	100.0
	167	424.2	MOL	29.7	1.94	1.50	99.0
6-DM	86	218.4	OL	34.0	1.90	1.42	100.0
	113	287.0	MOL	31.9	1.92	1.46	100.0
	123	312.4	MOL	29.8	1.96	1.51	100.0
	128	325.1	MDL	29.6	1.95	1.50	100.0
	142	360.7	MDL	30.4	1.94	1.48	100.0
	158	401.3	BWS	26.5	1.98	1.57	98.0

Site	Depth in.	cm	W. Zone	M %	Dbm gm/cc	Dbd gm/cc	S %
2-1	88	223.5	OL	17.2	1.70	1.45	55.0
	106	269.2	OL	18.1	1.84	1.56	68.6
2-4	63	160.0	MOL	19.0	1.75	1.47	62.7
	76	193.0	MOL	20.0	1.80	1.50	69.1
	120	304.8	DU	23.8	1.96	1.58	93.1
2-6	106	269.2	OL	27.0	1.88	1.48	90.5
	140	355.6	MOU	24.0	2.07	1.67	100.0
	170	431.8	DU	24.6	2.03	1.63	100.0
2-8	95	241.3	MOL	27.0	1.73	1.36	75.4
	138	350.5	DU	24.5	1.97	1.58	95.8
	170	431.8	DU	24.6	2.01	1.61	100.0
2-10	131	332.7	MOL	21.2	1.64	1.35	92.1
	202	513.1	DU	25.5	1.91	1.52	91.1
	280	711.2	DU	25.1	2.02	1.61	100.0
2-11	91	231.1	OL	22.3	1.54	81.9	21.4
	117	297.2	MOL	23.0	1.90	1.54	84.9
	130	330.2	MOU	24.5	1.94	1.56	92.9
	166	421.6	DU	23.9	2.01	1.62	99.5
	180	457.2	DU	24.0	2.03	1.64	100.0
2-12	84	213.4	MOU	17.0	1.82	1.56	64.5
	128	325.1	DU	21.3	1.91	1.59	84.8

Site	Depth in.	cm	W. Zone	M %	Dbm gm/cc	Dbd gm/cc	S %
2-14	78	198.1	OL	25.1	1.78	1.42	76.7
	124	315.0	DL	17.2	2.04	1.74	87.2
2-15	63	160.0	MOL	23.0	1.89	1.54	84.5
	106	269.2	DU	20.3	1.97	1.60	82.1
	136	345.4	DU	23.0	1.98	1.61	93.4
	171	434.3	DU	23.6	1.98	1.60	95.5
	185	469.9	DU	21.2	1.91	1.58	82.9
	211	535.9	UU	24.4	2.00	1.61	100.0
2-16	75	190.5	OL	12.0	1.62	1.45	38.4
	95	241.3	OL	10.5	1.70	1.54	38.7
2-17	67	170.2	OL	24.0	1.82	1.47	79.3
	97	246.4	OL	26.0	1.77	1.40	77.1
2-18	62	157.5	OL	22.8	1.85	1.51	77.1
	83	210.8	OL	21.5	1.81	1.49	71.4
	99	251.5	MOL	26.8	1.91	1.50	92.2
	118	299.7	MOL	26.1	1.92	1.52	91.5
	124	315.0	MOL	27.1	1.98	1.56	99.5
64-LH-1	66	167.6	MO-DL	34.2	1.83	1.36	94.7
	97	261.9	MO-DU	31.2	1.93	1.47	100.0
44-L-1	39	99.1	DL	25.2	1.98	1.58	96.4
	47	119.4	DL	25.6	1.96	1.56	94.7
	68	172.7	MOL	27.0	1.92	1.51	93.0

Site	Depth in.	cm	W. Zone	M %	Dbm gm/cc	Dbd gm/cc	S %
44-L-1	74	188.0	MOL	29.1	1.92	1.49	96.0
	84	213.4	MOL	26.3	1.94	1.54	93.1
44-L-2	66	167.6	MOL	29.3	1.89	1.46	93.6
	70	177.8	MOL	28.8	1.94	1.51	97.6
	75	190.5	OL	26.8	2.00	1.59	99.7
44-L-3	50	127.0	DL	28.0	1.98	1.55	100.0
	54	137.2	DL	29.2	1.94	1.50	99.0
	58	147.3	DL	26.6	1.98	1.56	99.5
HF-1	132	335.3	OU	13.5	1.55	1.36	38.3
	252	640.1	OU	14.5	1.80	1.58	52.8
T-1	-	-	OU	19.4	1.60	1.34	51.6
T-2	39	99.1	OU	13.7	1.57	1.38	38.2
14-BHS-1[1]	80	203.2	OL	26.3	1.73	1.37	73.1
1-3	70	177.8	OL	28.8	1.91	1.48	95.2
23-120[1]	84	213.4	OL	18.8	1.74	1.46	61.0
	90	228.6	OL	18.8	1.74	1.46	61.0
29-NW-1[1]	72	182.9	DL	32.5	1.88	1.42	96.3
29-WH-5[1]	90	228.6	DL	33.1	1.88	1.41	98.4

[1]Data courtesy of G.R. Hallberg.

367

Site	Depth in.	cm	W. Zone	M %	Dbm gm/cc	Dbd gm/cc	S %
29-4-280[1]	50	127.0	MOL	23.0	1.82	1.48	75.2
	60	152.4	DL	26.0	1.86	1.48	84.1
42-163[1]	72	182.9	MOL	21.7	1.67	1.37	60.9
	94	238.8	MOU	28.5	1.86	1.45	88.6
44-H-2	35	88.9	S	30.9	1.84	1.40	91.4
	45	114.3	S	28.2	1.94	1.52	96.1
	75	190.5	DL	27.7	1.98	1.55	100.0
	92	233.7	DL	26.3	1.98	1.56	99.5
	101	256.5	DL	29.0	1.92	1.49	95.9

[1] Data courtesy of G.R. Hallberg.

APPENDIX G: REGRESSION MODELS FOR BULK DENSITY

Regression models for all observations. N = 206

Number of Variables in Model	R^2	Variables			
1	0.00004	X4			
1	0.03200	X1			
1	0.04562	X2			
1	0.12175	X3			
2	0.04271	X1	X4		
2	0.13000	X1	X2		
2	0.14472	X2	X3		
2	0.14559	X3	X4		
2	0.14704	X2	X4		
2	0.17830	X1	X3		
3	0.14765	X2	X3	X4	
3	0.17951	X1	X2	X3	
3	0.17976	X1	X3	X4	
3	0.18134	X1	X2	X4	
4	0.18222	X1	X2	X3	X4

Regression models for oxidized zone. N = 68

	R^2				
1	0.00391	X1			
1	0.02853	X4			
1	0.11741	X2			
1	0.15196	X3			
2	0.06238	X1	X4		
2	0.15402	X3	X4		
2	0.15419	X2	X3		
2	0.15532	X2	X4		
2	0.16906	X1	X3		
2	0.17369	X1	X2		
3	0.16144	X2	X3	X4	
3	0.18697	X1	X3	X4	
3	0.18719	X1	X2	X3	
3	0.18744	X1	X2	X4	
4	0.18821	X1	X2	X3	X4

Regression models for mottled zone. N = 74

Number of Variables in Model	R^2	Variables			
1	0.00018	X4			
1	0.00081	X1			
1	0.04720	X2			
1	0.10836	X3			
2	0.00163	X1	X4		
2	0.06496	X1	X2		
2	0.13118	X1	X3		
2	0.16556	X2	X3		
2	0.17708	X3	X4		
2	0.18834	X2	X4		
3	0.17244	X1	X2	X3	
3	0.18299	X1	X3	X4	
3	0.19483	X1	X2	X4	
3	0.19693	X2	X3	X4	
4	0.20412	X1	X2	X3	X4

Regression models for deoxidized zone. N = 51

1	0.00105	X1			
1	0.00223	X4			
1	0.00578	X2			
1	0.00732	X3			
2	0.00638	X1	X4		
2	0.00680	X2	X4		
2	0.00732	X3	X4		
2	0.00733	X2	X3		
2	0.01047	X1	X3		
2	0.01063	X1	X2		
3	0.01076	X1	X2	X4	
3	0.01100	X1	X2	X3	
3	0.01127	X1	X3	X4	
3	0.04484	X2	X3	X4	
4	0.05048	X1	X2	X3	X4

Regression models for East-Central Iowa. N = 57

Number of Variables in Model	R^2	Variables			
1	0.00695	X4			
1	0.20941	X2			
1	0.34944	X1			
1	0.35873	X3			
2	0.39451	X1	X4		
2	0.40476	X2	X3		
2	0.40548	X3	X4		
2	0.40639	X2	X4		
2	0.48426	X1	X2		
2	0.49498	X1	X3		
3	0.40816	X2	X3	X4	
3	0.49535	X1	X3	X4	
3	0.49538	X1	X2	X3	
3	0.49561	X1	X2	X4	
4	0.49594	X1	X2	X3	X4

Regression models for South-Central Iowa. N = 25

Number of Variables in Model	R^2	Variables			
1	0.01846	X4			
1	0.06903	X2			
1	0.21300	X3			
1	0.48493	X1			
2	0.21906	X2	X4		
2	0.23207	X3	X4		
2	0.23720	X2	X3		
2	0.48510	X1	X2		
2	0.48969	X1	X4		
2	0.49402	X1	X3		
3	0.46397	X2	X3	X4	
3	0.49767	X1	X2	X4	
3	0.49976	X1	X3	X4	
3	0.50165	X1	X2	X3	
3	0.61070	X1	X2	X3	X4

Regression models for Northeast Iowa. N = 39

Number of Variables in Model	R^2	Variables	
1	0.00451	X2	
1	0.16716	X3	
1	0.25901	X1	
1	0.31676	X4	
2	0.33393	X1	X2
2	0.35224	X1	X4
2	0.41741	X2	X4
2	0.41741	X3	X4
2	0.41741	X2	X3
2	0.48652	X1	X3

Regression models for Southeast Iowa. N = 17

1	0.00284	X1	
1	0.00812	X2	
1	0.00814	X3	
1	0.04126	X4	
2	0.00824	X1	X3
2	0.01063	X1	X2
2	0.04172	X2	X3
2	0.04172	X3	X4
2	0.04172	X2	X4
2	0.06587	X1	X4

Regression models for West-Central Missouri. N = 51

1	0.00043	X4	
1	0.00407	X2	
1	0.01912	X3	
1	0.03080	X1	
2	0.03341	X1	X2
2	0.03361	X1	X3
2	0.04730	X2	X3
2	0.04730	X3	X4
2	0.04730	X2	X4
2	0.05257	X1	X4

Regression models for East-Central Missouri. N = 17

Number of Variables in Model	R^2	Variables		
1	0.03596	X3		
1	0.22007	X1		
1	0.40368	X2		
1	0.51262	X4		
2	0.31541	X1	X3	
2	0.43503	X1	X2	
2	0.48550	X2	X3	
2	0.51446	X2	X4	
2	0.51554	X1	X4	
2	0.51922	X3	X4	
3	0.49901	X1	X2	X3
3	0.53023	X1	X2	X4
3	0.53926	X2	X3	X4
3	0.55078	X1	X3	X4
4	0.57128	X1	X2	X4

X1 = depth, cm

X2 = % coarse silt + sand (2mm-2μm)

X3 = % fine silt (20-2μm)

X4 = % < 2μm clay

APPENDIX H: SHEAR STRENGTH DATA

Site	Depth		φ	C		r
	in.	cm	deg.	psi	kN/m^2	
1-MW	150	381.0	31.1	1.1	7.6	1.000
4-MW	120	304.8	37.6	2.6	17.9	1.000
	300	762.0	27.1	3.4	23.5	0.986
5-MW	90	228.6	31.0	0.7	4.8	0.996
7-MW	78	198.1	31.7	2.5	17.3	0.993
	111	281.9	25.3	1.3	9.0	0.993
8-MW	72	182.9	20.4	1.9	13.1	0.991
	90	228.6	21.4	1.8	12.4	0.998
9-MW	84	213.4	17.5	2.4	16.6	0.985
10-MW	78	198.1	24.1	3.9	26.9	0.995
11-MW	84	213.4	23.3	2.5	17.3	0.997
12-MW	40	101.6	32.8	5.2	35.9	0.991
1-ME	66	167.6	28.2	5.1	35.2	0.985
3-ME	40	101.6	25.7	4.5	31.1	0.999
6-ME	48	121.9	12.6	2.9	20.0	0.992
7-ME	75	190.5	25.7	3.6	24.8	0.991
9-LH	206	523.2	41.5	1.8	12.4	0.998
18-LH	98	248.9	42.8	0.0	0.0	0.999
	214	543.6	40.9	0.7	4.8	0.999
2-1	84	213.4	43.5	0.4	2.8	1.000
2-4	72	182.9	40.2	1.4	9.7	1.000
	120	304.8	43.9	0.5	3.5	0.999
2-6	142	360.7	42.2	0.0	0.0	0.991
2-8	144	365.8	38.8	0.2	1.4	0.998
2-11	134	340.4	41.6	0.6	4.1	0.999
2-14	124	315.0	41.2	0.0	0.0	1.000
2-15	166	421.6	44.6	1.1	7.6	0.998
2-16	103	261.6	41.9	1.3	9.0	0.979
2-17	72	182.9	39.2	2.0	13.8	0.999
2-18	105	266.7	36.9	0.2	1.4	0.998

Site	Depth		ϕ	C		r
	in.	cm	deg.	psi	kN/m^2	
HF-1	132	335.3	38.3	0.6	4.1	0.998
	252	640.1	35.0	0.7	4.8	0.999
T-2	39	99.1	24.7	0.8	5.5	0.999
14-BHS-1[1]	80	203.2	35.0	1.6	11.0	0.998
1-3	70	177.8	38.4	0.8	5.5	0.989
23-120[1]	84	213.4	41.9	1.3	9.0	0.998
	90	228.6	44.2	0.8	5.5	0.992
29-NW-1[1]	72	182.9	36.3	0.0	0.0	0.995
29-WH-5[1]	90	228.6				
29-4-280[1]	50	127.0	20.0	1.6	11.0	0.998
	60	152.4	23.0	0.8	5.5	0.999
42-163[1]	98	248.9	33.4	0.2	1.4	0.999

[1]Data courtesy of G.R. Hallberg.

APPENDIX I: REGRESSION MODELS FOR SHEAR STRENGTH

Regression Models for Dependent Variable Y1   N = 35

Number of Variables in Model	R^2	Variables			
1	0.00095	X2			
1	0.03085	X3			
1	0.19034	X4			
1	0.28657	X1			
2	0.03504	X2	X3		
2	0.19252	X3	X4		
2	0.19918	X2	X4		
2	0.32300	X1	X2		
2	0.32339	X1	X4		
2	0.33021	X1	X3		
3	0.20298	X2	X3	X4	
3	0.34479	X1	X3	X4	
3	0.35970	X1	X2	X4	
3	0.38822	X1	X2	X3	
4	0.39800	X1	X2	X3	X4

Regression Models for Dependent Variable Y2   N = 35

	R^2	Variables			
1	0.00282	X2			
1	0.00507	X3			
1	0.10717	X4			
1	0.16758	X1			
2	0.00671	X2	X3		
2	0.11733	X2	X4		
2	0.13880	X3	X4		
2	0.16972	X1	X3		
2	0.18704	X1	X3		
2	0.19882	X1	X2		
3	0.14436	X2	X3	X4	
3	0.19875	X1	X3	X4	
3	0.19889	X1	X2	X3	
3	0.21820	X1	X2	X4	
4	0.22300	X1	X2	X3	X4

Y1 = friction angle, degrees
Y2 = cohesion, KN/m^2
X1 = depth, cm
X2 = bulk density, gm/cm^3
X3 = moisture content, %
X4 = % <2μm clay